Faculty of Science and Engineering
Department of Imaging and Applied Physics

Seabed Biotope Characterisation Based On Acoustic Sensing

Rudolf J Kloser

This thesis is presented for the Degree of
Doctor of Philosophy
of
Curtin University of Technology

September 2007

Declaration

This thesis contains no material which has been accepted for the award of any other degree or diploma in any university.

To the best of my knowledge and belief this thesis contains no material previously published by any other person except where due acknowledgment has been made.

Signature: …….

Date: ……...

Abstract

The background to this thesis is Australia's Oceans Policy, which aims to develop an integrated and ecosystem-based approach to planning and management. An important part of this approach is the identification of natural regions in regional marine planning, for example by establishing marine protected areas for biodiversity conservation. These natural regions will need to be identified on a range of scales for different planning and management actions. The scale of the investigation reported in this thesis is applicable to spatial management at 1 km to 10 km scale and monitoring impacts at the 10s of m to 1 km biotope scale. Seabed biotopes represent a combination of seabed physical attributes and related organisms. To map seabed biotopes in deep water, remote sensing using a combination of acoustic, optical and physical sensors is investigated.

The hypothesis tested in this thesis is that acoustic bathymetry and backscatter data from a Simrad EM1002 multi-beam sonar (MBS) can be used to infer (act as a surrogate of) seabed biotopes. To establish a link between the acoustic data and seabed biotopes the acoustic metrics are compared to the physical attributes of the seabed in terms of its substrate and geomorphology at the 10s m to 1 km scale using optical and physical sensors. At this scale the relationship between the dominant faunal functional groups and both the physical attributes of the seabed and the acoustic data is also tested. These tests use data collected from 14 regions and 2 biomes to the south of Australia during a voyage in 2000.

Based on 62 reference sites of acoustic, video and physical samples, a significant relationship between ecological seabed terrain types and acoustic backscatter and bathymetry was observed. These ecological terrain types of soft-smooth, soft-rough, hard-smooth and hard-rough were chosen as they were the most relevant to the biota in their ability to attach on or burrow into the seabed. A seabed scattering model supported this empirical relationship and the overall shape of backscatter to incidence angle relationship for soft and hard seabed types. The correlation between acoustic data (backscatter mean and standard deviation) and the visual and physical samples was most consistent between soft-smooth and hard-rough terrain types for a large range of incidence angles (16^o to 70^o). Using phenomenological backscatter features segmented into 10 common incidence angle bins from -70^o to 70^o the length resolution of the data decreased to 0.55 times depth. The decreased resolution was offset by improved near normal incidence (0^o to 30^o) seabed type discrimination with cross validation error reducing from 32% to 4%.

A significant relationship was also established between the acoustic data and the dominant functional groups of fauna. Faunal functional groups were based on the ecological function, feeding mode and substrate preference, with 8 out of the 10 groups predicted with 70% correctness by the four acoustically derived ecological terrain types. Restricting the terrain classification to simple soft and hard using the acoustic backscatter data improved the prediction of three faunal functional groups to greater than 80%. Combining the acoustic bathymetry and backscatter data an example region, Everard Canyon, was interpreted at a range of spatial scales and the ability to predict the preferred habitat of a stalked crinoid demonstrated. Seabed terrain of soft and hard was predicted from the acoustic backscatter data referenced to a common seabed incidence angle of 40^o. This method of analysis was selected due to its combined properties of high spatial resolution, consistent between terrain discrimination at the widest range of incidence angles and consistent data quality checking at varying ranges.

Based in part on the research reported in this thesis a mid-depth Simrad EM300 multibeam sonar was purchased for use in Australian waters. A sampling strategy is outlined to map all offshore waters with priority within the 100 m to 1500 m depths.

Acknowledgements

It is a pleasure to acknowledge my supervisory panel; Prof. John Penrose for his continued guidance and enthusiasm in physics and applications of marine acoustics; Dr Alan Butler who continually added to my reading list on ecological topics for which I greatly benefited and enjoyed; Dr Chris de Moustier who ensured that I tackled the technical aspects to the best of my ability.

This study would not have been possible without the continued support of CSIRO Marine and Atmospheric Research (CMAR) and my many colleagues. The study formed part of a National Oceans Office (NOO) project in collaboration with CMAR. I would like to thank my co-principal investigators Alan Butler and Alan Williams for their continued support throughout that project. Also the many staff from CMAR who helped mobilise for the long and demanding survey that provided the data for this project. In particular, the project team of Bruce Barker, Francis Althaus, Gordon Keith, Tim Ryan, Mark Lewis, Karen Gowlett-Holmes and Mathew Sherlock.

The data used in this project was funded by a joint NOO and CMAR study and I thank both organisations for supporting my access to the data for the thesis.

Lastly, my love goes out to all my friends and family: especially my ever patient wife Maureen and children, Josef, Patrick and Eliza. It has been a shared journey and your support kept me going.

Dedication:

I dedicate this thesis to my friend and partner Maureen who has been my constant companion and without whose support this would not have been possible.

Table of contents

1 Introduction

1.1 Introduction 1

2 Seabed biotope characterisation

2.1 Introduction 4

2.2 Classification of habitats 7

2.3 Geology 8

2.4 Biology/Ecology 10

2.5 Oceanography 13

2.6 Australian regional setting 15

2.7 Summary 18

3 Seabed Acoustics

3.1 Introduction 19

3.2 Plane waves and rays in a fluid medium 19

3.3 Sonar Equation 21

3.4 Geoacoustic sediment properties 26

3.5 Seabed roughness 27

3.6 Seabed scattering models at high frequency 30

3.7 High frequency acoustic model 32

3.8 Echo statistics 37

3.9 Summary 40

4 Acoustic and Towed Video Technology

4.1 Introduction 41

4.2 Acoustic systems overview 41

4.3 Multibeam sonar (MBS) 44

4.4 Video system 62

4.5 Summary 65

5 Field Experiment

5.1 Introduction 66

5.2 Survey design 66

5.3 Acoustics 73

5.4 Video system 83

5.5 Benthic invertebrates 86

5.6 Geological sampling 87

5.7 Field data summary 88

5.8 Summary 96
6 Reference site analysis
6.1 Introduction 98
6.2 Reference sites 98
6.3 Videography analysis 99
6.4 Physical sampling 103
6.5 Multibeam sonar reference site analysis 104
6.6 Model based classification 112
6.7 Statistical descriptors for seabed segmentation 118
6.8 Backscatter referenced to a given incidence angle 124
6.9 Summary 126
7 Acoustic interpreted maps for a region
7.1 Introduction 128
7.2 Horseshoe Canyon example 129
7.3 Summary 148
8 Summary and Discussion
8.1 Exploratory seabed biotope surveys 149
8.2 National scale seabed biotope mapping 152
8.3 Mapping Australia's marine regions 154
Appendix
A. References 157
B. Equipment description 167
C. Seabed biotope characterisation in deep water – initial evaluation of single and multi-beam acoustic 176

List of figures

Figure 1.1 Framework for marine habitat classification represented by a hierarchy of spatial habitat units and hierarchy of ecological units (NOO 2002;; Kloser *et al.*, 2004).

Figure 2.1 Conceptual model of the range of space and time scales in the marine environment for some physical processes (stippled ellipse) and a deep-water > 50 m sponge community (open ellipse). Adapted from Holling (1992).

Figure 2.2 Model of predicted currents at depth (1.5 m in this instance) and location based on seasonal climatologies of wind, sea level, temperature and salinity, horizontal resolution 20 km (described in Bruce *et al.*, 2001).

Figure 2.3 Demersal continental shelf regions of Australia based on a collation of geological, oceanographic and biological data highlighting the Twofold Shelf, Coorong and Eucla regions sampled in this thesis (IMCRA 3.3 1998).

Figure 2.4 Major geomorphic units of the a.) South East Australian province with the study areas in the Twofold shelf and Coorong regions circled and b.) the Great Australian Bight Province with the Eucla region circled.

Figure 3.1 Example of area ensonified on a horizontal seabed at normal incidence (beam width limited) and at 50^o angle of incidence (pulse length limited). The beam geometries shown are 10^o along-track and 10^o across-track at 0^o and 50^o incidence (10^o chosen for clarity in the diagram, labels referred to in Chapter 4).

Figure 3.2 Reduction coefficient $\Delta(\theta_i)$ based on equation 3.19 for (a) integration angular limits of 0^o to 6^o and for (b) incidence angles 0^o to 70^o for the system described in Ch. 3.3.1.

Figure 3.3 Representation of acoustic scatter from high impedance, (a) smooth; (b) rough surface and low impedance contrast, (c) smooth; (d) rough surface (modified from Urick 1983 p140).

Figure 3.4 Seabed scattering strength $S_b(\theta)$ of seabed types at 95 kHz with the contribution from volume scattering (dotted) and the total seabed scattering (solid) for rock (plus), coarse sand (circle), medium sand (cross), coarse silt (diamond) and sandy mud (triangle) using the geophysical parameters quantified in Table 3.2 and the model (APL94 1994).

Figure 3.5 Scattering strength model prediction for 'medium sand' (solid) as the sum of volume scattering (*) and interpolated roughness scattering from Kirchoff approximation (square), composite roughness (circle) and large scale roughness (dashed).

Figure 4.1 Diagram showing the different beam patterns of the commonly used commercially available instruments for seabed classification (ICES in press).

Figure 4.2 Across-track receive beam intensity polar plots for the, a) nadir 0^o incident beam (2^o at –3dB power) and the, b) oblique -75^o beam (2.5^o at –3dB power). Note the side lobe and grating lobe levels (< -20 dB and < -17 dB for the 0^o and 75^o incidence beams) that measure unwanted signal from the seafloor and increase noise.

Figure 4.3 Reference diagram for coordinate system for EM1002 (Modified from Simrad 1999c).

Figure 4.4 Comparison of beam sampling area for multibeam and single beam acoustics operating in 100 m water depth. The single beam sampling area is representative of acoustic roughness algorithm for 17^o – 34^o (Kloser *et al.* 2001b), whilst the multibeam sampling is for 111, 2^o beams at equi-distant spacing and 140^0 swath width.

Figure 4.5 Box plot of seabed slope along-track and across-track for 100 pings of a soft smooth reference site (a, b) and a hard rough reference site (c,d). The box contains the inter quartile range (50% of the data), '+' represents outliers and the vertical line the spread of the data. Beam 1 at –70^o, beam 56 at 0^o (nadir) and beam 111 at –70^o

Figure 4.6 Internally calculated emitted beam pointing angles for 85 pings (Fig. 4.2) incident on a horizontal flat seabed where beam 56 is at 0^o and beam 111 at 70^o.

Figure 4.7 Estimates of the Simrad EM1002E ensonified area (a) based on Eq. 4.5 and 4.6 (dashed) and equivalent ensonified area based on Eq. 3.12 and Eq. 3.17 (solid) at 100 m depth and pulse length 0.7 ms. Estimated seabed backscatter error, (b) between the two estimates of ensonified area in dB for incidence angles 0^o to 70^o on a flat horizontal seafloor.

Figure 4.8 Simrad EM1002 seabed backscatter area (Eq. (4.5 and 4.6)) resolution at the center of each beam (A_{bci}) on a horizontal flat seafloor for a range of incidence angles (0^o –70^o), depths, 50 m (plus), 100 m (square) and 400 m (circle) at pulse lengths of 0.2 ms, 0.7 ms and 2 ms respectively. Assumes a Simrad EM1002 with 2^o along-track and 3^o across-track conical receive beams.

Figure 4.9 Length of the ensonified region in the along-track (solid, Eq. (4.8)) and the across-track (dashed, min of Eq. (4.9 and 4.10)) directions at the beam centres for a horizontal flat seafloor at 100 m depth. Assumes a Simrad EM1002 with 2^o along-track and 3^o across-track conical receive beams and pulse length 0.7 ms.

Figure 4.10 Area compensation (Λ_{Ai} , Eq. (4.14)) required from that implemented in the real time Simrad algorithms (A_{rti}) assuming a real time implemented incidence angle and measured local seabed incidence angle difference of 0^o (solid), 3^o (dash-dot) and 10^o (dot) at constant range (positive starboard up). The emitted angle from the vessel ranges from -70^o to 70^o, assumes a Simrad EM1002 with 2^o along-track and 3^o across-track conical receive beams at 100 m depth and pulse length of 0.7 mS.

Figure 4.11 Area correction in dB required for along-track slope change of –10^o to 10^o within the beam width limited region at 100 m depth and 0.7 ms pulse length.

Figure 4.12 Variation of the absorption dB km^{-1} in seawater based on Francois and Garrison (1982) at a base case of frequency 95 kHz, pH 8, temperature 15 ^{o}C, depth 0 m, and salinity 35 ppt (asterix) and variations of temperature (5 to 30 ^{o}C), depth (0 to 300 m) and salinity (33 to 36 ppt).

Figure 4.13 Error (dB) in the measured seabed backscatter for absorption error ($\Delta_{\alpha_{set}-\alpha_{measured}}$) of 1 $dBkm^{-1}$ (solid), 5 $dBkm^{-1}$ (dashed) and 10 $dBkm^{-1}$ (dotted) at transmission angles (θ) 0^{o} to 70^{o} on a horizontal seafloor at 200 m depth (D).

Figure 4.14 Illumination (plan and elevation in cm) of the seafloor with camera and light at 30^{o} incidence and 101 cm above the seafloor.

Figure 5.1 The range of acoustic and ground-truth sampling gears used from Southern Surveyor during mapping survey SS01/00. For detailed specifications of the equipment refer to Kloser et al., 2001b.

Figure 5.2 Map showing the general locations (small and large black dots) of survey areas during SS01/00 at a regional scale .

Figure 5.3 Map of MBS survey track areas mapped in the Twofold Shelf and upper slope region 1. Areas are named and numbered as per Table 5.1.

Figure 5.4 Map of MBS survey track areas mapped in the Coorong region 2. Areas are named and numbered as per Table 5.1.

Figure 5.5 Map of MBS survey track areas mapped in the Eucla region 2. Areas are named and numbered as per Table 5.1. Also shown is the Great Australian Bight Marine Protection Zone.

Figure 5.6 Example of MBS mapped Area 3 (Gabo Reef) showing bathymetric texture (shaded-bathymetry, 8 times vertical exaggeration), acoustic reference sites marked and associated targeted video and sediment grab/core stations.

Figure 5.7 Example of the a) bathymetry (red 115 m to yellow 130 m), b) beam center backscatter imagery –5 to –60 dB (black to white), c) seabed slope (yellow 0.5^{o} to blue 10^{o}), d) bathymetry-contrast (shaded-bathymetry 8 times vertical exaggerated) with visual megahabitat analysis of the region characterized by a low relief limestone reef (1.1 hard-rough), reef edge (1.2 hard-rough) and sediment flat of changing substrate (1.3 - 1.5 soft-smooth).

Figure 5.8 Simrad EM1002 centre beam backscatter of Gabo Reef (Fig. 4) with, a) recorded backscatter with incidence angle (scale range –5 to –60 dB) and b) removal of incidence angle backscatter dependence referenced to 40^{o} incidence angle (scale –20 to –40 dB).

Figure 5.9 Example of a) preprocessed MBS bathymetry texture (shaded-bathymetry vertical exaggeration 8 times) in the flatly sloping <1^{o} Great Australian Bight (Area 14), depth 135-145 m, showing the depth rippling at high incidence angle (60^{o} to 70^{o}) on the outer beams due to vessel motion and/or incorrect surface sound speed ; b) preprocessed MBS backscatter per central beam in areas with and without large sand waves (high backscatter is black).

Figure 5.10 Shaded bathymetry of the Big Horseshoe (Area 6 and 7), a productive fishing ground, showing the depth limitation of the swath mapper at approximately 600 m at 120^{o} seabed ensonification.

Figure 5.11 Preprocessed bathymetry texture (Sun illuminated bathymetry with 8 times height exaggeration) for Broken Reef (Area 5, depth 112 – 116 m) showing limestone outcrops of 0.5 to 1 m height. North-south lines highlight MBS artifacts due to incorrect sound speed profile or surface sound speed compensation.

Figure 5.12 Example of single beam 38 kHz backscatter: (at Gabo Reef Area 3, Fig. 5.7) a) second echo (E2) overlaid on uncorrected EM1002 backscatter and b) tail of first echo (E1) overlaid on MBS texture (sun illuminated bathymetry, 8 times vertical exaggeration). The size of the sampling dots represents the approximate 50 m sampling diameter of the single beam system (Kloser *et al.,* 2002a).

Figure 5.13 MBS backscatter referenced to 40^{o} incidence angle (high backscatter dark and prominent horizontal line normal incidence) of small feature (~4 x 4 km) showing overlay of two georeferenced and scored video transects (soft terrain classes, circles, hard terrain classes, asterisk) of varying geological and biological characteristics (Table 2.4). Geolocated sediment grab composition (pie chart) in percentage gravel (red), sand (yellow) and mud (brown).

Figure 5.14 Example video frame grabs of the typical substrate, geomorphology and fauna types.

Figure 5.15 Length scales for video scores (all areas) of contiguous patches of seabed attributes, substrate and geomorphology (solid) and fauna (dashed).

Figure 6.1 Box plot of contiguous terrain length (m) frequency for the soft-smooth, soft-rough, hard-smooth and hard-rough terrain types. The box contains the median (bar) and interquartile (50%) range and outliers (plus sign) being 1.5 times this range.

Figure 6.2 Variation in relative seabed backscatter (dB) for two reference sites >50 pings one side of the swath width, soft-smooth (lower) and hard-rough (upper) for seabed incidence angles of 0 to 70 degrees being. Box plot shows variation of site backscatter dB with median and inter quartile (25% to 75%) range of dB values, solid line is linear mean of backscatter.

Figure 6.3 Variation of relative between site backscatter for 11 soft-smooth (solid mean) and 15 hard-rough sites (dotted mean) according to seabed incidence angle. Box plot shows variation of site means (dB) with median and inter quartile (25% to 75%) range.

Figure 6.4 Variation of mean relative standard deviation of backscatter for 11 soft-smooth (dotted mean) and 15 hard-rough sites (solid mean) according to seabed incidence angle where 0^{o} is normal to the seabed. Box plot shows variation of site standard deviation means with median and inter quartile (25% to 75%) range.

Figure 6.5 Variation of backscatter mean (a) and standard deviation (b) for soft-smooth reference sites, 4 with mud composition < 10 % (dotted mean) and 6 with mud

> 10% (solid mean). Box plot shows variation of site mean and standard deviation means with median and inter quartile (25% to 75%) range.

Figure 6.6 Comparison of the a) mean and b) standard deviation of relative seabed backscatter of a soft-rough site (solid) with 11 soft-smooth sites (dash-dot) and 15 hard-rough sites (dashed).

Figure 6.7 Variation of mean backscatter (a) and its standard deviation (b) for 15 hard-rough reference sites (solid), 7 within 30 to 100 m depth (dotted), 8 within 100 to 200 m depth (dashed) according to incidence angle. Box plot shows variation of between site means and standard deviation with median and inter quartile (25% to 75%) range.

Figure 6.8 Variation of mean backscatter (a) and its standard deviation (b) for 5 reef reference sites (solid mean) and soft-smooth reference sites (Fig. 6.5) with mud composition < 10 % (dashed mean) and 6 with mud > 10% (dotted mean) according to incident angle. Box plot shows variation between sites with median and inter quartile (25% to 75%) range.

Figure 6.9 APL94 model predictions (adjusted by –12 dB) of typical seabed types ranging from rock to clay terrains assuming geoacoustic properties in Table 3.2 at 0^o to 70^o incident to the seafloor, and mean backscatter for soft-smooth (dotted) and hard-rough (solid) reference sites (Figure 6.3).

Figure 6.10 Box plot of difference in mean backscatter data at each incidence angle to that predicted by the APL94 (1994) seabed backscattering model from 11 soft-smooth reference sites (50 to 200 m depth) using two methods of fitting; a) using simulated annealing, b) best fit to historic geoacoustic values (Table 3.2).

Figure 6.11 Predicted sediment size (phi) based on model values (Table 3.2) and minimum Kolmogorov-Smirnov test fit to 36 reference sites with sediment composition of gravel (o) and mud (*), dry weight fraction (%).

Figure 6.12 Prediction of surface roughness assuming power law relief spectrum and isotropy for a soft-rough site using model values (solid) (Table 3.2) and simulated annealing (dotted).

Figure 6.13 Model predicted a) mean sediment grain size (phi) and b) spectral strength based on model values (Table 3.2) for the 11 soft smooth and 14 hard rough reference sites 50 – 200m depth.

Figure 6.14 Box plot of APL94 (1994) model predicted roughness values a) spectral exponent and b) spectral strength for soft smooth and hard rough reference sites using simulated annealing with limits specified in Table 3.3.

Figure 6.15 Simulated annealing APL94 (1994) model prediction of surface roughness assuming power law relief spectrum and isotropy for two reference sites; soft-smooth (o) and reef (*) with orthogonal sampling, north-south (solid) and east-west (dotted).

Figure 6.16 Mahalanobis distance measure of separation between the four ecological terrain types and 6 sectors, grouped by the three similar incident angle segments,

S16(incidence angles from 61^{o} to 71^{o}), S25(incidence angles from 30^{o} to 60^{o}) and S34 (incidence angles from 0^{o} to 29^{o}).

Figure 6.17 Classification of a complex reference site using four ecological terrain types, 6 sectors and 4 ping ensemble as training sites, a) not using and b) using between sector information parameter, 'bps', with scored video transect overlaid. Terrain type key, soft-smooth blue, soft-rough green and hard-smooth, brown.

Figure 6.18 Classification of a complex reference site using four ecological terrain training types, 10 sectors and 4 ping ensembles using all parameters with scored video transect overlaid. Terrain type key, soft-smooth blue, soft-rough green and hard-smooth, brown.

Figure 7.1 Location of study site within the Bass Canyon and Twofold shelf province on the east coast of Australia (Harris *et al.,* 2002).

Figure 7.2 Detailed bathymetry of the Bass Canyon using historic data from deep water MBS surveys (figure B2, Hill *et al.*, 2001) with Horseshoe Canyon study site marked.

Figure 7.3 Bathymetric data from the Simrad EM1002 of Horseshoe canyon, illumination 20^{o} elevation, 35^{o} azimuth, depth 130 m (brown) to 600 m (blue).

Figure 7.4 Direction and relative amplitude of a.) surface (20 m) currents shown with arrows recorded during the mapping of the canyon. Note the circulatory nature of the currents over the canyon with minimal current in the centre and higher currents over shallow water (Kloser *et al.,* 2001b), b.) lantern fish (*Lampanyctodes hectoris*) aggregated in the canyon.

Figure 7.5 Bathymetry of Horseshoe canyon ranging from 150 m depth (brown) to 600 m depth (aqua) with illumination elevation (20^{o}), azimuth (35^{o}), depth 130 m (brown). Segmentation of the region based on visual classification of bathymetry, slope, shaded bathymetry and backscatter into 25 acoustic terrain types as outlined in Ch. 5 Table 5.3. Boxed region (dashed) detailed in Figure 7.12.

Figure 7.6 Slope derived from the MBS bathymetry (30 m grid) and segmented into 4 slope classes being, 0^{o} to 3^{o} (white to blue), 3^{o} to 5^{o} (aqua), 5^{o} to 10^{o} (yellow) and greater than 10^{o} (red).

Figure 7.7 Relative backscatter (dB, 30 m grid), a.), referenced to 40^{o} incidence angle –40 to –20 dB (white to black); b.), segmented by soft (blue) < -33.5 dB, transition (cyan) -33.5 dB to -31 dB, hard (red) > -31 dB terrain (Table 7.1). Backscatter at depths greater than 550 m removed due to increased noise interference.

Figure 7.8 Cumulative probability of slope derived from an acoustically soft seabed (solid) and an acoustically hard seabed (dashed).

Figure 7.9 Location of, a.), sediment grab samples as percentage by weight of sand (yellow), mud (brown) and gravel (red) and, b.), video terrain type of soft-smooth (orange), soft-rough (yellow), hard-smooth (pink), hard-rough (red), c.), video terrain type of soft (blue) and hard (red). Relative backscatter (30 m grid) referenced to 40^{o} incidence angle white to black (-40 to –20 dB).

Figure 7.10 Relative backscatter (grid 30 m) referenced to 40^{o} incidence angle for video classified terrain type of soft (dashed) and hard (solid) within acoustic defined terrain of soft (blue) and hard (red), a.), occurrence and b.), relative proportion in 2 dB bins.

Figure 7.11 Contiguous patch length of video terrain, soft (dashed) and hard (solid) within acoustic terrain of soft (blue) and hard (red) for a.), all regions and b.), the Big Horseshoe region (areas 6 and 7).

Figure 7.12 Contiguous patch length of video fauna in video soft (dashed) and hard (solid) terrain within acoustic terrain of soft (blue) and hard (red) for a.), all regions and b.), the Big Horseshoe region (areas 6 and 7).

Figure 7.13 The cumulative video classified fauna of types 0 to 9 (Table 4.xx) associated with increasing values of backscatter where soft type fauna are associated with lower backscatter (dashed) and hard associated fauna associated with high backscatter (solid) and no affinity dotted.

Figure 7.14 Section of the Horseshoe Canyon (Fig. 7.5, 30 m grid) showing the, a.), slope (details Fig. 7.6), b.), backscatter (details Fig. 7.7a) and c.) segmented backscatter into soft and hard terrain (details Fig. 7.7b) with sediment grab samples (pie charts, gravel (red), sand (yellow) and mud (brown)) and video classified terrain into soft (blue) and hard (red) terrain. Reference sites 4, 5, 6, 7, 8 are shown within terrain areas 7.06, 7.07 and 7.11.

Figure 7.15 Example images of the stalked crinoid (*Metacinus rotundus)* observed in reference site a.), 5 at 185 m depth and b.), site 7 at 229 m depth (Fig. 7.14).

Figure 7.16 Relationship of video classified fauna type 4 (crinoids, 738 scores) with MBS variables of depth, slope and backscatter at 30 m grid for a.), all records and b.) where the cover was greater than 10% of the viewing area (159 scores).

Figure 7.17 Potential distribution of the Fauna category 4 (Crinoids) based on the 90th percentile (green) and the 50th percentile (red) range for the entire MBS dataset (blue).

Figure 8.1 Example of the EM300 MBS bathymetry and improved knowledge from the outer shelf upper slope: (A) image from previous information with canyons marked (Harris *et al*., 2002); (B) the extra detail of the topography provided with the MBS; proposed marine protected area boundary in red. (C) map of the bathymetry joined with deeper water Simrad EM12 MBS data showing the outer shelf and the continental slope of the region.

List of Tables

Table 2.1 Example of how surrogate variables can be used to infer variables of interest based on acoustic and video metrics.

Table 2.2 Relating needs of spatial management planning to sizes resolvable by sampling; a pseudo-spatial hierarchical habitat classification scheme (NOO, 2002) and terms from a spatially explicit classification scheme (Greene et al., 1999). Micro-scales (< 1 m) not shown (Kloser et al. 2004).

Table 2.3 Clastic term of diameter size range in mm and phi size based on the Wentworth scale (Wentworth 1922).

Table 2.4 Attributes of seabed habitats recorded from the video data at 1 s intervals (approx. 0.25 m) following Kloser *et al.* (2001b) ordered in terms of hypothesised gradients of increasing seabed hardness and roughness and inferred current and potentially nutrient availability for fauna.

Table 3.1 Definition of parameters used in Table 3.2 for a model of seabed reflectance based on Jackson and Briggs (1992).

Table 3.2 Characteristics of seabed terrains at 95 kHz and sound speed 1500 ms^{-1} to determine seabed backscatter (APL94 1994).

Table 3.3 Recommended limits for the model of seabed backscattering, (APL94 1994).

Table 3.4 Parameters derived from the MBS backscatter and depth used in the phenomenological segmentation of the seafloor in Ch. 6.7.

Table 4.1 Acoustic sampling devices for surficial seabed properties and typical sampling resolution expected in 100 m water depth.

Table 4.2 Theoretical depth data densities on a horizontal flat seafloor based on a Simrad EM1002 with 111, 2^o conical, equispaced beams covering 140^o and surveying at a speed of 5 ms^{-1} (ignoring attitude and refraction effects). Minimum grid size requiring at least 2 samples within a grid cell.

Table 4.3 Resolution of the video system at center of viewing from visual viewing and digital screen captures range length 250 – 350 cm (vertical V) and center width 203 and 280 cm (horizontal H).

Table 5.1 Areas sampled within biogeographic regions during survey SS01/00 using the Simrad EM1002 MBS showing, area, depth range, pulse length and on-board produced bathymetric grid. Region 1, 2 and 3 are Twofold Shelf, Coorong and Eucla respectively.

Table 5.2 Physical and visual operation types and frequency within survey areas during SS01/00 (Kloser *et al.* 2001b; "S"=existing data from previous surveys, Bax and Williams [Eds] 2000). Note only invertebrates retainedfrom the benthic sled sampling devices are shown here.

Table 5.3 Classes of depth, bathymetry-contrast, slope and backscatter attributes used to visually score benthic terrain at 1 to 10s km feature sizes in MBS maps gridded at 10 – 50 m intervals (Fig. 5.7): also shown are the inferred simplified terrain types for comparison with video terrain types.

Table 5.4 Summary of methods to analyse the MBS data, based on Kloser *et al.,* 2002a (Appendix C).

Table 5.5 Calibration settings for the EK500 acoustic instrument.

Table 5.6 The functional unit classification scheme based on the ecological association of the species mobility, dominant feeding mode and preferred (inferred) substrate type (Althause *et al.* 2004).

Table 5.7 MBS survey areas with number of acoustic terrain and reference sites with associated physical and visual samples.

Table 5.8 Area of acoustic terrains (km^2) at each depth strata (m) scored for bathymetry contrast, slope and backscatter based on visual scoring of the MBS data, Table 5.3.

Table 5.9 Criteria for segmentation of the visual acoustic terrains scoring (Table 5.3) into generic seabed characteristics ranging from soft to hard and smooth to rough consistent with the ecological preference of functional units of fauna (Table 5.6).

Table 5.10 Distribution of visually scored acoustic terrains area (km^2) by depth for the generic seabed classes ranging from soft-smooth to hard-rough defined in Table 5.9.

Table 5.11 Classes of substrate, geomorphology and fauna used to score benthic terrains and proportions of each across the 14 study areas; also shown are the inferred terrain types for comparison with acoustic terrain types.

Table 5.12 Comparison of video terrains (% composition) of substrate and geomorphology within the acoustic terrains defined at 1-10 km scale. Each data set independently grouped into four terrain classes (see Tables 5.9 and 5.11) and two terrain classes of soft and hard terrain.

Table 5.13 Proportion (%) of faunal types in four terrain classes defined by video at 1-10 m feature size. Grouping of video data into terrain classes shown in Table 5.11.

Table 5.14 Proportion of soft and hard substrate preference of 5 sessile faunal groups within the 8 functional units (Table 5.6) separated into the acoustic terrains of varying backscatter and inferred hardness (Tables 5.3 and 5.9).

Table 5.15 Sediment stations mean proportion by weight of gravel, sand and mud (s.d. in brackets) for each acoustic depth class.

Table 5.16 Sediment stations mean proportion by weight of gravel, sand and mud (s.d. in brackets) for each acoustic backscatter class (Table 5.3).

Table 5.17 Visual inspection of lithology (Harris et al. 2000) and associated porosity from hard-rough (reef) acoustic terrains and video scoring (soft-smooth (SS), soft-rough (SR), hard-smooth (HS) and hard-rough (HR).

Table 6.1 Proportional composition of reference sites designated by videography scores Table 5.11 as soft to hard and smooth to rough terrain.

Table 6.2 Proportion (%) of video scored fauna in the seabed terrains of Table 6.1 weighted by terrain type then fauna group.

Table 6.3 Proportion of video scored fauna group in the seabed terrains soft, hard, smooth and rough weighted by terrain type then fauna type.

Table 6.4 Proportion of video scored fauna where the cover is greater than 10% or greater than 50% (in brackets) for the seabed terrains of soft-smooth, soft-rough, hard-smooth and hard-rough.

Table 6.5 Sediment composition, percentage gravel (G%), sand (S%) and mud (M%) with associated standard deviation (s.d.) with the video scored homogeneous reference sites outlined in Table 6.1.

Table 6.6 Visual inspection of lithology (Harris *et al.,* 2000) and associated porosity from hard rough (reef) acoustic terrain and video scoring (soft-smooth (SS), soft-rough (SR), hard-smooth (HS) and hard-rough (HR)).

Table 6.7 Prediction of sediment size (in phi units) based on model values (Table 3.2) and minimum Kolmogorov-Smirnov (KS) fit to 11 homogeneous soft-smooth terrain reference sites with measured sediment composition (gravel, G, sand, S, mud, M).

Table 6.8 Geoacoustic properties of density ratio and sound speed ratio of two soft smooth sites based on box core samples.

Table 6.9 The effective sampling distance of segmenting the across-track ensonification of the MBS backscatter data assuming 111 equidistant spaced beams into 5 and 10 segments for a flat horizontal seafloor.

Table 6.10 The effective sampling distances of segmenting the along and across track ensonification of the MBS backscatter data assuming a swath sampling of 140 degrees and speed of 10 knots for various depths.

Table 6.11 Parameters derived from the MBS backscatter and depth used in the phenomenological segmentation of the seafloor (described in Ch. 3.8).

Table 6.12 Number of times the correlation between parameters within the 4 ecological terrain types is greater than 0.5 or less that –0.5.

Table 6.13 Number of times the Mahalanobis distance for a given parameter between the four ecological terrain types was greater than 5 for the 6 segments (1 to 6) combined by common incidence angles 1&6, 2&5, and 3&4 for the 4 ping ensemble (Table 6.9).

Table 6.14 Cross validation error for the four ecological terrain types using the 6 beam segments with and without the cross segment mean backscatter 'bps' metric.

Table 7.1 Probability of seabed being classified as hard or soft based on the mean amplitude of 26 reference sites referenced to 40^{o} incidence angle Figure 6.3.

Table 7.2 Summary of the 25 acoustic terrain types for the Horseshoe Canyon (Fig. 7.5 for key) based on the backscatter, bathymetry and slope metrics of mean (m) standard deviation (s.d.) and kurtosis (k) with a description of major features (Kloser *et al.,* 2001b). Predominantly soft acoustic terrain highlighted in italic bold.

Table 7.3 Proportion of video terrain class of soft and hard and video fauna classes as defined in Table 2.4 segmented by the acoustic terrain type areas shown in Table 7.2 and Fig. 7.5. Soft acoustic terrain and predicted soft fauna type in italic bold.

Table 7.4 Proportion of video classified fauna (Table 2.4) segmented into the video terrain types of soft and hard defined by the substrate and geomorphology classes (Table 2.4). Predicted soft fauna type highlighted in bold italic.

Table 8.1 Theoretical depth data densities on a horizontal flat seafloor based on a Simrad EM1002 (2^{o} conical 111 beams) and Simrad EM300 (1^{o} conical 132 beams) equispaced covering 140^{o} and surveying at a speed of 5 ms^{-1} (ignoring attitude and refraction effects). Minimum square grid size requiring at least 2 depth samples within a grid cell.

Table 8.2 Approximate time in days to provide 100% multibeam cover using a Simrad EM300 multibeam sonar operating at 5 ms^{-1} from 25 m to 6000 m depths for each Australian Large Marine Domain excluding islands and Antarctic territory.

1 Introduction

This thesis explores the development of acoustic seabed survey methodology in response to management needs for seabed maps of offshore regions of the Australian marine jurisdiction. The context is *Australia's Oceans Policy*, launched in 1998, which aims to develop an integrated and ecosystem-based approach to planning and management for all ocean uses through spatially-structured Regional Marine Plans (NOO, 2002). This management approach includes the establishment of a national representative system of marine protected areas (MPAs) to aid in biodiversity conservation and is based on the identification of natural regions as planning units (NOO, 2002). These natural regions need to be identified on a range of hierarchically nested scales for different planning and management actions as the structures and functions of marine ecosystems are organised at multiple scales, and because of the multi-scale nature of human interests and impacts (*e.g.,* Langton *et al.*, 1995; Roff and Taylor, 2000). As an example of management within natural regions, the Australian Fisheries Management Authority has spatial spawning closures and is planning for wide-ranging spatial management of seabed-contact fishing effort to supplement the existing fishery management arrangements based on Total Allowable Catches.

The term "biotope" is used in this thesis to refer to a type of seafloor defined by both its physical characteristics (*e.g.* seabed hardness and roughness, regime of currents, temperature, depth) and the organisms that typically inhabit it. Spatial management planning would ideally start with a regional view of seabed biotopes - what they are, where they are, how much of each – together with an evaluation of biotope use which should identify biotopes with high ecological value (*e.g.* for biodiversity or fishery production) and those that may be vulnerable to impact from human activity (Bax and Williams 2001; Williams *et al.*, 2004). This is a multi-scale question which, in Australia's offshore regions, has to be addressed using a variety of existing information that is usually not comprehensive, is collected at a range of spatial and temporal scales and precisions, and may be difficult to access. As an example, the establishment of MPAs will be based primarily on the analysis of historic data using seabed geomorphology (Harris *et al*., 2002). An unfortunate part of this approach has been the lack of detailed historic information on seabed biotopes in 100 to 600 m – the region of highest current commercial fisheries interest. Clearly it would be of benefit to map these regions to better understand their biotopes and in turn assess how MPAs would affect the fishing industry and the protection of the biodiversity values of the offshore regions.

Within the offshore regions a major source of seafloor disturbance occurs through demersal trawl fishing, which is highly concentrated in 100 to 1000 m depths in the south east Australian region. The vulnerability of seabed biotope to fishing is defined as the resistance to physical modification and its resilience once modified (Bax and Williams, 2001). Fishing effort in the 200 – 600 m depth range in the south east Australian region has increased from 1995 to 1999, and due to the narrow area of the steep upper slope, the repeated impact was 7 times higher than in the 0 - 200 m depth range (Larcombe *et al.,* 2001). Another major fisheries change in recent years has been the targeting of specific terrain types using fixed gears such as traps, long lines and nets to depths of 500 m. This has the effect of moving effort from the relatively flat trawl grounds to harder and rougher substrate types. Understanding the changing use and its impact on the seafloor requires maps of seabed regions segmented into soft, hard, rough and smooth, which in turn determines the biological communities that can attach to the substrate and burrow into the substratum (Bax and Williams, 2001; Kloser *et al.*, 2001a). To map seabed biotopes of the whole Australian Marine Jurisdiction ($16*10^6$ km^2), will require the development of surrogates for biotopes, due to the large region and difficulty/expense of sampling the marine environment. From these seabed surrogates, we will need to infer the geological, biological and oceanographic features of the marine environment. The term surrogate is used throughout this thesis to imply that a strong correlation exists between the surrogate variable and the variable/parameter of

interest. It does not imply that there is a clear deterministic relationship between the surrogate variable and the parameter of interest which is also how the terminology is used by others.

The seabed maps at a given spatial scale can be placed in context using a conceptual framework provided by a hierarchical habitat classification scheme adopted by the Australian National Oceans Office (NOO, 2002). The classification scheme has seven primary 'Levels' and treats habitats and ecological attributes as complementary assessments of biodiversity, linked by ecological processes (Fig. 1.1). These Levels are: Realms, Provinces, Biomes, Biogeomorphological Units, Primary Biotopes, Secondary Biotopes, Facies. The scheme is not spatially hierarchical because, although smaller sizes are generally associated with lower levels in the hierarchy, scale is variable within levels. For example, an extensive facies at Level 6 may have a larger spatial extent than a secondary biotope at Level 5. In reality, the technology available for obtaining surrogates for habitat mapping has finite resolution and mapping is carried out at various scales to suit different management and scientific needs (Kloser *et al*., 2004).

Acoustic methods of sensing the water column and seabed habitats provide a potential method for developing these surrogates when used in conjunction with direct capture and visual sampling methods. Simple normal incident single and multi-frequency acoustic methods provide a useful sampling tool to map the seabed environment in terms of broad scale bathymetry and seabed hardness and roughness on flat seabeds with associated ground truthing (*e.g.* Chivers *et al.,* 1990; Kloser *et al.*, 2001a). To improve seabed sampling resolution, depth resolution and to account for seabed slope, multibeam sonars (MBS) are being used (e.g. Kloser *et al.,* 2001b). A MBS provides detailed bathymetry along the line of the vessel's track with swath widths of 2 to 5 times water depth and produces detailed acoustic backscatter maps of the seabed. The backscatter maps produced with data collected from hull-mounted MBS systems have lower resolution than those produced by towed sidescan instruments because the MBS transmits pulses of lower bandwidth over a wider fore-aft beamwidth. However, the higher positioning accuracy of hull-mounted sonars, and the angular resolution afforded by beam forming, MBS can correct for seabed slope and geo-reference the backscatter. Investigations using multi-beam backscatter maps to date have concentrated on geological mapping, (*e.g.* Todd *et al.*, 1999, Dartnell and Gardner 2004) and only recently habitat mapping (*e.g.* Kostylev *et al.,* 2001; Edwards *et al.*, 2003). What is less certain is whether the bathymetry and associated backscatter data can serve as a surrogate for biotope maps of a given region and, across regions the level of physical and optical (visual) sampling required.

This thesis explores the use and interpretation of commercially available acoustic and video survey technologies to provide surrogates of seabed attributes in water depths from 50 to 600 m at the biotope level (10s of m to 1 km) and at the 1 km to 10 km feature size.

Two hypotheses are tested in this thesis;

- At the 10s of m to 1 km scale, that the acoustic metrics can be used to describe the form and nature of the seabed terrain (substrate type and geomorphology) over a range of depths and between bioregions.
- At the 10s of m to 1 km scale, that the acoustic metrics can be used to predict the dominant functional groups of large epibenthic fauna over a range of depths and between bioregions.

To test these hypotheses, multibeam sonar data were collected from 14 regions within 2 biomes in the South of Australia. In these regions well described biotope reference sites were established using video and physical sampling of the sediment, rocks and large epifauna.

This thesis provides the context of seabed biotope characterisation within nested spatial and temporal scales of geological, biological and oceanographic variables in Ch. 2. Chapter 2 then introduces the need for acoustic remote sensing to provide surrogate measures of biotopes given the size and cost of physical sampling in the Australian deep water regions. A summary of high frequency seabed acoustic theory leading to a simple model of seabed roughness and volume scattering as well as phenomenological characteristics in the seabed backscatter are outlined in Ch. 3 and refered to in all subsequent chapters when using acoustic equipment. The MBS and video equipment used in experiments is described in Ch. 4 with context to spatial scales of measurements and known sampling errors. Errors with measurement of acoustic backscatter at a given angle of incidence to the seabed due to seabed slope, water column characteristics, ensonified area and instrument performance are explored. Using the instruments outlined in Ch. 4, Ch. 5 describes the field experiment carried out in April 2000 and characterises the seabed terrain and habitat at the scale of 1 to 10s of km. At this scale a major factor in determining the terrain is the morphology provided by the MBS. In this chapter the finer scale character of the seabed at 10s of m detected by video sensing is described. Chapter 6 explores the testing of the hypotheses in the thesis at the 10s of m to 1 km feature size. Based on the well described reference sites established in Ch. 5 the relationship between the video data and acoustic backscatter data is provided. Acoustic data is compared to the simple model and phenomenological characters outlined in Ch. 3. In particular the effect of video data correlations with angle of incidence and spatial scale at different aggregations of acoustic backscatter data is explored. Chapter 7 gives an example of how the acoustic interpreted maps of a region could be interpreted based on the Australian marine habitat classification framework (Fig. 1.1). A canyon off eastern Bass Strait is placed in context at the 100s of km scale and then described from the 10s km to 10s m scale using the acoustic data. The ability of the acoustic data to act as a surrogate and predictor of preferred habitat for a species is explored. Finally Ch. 8 provides a summary of the work and outlines a sampling strategy for the deepwater seabed habitats from 100 m to 1500 m as a first priority based on current human activity.

Figure 1.1 Framework for marine habitat classification represented by a hierarchy of spatial habitat units and hierarchy of ecological units (NOO 2002; Kloser *et al.*, 2004).

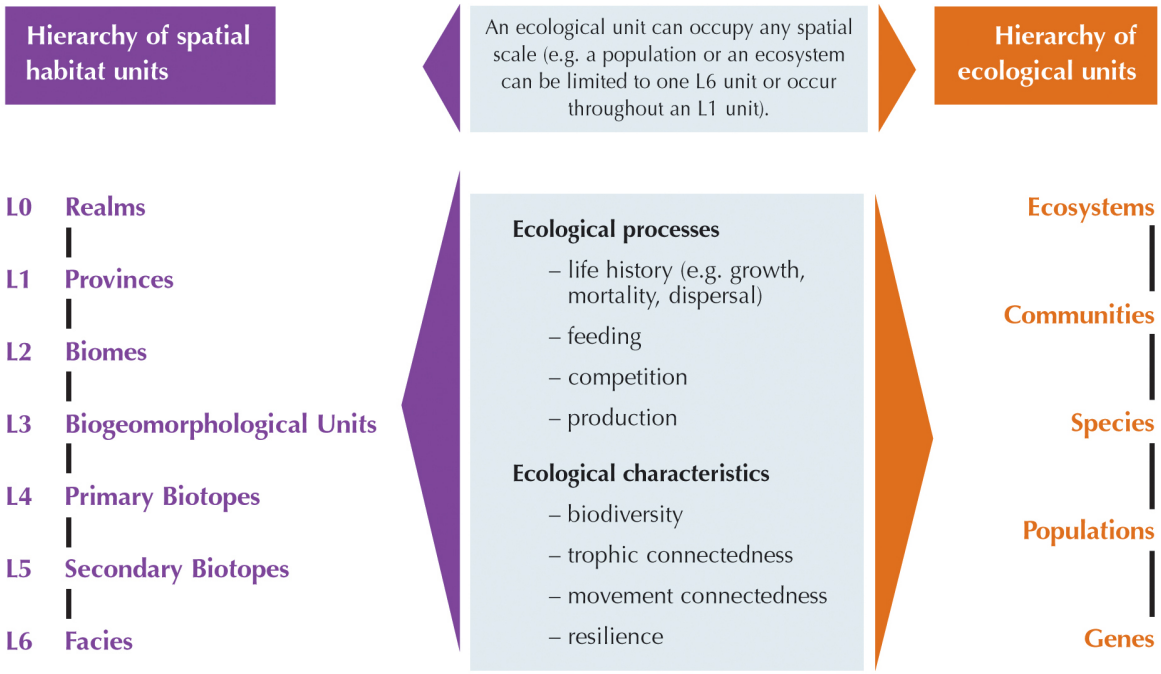

2 Seabed biotope characterisation

2.1 Introduction

The present day seafloor represents the accumulation of geological, oceanographic, chemical and biological processes over eons (*e.g.*, Seibold and Berger 1996; Neshyba 1987). Within Recent geological time (10-15 000 yrs) the space and time scales of dominant physical processes and their relationship within the hierarchical habitat scale (Fig. 1.1) provides a conceptual view of the dynamics within the marine environment (Fig. 2.1). At the "Province" habitat unit, some dominant change processes are evolution and climate change, these have occurred over 10 000s of years; at the sponge assemblage 10s m to 1 km habitat scale, important processes include growth, feeding, reproduction, dispersal and competition, which occur over hours to years. Figure 2.1 illustrates the continually changing nature of the oceanic environment and seabed habitats over time (Holling 1992; Gunderson *et al.,* 1995). In addition some aspects show variability over time scales short enough to be of significance to management and environmental assessment practice. Such space and time scale variability has led to attempts to develop rapid assessment and monitoring techniques, usually involving some form of remote sensing. The composition of the present day seafloor geology and its biota is the focus of this study, in particular how to observe, describe and measure biotopes using remote sensing.

Figure 2.1 Conceptual model of the range of space and time scales in the marine environment for some physical processes (stippled ellipse - dashed) and a deep-water > 50 m sponge community (ellipse - solid). Adapted from Holling (1992).

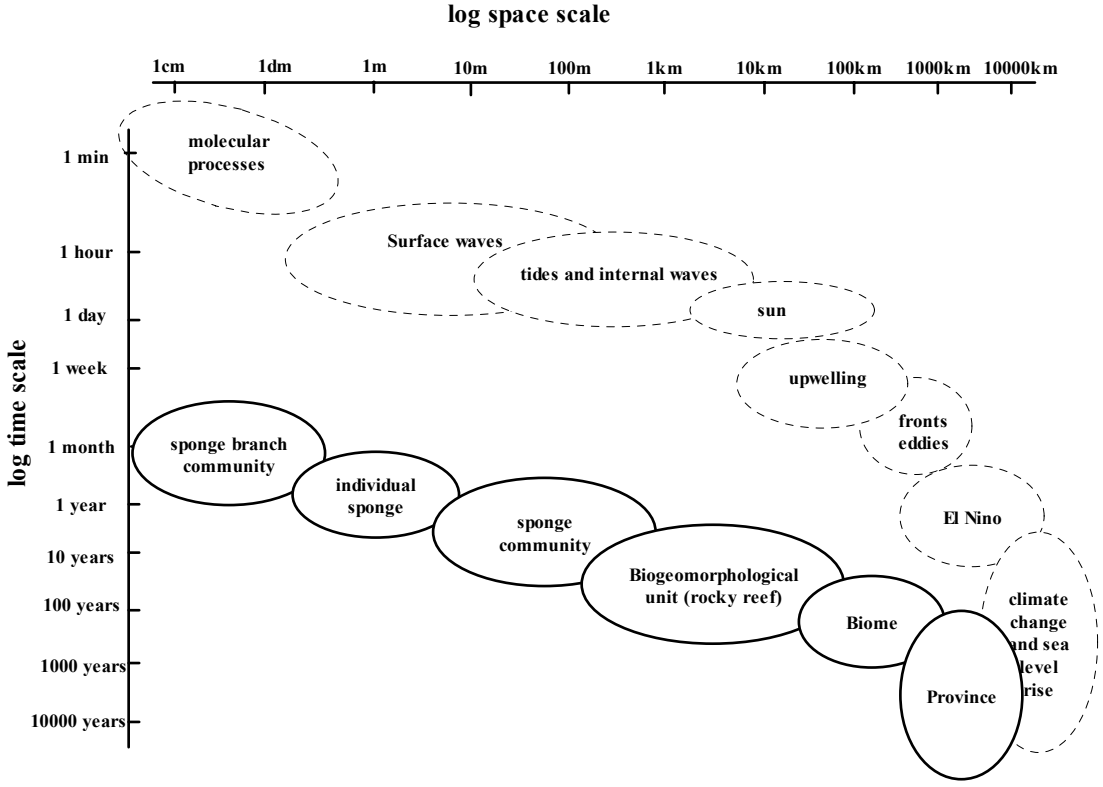

The seabed system is studied by measuring geological, biological, physical and chemical variables to varying degrees of accuracy. The measurements undertaken are necessarily limited in spatial and temporal extents based on the equipment involved and the types of

variables measured. In many cases it is not possible to obtain direct measurements of the quantities required (*e.g.*, biological factors of life history, trophic connections and biodiversity). Therefore, based on these sampling limitations, measured variables and observed patterns are hypothesised to represent surrogates of the variables of interest (Table 2.1). Physical, statistical or conceptual models are used to infer the behaviour of the variables of interest from the available measurements. These models do not eliminate the need to be cautious about extrapolation beyond the relevance of the data. As an example, there may be a need to understand the impact of fishing on the seabed biodiversity at a site and monitor this change over time between sites. Rather than collecting all the species (where the taxonomy is poorly known) at the site, it may be appropriate to create a surrogate measure (*e.g.*, weight, numbers, seabed coverage) of species groups (grouped by feeding mode, substrate preference, mobility or morphology) as representative of the site and compare this metric between sites (Table 2.1). This chapter discusses the geological, biological and oceanographic (physical and chemical) variables of interest within the context of biotope mapping in deep water at the 10s of m to 10s of km scale and those resolvable with remote sensing instruments such as acoustics and video.

In this context, habitat (Elton 1927) is defined as a place where an organism lives (its home) described by the physical, chemical and biological variables at a particular time. Therefore habitat needs dimensions of latitude, longitude, depth and time when it is described. The habitat of a species is the tangible and actual location in space and time of a species' niche. A niche is a conceptual abstraction of the location of a species within the multidimensional space of resources and ecological interactions (Hutchinson 1958). The niche concept is important when physical and chemical variables are proposed as surrogates of biological distributions. It may be that the physical and chemical variables are suitable for a species to exist (fundamental niche) in the space but external factors such as competition, dispersal, predation and disease preclude it so it occupies a smaller "realised niche" (Hutchinson 1958). Therefore, habitat is the geography of the realised niche where the species can persist given the suppressing factors of competition, predation and disease. It follows that habitat mapping is the process of mapping the locations where a species persists. This is different from biotope mapping that describes the physical and chemical environment and also the organisms at a specific location together with their relative abundances and sizes as a minimum. Therefore in its simplest form seabed biotope mapping is a description of the geological environment at a location along with the biota, interacting and inseparable. This thesis is concerned with the process of obtaining biotope maps using remote sensing to map components of the geological (acoustics) and biological (video) characteristics.

Table 2.1 Example of how surrogate variables can be used to infer variables of interest based on acoustic and video metrics.

Character	Variable of interest	Physical sampling	Remote sensing	Hypothesised surrogacy example
Geology	Geomorphology Bottom depth, slope, aspect, feature, undulations.	Limited –lead lines, poles have been used.	Multibeam sonar (MBS) Video	Acoustic MBS measures irregular bathymetry (i.e. not regular as with sand waves) this is a surrogate for hard substrate which in turn is a surrogate for a distinct range of epifauna adapted to attach to the hard substrate.
	Substrate Sediment/rock type	Samples obtained via grabs , cores, dredge operations	Acoustic backscatter combined with targeted physical sampling. Photography/ video.	Acoustic backscatter validated with physical samples is a surrogate for the sediment type and can be used to extrapolate over the region where physical sampling is not available.
Biology	Species diversity	Species collections through grabs and dredge/trawl operations.	Use of video to measure the dominant species and morphology of large epifauna. Use of acoustics to measure the geomorphology and substrate type.	A high diversity of shapes within a video image indicates a high range of species diversity.
	Species population density	Count all species in a region using physical sampling or video methods	Acoustic measures of the geomorphology and substrate type	The diversity of organisms at a location depend on a complex interaction of a number of factors that are unrelated to the geomorphology and substrate and it would be necessary to combine a number of variables, including acoustics to establish a surrogate measures.

2.2 Classification of habitats

To place biotope mapping in context of the various spatial and temporal scales and spatial management needs, the Australian National Oceans Office's generalised habitat mapping framework is adopted (Fig. 1.1, NOO 2002). This framework is not spatially explicit and to assist in defining scale, the nomenclature of Greene *et al.,*(1999) is adopted and, placed in a hierarchy of management needs (Table 2.2, Kloser *et al.,* 2004).

Table 2.2 Relating needs of spatial management planning to sizes resolvable by sampling; a generic hierarchical habitat classification scheme (NOO, 2002) and terms from a spatial classification scheme (Greene *et al.,* 1999). Micro-scales (< 1 m) not shown (Kloser *et al.,* 2004).

Management needs	Spatial size for resolving features	Common level in hierarchical habitat classification scheme	Terms for scaled spatial units
Visualisation and over-arching framework for regional planning based on identifying large marine domains	100s km	Biomes and sub biomes (*e.g.* major sub-divisions of shelf, slope, abyss)	Regional
Seabed features and terrains that give boundaries to generally defined ecosystem structures and processes	1 - 10 km, and larger	Biogeomorphological units (*e.g.* fields of sand waves, seamounts, canyons, plains and valleys)	Large -- Megahabitat
Values and habitat associations defined by types and compositions of habitats and communities	10s m - 1km	Primary and secondary biotopes (substrate type and animals identified)	Medium-- Megahabitat/mesohabitat
Impacts/ boundaries/ monitoring (biological indicators)	1 – 10s m	Biological facies	Small -- Macrohabitat

Following Greene *et al.* (1999) the seafloor can be described at a set of nested hierarchical scales based on the physiography, geomorphology, substrate type and modifiers (Table 2.2). At the mega- and mesohabitat scales the seafloor is defined by physiography and depth, with depth intervals being appropriate for fisheries assessment and management within the region. Typically these are coastal (~<50 m depth), midshelf (>50 and <150 m) outer shelf and upper slope (>150m and <500 m) but will change to suit particular species. The depth range considered in this thesis is 50 to 500 m; this range is subdivided from 50 to ~100 m and ~100 to ~200 m to incorporate recent sea level rise during the Holocene period (~ 140 m over past 10 000 to 15 000 years) and the approximate location of the continental shelf break; the depth range ~200 to 500 m is termed the upper continental slope. At the meso- and macrohabitat scale the seafloor habitats are determined by the geomorphology and substrate. The geomorphology includes forms such as reef (carbonate feature) ledge and sediment waves, whilst the substrate includes description of the sediments and lithology (Wentworth 1922; Folk 1968). An extra description of meso- and macrohabitat could include the underlying seabed slope or aspect of the region. Layered on these physical descriptors of seabed geology are the descriptions of the seabed modifiers. Modifiers are based on geological, oceanographic, chemical, biological and anthropogenic processes. Within the biological processes, modifiers include descriptions of bioturbation (tracks, burrows etc), cover of

encrusting organisms and communities (examples of conspicuous species). Combining both geophysical and biophysical information at this level describes the meso- and macrohabitat biotopes. The general outline of the scheme proposed by Greene *et al.* (1999) will be adopted when analysing the remotely sensed acoustic and video data in Chapters 5 to 7. In practice the exact naming of elements within the habitat scale levels changes depending on the region (biota types and geological types) and the particular management focus (*e.g.* fishing, marine parks) of the study.

A management focus for habitat mapping is the human induced modification of the seabed due to bottom contact fishing (Bax and Williams 2001). The long term effect of fishing will depend on the substrate type and the time given for the biotic communities to recover. Bax and Williams (2001) categorise habitat vulnerability by a two axis plot of resistance and resilience. Habitats, and in turn their benthic communities, that are vulnerable to fishing have low resistance to modification and take a long time to recover. Examples include substrata consolidated by slow growing structural biota such as low profile limestone reefs. Low profile limestone reefs are a major component of the substrate in the study region. Less vulnerable are hard elevated granite habitats that provide high resistance to modification by fishing gears, although the benthic communities may take a long time to recover if modified (Langton *et al.*, 1995). Advances in fishing technology (primarily accurate positioning with GPS) which allows new grounds to be opened up to fishing with accurately targeted fishing gear have increased the pressure on vulnerable habitats. In order to evaluate the vulnerability of habitats to fishing it is recommended to map the biotopes at the 10s of m to 1 km feature size (Bax and Williams 2001).

To place biotope mapping in context the geological, biological and oceanographic properties of biotopes need to be considered in the larger spatial and temporal context. With each of these properties the limitations of physical sampling over large areas encourage the development of models and surrogates to represent the dominant character of the oceanographic, geological and biological variables as outlined below.

2.3 Geology

The present day form and nature of the seafloor has been developed over eons by endogenic (energy from inside the earth) and exogenic (energy derived from the sun) processes. Examples of endogenic processes are those associated with seafloor spreading; the production of new seafloor at mid-oceanic ridges and its subduction in the great trenches. The large size features on the seafloor can be thought of as being caused by these endogenic processes that tend to roughen the seabed on large scales of kilometers to tens of kilometers. Exogenic processes such as erosion and sedimentation tend to smooth the seafloor, although coral reefs that are built from calcium carbonate can form significant features that extend over kilometres on the seafloor, the Great Barrier Reef being an example. In this case we are interested in the biotic assemblages that are associated with the existing seafloor (50 – 500 m deep) and related to recent geological history. The greatest exogenic influence in forming the current nature of the seafloor has been sea level rise. Over the past 10 000 – 15 000 years the sea level has risen 120 – 140 m and has had a profound impact on the form and nature of the seafloor over that depth range (Seibold and Berger 1996, fig. 5.6). During this time the sea level rise has not been monotonic and fluctuations have also been important in shaping the current geological and biological structure of the seafloor (Seibold and Berger 1996, fig. 5.6).

To characterise the surficial nature of the seafloor (relevant to the biota that can attach and burrow into it) it is necessary to describe the seafloor consolidation (hardness) and geomorphology (roughness or rugosity). Sedimentology and lithology (type of rocks) describe the substrate and its character whilst the geomorphology describes the seafloor shape from seamounts and canyons to sand waves and rock shape. The hypotheses explored in this thesis

are that the hardness and roughness attributes of the seafloor are an important factor in the distribution of biological assemblages; that the acoustic method can obtain measures of hardness and roughness, and that these measures may act as surrogates for biological assemblages at various scales.

Hard substrates are defined here as being composed of rock or biogenic material, either buried or exposed forming outcrops or subcrops from the surrounding sediment. Hard substrate outcrops occur where currents and waves have exposed them and kept them free from sediments or in areas of active erosion. Outcrops also occur as a consequence of bioactivity forming bryozoan and coral reefs (calcium carbonate deposits). These deposits can form large limestone regions that can be relatively friable and easily eroded by current, wave, bio-erosion and anthropogenic forces. Hard substrates provide anchoring points for a range of sessile benthic fauna and have benthic biota that are usually distinctly different from those supported by soft substrates. Hard substrates are classified as igneous, sedimentary, chemical, biogenic and metamorphic following the nomenclature of Folk (1968).

A soft substrate is defined here as material that biota can burrow into over a short time frame and is typically associated with unconsolidated sediments. Biogenic reefs are not classed here as soft substrate but due to their ability to maintain roughness are classified as hard. The sedimentation processes that make up the seafloor are mainly due to riverine and large scale ocean processes through storm events and deposition of planktonic/benthic organisms, and chemicals. The sediment composition can therefore be divided into lithogenous (disintegration of pre-existing rocks), biogenous (remains of organisms) and hydrogenous (precipitates from seawater) sediments. The bulk of the sediments around the continents consist of debris washed off the continents and are therefore lithogenous.

A simple method of characterising sediment and assessing its potential source and transport due to currents is grain size. However, inferring current energy from sediment samples alone is a non-trivial task (Seibold and Berger 1996). In general, sediment diameter ranges from boulders (> 256 mm) to clays (< 4 μm). Several classification scales are used to separate out the various size classes with the Wentworth Scale being the one adopted here (Table 2.3). To describe particle size of many orders of magnitude, the "Phi" logarithmic scale is often used, defined as:

$$\varphi = -\log_2 \frac{d}{d_{ref}} \qquad (2.1)$$

where d is particle diameter in mm and d_{ref} is 1 mm (Wentworth, 1922 and Krumbein, 1936).

Table 2.3 Clastic term diameter size range in mm and phi size based on the Wentworth scale (Wentworth 1922, Folk 1954).

Clastic term	Diameter range (mm)	Phi range
gravel boulders	> 256	φ < -8
gravel cobbles	64 - 256	-8 < φ < -6
gravel pebbles	4-64	-2 < φ < -6
gravel granules	2 - 4	-1 < φ < -2
sand	0.0625 – 2	-1 < φ < 4
silt	0.004 - 0.0625	4 < φ < 8
clay	< 0.004	φ > 8

Intuitively it would be expected that the deposition of fine to large grains would occur at low to high near seabed currents respectively. This has been shown to be true for a range of well-sorted sediment sizes but depends on the consolidation of the material for fine grains. The actual mechanisms of sediment transport and deposition are complex and involve knowledge of at least seabed roughness and consolidation, current velocities, dynamics of current events, historic sediment deposition (relic or modern) and level of bioturbation (Seibold and Berger 1996, fig. 4.2). Using sediment samples as an accurate surrogate for current energy is therefore non trivial for the smaller grain sizes of clay and silt that can, depending on the consolidation of the sediment, resist erosion at high current speeds (Seibold and Berger 1996, fig. 4.2).

The present composition of the surficial sediment on the seafloor has been reworked by both current stress and biological activity. Benthic organisms burrow and rework the top 5-25 cm of the sediment by a process known as bioturbation (Seibold and Berger 1996 pg. 172). Bioturbation can mix the fine layering of sediments and limits the use of sediment samples to unravel recent hydrodynamic or chemical processes. Likewise the use of sediment size as a primary surrogate for infaunal species distribution has not been proven. Snelgrove and Butman (1994) concluded that the complexities of soft-sediment infauna assemblages may defy any simple paradigm relating to a single factor, and propose a shift towards understanding relationships between organism distributions and the dynamic sedimentary and hydrodynamic environment. In contrast, epifaunal assemblages as judged from photographs were highly correlated to broad sediment types and the correlation were shown to improve with depth and current metrics (Kostylev *et al.,* 2001).

Seabed roughness occurs at various spatial scales from 1 to 100 km features such as canyons and raised reefs to features <1 m to 10s of m such as sand waves and 1 m high limestone outcrops. The 1 to 100 km features are described as being continental shelf, slope, canyons and seamounts etc based on their depth and physiography (Greene *et al.,* 1999). At the biotope size (10s m to 1 km) the seafloor roughness is described in terms of reef, mound, slabs, sediment wave, vents, bar etc (Geene *et al.,* 1999). The seafloor roughness can be a surrogate for seabed substrate (*e.g.*, Roff and Taylor 2000) and can be a major contributor to acoustic backscatter depending on the acoustic wavelength, (*e.g.*, Todd *et al.,* 1999). Benthic biota are also associated with certain roughness and hardness features of the seabed due to the availability of anchorage points and a combination of other conditions required by different plants and animals to survive and persist in a region (*e.g.*, delivery of nutrients and or shelter, Mann and Lazier 1996 pg. 55; Wildish and Kristmanson 1997).

Acoustic bathymetry and backscatter data are widely used to characterise the seafloor roughness, which is used increasingly as a surrogate of the seafloor substrate (*e.g.*, Todd *et al.,* 1999). Acoustic backscatter data are influenced by the combined geoacoustic properties of

sediments incorporating porosity, bulk density and roughness (Jackson *et al.,* 1986). These combined qualities may be a more effective measure of the hardness of the sediment than just grain size, and be a better determinant of the ability of biota to attach and burrow at the biotope scale. Therefore an acoustic system could, in theory, discern between consolidated and unconsolidated sediments of the same grain size, hence help infer that different biota would be associated with each type.

2.4 Biology / Ecology

A five-kingdom classification system recognises organisms as belonging to the largely unicellular kingdoms Monera (*e.g.*, bacteria) and Protista or the predominantly multicellular kingdoms Plantae, Animalia and Fungi kingdoms (Raven and Johnson 1986). Organisms of interest in this thesis are the larger multicellular plants and animals which can be separated into three major categories, plankton (drifters), nekton (swimmers) and benthos (bottom-living organisms). Demersal organisms are the subcategory of nekton that generally stay near the seafloor. As the depth range of this study is greater than 50 m and on the outer region of the zone where there is enough light to support photosynthesis (the photic zone) most multicellular organisms observed in this work are classed in the kingdom Animalia. Ninety-eight percent of the marine animal species classified in the sea are benthic and 2% are planktonic or nektonic (Seibold and Berger 1996). The seabed therefore represents an important region for biodiversity of both sessile (permanently attached) and vagile (free to move) fauna. Sessile organisms include sponges, corals, brachiopods and bryozoans. Vagile organisms can move at a variety of speeds and include fast moving crabs and slow moving sea urchins, crinoids, starfish, most bivalves, snails and worms. Animals that live on and above the seafloor are termed “epifauna” whilst those that live hidden within rocks and sediment are termed “infauna”. Of the 155 000 marine animal species identified as benthic 81% are epifauna and only 19% infauna. Whilst the number of species identified continues to increase the ratio is expected to remain stable assuming even sampling of both the epifaunal and infaunal habitats. This suggests that the biodiversity or variety of ecological niches of the epifauna is far greater than the infauna (Seibold and Berger 1996). Alternatively, it is also possible that the ratio represents a bias in sampling or specialisation of taxonomists in the previous studies. A challenge is to explore the ability of remotely sensed acoustic and video surrogates to improve our classification of epifaunal communities and improve our knowledge of epifaunal ecology as it relates to the geological and oceanographic environment.

The community level of organisation relates the patterns in the structure and behaviour of multispecies biological assemblages. Communities of organisms have properties that are the sum of the properties of the individual organisms plus their interactions (Begon *et al.*, 1996 pg. 679). Communities occur over a range of spatial scales being defined by the suite of organisms and the purpose of the study, as communities are often continuous without distinct boundaries. Some useful characteristics of communities are species richness, diversity, resilience, succession, and energy flow. An important aspect of obtaining metrics of communities is an understanding of community dynamics (*e.g.*, succession). Dynamics of a community at a site are due to the non-seasonal, directional and continuous pattern of colonization and extinction of species populations (Begon *et al.*, 1996 pg. 692). Often, in deep-water the dynamic state of the biological community being observed is not known or poorly understood. For example a limestone reef populated with sponges is a long-term dynamic community. On long time scales the sponge community associated with the limestone reef is slowly eroding the reef structure and would eventually erode it away removing the very substrate that it relies on for its attached habitat. On shorter time scales, anthropogenic influences such as bottom trawl impact can remove attached biota creating new surfaces for colonisation and even remove substrate thereby reducing available terrain. Deep-

water sponge communities have poorly understood life histories and their natural temporal and spatial dynamics are largely unknown within the temperate regions of Australia.

Measures of communities (species richness, diversity, resilience, succession, and energy flow) are difficult to obtain in the deep water benthic environments due to limited repeat sampling at sites and the expense of obtaining accurate geolocated physical samples and associated taxonomic identification of species. An alternative or surrogate to costly taxonomic approaches to measure diversity at the 1 to 10s km feature scale is to aggregate the large number of highly diverse taxa into 'usable' groups of simple categories, Functional Units (FUs). Classification and grouping into FUs is based on the organisms' preferred substrate type (hard, soft), mobility (sessile, vagile) and feeding mode (active/passive filter feeder: scavenger/predator). Using functional units (FUs) has several practical and ecological advantages. The functional units reflect the ecological requirements of the community, are relatively easily applied in the field with semiskilled taxonomists, and are potentially identifiable from non-destructive sampling techniques such as video (Althaus *et al.*, in prep). The potential for lower cost remotely sensed video observations to measure a surrogate of communities (FUs) supported with only limited, targeted physical sampling is explored further in Chapters 6-7. Another surrogate measure of species diversity at a location may be obtained using morphological units. Based on remote video or photographic images the diversity in shapes of biota may be a useful surrogate for species diversity.

This thesis takes a surrogacy approach to mapping the geomorphologic (1 to 10 km) and biotope (10s m to 1 km) scale using acoustic and video remote sensing supported with physical samples. Biota of a region will be described based on the sampling method used and compared to the geological attributes to explore surrogacy variables. Physical samples from benthic dredges have been sorted into Functional Units as described above. Video data have been scored as relating to the dominant species or species group within an image (Table 2.4, Kloser et al., 2001b). The morphology of the species within a video image as a surrogate for biodiversity is not treated in the present work.

The definition of the video categories have been reordered to follow a hypothesised increase from soft-smooth substrates and low current velocities moving to hard-rough substrates with expected higher current velocities. The scoring of soft to hard substrate may be an effective surrogate for low to high currents. This is generally true for unconsolidated sediments but highly variable for consolidated muds (Seibold and Berger 1996 p 99). The geomorphology score moves from soft-smooth (0) to soft-rough (3) through hard-smooth (5) to hard-rough (9). Category (4) Debris flow /rubble bank could be classified as either soft rough or hard rough depending on the type of rubble (sedimentary or igneous/metamorphic). The faunal categories are difficult to organise in strict soft to hard, smooth to rough categories. A starting hypothesis is that organisms that need soft substrates to burrow into will be found in dominance on those substrates whilst organisms that can attach to hard substrates will be more dominant on those substrates. When hard substrates are not covered by sediment, currents of higher velocity are present or high slopes are more likely. Sub-cropping hard substrate categories often required knowledge of past and future video images to score consistently. A characteristic sign of sub-cropping hard substrate was high densities of attached sponge macro epifauna. The use of a sequence of previous video images and faunal distributions to infer sub-cropping hard substrate introduces a level of subjectivity in the scoring process. To eliminate between-scorer bias a single scorer analysed the entire video data set (Kloser *et al.,* 2001b).

Table 2.4. Attributes of seabed habitats recorded from the video data at 1 s intervals (approx. 0.25 m) following Kloser *et al.*, (2001b) ordered in terms of hypothesised gradients of increasing seabed hardness and roughness and inferred current and potentially nutrient availability for fauna. (numbers refer to original scoring metrics used).

	1. Substrate (S)		2. Geomorphology (G)
0	Mud	0	Unrippled
1	Fine sediments	1	Current rippled/directed scour
2	Coarse sediments	2	Wave rippled
3	Gravel/pebble	3	Highly irregular
4	Cobble/boulder	4	Debris flow/rubble banks
6	Sedimentary rock	5	Subcrop
5	Igneous/metamorphic rock	6	Outcrop (low <1m); no holes/cracks
		7	Outcrop (low <1m); with holes/cracks
		8	Outcrop (high >1m); no holes/cracks
		9	Outcrop (high >1m); with holes/cracks

	3. Fauna (F) (dominant faunal community)		4. Faunal Abundance (A)
0	None - no apparent epifauna or infauna	1	Low/sparse (<10%)
9	Distinct infauna bioturbators	2	Medium/intermediate (<50%)
6	Small encrustors/erect forms (including bryozoans)	3	High/dense (>50%)
7	Sedentary: *e.g.* seapens		
2	Small sponges - community		
1	Large sponges - community		
3	Mixed sponges, seawhips and ascidians		
5	Octocorals (gold corals/seawhips)		
8	Mobile: *e.g.* echinoids/holothurians/asteroids		
4	Crinoids		

2.5 Oceanography

Life in the ocean is governed largely by ocean dynamics (Neshyba 1987; Mann and Lazier 1996). To predict biotic assemblages on the seafloor will require an understanding of the hydrodynamic, chemical and biological processes at the sediment-water interface. A seabed of given composition and morphology has developed over eons governed by both large and fine scale oceanographic processes (Fig. 2.1). The scales of influence range from micro-mixing (1 cm), daily sun and moon excited events (1 m to 1000 km) through to global events such as El Niño and sea level change (1000 km – Global) (Fig. 2.1). At the 10s of m to 1 km scale, hydrodynamic differences between patches of habitat arise due to local topographic variability including the roughness and steepness of the terrain within the 1 to 10s km region (*e.g.* canyon, seamount). Within a 10s of m to 1 km region, it should be possible to predict the probability of occurrence of functional/morphological types of benthic communities based on general location, depth, temperature, salinity, nutrients, current stress and boundary layers. A community may be constantly dynamic due to the distribution of sediments by locally

strong currents (Seibold and Berger 1996). It is also postulated that current strength and variability influence the distribution of benthic organisms. In strong currents, mature organisms can be physically damaged or dislodged and the settlement and recruitment of benthic organism may be inhibited. In regions of weak currents, survival of filter feeders may be limited by the low influx of suspended food material (Mann and Lazier 1996; Wildish and Kristmanson 1997).

Prediction of fine scale (10s m to 1 km) seabed current stress and its temporal variability is limited in this study. In general seabed current stress is obtained by extrapolation from water column current meters. Current meters can only cover a small number of sites so hydrodynamic models are used to provide current and seabed stress over large areas (Fig. 2.2) (*e.g.*, Condie *et al.*, 1999; Bruce *et al.*, 2001). The main variables required to predict seabed current stress are bathymetry, local wind, tides and the large scale geostrophic flow causing upwelling, downwelling, internal waves, and along shore transport. Maps of generic bottom stress derived from these physically based models can be used to predict sediment transport and larval dispersal and settlement. Generally, the oceanographic models are poorly tested with real data at fine scales (Scott Condie *pers comm.*).

Understanding the oceanography at a location and its relationship to the biota firstly requires a general description of oceanographic conditions that prevail at a given location and depth, with an understanding of the major water masses and their seasonal fluctuations. Here, physical measures of temperature, salinity, nutrients and mean flow are major indicators of biota distribution. Secondly, there is a need to understand the local variations at various spatial scales that occur due to depth, seabed morphology, wind, waves and tides. This can provide current stress indicators for a particular depth, substrate type and geomorphology. Using current stress indicators may assist in predicting typical fauna (Kostylev *et al.*, 2001). In the present work, large scale oceanic variables are used to set the provinces and biotones within which we sampled at finer scale (IMCRA 3.3 1998).

Figure 2.2 Model of predicted surface currents at depth (1.5 m in this instance) and location based on seasonal climatologies of wind, sea level, temperature and salinity, horizontal resolution 20 km (described in Bruce *et al.*, 2001).

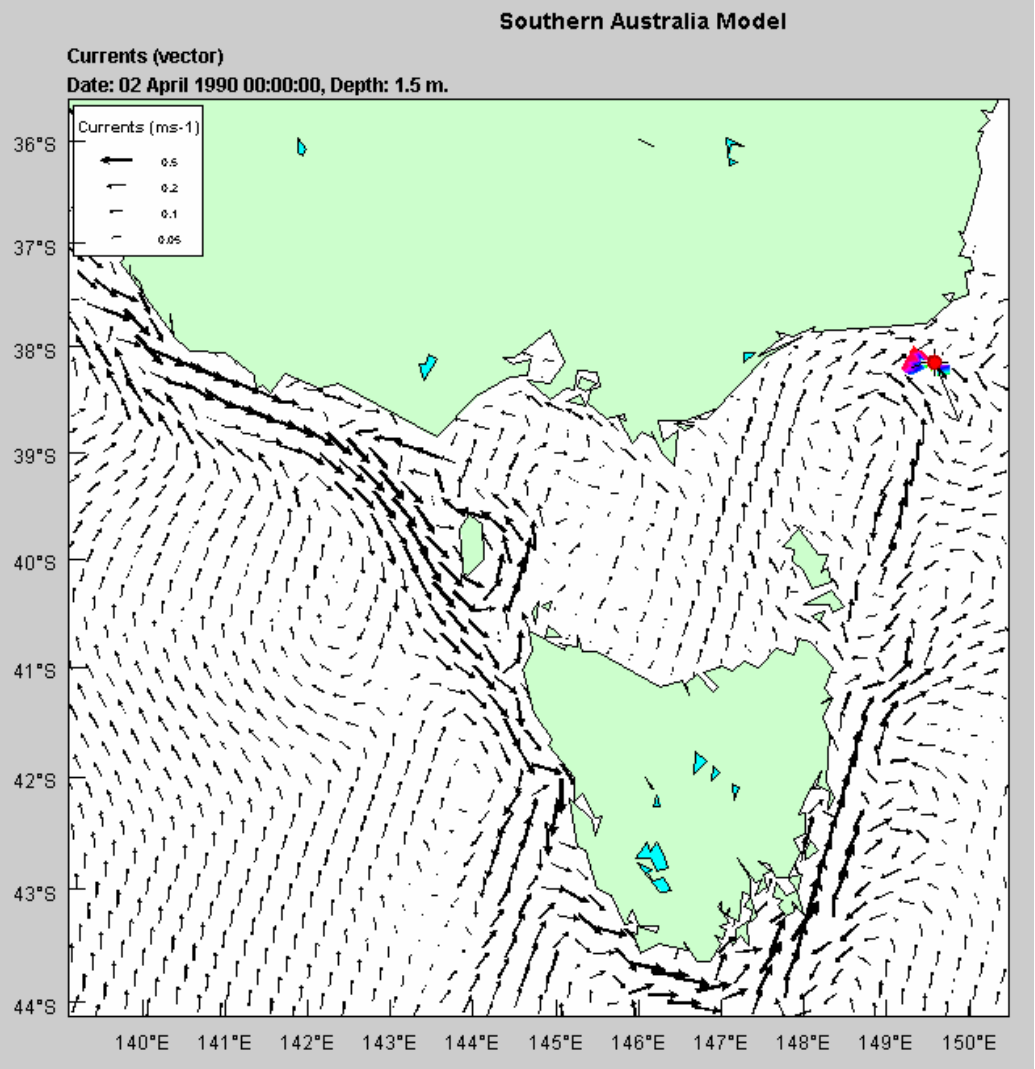

2.6 Australian regional setting

Based on a collation of existing geological, oceanographic and biological data, the marine continental shelf region was zoned at the province and biome levels (IMCRA 3.3 1998). The zonation described below (Figs. 2.3, 2.4) reflects the information available at the time and provides a context for this work as the sites are nested within a hierarchy of spatial scales (Fig. 1.1). The Australian continental shelf biota boundaries were developed jointly by a collaboration of Australian scientists and environmental agencies (IMCRA 3.3 1998) into 9 provinces and 8 biotones at the regional scale of 1000s of km. Biotones are defined to be zones of transition between core provinces (IMCRA 3.3 1998). Demersal continental shelf provinces/biotones were derived primarily by the distribution of demersal fishes. The boundaries of provinces/biotones are best thought of as fuzzy and not fixed as outlined on maps, because sharp boundaries rarely apply in nature (e.g. Roff and Taylor, 2000 and Hubbell 2001). Within these major provinces and biotones the IMCRA 3.3 (1998) working group identified 60 regions at 100s – 1000s km scale based on an analysis of inshore fish species extended out to the 200 m isobath.

The sampling in this study, outlined in Chapter 5, occurred in three major demersal provinces/biotones: the South East Province (SEP), Gulf Province (GP) and Great Australian Bight Biotone (GABB). Within these provinces/biotones at the regional scale the sampling occurred within three regions: Twofold Shelf (TWO), Coorong (COR) and Eucla (EUC) (Fig. 2.3).

Figure 2.3. Demersal continental shelf regions of Australia based on a collation of geological, oceanographic and biological data highlighting the Twofold Shelf, Coorong and Eucla regions sampled in this thesis (IMCRA 3.3 1998).

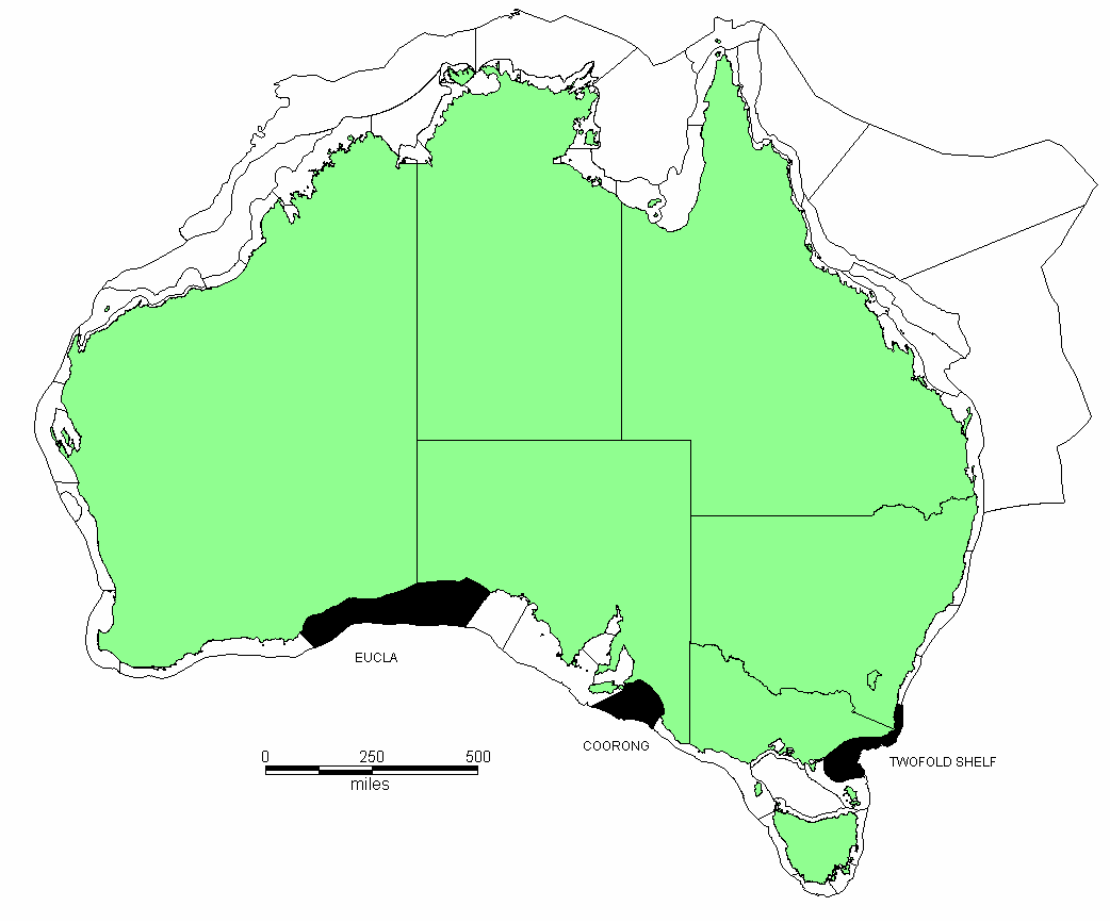

Since the 1998 IMCRA bioregionalisation of shelf waters, many projects have been updating the physical, geological and biological knowledge at shelf, slope, and abyssal depths. An example of this is the reanalysis of geological information summarised into major geomorphic features at a regional scale (Harris *et al.*, 2002; IHO, 2001). Within the South East Australian and Great Australian Bight management region, the major geomorphic units are shown in Figure 2.4.

Figure 2.4. Major geomorphic units of the (a) South East Australian province with the study areas in the Twofold shelf and Coorong regions circled and (b) the Great Australian Bight Province with the study area in the Eucla region circled (Harris et al., 2002).

a.)

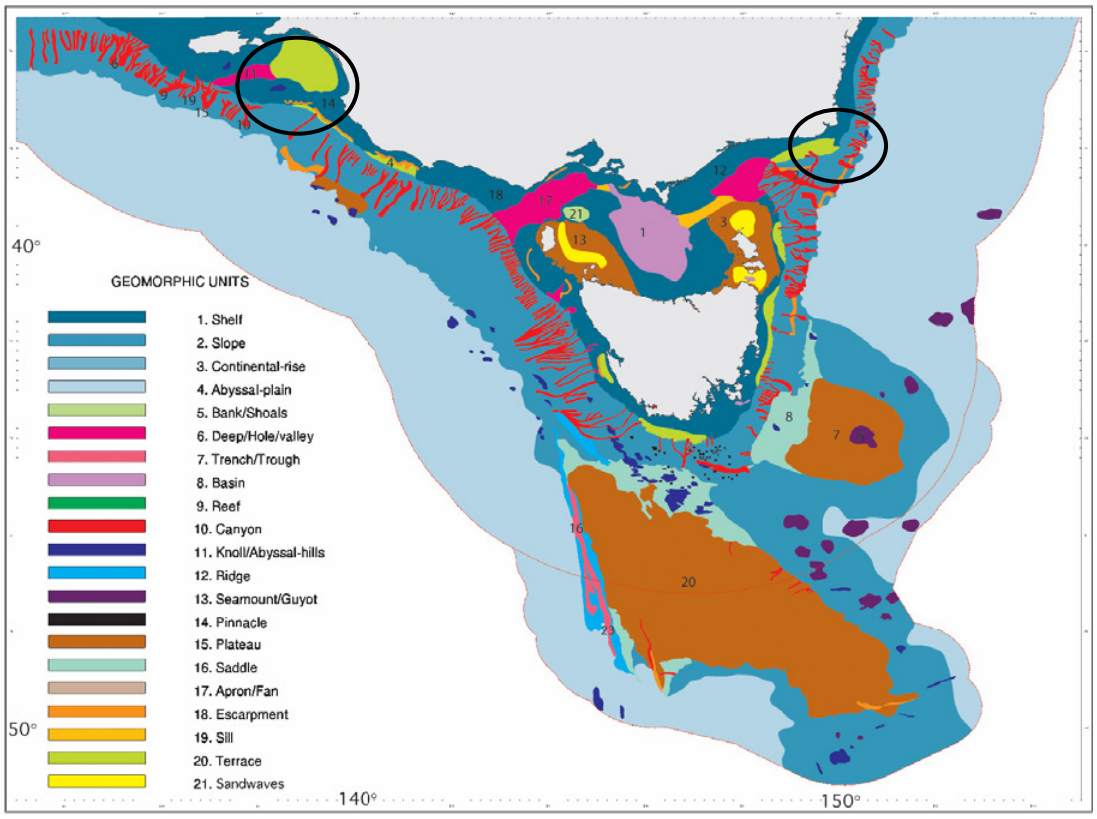

b.)

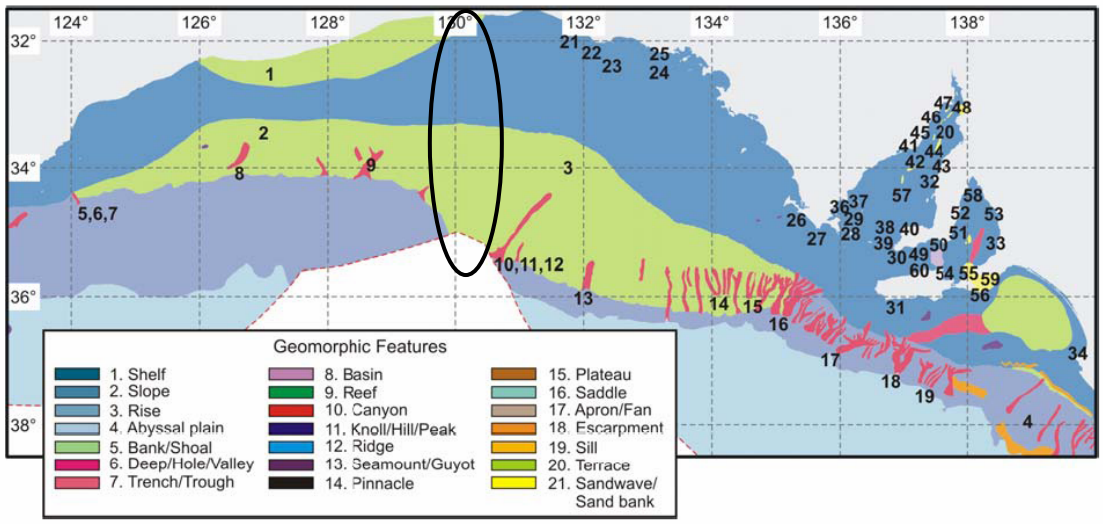

2.7 Summary

The characterisation of the seafloor requires an understanding of the geological, biological, and oceanographic features that are nested within spatial and temporal scales and inseparable. The focus of this thesis is on biotope mapping that requires a description of the geology (substrate type and geomorphology) and the biota at a site. The feature sizes of interest are 10s m to 1 km for biotope mapping and 1 km to 10s of km for geomorphological mapping. An example of management need for mapping at these scales is the potential distribution and impact of demersal fishing. To determine and monitor impacts of fishing on habitats, mapping needs to be at the 10s of m to 1 km scale (Bax and Williams 2001). The use of surrogate measures of the geological and biological variables of interest using acoustic and video remote sensing is proposed, acknowledging that physical sampling at these spatial scales in deep water is costly.

It is proposed that Functional Units and Morphological Units may serve as practical, low cost measures of the biota relevant to management. These units are hypothesised to be sensitive to human activities where Functional Units separate hard substrate biota from soft substrate biota. Morphological units (MUs) that describe the structural complexity of organisms may be a surrogate for species diversity and may also be an indicator of seabed disturbance due to demersal trawling where large erect organisms are removed, leaving smaller organisms.

This thesis explores the proposition that acoustic remote-sensing metrics of the seafloor can separate hard from soft seabeds and that this in turn predicts the biota to a Functional Unit level with high probability.

3 Seabed Acoustics

3.1 Introduction

Ocean acoustics involves the study of compressional waves within an inhomogeneous fluid medium and how they interact at the boundaries (seafloor and surface), and scatter at objects. The reflection of acoustic waves at the seafloor depends on the physical properties of the substrate, largely density, compressional wave velocity, shear wave velocity, and absorption loss (*e.g.*, Clay and Medwin 1977; Urick 1983; Frisk 1994). The seabed boundary is often rough compared to the acoustic wavelength, requiring theoretical understanding of scattering from rough surfaces (*e.g.*, Ogilvy 1992). A conceptual method of describing the properties of acoustic waves was given by Christian Huygens by his hypothesis: "each point on an advancing wave front can be considered as a source of secondary waves, which move forward as spherical wavelets in an isotropic medium". Based on this conceptual framework a phenomenological understanding of acoustic waves and their interaction at boundaries can be explained (*e.g.*, Clay and Medwin 1977 pp 30-36; Urick 1983 pp 120-128). To quantify the interaction of waves within and between mediums the wave equation is developed to varying degrees of generality and solutions obtained by solving for boundary conditions (Frisk 1994).

This chapter looks at the specific use of high frequency (95 kHz) acoustics to study the surficial (seabed substrate to approximately 0.1 – 0.3 m depth) properties of the seafloor from a vessel at water depths ranging from 50 – 500 m and incident angles less than 70^o. The transmitter emits a pulsed sinusoidal wave. The transmitter and receiver are coincident (monostatic) and combine to form narrow beams (approx. 2^o at –3 dB power full angle) to receive seabed acoustic backscatter signals. To interpret the received backscatter signals, a physical model is outlined for propagation of high frequency waves and absorption in the fluid medium and its interaction with a nominally rough boundary seabed. Acoustic models for seabed scattering are aimed at providing a quantitative understanding of the seabed scattering mechanisms that are predictive and independent of water depth and sounder systems. These models can be used to solve the forward problem where the model predicts the seabed backscatter characteristics based on the physical nature of the scattering at the seabed surface and volume. The inverse problem reverses this process where the physical and biological attributes of the seabed are estimated from the seabed backscatter. Inversion of the model to provide seabed properties may not however give a unique solution.

An alternative to interpreting received seabed acoustic backscatter using a physical model is to investigate the echo statistics and phenomenological characteristics of the received signal to characterise the seafloor roughness or the seabed acoustic diversity as discussed in more detail in this chapter.

3.2 Plane waves and rays in a fluid medium

It is possible to consider sound waves as plane waves when the curvature of the wavefront is small compared to the size of the measuring device (radius of curvature much larger than the aperture of the measuring sonar) (Clay and Medwin 1977 p52); and when sound waves are in the far-field of the source propagating spherically. The transition of near-field to far-field occurs approximately at a range R_f (Urick 1983 p 72), and for a piston transducer:

$$R_f = \frac{a^2}{\lambda}, \tag{3.1}$$

where 'a' is the longest linear dimension across the transducer face and λ is the acoustic wavelength (MacLennan and Simmonds 1992). Transition from near-field to far-field

conditions occurs gradually and in fisheries acoustics, acoustic measurements are assumed to be in the far field at distances greater than $2R_f$ (MacLennan and Simmonds 1992). For a 95 kHz 2^o acoustic receiver assuming a = 0.41 m and λ= 0.0158 m, the recommended far-field measurement distance is 10.6 to 21.2 m based on these two estimates.

An assumed plane wave propagates through an inhomogeneous ocean medium based on the material properties of density and sound speed. The speed of sound c in the ocean varies as a function of temperature, salinity and depth (McKenzie 1981). Sound speed is sensitive to temperature variations, where a rise in sea surface temperature of 1^o C at 5^o C and 20^o C leads to increases in sound speed of 4 and 3 $m.s^{-1}$ respectively. The density ρ of seawater is related to pressure p, temperature T and salinity S (Fofonoff and Millard 1983). Seawater density varies between 1026.4 kgm^{-3} ($p = 5\ 10^5$ Pa, T = 16^o C and s = 35.5 psu) and 1029.6 kgm^{-3} ($p = 5\ 10^6$ Pa, T = 10^o C and s = 35.5 psu) at depths from approximately 50 m to 500 m at sites within our study area. The quantity ρc of a medium is defined as the acoustic impedance. Acoustic impedance changes within and between media leading to reflected and transmitted waves based on the impedance contrast at boundaries; the pressure reflection R and transmission T coefficients of a plane wave at incident angle θ_{1i} to a flat boundary of density contrast ρ_1 to ρ_2 and sound speed contrast c_1 to c_2 is defined by:

$$R_{12}(\theta_i) = \frac{\rho_2 c_2 \cos\theta_{1i} - \rho_1 c_1 \cos\theta_{2i}}{\rho_2 c_2 \cos\theta_{1i} + \rho_1 c_1 \cos\theta_{2i}} \text{ and} \qquad (3.2)$$

$$T_{12}(\theta_i) = \frac{2\rho_2 c_2 \cos\theta_{1i}}{\rho_2 c_2 \cos\theta_{1i} + \rho_1 c_1 \cos\theta_{2i}}. \qquad (3.3)$$

These coefficients hold for the boundary conditions of:

- no excess pressure on either side of the interface,
- the two media remain in contact at the interface as the signal reflects and passes through it and
- the relationship between θ_{1i} and θ_{2i} is related by Snell's law such that:

$$\frac{\sin\theta_{1i}}{c_1} = \frac{\sin\theta_{2i}}{c_2} \text{ (Clay and Medwin 1977).} \qquad (3.4)$$

For a plane wave where λ is very much less than the water depth z; and hence the distances from source to seabed; seabed to receiver and the change in sound speed is negligible over several wavelengths, ray tracing applies using Snell's law. At 95 kHz assuming c=1500 $m.s^{-1}$, λ = 0.0158 m, z ranges from 50 – 500 m and the maximum change of c over several wavelengths is less than 0.02% justifying the conditions for using Snell's law. Using Snell's law the angle of incidence $\theta_{(i+1)}$ at depth $z_{(i+1)}$ is calculated based on the initial incident angle θ_i at depth z_i and sound speed $c(z_i)$ where:

$$\theta_{(i+1)} = arc\sin\left(\frac{c(z_{(i+1)})\sin\theta_i}{c(z_i)}\right). \qquad (3.5)$$

A critical incident angle θ_c is reached at an interface $c_2 > c_1$, when $\sin\theta_c = \frac{c_1}{c_2}$ and the acoustic wave travels along the boundary and refracts back into the upper medium. Typically

for sandy sediments the sound speed varies between 1836 to 1711 m.s^{-1} (Hamilton 1972) leading to critical angles of 55^o to 61^o incident on the seabed and within the present operating emitted MBS incident range of 70^o depending on seabed slope. The effect of operating at seabed incident angles in excess of the critical angles is discussed further when interpreting the acoustic measurements.

As a sound wave propagates in an unbounded homogeneous medium it reduces in intensity due to spherical spreading proportional to the square of the distance from the source and by absorption due to conversion of the acoustic energy to heat. Absorption α_w of sound in seawater can be associated with three major sources. Firstly, a pure water component due to shear viscosity and bulk viscosity that becomes the dominant term in sea water above 200 kHz. Secondly, at low frequencies (< 1 kHz) boric acid chemical relaxation dominates the absorption loss. Thirdly, in the mid-frequency range (10 to 200 kHz) magnesium sulphate represents the dominant contributor of absorption (Francois and Garrison 1982). The Francois and Garrison (1982) formula for absorption is adopted here as it is based on a compilation of field based data whereas the earlier Fisher and Simmons (1977) formula is based on laboratory experiments. The accuracy of the Francois and Garrison (1982) formula for the temperatures and pressures used in this study remains uncertain. Field based measurements used in the Francois and Garrison (1982) regression were based on lower temperatures, range –1^o to 10^o C, whereas temperatures used in this study had a higher, range 10^o to 20^o C. An error in measured α_w at 95 kHz of 10% would translate to a 1 dB error at 100 m depth or 5.4 dB in 500 m in the relative measured seabed backscatter at 70^o incidence.

3.3 Sonar Equation

Consider a simplified acoustic system where a narrow band monostatic sonar at incident angle θ_i to the seabed with transmitting sensitivity $b(\varphi,\psi)$ and receiving sensitivity $b'(\varphi,\psi)$ emits a short sinusoidal pulse of duration (τ) and average source intensity $I_s(\theta_i)$ measured at a unit distance from the source. The pulse propagates through an unbounded medium spherically spreading and being absorbed with straight ray paths (no refraction). At a range R the pulse interacts with a horizontal and flat seafloor and ensonifies an area A of random homogeneous distribution of scatterers producing surface reverberation s_s at any one instant. Neglecting volume scatter within the seafloor, the signal is backscattered towards the source as the incoherent sum of signals emanating from randomly distributed scatterers within the area A. This incoherent surface reverberation s_s throughout the ensonified area is further spherically spread, absorbed and refracted back to the source.

At the receiver the signal intensity $I_r(\theta_i)$ can be derived from the sum of the elemental areas dA within A by:

$$I_r(\theta_i) = \frac{I_s(\theta_i)}{R^4 10^{\frac{2\alpha R}{10}}} \int_A s_s b(\theta_i) b'(\theta_i) dA \,. \qquad (3.6)$$

Often this equation is expressed in logarithmic form as the sonar equation to conveniently describe and evaluate the performance of acoustic systems (*e.g.*, Urick 1983 p 246) as;

$$EL(\theta_i) = SL(\theta_i) - 2TL(\theta_i) + TS_b(\theta_i) \,. \qquad (3.7)$$

The sonar equation is usually expressed in decibels with reference distances (1 m) and reference sound pressures (1μPa). The source level ($SL(\theta_i) = 10\log I_s(\theta_i)$) at 1 m from the

projecting transducer face and echo level ($EL(\theta_i) = 10\log I_r(\theta_i)$) at the receiving transducer is at a reference intensity I_{ref} of a plane wave of rms pressure 1 μPa. The two-way transmission loss ($2TL = 10\log(R^4 10^{\frac{2\alpha_w R}{10}})$ at range R with sound absorption α_w dBm^{-1} for spherical spreading is given by;

$$2TL = 2\alpha_w R + 40\log R\,. \tag{3.8}$$

The backscattered cross section (m^2) of the seafloor in logarithmic form of target (backscatter) strength (TS_b) after being made dimensionless using length squared (Clay and Medwin 1977 pg 182) is,

$$TS_b(\theta_i) = 10\log\int_A s_s b(\theta_i) b'(\theta_i) dA \text{ dB re m}^2. \tag{3.9}$$

The evaluation of the integral in Eq. 3.9 at a given incidence angle θ_i for acoustic systems that have known beam geometries is outlined below.

3.3.1 Equivalent area ensonified

Assuming that the seabed surface backscattering coefficient s_s is constant within the pulse resolution area in Eq. 3.9, s_s can be taken outside the integral to yield:

$TS_b(\theta_i) = S_s(\theta_i) + 10\log A(\theta_i)$, the backscatter strength $S_s(\theta_i)$ from Eq. 3.7 is,

$$S_s(\theta_i) = EL(\theta_i) - SL(\theta_i) + 2TL(\theta_i) - 10\log A(\theta_i)\,. \tag{3.10}$$

Note that Eq. (3.10) is an average of the true backscatter strength $S_s(\theta_i)$ within the pulse resolution area. In the near nadir region, where the true backscatter strength changes rapidly within the pulse resolution area this integration yields a bias (*e.g.,* Matsumoto *et al.,* 1993). Hellequin *et al.* (2003) showed that for the Simrad EM1000 multi-beam system the magnitude of this bias varies with seabed type and backscatter processing method implemented within the MBS software.

Assuming the simplification in Eq. 3.10 is consistent within a common seabed type (no relative error) the equivalent area ensonified $A(\theta_i)$ is determined by:

$$A(\theta_i) = \int_A b(\theta_i) b'(\theta_i) dA\,. \tag{3.11}$$

Note that the equivalent area ensonified, $A(\theta_i)$, is a representation of the physical area ensonified defined by the pulse length and beam geometry, and the intensity variations within the beam geometry over that area. The integral of the beam geometry represents an ideal beam aperture of unity response within the aperture and zero outside. This is analogous to the concept of an ideal sampling volume used in fisheries acoustics for volume scattering (MacLennan and Simmonds 1992). The pulse length dependent equivalent area ensonified $A_p(\theta_i)$ on a flat horizontal seabed can be separated into two components, one being circular

or elliptical at near normal incidence (nadir) and a thin section of an annulus at high incident angles (Fig. 3.1; de Moustier and Alexandrou 1991).

Figure 3.1 Example of area ensonified on a horizontal seabed at normal incidence (beam width limited) and at 50° angle of incidence (pulse length limited). The beam geometries shown are 10° along-track and 10° across-track at 0° and 50° incidence ($\varphi = \psi = 10°$ chosen for clarity in the diagram (labels referred to in Section 4.3 when describing the system used).

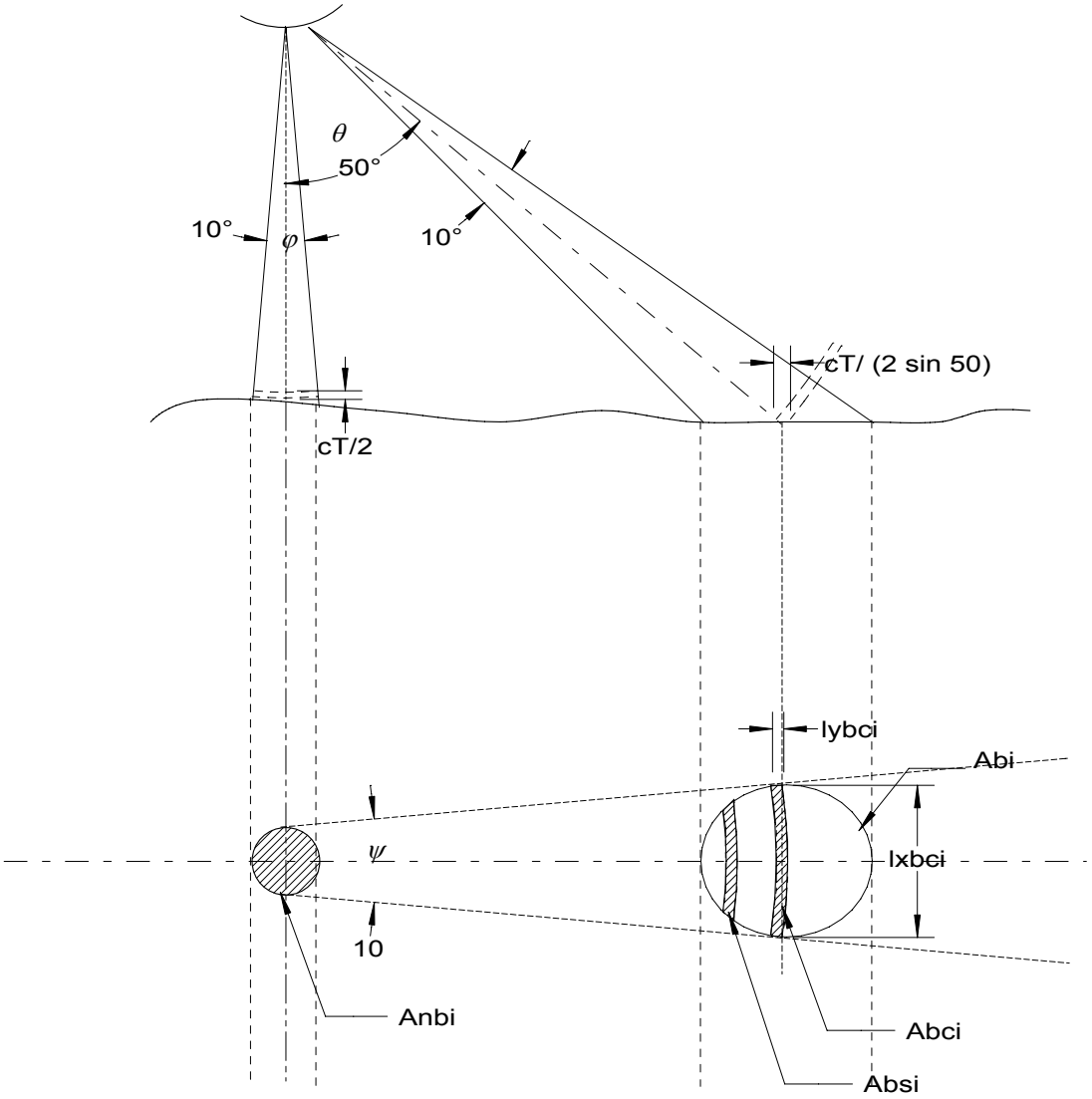

Near nadir the maximum area ensonified is that of a circle or ellipse (circle shown in Fig. 3.1) with transmitting sensitivity $b(\varphi,\psi)$ and receiving sensitivity $b'(\varphi,\psi)$ bounded by the pulse resolution length $\frac{c\tau}{2}$ where c is sound speed and τ is the pulse duration such that;

$$A_p(\theta_i) = \frac{\pi \tan(\frac{\varphi''}{2}) \tan(\frac{\psi''}{2}) R_i^2}{cos(\theta_i)}. \qquad (3.12)$$

The along-track and across-track beam apertures are the effective beam widths of unity response defined by;

$$\varphi'' = \int_{-\varphi'}^{\varphi'} b(\varphi)b'(\varphi)d\varphi \quad \text{and} \tag{3.13}$$

$$\psi'' = \int_{-\psi'}^{\psi'} b(\psi)b'(\psi)d\psi\ , \tag{3.14}$$

where the limit of integration is

$$\psi' = a\cos\left(\frac{R_i}{R_i + \frac{c\tau}{2}}\right) \tag{3.15}$$

$$\text{and } \varphi' = a\cos\left(\frac{R_i}{R_i + \frac{c\tau}{2}}\right) \tag{3.16}.$$

This integration holds for angles of incidence θ_i less than φ'. In the across-track direction the transition from an elliptical ensonified area to that approximating a section of an annulus occurs at $\frac{\varphi'}{2}$ and at high incident angles the equivalent area $A(\theta_i)$ is defined by;

$$A_p(\theta_i) = \frac{\Delta(\theta_i)c\tau\psi'' R_i}{2\sin\theta_i} \tag{3.17}$$

$$\psi'' = \int_{-\pi}^{\pi} b(\psi)b'(\psi)d\psi \tag{3.18}$$

where the limits of integration are -π to π as the pulse resolution area describes an annulus shape on the seafloor acrosstrack. A reduction coefficient $\Delta(\theta_i)$ in the effective area is required if the beam intensity varies within the pulse resolution width $\frac{c\tau}{2\sin\theta_i}$ ensonified on the flat seafloor alongtrack where,

$$\Delta(\theta_i) = \frac{\int_{\psi_l}^{\psi_u} b(\psi)b'(\psi)d\psi}{\int_{\psi_l}^{\psi_u} d\psi}, \tag{3.19}$$

with integration limits assuming $R_i >> \frac{c\tau}{2}$ of,

$$\psi_l = \theta_i - a\cos\left(\frac{R_i\cos\theta_i}{R_i - \frac{c\tau}{4}}\right) \text{ and} \tag{3.20}$$

$$\psi_u = a\cos\left(\frac{R_i\cos\theta_i}{R_i + \frac{c\tau}{4}}\right) - \theta_i \tag{3.21}.$$

In practice for large R the upper and lower integration limits are equal and $\psi_l = \psi_u$.

Consider as an example a MBS (Simrad EM1002) operating on a flat horizontal seafloor with along-track beam power patterns defined by $\frac{\sin x}{x}$ and half power full angles of $b_i(\varphi) = b_i^{'}(\varphi) = 3^o$, sound speed c=1500 m.s^{-1}, pulse length τ = 0.0007 s and depth =100 m. In the across-track the receive beam has a beam pattern of $\frac{\sin x}{x}$ $b_i^{'}(\psi) = 3^o$ (half power full angle) and the transmit beam pattern is assumed to have unity intensity over the receiver beamwidth. Near nadir the unity response ideal beam aperture is 2.17^o along-track, (Eq.3.13, 3.15) and 3.08^o across-track (Eq. 3.14, 3.16) using $\varphi^{'} = \psi^{'}$=5.9^o.

At incident angles greater than 5.9^o the along-track ideal beam aperture $\psi^{"}$ is 2.17^o (Eq. 3.18) and the across-track is defined by the pulse resolution length $\frac{c\tau}{2\sin\theta_i}$ and reduced by the integral of the beam pattern within the pulse resolution $\Delta(\theta_i)$ (Eq. 3.19). Assuming that at large R the angular integration limits are equal and $\psi_l = \psi_u$ the reduction coefficient in equivalent scattering area due to the across track ideal beam aperture $\Delta(\theta_i)$ is less than 1dB for angular limits less than 1.5^o and greater than 3 dB for angular limits greater than 3^o (Fig. 3.2a). This translates to reduction coefficients at 100 m depth to be less than 1dB for incidence angles greater than 6^o (Fig. 3.2b).

Figure 3.2 Reduction coefficient $\Delta(\theta_i)$ based on equation 3.19 for (a) integration angular limits of 0^o to 3^o and for (b) incidence angles 0^o to 40^o for the system described in Sec. 3.3.1.

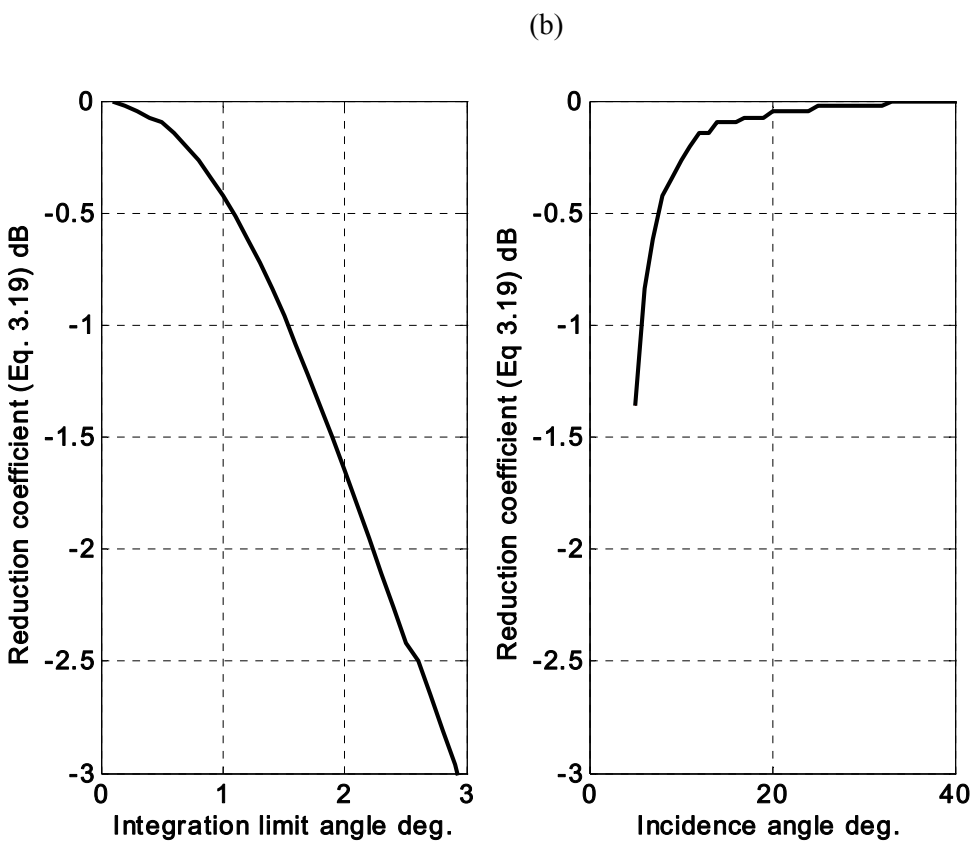

3.3.2 Acoustic system limitations

There are some practical limits to acoustic system capabilities that can be expressed using the sonar equation. An acoustic transmitter at high frequency has a maximum SL limited primarily by the mechanical characteristics of the transducer, and cavitation bubbles (Urick 1983 p 76). Bubbles are generated at high negative pressures at the transmitter face and their onset is a function of transducer directivity, pulse length, frequency, pressure, medium impurities and fluid impedance. The two-way transmission loss $2TL(\theta_i)$ at a fixed range R increases with increasing frequency squared due to increased absorption. This represents a significant limitation on range performance using high frequencies (Urick 1983). Therefore it is common to use low frequency acoustic systems in deep-water and high frequency systems in shallow water when operating as a depth-sensing device from a vessel. The frequency and hence wavelength of an acoustic system also determines to a large extent the sampling resolution and the transducer size.

3.4 Geoacoustic sediment properties

The geoacoustic surficial sediment properties of interest include the compression and shear sound speeds, density, porosity, homogeneity and biotic inclusions and vary widely with sediment types (Hamilton and Bachman 1982). It is convenient to express the geoacoustic sediment properties to an easily identifiable measure of sediment particle size using the

Wentworth Phi 'ϕ' scale (Ch. 2). The geometric mean, of the sediment diameters in mm of the corresponding ϕ distribution is M_ϕ:

$$M_\phi = \frac{1}{3}(\phi_{84} + \phi_{50} + \phi_{16}), \tag{3.22}$$

where ϕ_{16}, ϕ_{50} and ϕ_{84} are the 16 , 50 and 84 percentage points of the cumulative distribution. This method of estimating M_ϕ removes a potential small bias when averaging only the 16 and 80 percentage points (Hamilton and Bachman 1982; Inman 1952; Ch. 2). Alternatively the arithmetic mean of the sediment diameters can be calculated in the phi notation, $M_{\phi AM}$,

$$M_{\phi AM} = -\log_2 \overline{d} \tag{3.23}$$

where $\overline{d}$ is the mean grain size diameter in mm. Incomplete description of the method of determining the mean sediment size (geometric or arithmetic mean of the sediment diameters mm) when using the Phi scale leads to large uncertainties and confusion (Pierce and Grause 1981). Phi sizes contained in this work will refer to the geometric mean of the sediment diameters in mm (Eq. 3.22). Naming of sediment mixtures of gravel, sand and mud (silt plus clay) follows the convention of Folk (1952).

On the continental terrace (shelf and slope) geoacoustic properties of porosity, density and sound speed can be determined at high frequencies for sediment grain size M_ϕ using linear regression equations with standard error based on the compilation of numerous experimental results (Hamilton and Bachman 1982). These will be used later in the seabed scattering model (APL94 1994) to explore acoustic backscatter profiles.

A limitation with using these sediment particle size derived equations is the large scatter that surrounds an individual geometric mean sediment grain size and the effects of live and dead epifauna and infauna. The relationship does not consider grain sizes higher than 2 mm or lithology (*e.g.* limestone and sandstone features) that were a dominant feature in the study areas (Ch. 5).

The attenuation, α_s dBm^{-1}, in sediments can be expressed in the form $\alpha_s \equiv bf^m$ where frequency, *f*, is in kHz and 'b' is a constant and 'm' is approximately unity (Clay and Medwin 1977 p261). Experimental measurements show that α_s varies linearly with frequency although there is considerable variation at a given frequency depending on seabed type and porosity. The actual range of m has been shown to vary between 0.5 to 2 (Stewart and Chotiros 1992). Typical values of absorption α_s, m = 1, for unconsolidated sediments give ranges of 'b' from 0.5 for sand, 0.5 to 0.7 for fine sand, 0.8 to 0.1 for mixed and 0.1 to 0.05 for silty clay (Hamilton 1972). At 95 kHz α_s for sand is approximately 47.5 dBm^{-1}, with a return path within sediment signal, attenuated by 10 dB at a depth of 0.1 m. This large signal attenuation demonstrates that at high frequencies (95 kHz) the penetration of acoustic waves into the seabed is limited to a few 10's of wavelengths, the top 0.10 to 0.30 m at 95 kHz for most sediment types considered here.

3.5 Seabed roughness

The surface roughness of the seafloor can be described in terms of the spatial statistics such as mean, variance, and correlation lengths or areas of elevations about a mean plane. However these statistics are usually insufficient to describe surface roughness unambiguously. A more complete description is obtained through the roughness energy density spectrum (1D or 2D) and used to compute the average phase shift within an elemental area due to elevation differences.

Height statistics

Acoustic waves are imperfectly reflected and partly scattered by rough surfaces. In acoustic scatter terms a surface is thought to be rough if the surface root mean square (rms) roughness (std), σ, is significant compared to the wavelength, λ, of the acoustic signal. From Rayleigh (1945) we have the characterisation of acoustic roughness by the Rayleigh parameter (Ra) where the round trip rms phase difference introduced by the height statistics of the surface is

$$Ra = 2k_a hCos\theta_i , \tag{3.24}$$

where $k_a = \frac{2\pi}{\lambda_a}$ is the acoustic wave number, and $h = \left\langle \sigma^2 \right\rangle^{\frac{1}{2}}$ is the rms height of the surface (Brekhovskikh and Lysanov 1991).

A surface is considered to be rough where Ra >> 1, and results in incoherent scatter. A smooth surface is one where Ra << 1, and results in coherent scatter.

For example, when using a frequency, f=95 kHz, multi-beam sonar in seawater with speed of sound, c = 1500 m.s^{-1}, the wave length is

$$\lambda_a = \frac{c}{f} = \frac{1500}{95000} = 0.0158 \text{ m.}$$

The seabed surface will appear rough, Ra >> 1, when $hCos\theta_i$ >> 0.0013 m. Therefore at 0^o incidence (nadir) h = 0.0013 m and at 70^o incidence h = 0.0038 m. This very small rms height deviation coupled with a large horizontal sampling resolution of most acoustic instruments at depth (area > 4 m^2 at 100 m depth, see Ch. 4) indicates that all practical surfaces encountered on the seafloor will appear as rough and provide incoherent scatter under this criteria.

In many cases we can treat randomly rough surface heights as Gaussian in distribution at scales of kilometres to meters, (Krause and Menard 1965; Stewart *et al.,* 1994a).

Spatial statistics

Two surfaces of equal height statistics can have different spatial statistics leading to differences in acoustic scatter. Such surfaces can be distinguished by their autocorrelation functions:

$$C(R) = \frac{\left\langle h(r_o)h(r_o + R)\right\rangle_s}{\sigma^2}, \tag{3.25}$$

where r_o is the two-dimensional vector giving horizontal position and R represents a vector separating two surface points.

This function has the property that C(0) = 1 indicating exact surface match and as R increases C(R) will usually decay to zero. The shape of the decay is dependent on the type of surface and the rate of decay is dependent on the distance over which the points become uncorrelated (Ogilvy 1992 p13). This has important implications for corrugated surfaces (e.g. sandwaves) where the sample area (shape and size) may not be large enough for the surface to be treated as being random. Two important points need to be considered when comparing autocorrelated functions. Firstly, the spatial sampling and resolution need to be similar for both surfaces and secondly, the functions are generally not valid for sampled lengths greater than $1/10^{th}$ of the surface extent (Ogilvy 1992 p14-17).

Relief spectrum

The spectrum of surface roughness describes both the height statistics and the spatial separation statistics and is usually defined as the Fourier transform of the un-normalised correlation function expressed here in 2 D form:

$$P(k_s) = \frac{\sigma^2}{(2\pi)^2}\int_{-\infty}^{\infty}\int_{-\infty}^{\infty} C(R)e^{ik_s.R}d^2R\,, \tag{3.26}$$

where R represents the magnitude of the 2D vector R, $k_s = (k_x,k_y)$ represents the spatial wave number and P has dimensions of length^4. It is convenient to simplify this expression using continuous functions that tend to smooth the surface and this rarely occurs in nature (Ogilvy 1992). The seabed scattering model (APL94 1994, explained next section) uses a power law representation of the relief spectrum in the form:

$$P(k_s) = w_2 k_s^{-\gamma}\,, \tag{3.27}$$

where w_2 represents the spectral strength and the spectral exponent γ dictates the relative distribution of energy in the spectrum. This power law representation assumes that the interface roughness can be described as a random process with "stationary increments" when the 2D roughness statistics are Gaussian and isotropic. The term stationary increments implies that, while $h(r)$ may not be stationary, the random process defined as the difference $h(r+r_o)-h(r_o)$ is stationary and depends only on the horizontal distance r between the two points where r_o is an arbitrary horizontal displacement (Jackson *et al.,* 1986).

Following Jackson *et al.* (1986) the relief spectrum $P(k_s)$ is related to the structure function $D(r)$, where $D(r)$ is defined as the expected value of the square of the increment in $h(r)$ for fixed horizontal displacement:

$$D(r) = E\{[h(r+r_o)-h(r_o)]^2\}. \tag{3.28}$$

Assuming the roughness statistics are isotropic, the spectrum and the structure function take the form:

$$D(r) = G_h^2 r^{2\varsigma}\,, \text{ where} \tag{3.29}$$

$G_h^2 = \frac{[2\pi w_2 \Gamma(2-\varsigma)2^{-2\varsigma}]}{[\varsigma(1-\varsigma)\Gamma(1+\varsigma)]}$, and

$\varsigma = (\frac{\gamma}{2} - 1)$ (Ishimaru 1978; Jackson *et al.,* 1986), where γ is the spectral exponent used in Eq. 3.15 and Γ is the gamma function.

For directionally isotropic seabeds the positive square root of the structure function, ($G_h r^{\varsigma}$), represents the rms height difference for points on the seafloor separated by distance vector r. Typical values of the isotropic structure function variables, w_2 and γ have been measured for a variety of seabed types, and are used in the APL94 (1994) seabed scattering model discussed in section 3.7. As an example, for sandy gravel and sandy clay seabeds , γ is estimated to be 3.25 for both seabed types and w_2 , 0.012937 cm^4 and 0.000518 cm^4 respectively. Assuming the power law holds, sandy gravel and sandy mud sediment types will have an approximate rms height difference of 6.8 cm and 1.4 cm respectively for a separation distance of 1 m. Experimental validation for sandy sediments of the structure function and relief spectrum have generally supported this representation of seabed roughness (*e.g.*, Jackson and Briggs 1992; Williams *et al.,* 2002). In particular the anisotropic nature of sand waves on the seafloor for selected seabed sites did not greatly affect the mean power law representation of the seabed roughness and hence the mean seabed backscatter using the APL94 (1994) model (*e.g.,* Jackson and Briggs 1992). Gensane (1989) showed that although the mean backscatter may be similar in the presence of anisotropic sand waves for a given substrate type the statistical properties of the seabed backscatter have changed measurably.

3.6 Seabed scattering models at high frequency

High frequency scattering from the seafloor is related to the roughness of the sediment water interface, roughness of interfaces between the sediment layers, discrete scatterers within the sediments and fluctuations in the sediment volume density and sound speed. The diversity of sediment types encountered in the ocean and the wide range of acoustic frequencies used has led to a range of model realisations (Jones and Jackson 2001). The sediment can be modelled as a fluid (Ivakin and Lysanov 1988), an elastic (Jackson and Ivakin 1998) or poro-elastic medium (*e.g.,* Chotiros 1995), or as a system whose dynamics are governed by grain-grain contact (Buckingham 1997). Modelling and validated measurements at high frequencies have been limited due to the difficulty of accurately characterising seabed properties at centimetre scales. Advances in two-dimensional digital photogrammetry and three-dimensional X-Ray computed tomography are changing this situation (Pouliquen and Lyons 2002). Physical measurement techniques are now able to take into account the effects of bioturbated sediments.

The motivation of developing acoustic seabed models is that they lead to solving the inverse problem where the acoustic backscatter from a region is used to predict the sediment characteristics. In practice the inversion of backscatter incident and frequency limited measurements of seabed backscatter to seabed types is not unique. This is illustrated by looking at the monostatic reflectance as a function of angle for various typical seabed types that exhibit various degrees of coherent and incoherent scatter (Fig. 3.3). At some incidence angle a high impedance smooth surface (Fig. 3.3a) could reflect back towards the source the same intensity as a low impedance rough surface (Fig. 3.3d).

Figure 3.3 Representation of acoustic scatter showing direction of incident wave and expected direction of specular wave from high impedance, (a) smooth; (b) rough surface and low impedance contrast, (c) smooth; (d) rough surface (modified from Urick 1983 p140).

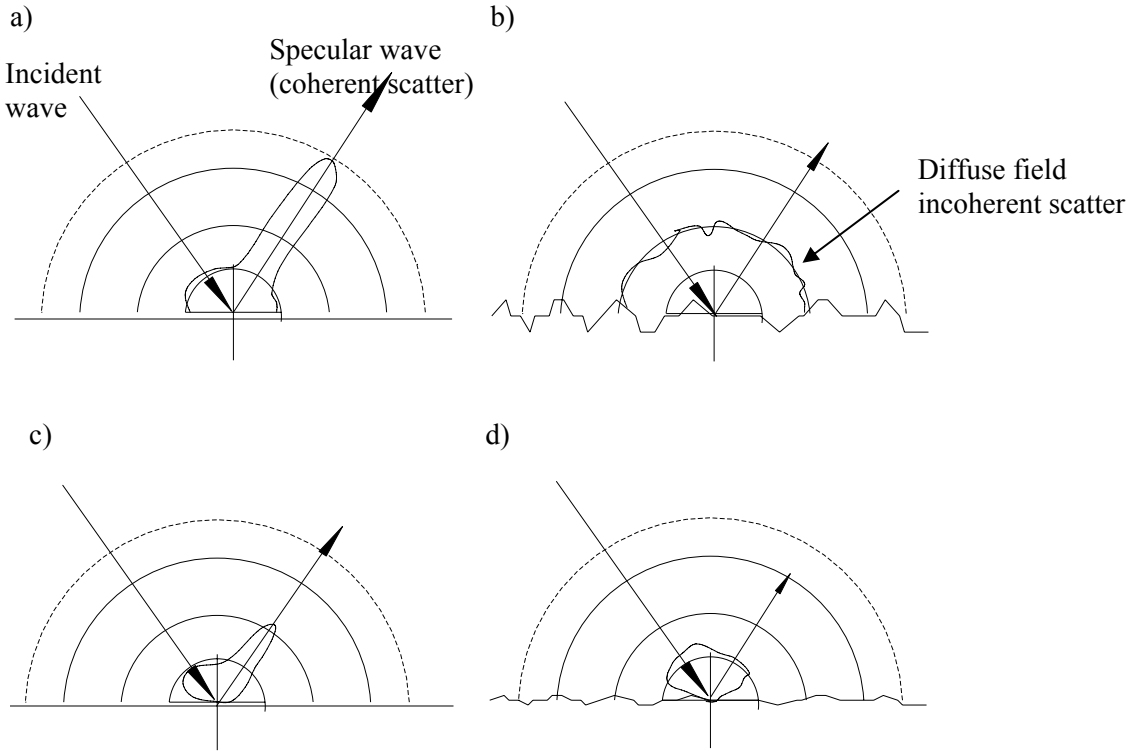

In most cases of acoustic sensing of the seafloor and certainly the examples presented here the seabed is poorly described in terms of its roughness and geoacoustic properties including the effects of epifauna and infauna.

3.7 High Frequency Acoustic Model

In the frequency range of interest 10 to 100 kHz a useful fluid sediment model has been developed over a variety of soft to hard seabed types validated with acoustic measurements (Jackson *et al.,* 1986; Jackson and Briggs 1992; APL94 1994). The Applied Physics Laboratory at the University of Washington (APL94 1994) model combines the most dominant dimensionless seabed scattering mechanisms of homogeneous sediment volume scattering coefficient $s_v(\theta)$ and surface roughness coefficient $s_s(\theta)$ as a superposition of incoherent scatter to estimate the seabed backscattering strength $S_b(\theta)$, where

$$S_b(\theta) = 10\log_{10}\left[s_s(\theta) + s_v(\theta)\right] \quad \text{dB.} \qquad (3.30)$$

This simple fluid sediment model will have poor geoacoustic parameter prediction for the following sediment compositions and seabed roughness characteristics,

- inhomogeneous sediment layers (Jackson and Ivakin 1998).
- shear waves for rock seabeds (Ivakin and Jackson 1998).
- poroelastic (Biot) effects of sands (Williams *et al.,* 2002).
- other volume scattering mechanisms, compressional-compressional, shear to shear, compression to shear (Jackson and Ivakin 1998).
- non isotropic surfaces (Pouliquen and Lyons 2002)
- very rough surfaces that violate the Kirchhoff scattering criteria.
- inclusion of discrete inclusions within the sediment volume such as shell fragments and other biological material.
- representation of texture and higher order echo statistics.

Despite the potential for a number of limitations in the APL94 (1994) model, measurements on a variety of seabed types has supported the role of the dominant physical scattering mechanisms it represents over a wide range of incidence angles (*e.g.*, Jackson and Briggs 1992; Williams *et al.,* 2002; Sternlicht and de Moustier 2003).

Surface roughness scattering

The surface roughness is assumed to be described by the power law spectrum outlined in section 3.5. The elemental surface area curvature radius is assumed to be much larger than the acoustic wavelength (the Kirchhoff approximation, Ogilvy 1992 p104). Here the sum of the contributions of each elemental surface area can be calculated by the Helmholtz-Kirchhoff integral to estimate the surface roughness scattering at incident angle θ. Surface roughness scattering $s_s(\theta)$ under these conditions can be expressed as a function F of the following variables:

$$s_s(\theta) = F(f, \theta, \rho, \nu, \gamma, w_2) \qquad (3.31)$$

where the terms are defined in Tables 3.1 and 3.3.

Sediment volume scattering

Based on the assumptions of a homogeneous seabed with the limitations outlined as above the sediment volume scattering $s_v(\theta)$ can be expressed as a function of:

$$s_v(\theta) = F(f, \theta, \rho, \nu, \delta, \sigma_s), \qquad (3.32)$$

where the terms are defined in Tables 3.1 and 3.3. The loss parameter δ can be expressed in terms of the sediment sound attenuation, α_s, sediment and seawater sound speed ratio ν and frequency f.

$$\delta = \frac{\alpha_s}{f}\frac{\nu c_w \ln(10)}{40\pi}. \quad (3.33)$$

The sediment volume parameter σ_s has been derived empirically comparing models to experimentation (APL94 1994).

The model input parameters are outlined in Table 3.1 and typical geoacoustic values for a range of seabed types are outlined in Table 3.2 based on historical measurements (APL94 1994). Figure 3.4 shows the realisation of the model output for five seabed types at 95 kHz and incident angles 0^o to 70^o. The model realisations show that larger grain size (harder) and hence rougher substrates generate increasingly higher backscatter for incident angles 20^o – 70^o. For rough rock substrate multiple surface roughness dominates resulting in high backscatter over the entire incident angle range (Fig. 3.4). As the grain size of the sediment decreases the contribution from surface roughness scattering decreases whilst the contribution of volume scattering increases (Fig. 3.4). The coarse sand seabed type has less than 2 dB influence from volume scattering and the dominant scattering mechanism is predicted to be multiple roughness scattering. Whereas, multiple roughness scattering has negligible contribution above 20^o incidence for the coarse silt and sandy mud seabed types backscatter profile. The medium sand seabed type backscatter profile shows a mixture of volume scattering and roughness scattering dominance over the 0^o to 70^o incidence range (Fig. 3.4). At low incidence angle (0^o to 20^o) multiple roughness scattering is dominant, between 20^o to approximately 55^o both volume and roughness scattering contribute significantly and higher than 55^o incidence roughness scattering dominates (Fig. 3.4). Figure 3.4 demonstrates that the historical geoacoustic measurements and APL94 (1994) model predictions of seabed type conclude that finer grained sediment backscatter measurements are dominated by volume scattering and roughness scattering is small. As the sediment grain size increases the roughness of the seafloor increases and roughness scattering dominates the seabed backscatter.

Table 3.1 Definition of parameters used in Table 3.2 for a model of seabed reflectance based on Jackson and Briggs (1992).

Symbol	Definition	Short Name
ρ	Ratio of sediment mass density to water mass density	Density ratio
ν	Ratio of sediment sound speed to water sound speed	Sound speed ratio
δ	Ratio of imaginary wave number to real wave number for the sediment	Loss parameter
σ_s	Ratio of sediment volume scattering cross-section to sediment attenuation coefficient	Volume parameter
γ	Exponent of bottom relief spectrum	Spectral exponent
w_2	Strength of bottom relief spectrum (cm^4) at wave number 2π/λ in 1rad.cm^{-1}	Spectral strength

Table 3.2 Characteristics of seabed terrains at 95 kHz and sound speed 1500 m.s^{-1} to determine seabed backscatter (APL94 1994).

Sediment Name	Bulk grain size Mz (f)	Rho ρ	Nu ν	Delta δ	Sigma σ_s	Gamma γ	w_2 w_2 (cm^4)
rough rock	-	2.500	2.500	0.01374	0.002	3.25	0.206930
rock	-	2.500	2.500	0.01374	0.002	3.25	0.018620
cobble, gravel, pebble	-	2.500	1.800	0.01374	0.002	3.25	0.016000
sandy gravel	-1.0	2.492	1.337	0.01705	0.002	3.25	0.012937
very coarse sand	-0.5	2.401	1.307	0.01667	0.002	3.25	0.010573
muddy sandy gravel	0.0	2.314	1.278	0.01630	0.002	3.25	0.008602
coarse sand, gravelly sand	0.5	2.231	1.250	0.01638	0.002	3.25	0.006957
gravelly muddy sand	1.0	2.151	1.224	0.01645	0.002	3.25	0.005587
medium sand	1.5	1.845	1.178	0.01624	0.002	3.25	0.004446
muddy gravel	2.0	1.615	1.140	0.01610	0.002	3.25	0.003498
fine sand	2.5	1.451	1.107	0.01602	0.002	3.25	0.002715
muddy sand	3.0	1.339	1.080	0.01728	0.002	3.25	0.002070
very fine sand	3.5	1.268	1.057	0.01875	0.002	3.25	0.001544
clayey sand	4.0	1.224	1.036	0.02019	0.002	3.25	0.001119
coarse silt	4.5	1.195	1.018	0.02158	0.002	3.25	0.000781
sandy silt, gravelly mud	5.0	1.169	1.000	0.01261	0.002	3.25	0.000518
medium silt, sand-silt-mud	5.5	1.149	0.989	0.00676	0.001	3.25	0.000518
sandy mud	6.0	1.149	0.987	0.00386	0.001	3.25	0.000518
fine silt, clayey silt	6.5	1.148	0.986	0.00306	0.001	3.25	0.000518
sandy clay	7.0	1.147	0.985	0.00242	0.001	3.25	0.000518
very fine silt	7.5	1.146	0.984	0.00194	0.001	3.25	0.000518
sily clay	8.0	1.146	0.982	0.00163	0.001	3.25	0.000518
clay	9.0	1.145	0.980	0.00148	0.001	3.25	0.000518

Figure 3.4 Seabed scattering strength $S_b(\theta)$ of seabed types at 95 kHz with the contribution from volume scattering (dotted) and the total seabed scattering (solid) for rock (plus), coarse sand (circle), medium sand (cross), coarse silt (diamond) and sandy mud (triangle) using the geophysical parameters quantified in Table 3.2 and the model (APL94 1994).

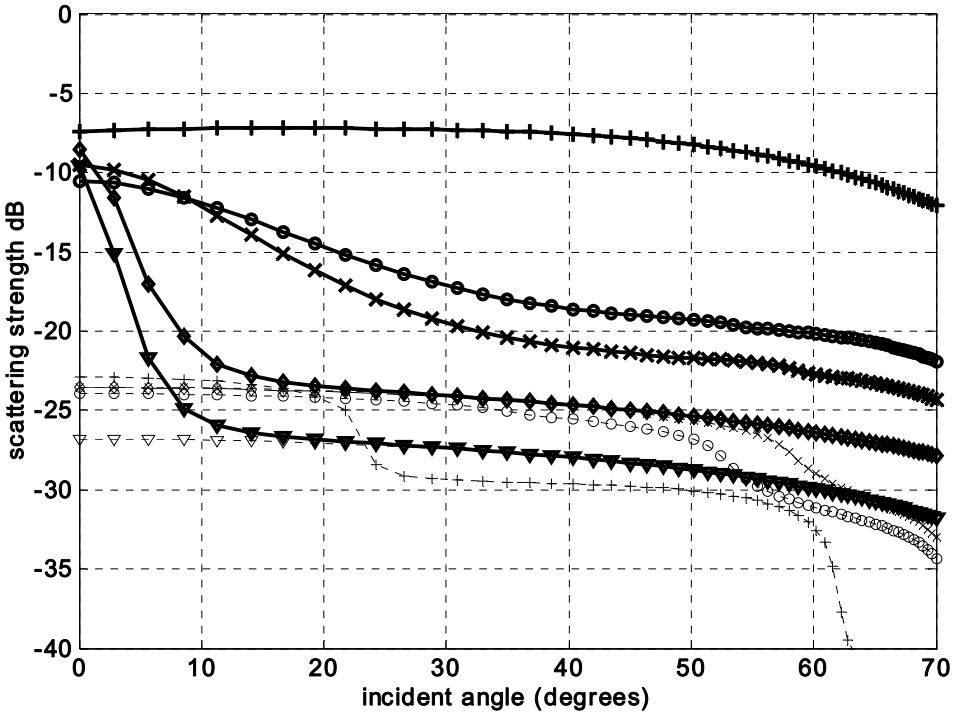

Within the APL94 model the surface roughness scattering is further divided into the Kirchhoff approximation for incidence angles near 0^o and the composite roughness approximation for all other angles. In the composite roughness approximation, the small-roughness perturbation approximation is used with corrections for shadowing and large-scale rms bottom slope. For rough seabeds outside the Kirchhoff and composite-roughness approximations (*e.g.* cobble and rock), an empirical large-roughness scattering strength expression was derived (APL94 1994). Interpolation between the Kirchhoff, composite and large roughness conditions is carried out to smooth the transition between approximations at their limits and is empirically derived (APL94 1994). The interpolation between the roughness approximations places a large emphasis on the empirical large scale roughness (Fig. 3.5). For 'medium sand' (Table 3.2) Figure 3.5 shows that at the critical angle (approx 55^o incidence) the interpolation method has ignored the increased backscattering strength contribution from composite roughness scattering. The experimental results presented in Chapter 6 support the increase in scattering strength at the critical angle for sandy seabed types.

Figure 3.5. Scattering strength model prediction for 'medium sand' (solid) as the sum of volume scattering (*) and interpolated roughness scattering from Kirchhoff approximation (square), composite roughness (circle) and large scale roughness (dashed).

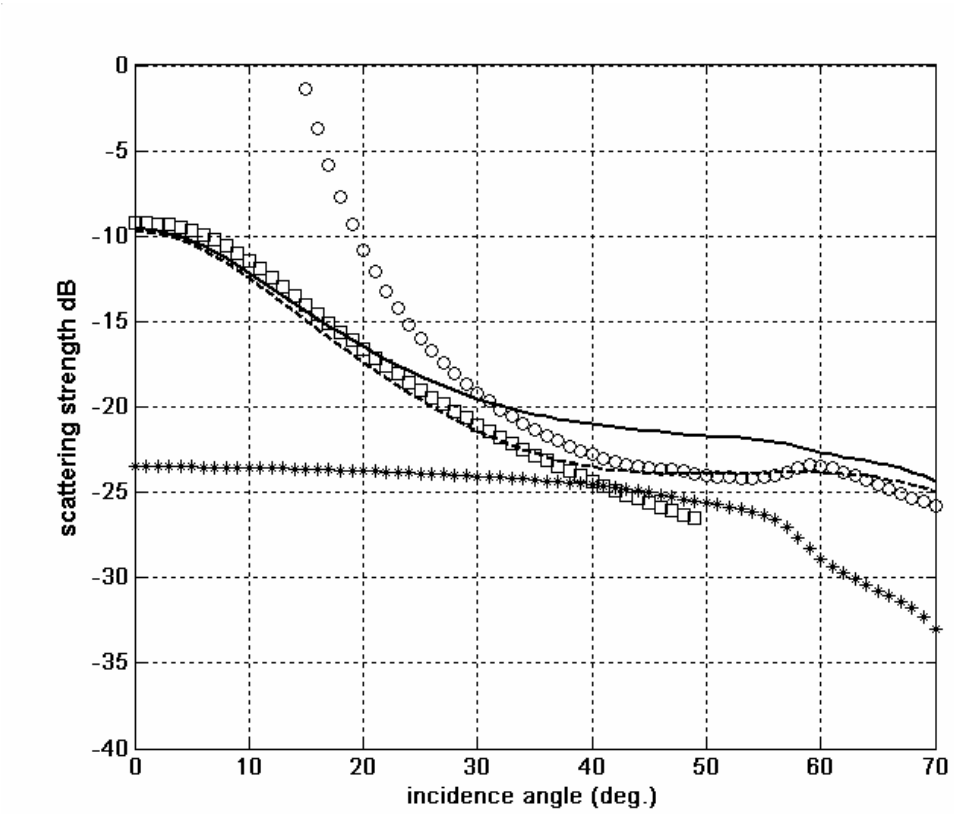

Prediction of seafloor properties based on the APL94 model

To solve the inverse problem of predicting seabed geoacoustic properties based on the monostatic acoustic seabed backscatter requires an understanding of the limitations in the model parameters (Table 3.3). To optimise for seafloor properties and fitting of experimental measurements to those parameters that cause large variations it is recommended to classify sediments according to being either soft (unconsolidated) with $M\varphi_{GM} > 3.0$ or hard $M\varphi_{GM} <= 3.0$ (APL94 1994). To determine whether the sediment is either hard or soft the experimentally derived seabed backscatter profile is compared to the model backscatter predictions (Fig. 3.4) using the Kolmogorov-Smirnov (KS) test to select between $M\varphi_{GM} > 3.0$ or hard $M\varphi_{GM} <= 3.0$. For soft sediments ($M\varphi_{GM} > 3.0$), it is assumed that volume scattering dominates whereas for hard sediments ($M\varphi_{GM} <= 3.0$) seabed roughness is assumed to dominate. Using the hard to soft sediment characterisations as the initial starting parameters simulated annealing optimising can be used to obtain a prediction of the seabed geoacoustic properties for calibrated seabed backscatter measurements (see Ch. 6).

Table 3.3 Recommended limits for the model of seabed backscattering, (APL94 1994).

Symbol	limit	Short Name
$M\varphi_{GM}$	$-1 <= M\varphi_{GM} <= 9$	Mean grain size
ρ	$1.0 <= \rho <= 3.0$	Density ratio
ν	$0.8 <= \nu <= 3.0$	Sound speed ratio
δ	$0.0 < \delta <= 0.1$	Loss parameter
σ_s	$0.0 <= \sigma_s <= 1.0$	Volume parameter
γ	$2.4 <= \gamma <= 3.9$	Spectral exponent
w_2	$0.0 < w_2 <= 1.0$	Spectral strength
θ	$0.0 <= \theta <= 90$	Incident angle (degrees)
c_w	$1400 <= c_w <= 1600$	Sound speed of water $m.s^{-1}$
f	$10.0 <= f <= 100.0$	Frequency kHz

3.8 Echo statistics

Model and phenomenological

Rough surface backscatter measurements from high-resolution radars and sonars have measured scattered envelope amplitude distributions that are described by Rician, Gaussian, Rayleigh, log-normal, Weibull or other more complex probability density functions (pdf) (Stanic and Kennedy 1992). The Rician pdf is a generalisation that encompasses the Gaussian and Rayleigh pdf; it is analogous to the complex sum of a sinusoidal signal and narrow band random noise. When all the signals are large with random intensity but similar phase the Gaussian pdf is produced. If the signal is the sum of many sine waves of similar intensity (no concentrated component) having the same frequency but at random phases the Rayleigh pdf is produced.

The scattering statistics from the seabed are highly dependent on sonar frequency, pulse length and beam width (Stewart *et al.,* 1994a; Gensane 1989). Neglecting subsurface volume scatter the backscatter strength pdf (now referred to as pdf) shape can provide a measure of coherent and incoherent backscatter (Stanton 1985a and 1985b). The pdf shapes can be used to estimate bottom roughness, correlation lengths and bottom microstructure (Stanton 1985b). Backscattering pdf of echo amplitudes from a rough surface at normal incidence follows a Rician pdf (Stanton 1985b). For small scale roughness, when the coherent component dominates, the Rician pdf approaches a Gaussian: whereas for large roughness, when the incoherent component dominates, the Rice pdf approaches a Rayleigh distribution. The echo amplitude from rough horizontal seabeds can generally be characterised by a Rayleigh pdf at incidence angles greater than normal since incoherent scattering dominates. When the seabed topography is more complex the pdf presents non-Rayleigh pdf distributions (Stanic and Kennedy 1992). On real seabeds there are different large-scale features with different scales of roughness and at each spatial scale of roughness the incoherent backscattering signal due to surface roughness can be modelled as the superposition of a set of Rayleigh pdfs (Stewart *et al.,* 1994a). Superposition of a set of Rayleigh pdfs has been successfully applied to situations where different incident angles and ensonified areas are employed such as the case with multi-beam sonars (Stewart *et al.,* 1994b; Lyons and Abraham 1999).

Simulations based on the pdf distributions generated by the point scatter model have identified acoustic signatures that could be used in seafloor classification (Alexandrou *et al.,* 1992). The methodology employed required quadrature sampling of the seafloor backscattered echoes and is not available in this study. Likewise, Alexandrou and Pantzartzis (1993) used a simulation of the point scattering model to distinguish between a number of

seabed scatter distributions. Depending on the simulated acoustic scattering density they were able to achieve a synthetic seabed correct classification rate of 70 to 100 % using several pattern recognition techniques.

Due to the complexity of real sediment interfaces and the contribution of roughness and volume scattering in what is essentially an inhomogenous layered medium no current theory can completely describe the effects of the various scatterer distributions on the model dependence of the reverberation statistics (Stanic and Kennedy 1992). The present use of echo statistics relies on a phenomenological approach.

Phenomenological

The use of phenomenological echo statistics to classify seabed types has been applied to single beam normal incident, sidescan and multibeam sonars (*e.g.,* Pace and Gao 1988; Huseby *et al.,* 1993; Collins *et al.,* 1996). Statistical classification consists of two steps: extracting a vector of feature components from the echo data in a region and assigning for each feature vector a class. The determination of the vector has received considerable attention and changes depending on the instrument employed. Many features can be derived from the acoustic signals and the derived maps (*e.g.,* Pace and Dyer 1979). Specifically for the multi-beam sonar that will be described in Chapter 4 several parameters have been shown to be useful (Pace and Gao 1988; Huseby *et al.,* 1993; Simrad 1999a, Preston et al., 2003 and Dartnell and Gardner, 2004). These involve obtaining mean, standard deviation, quantile and "power spectral" parameters of the amplitude of the backscattering strength fluctuations and textural features of the backscatter strength image using a grey-level co-occurrence matrix (Table 3.4). Using a multibeam sonar it is also possible to obtain parameters of the depth data being standard deviation, slope, slope standard deviation and a power spectral parameter (Table 3.4).

Table 3.4. Parameters derived from the MBS backscatter and depth used in the phenomenological segmentation of the seafloor in Sec. 6.7.

Parameter	Description
mn	Mean ensemble of backscatter.
q8	80% quantile.
sd	Standard deviation of backscatter.
bps	Ratio of central mean backscatter to adjacent sectors
df3	Power spectrum of backscatter
ddf3	Power spectrum of depth data
co	Contrast of GLCM
en	Entropy of GLCM
dsd	Standard deviation of depth
ssd	Standard deviation of slope
smn	Mean slope

The parameters outlined in Table 3.4 are described here and applied in Chapter 6. The mean and standard deviation of the backscatter for a multibeam sonar's centre of each beam backscatter BS for n observations, where n is defined by the number of pings times the number of beams within a region of interest is:

$$\text{mean } \overline{bs} = \frac{1}{n}\sum_{j=1}^{n} 10^{\frac{BS_j}{10}}, \tag{3.34}$$

$$\text{log-mean 'mn': } \overline{BS} = 10\log_{10}(\overline{bs}), \tag{3.35}$$

with log-standard-deviation 'sd' : $SD = 10\log_{10}((\frac{1}{n-1}\sum_{j=1}^{n}(bs_j - \overline{bs})^2)^{\frac{1}{2}})$, (3.36)

The quantile parameter of the mean backscatter is reported to be less sensitive to occasionally high or low outliers (Huseby *et al.,* 1993). In particular the 80% quantile 'q8' of the backscatter (bs_j) has been shown to provide a strong discriminator between distinct seabed sites (Huseby *et al.,* 1993). The 80% quantile parameter is calculated from the n sorted mean backscatter values where 80% of the values are less that or equal to the 'q8' parameter. Similarly, the 50% quantile is known as the median of the backscatter values.

The "power spectrum parameter" 'df3' has been shown by Pace and Gao (1988) and Huseby *et al.* (1993) to be important for sidescan and multibeam systems respectively. The implementation of the parameters here follow in large part those outlined in Pace and Gao (1988) and Huseby *et al.* (1993). Specifically for each ping the backscatter values within a defined number of beams are normalised:

$bs_n = bs_j - \overline{bs}$.

A w point Fast Fourier Transform (F) was calculated from the bs_n spatial series (s) where the window size w ranged from 32 to 128 points (MatLab 2000). The average power spectrum $\overline{P}(f)$ of F for window size w was defined as,

$\overline{P}(f) = \frac{1}{w}\sum_{1}^{w}\left|F\left[bs_n(s)\right]\right|^2$ and the "log-power spectrum" defined as,

$P_L(f) = \frac{l\log_{10}(\frac{A\overline{P}(f)}{P_m}+1)}{\log_{10}(A+1)}$, where P_m is the maximum value of $\overline{P}(f)$ and A is a constant multiplier (10^{-4} in this work).

The log-power spectrum $P_L(f)$ is normalised for the Nyquist frequency being half the spatial separation of the beams:

$P_{NL}(f) = \frac{P_L(f)}{\sum_{1}^{N}P_L(f)}$ and then the 'df3' parameter extracted: $df3 = \frac{\sum_{\frac{1}{2w}}^{\frac{1}{2}}P_{NL}(f)}{\sum_{\frac{3}{4N}}^{\frac{1}{N}}P_{NL}(f)}$. (3.37)

Similarly a "power spectrum parameter" from the depth data 'ddf3' was calculated following the same procedures as outlined for 'df3'. One of the advantages of the power spectral parameter is the normalisation process and therefore non reliance on absolute values. This should make it insensitive to both relative and absolute changes in backscatter which was its original aim when developed for sidescan systems (Pace and Gao 1988).

An important set of parameters derived from seabed backscatter data using sidescan sonars and multibeam sonars are those that describe the texture of the backscatter images (Pace and

Dyer 1979; Huseby *et al.,* 1993). To quantify the texture of an image region three principle approaches are followed, these being spectral, statistical and structural. The textural features that have been demonstrated to be important in other studies are those that are derived from the normalised grey level co-occurrence matrix (GLCM) such as contrast 'co' and entropy 'en' (Huseby *et al.,* 1993). The normalised GLCM is calculated from acoustic backscatter data as relative integer dB values from 0 to 64. This gives an effective 64 dB dynamic range of seabed backscatter values that is twice the expected backscatter range predicted from the APL94 (1994) model for a large range in seabed types (Fig. 3.3). The direction of the co-occurrence matrix is typically calculated for 0^o, 45^o, 90^o and 135^o with only the 0^o direction (the direction across the vessel track) discussed here. Hence, the co-occurrence $P_d(i,j)$ for a ping sequence of data containing a number of beams of relative seabed backscatter values i and j, is defined as the number of pairs of samples having reflectivity i and j, respectively, and which are in a fixed spatial relationship (Huseby *et al.,* 1993). Normalisation $p_d(i,j)$ of the co-occurrence matrix $P_d(i,j)$ is obtained by dividing each element using the sum of the entire matrix values. Using the normalised co-occurrence matrix the parameters of contrast 'co' and entropy 'en' can be calculated by,

$$co = \sum_i \sum_j p_d(i,j)(i-j)^2 \text{ and} \tag{3.38}$$

$$en = \sum_i \sum_j p(i,j)\log_{10}(p_d(i,j)). \tag{3.39}$$

Parameters of entropy and contrast derived from the normalised co-occurrence matrix should be relatively insensitive to both absolute and relative changes in seabed backscatter. A parameter that describes the ratio of the central mean backscatter (approximately 0 to 30 degrees incidence) to the backscatter at higher incidence 'bps' (~ 30 to 70 degrees incidence) is discussed in more detail in Section 6.7.

3.9 Summary

To interpret experimental data gathered at high frequencies (95kHz) for a variety of seabed types and depths two major approaches are outlined in this chapter which will be used in Chapter 6. Firstly, a simple model of seabed scattering is outlined that incorporates the incoherent sum of seabed roughness and volume scattering. Whilst a number of limitations in the model are known, its simplicity and its general fit to a number of experimental studies makes it worthy of further consideration. The greatest limitation of the simple model is its inability to describe the statistical differences between seabed types.

Secondly, the echo statistics and phenomenological characteristics of seabed backscatter systems are investigated. Echo statistic methods to interpret the seafloor roughness using the point scattering model and comparisons with probability density functions were briefly reviewed. As only coarsely quantised amplitude data were available in this study it was not deemed appropriate to pursue a theoretical analysis of the echo statistics pdf functions based on the point scattering model. A phenomenological rather than model based approach is outlined that describes features that have been found to be successful in discriminating seabeds in past studies using sidescan and multibeam sonar instruments. These phenomenological parameters will be explored in more detail in Chapter 6.

4 Acoustic and Towed Video Technology

4.1 Introduction

Chapter 3 provided an overview of the physical theory of acoustic seabed scattering at high frequencies (10-100 kHz) that forms the basis of interpreting data obtained from the acoustic technologies used in the present work. Recent advances in commercial acoustic and video technology have led to new ways of carrying out exploratory seabed biotope studies (Kloser *et al.,* 2001b). Commercially available acoustic (multi-beam sonars) and video technology used in the research carried out in this thesis are discussed in this chapter, as are the metrics that can be derived from the data, and the spatial scales over which they operate. The potential bias and sensitivity of the acoustic metrics arising from instrument configuration and compensation for terrain and oceanic conditions are also discussed.

4.2 Acoustic systems overview

Acoustic sensing of the surficial seabed is required to provide information on the depth, roughness and hardness of the seafloor at appropriate scales (discussed in Chapter 2). The acoustic systems discussed here send out a pulse of directed sound and ensonify a region on the seafloor that scatters sound back (backscatter) to the source to infer seabed depth, roughness and hardness. Depth and large scale roughness from the depth soundings are calculated by knowing the time of echo return with associated angle of arrival, whilst hardness and roughness are inferred from the magnitude and variability in time and space of the backscattered signal as a function of angle. The resolution of the sampling is related to sounding range, frequency, number of beams, beam pattern, platform motion compensation and methods of signal transmission, reception and processing. The acoustic backscatter is made up of a combination of many geoacoustic variables at a particular frequency and is not directly related to physical seabed roughness and hardness (*e.g.*, Jackson and Briggs 1992; Ch. 3). It should be noted that the resolution of sampling for depth soundings and backscatter may be different within the same instruments. For example a multibeam sonar calculates a depth sounding for each resolved beam whereas the backscatter is derived within and between beams.

Acoustic devices range in increasing cost and complexity from simple single beam normal incidence sonars (SBS), through to side scan sonars (SSS), interferometric sonars (IFS), multibeam sonars (MBS) and experimental (hence expensive) synthetic aperture sonars (SAS) (Table 4.1). These systems are largely distinguished by their transducer transmitting and receiving beam patterns (Fig. 4.1). Within these general categories of acoustic systems there are also different signal transmission and reception methods, namely continuous, multiband, broadband or parametric frequency mixing. For deep-water surveys operating at full survey speeds of 10 knots, the simple single beam sonar (SBS) and multi beam sonars (MBS) provided the desired range of cost, resolution and availability in the present work (Kloser *et al.,* 2001b).

Figure 4.1 Stylised diagram showing the different beam patterns of the commonly used commercially available instruments for seabed classification (ICES 2007; B. Michaels personal communication).

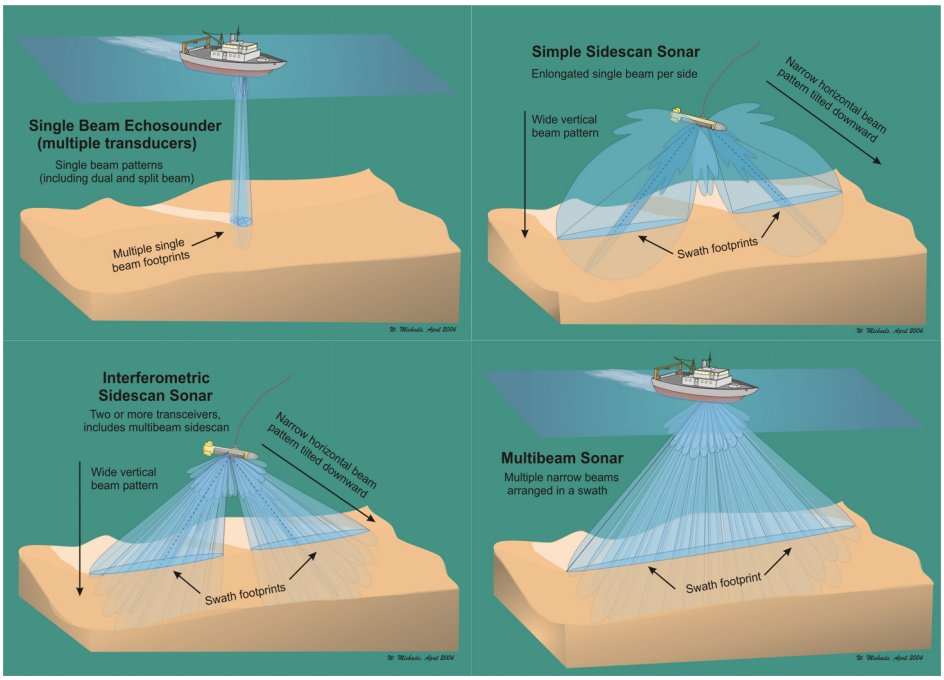

The single beam normal incident sonar (SBS) represents the simplest form of acoustic sampling and is found on most marine vessels for seabed depth sounding. This SBS is monostatic having a directive conical beam (commonly 7^{o} to 20^{o} wide full angle at the half peak power level) with the same transmit and receiver beam sensitivity functions. The SBS commonly operates by sending a short single frequency pulse of sound towards the seafloor. The seabed reflected echo returned is a convolution of the transmitted source signal, transmit and receive beam sensitivities and the ensonified seabed including surface roughness and volume scattering (Sternlicht 1999; Sternlicht and de Moustier 2003). Range or depth of returns are determined by time arrivals and echo magnitude resulting in no or minimal angular resolution. Sidescan sonars are usually towed close to the seafloor to obtain high incidence angles often producing shadows for a detailed view of seafloor topography. The sidescan sonar is monostatic and in its simplest form consists of two transducer arrays on either side of the towfish for directing sound across-track at a high incident angle as it is towed. Typically sidescan sonars have a narrow beam along-track (0.3^{o} to 1^{o}) and wide beam across-track (70^{o}). They send a pulse of sound across the seafloor and record the reflected echoes as a function of time. Sidescan sonars in general need to be towed at slow speed to ensure even sampling of the seafloor. More sophisticated and costly systems use beam focusing to survey at higher speeds (*e.g.*, Klein 5000). The position, relative to the towfish, where an echo originates on the seafloor is estimated by time of arrival and height above the seabed. Errors in location of the towfish relative to the vessel and non flat seabeds add to the positional errors. To improve the accuracy of locating originating echoes a combination of phase difference and arrival time is used (*e.g.,* Denbigh 1989). Phase measurements require that a pair of receiving transducers be spaced closely, usually a multiple of a wavelength apart. The phase difference (within a wavelength) resolves the angle to the originating echo when the positioning and orientation of the transducer are accurately known. Bathymetric side scan sonar systems using only one pair of transducers are unable to resolve the angular location of two echoes arriving at the same time but originating from different locations within the wide across-track beam (70^{o}).

Multibeam sonars have different transmitter and receiver beam sensitivity functions; on transmission a directed pulse, wide beam across-track but narrow beam along-track is transmitted towards the seabed; on reception a large number of receive beams with narrow across-track but wide along-track beam pattern directivities are formed from the multi-element array. Transmit and receive beam patterns combine to form a set of narrow conical beams. The angular locations of the combined transmit and receive beams is known by interfacing to a motion reference system. A multibeam sonar system calculates within each beam angle the corresponding travel time and intensity of the reflected seabed echo. The overall length of the array of elements used to form the beams determine the angular resolution of multibeam sonars. In general, a MBS system produces better bathymetry in complex seabed terrain when compared to interferometric sonars. Also, the narrow beams of MBSs create high receiver gains in the direction of interest, significantly reducing the noise from other directions. This increased signal and reduced noise improves their operation in greater depths and for a wider range of sea states. A multibeam sonar was selected for use in this study as such systems provide both high resolution geolocated bathymetry and backscatter data at survey speed of 8-12 knots (Table 4.1).

Table 4.1 Acoustic sampling devices for surficial seabed properties and qualitative description of resolved ensonified area expected.

Technology	Resolved ensonified area		Main application -
	Bathymetry	Backscatter	
Simple Single Beam normal incident sonar (SBE)	Large	Large	Low cost. Bathymetry and reflectivity can be used for seabed characterization. Note that chirp systems and parametric arrays with active motion correction can produce very small footprints.
Side Scan Sonar (SSS)	N/A	Small	Low cost fine scale work for object detection, highest width sampling but no associated bathymetry. Needs to be towed to maintain high aspect ratios with increasing depth and requires towed body tracking to provide accurate positioning of targets.
Interferometric Sonar (IFS)	Medium to Small -	Small	Medium cost compared with multibeam sonar with lower resolution bathymetry. Needs accurate motion sensing to maintain accuracy. Shorter effective ranges and narrower swath coverage for equivalent frequencies due to wide reception beam.
Multi-beam sonar (MBS)	Small	Small	Medium- high cost bathymetry and reflectivity needing associated motion and georeferencing equipment.
Synthetic aperture sonar (SAS)	Unknown	Unknown	Under development; needs accurate positioning and motion information. Has the ability to produce very high resolution and due to its developmental nature is high cost.

4.3 Multi-beam sonar (MBS)

4.3.1 Historic use

Commercial multi-beam echo sounders (as distinct from phase differencing sidescans, Denbigh 1989) are a relatively new instrument designed initially to measure the topography of the seafloor (*e.g.*, Kleinrock *et al.,* 1992). Initially only low frequency (12 kHz) instruments were used in deep water with minimal number of beams (de Moustier 1986; Mitchell and Clarke 1994). Over the past decade there has been significant advance in the frequency range of instruments (10- 500 kHz) and reductions in beam widths (3^o to 0.5^o), increase in number of beams (60 to > 300) and reduction in cost (MBSTC21 2000). These developments have coincided with improved and less costly (since ~1986) differential global positioning system (DGPS) accuracy and platform motion measurement devices.

Methods have also been evolving to process and interpret the depth and seabed backscatter data from these instruments. The processing of depth data, removing unwanted errors caused by ray bending, platform motion, fish schools, bottom detection method and noise has been investigated (*e.g.*, Mitchell 1996; Canepa *et al.,* 2003). Advances are also being made in the processing and understanding of seabed backscatter from multi-beam instruments (*e.g.*, de Moustier 1986; Hughes-Clark *et al.,* 1993; Hellequin *et al.,* 2003). Several commercial software products provide a phenomenological seabed backscatter processing system (*e.g.*, Simrad 1999a; Preston *et al.,* 2003). Scientific applications of multibeam sonars in shallow waters (< 500 m) have concentrated on describing the geology of the seafloor using both the detailed bathymetry and seabed backscatter (*e.g.*, Goff *et al.,* 1999; Todd *et al.,* 1999; Gardner *et al.,* 2003). Recently there has been an effort to use multi-beam sonars for habitat mapping (*e.g.*, Kostylev *et al.,* 2001; Kloser *et al.,* 2002a; Edwards *et al.,* 2003).

4.3.2 Equipment description

Three commercial multibeam sonar instruments were considered for this study to operate at depths from 30 m to 500 m. The Simrad EM 1002 was selected based on its stated capability of achieving high angle of incidence at 500 m depth giving wider coverage at a given frequency; number of narrow formed receive beams (111 at 2^o to 2.5^o half power full beam angle); seabed backscatter positioned on the seafloor at a given angle of incidence; seafloor classification software (Simrad 1999a) and active roll compensation. Roll compensation attempts to maintain a relatively even swath width about the ships track. This is achieved by aligning the centre of the transmit beams to be normal to the sea surface within a finite range (+/- 10^o) of vessel roll positions. On reception the received beams are phased with a finite range of roll angles (+/- 10^o) to maintain a constant angle of incidence to a nominally horizontal seafloor. No pitch or yaw compensation was operational for any of the instruments considered. Active pitch and yaw compensated instruments steer the transmit and receive beams to ensure even sampling of the bathymetric values across the vessel's path (*e.g.*, Hughes-Clark *et al.,* 1998). In March 2000 a nominally 95 kHz multi-beam sonar (Simrad EM1002, Seatex motion reference system) was hired and fitted to the 65 m CSIRO research vessel *Southern Surveyor* (see Ch. 5 for details of the survey).

The Simrad EM1002 is a phase interpolated beam-forming multi-beam sonar with 128 transducer elements forming 111 beams in a semicircular array, 45 cm radius, that reduce beam forming errors due to incorrect sound speed measurements at the transducer face (MBSTC21 2000). Beams formed at +/- 60^o incidence angles (no vessel roll) are a sum of appropriate transducer elements without sound speed dependent phase delays. At incident angles greater than +/-60^o (or the compensation of the maximum +/- 10^o of vessel roll) a phase delayed sum of elements is required to achieve beam steering and these formed beams are sensitive to sound speed measurement errors at the transducer face (MBSTC21 2000). The transmit beam pattern

can vary from 60° to 200° across-track and 3.3° fore and aft, whilst the receive beam width is nominally 2° across-track and 3.3° along-track. To reduce bottom reflection coupling between beams, the unit uses frequencies of 98 kHz for the inner sector (less than nominally ±50° incidence) and 93 kHz on the outer sectors (greater than nominally ± 50° incidence). On reception the effective transmit and received beamwidth (-3dB power) for the inner sector beams are approximately 2° whilst the outer sector beams are 2.5°. Measurements of the fore-aft transducers receiver beams (half power full beam angle) vary between 2.3° to 3.2°, -175.7 to -182.3 dB re 1V/µPa at 93 kHz for angles greater that 50° and 2.3° to 2.6°, -178.1 to -178.7 dB re 1V/µPa at 98 kHz for angles less than 50° (Simrad data sheet EM1002 Reg.nr: 211716). Of note is the side lobe power levels for the received beams where at normal (0° incidence) and oblique (75° incidence) the power is approximately -21 dB and -17 dB respectively (Fig. 4.2). At high incidence angles a grating lobe is formed with a -22 dB power level (Fig. 4.2b). High off axis lobe levels increase distortion of the measured seabed backscatter, especially when the lobes are directed near normal incidence (*e.g.*, Hellequin *et al.,* 2003).

Figure 4.2. Across-track receive beam intensity polar plots for the, a) nadir 0° incident beam 98 kHz (2° at –3dB power) and the, b) oblique -75° beam 93 kHz (2.5° at –3dB power). Note the side lobe and grating lobe levels (< -20 dB and < -17 dB for the 0° and 75° incidence beams) that measure unwanted signal from the seafloor and increase noise.

a) b)

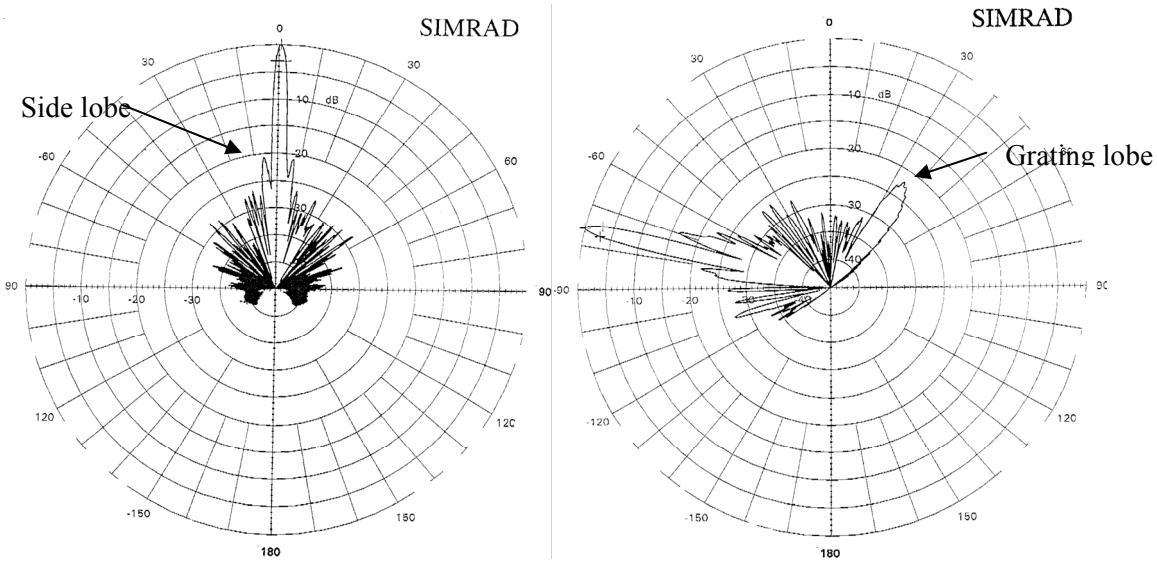

The seabed depth and associated seabed backscatter amplitude at the instance of depth determination is calculated for the 111 beams. The system was operated in an equi-distant mode where the angle of incidence of each beam is adjusted to give evenly spaced depth sampling across a nominal flat horizontal seafloor. The other operational modes are equi-angular where the depth is sampled at evenly spaced received angles from the transducer or "in-between" mode. The swath width was set to 140° with pulse duration varying with depth: 0.2 ms at 0-100 m, 0.7 ms at 100-200 m and 2 ms for 200-600 m.

4.3.3 Data quality assurance

The Simrad EM1002 was installed and calibrated following a "patch test" to minimise navigational and motion errors as outlined in the Simrad EM1002 installation manual (Simrad 1999c). To improve the quality of the seabed bathymetry a local sound speed profile was calculated (McKenzie 1981) based on a temperature depth profile as well as temperature measurements at the transducer face for beam forming calculations. Once collected the data

were processed following the procedures in the Simrad Neptune software package (Simrad 1999b). At the reference sites discussed in Chapter 6 the bathymetry and backscatter were quality checked for outliers and inconsistent values. Typically outliers occurred in the center beam depths and motion errors were highlighted in the outer beams (Ch. 5, Fig. 5.8). Data collected from depths greater than 500 m were excluded due to noise.

A local absorption profile was calculated (François and Garrison 1982) for each region surveyed based on a conductivity, temperature and depth profile. Anomalous backscatter data was evident when there were inconsistent measured depths and due to aeration under the hull of the vessel. These values were excluded from further computations at the reference sites (Ch. 6). The following sections provide an overview of the spatial resolution of the EM1002 MBS and the backscatter sensitivity and corrections required due to seabed slope, water column absorption and noise.

4.3.4 Horizontal Spatial Resolution of Depth Soundings

The Simrad EM1002 multibeam sonar operated at 5 $m.s^{-1}$ (10 knots) in an equi-distant mode with evenly spaced sampling of depth at the beam b_i centres (i = 1 to 111) across a flat seafloor with a swath width of 140° ($2\theta_{max}$°, where θ_{max} =70°) and pulse duration of τ ms. The position of the n = 111 beam centres (assuming no ray bending effects and coordinate system of Fig. 4.3), y_{bi}, across-track at depth, D meters, is determined by,

$$y_{b_i} = \frac{D \tan \theta_{\max}}{\frac{n-1}{2}} (b_i - \frac{n+1}{2}) \text{ m ; } b_i = 1,2, \ldots 111 \quad (4.1)$$

The along-track, $x_{bi,}$ spacing, assuming no rotational (yaw, pitch and roll) vessel motion, is determined by the ping rate, p_r s^{-1}, and vessel speed, s $m.s^{-1}$, by,

$$x_{bi} = \frac{s}{p_r} \text{ m.} \quad (4.2)$$

In this case p_r is restricted on a flat seafloor by the maximum slant range at a given depth and sound speed c $m.s^{-1}$ by,

$$p_r = \frac{c \cos \theta_{\max}}{2D} \text{ } s^{-1}. \quad (4.3)$$

Note the Simrad EM1002 operates by waiting until the last echo has been received from the furthest range before it transmits another ping.

Figure 4.3. Reference diagram for coordinate system for EM1002 (Modified from Simrad 1999c). The emitted incidence angle from the vessel θ is referenced from 0 degrees by the downward z axis and positive in the across tack y positive direction.

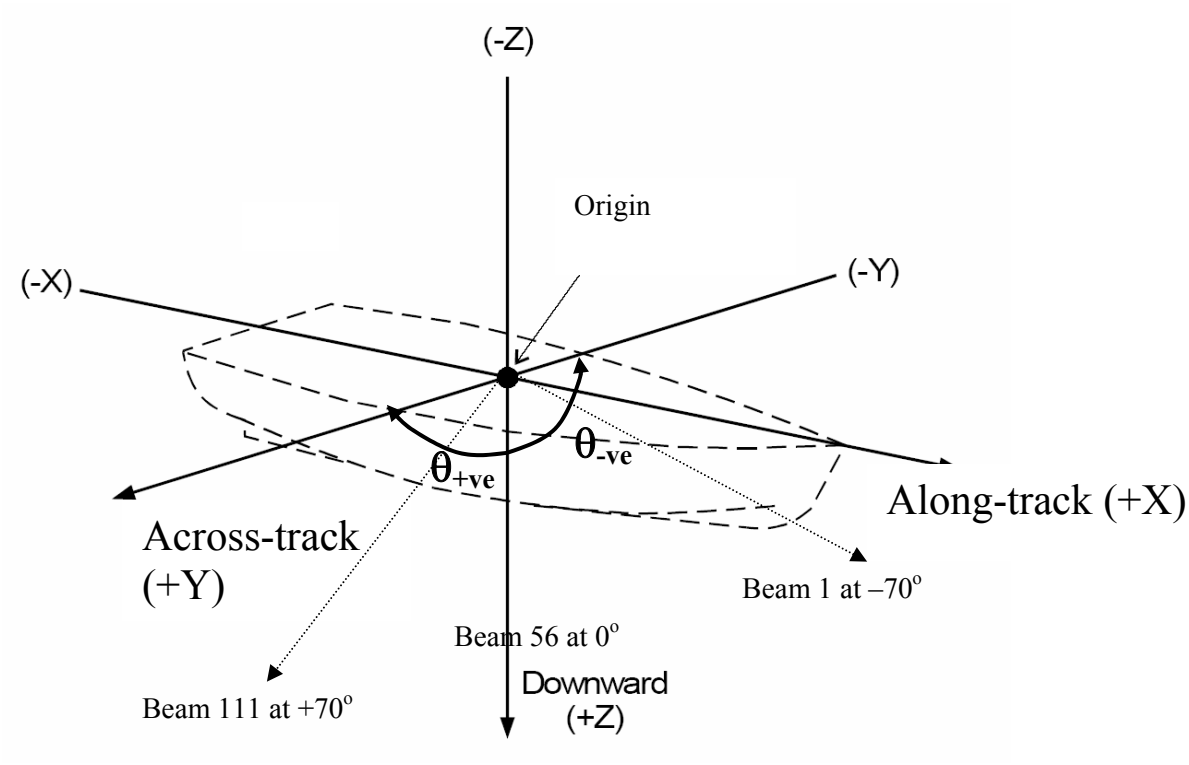

The beam area, A_{bi}, ensonified on a flat horizontal seafloor by the beam pattern (-3dB power) neglecting pulse duration effects is approximated by a rectangle in the EM1002 software:

$$A_{b_i} = \frac{\psi_{xb_i}\psi_{yb_i}R^2}{\cos\theta_i} \quad \text{m}^2 \text{ (Hammerstad 1994).} \qquad (4.4)$$

Here ψ_{xbi} and ψ_{ybi} are the along and athwart -3 dB beam angles for beam, 'i', in radians; θ_i^o is the angle of incidence at beam 'i' and R is range to the seafloor on the beam axis in meters. Surveying in 100 m depth, 2 pings per second and at a speed of 5 $m.s^{-1}$ (10 knots) the beam pointing centres are nominally spaced 5 m apart across-track and 2.5 m along-track (Fig. 4.4). Ignoring beam pattern, attitude and refraction effects this represents the theoretical horizontal resolution of the system increasing, linearly with depth across-track (25 m spacing at 500 m depth) and along-track determined by the ping rate. Figure 4.4 illustrates the small seafloor beam footprint compared with a single beam seabed classification system (Kloser *et al.,* 2002a) directly below the vessel increasing to a wide (10.2 m) and long (29.9 m) footprint at 70° off normal. Also as the vessel moves forward the overlap of adjacent ping beams is high for beams at 70° and with no overlap for beams at 0° (Fig. 4.4. At D = 600 m, the along-track depth spacing would be no less than 11.7 m at c = 1500 $m.s^{-1}$, θ_{max} = 70° and vessel speed 5 $m.s^{-1}$(Table 4.2). It should be noted here that the ensonified along-track width increases with depth due to spherical spreading and this places a greater footprint on the seafloor that has the effect of smoothing along-track depth changes.

The MBS bathymetric data density on the seafloor changes as a function of depth, slope, oceanographic conditions, vessel speed and motion. In practice there are a number of effects

that alter the minimum bathymetric grid including seabed slope, roll, pitch and yaw beam pointing. The precision of an individual depth value will be uncertain based on errors in correction of vessel motion, vessel position, acoustic and electrical noise, seabed type and bottom detection method (amplitude or phase). The accuracy of a depth value is also dependent on the compensation of the absolute beam pointing angle, absolute geolocation and ray bending effects from Snell's law (Ch. 3). To reduce positioning errors a "patch test" is commonly carried out and appropriate compensation factors calculated (Simrad 1999c). In the experiments discussed in Chapter 5 a number of dynamic positioning errors remain that show up as artefacts in the data correlated with the vessel motion and oriented to the vessel's track.

According to the manufacturer the Simrad EM1002 depth determination on a horizontal flat seabed within a beam 'i' is governed by the number of digitised sample values bs_{ij} j = 1 to n. Here the number of samples 'j' within a beam is a function of the angle of incidence, the digitisation rate (11.97 kHz) and the method of averaging samples (on the band passed enveloped detected 95 kHz (nominally) carrier signal for the EM1002 MBS according to Simrad (1999c)). Around normal incidence when the number of samples is less than 10 the depth is determined at the maximum amplitude detection within the –3 dB power levels (Hammerstad 2000). At sample densities greater than approximately 10 the bottom depth is determined by measuring the phase difference of two "half beams" formed from different sub arrays of the received transducer pointing in the same direction as the original beam (Simrad 1999c). Near normal incidence, measured depths are more sensitive to noise and off axis seabed terrain influence. Also, as the incidence angle increases (greater than 60^o incidence) the signal strength decreases and the depth values are more sensitive to electrical and acoustic noise as well as the increased along-track spread of the acoustic footprint on the seabed. Depth measurement uncertainty has the effect of introducing outliers in the measured depth data. Methods of removing outliers vary depending on the instrument and the objectives of the study and are discussed by Mitchell (1996), Calder and Mayer (2003) and Canepa *et al.,* (2003).

It is common practice to grid MBS bathymetric data, requiring 1 or more data points to be located within a square grid cell. Defining a minimum grid cell density of 2 a minimum expected square grid size at a given depth was calculated (Eq 4.1 and 4.2) (Table 4.2). The minimum theoretical grid size for the EM1002 operated at 5 $m.s^{-1}$ and 140^o seabed ensonification over a horizontal flat seafloor is 2.5 m at 50 m depth increasing to 30 m at 600 m depth. In practice due to vessel motion and slower ping rates or a requirement for higher data densities per cell, the grid sizes are increased.

Table 4.2. Theoretical depth data densities on a horizontal flat seafloor based on a Simrad EM1002 with 111, 2^o conical, equispaced beams covering 140^o and surveying at a speed of 5 $m.s^{-1}$ (ignoring attitude and refraction effects). Minimum grid size requiring at least 2 samples within a grid cell.

Depth	Beam spacing		Side length of square grid
m	Minimum Along-track m	Across-track m	Minimum m
50	1.0	2.5	2.5
100	2.0	5.0	5.0
200	3.9	10.0	10.0
400	7.8	20.0	20.0
600	11.7	30.0	30.0

Figure 4.4. Comparison of beam sampling area for multibeam and single beam acoustics operating in 100 m water depth. The single beam sampling area is representative of acoustic roughness algorithm for 17^o – 34^o (Kloser *et al.*, 2001b), whilst the multibeam sampling is for 111, 2^o beams at equi-distant spacing and 140^0 swath width.

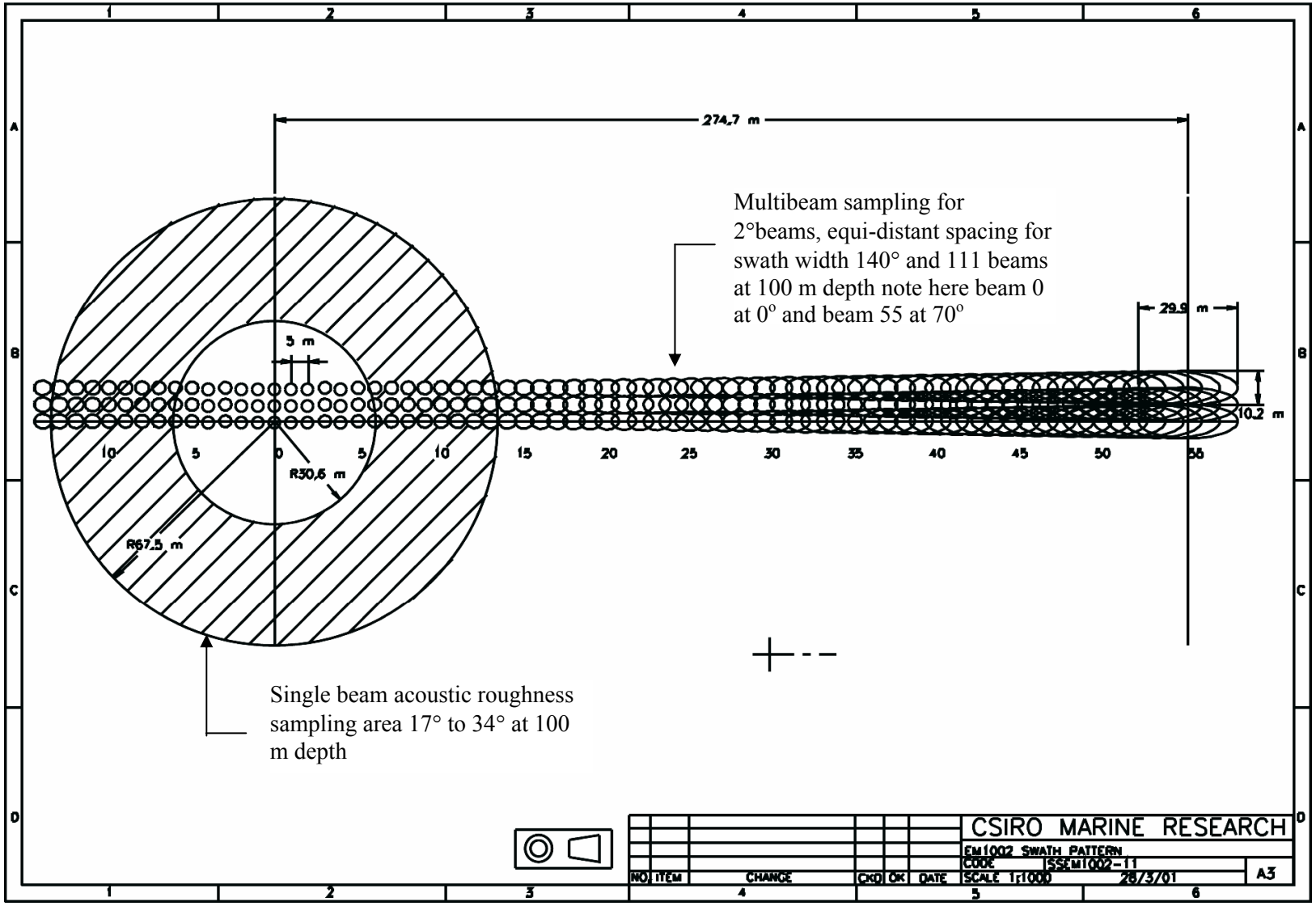

4.3.5 Bathymetric slope

The seabed slope in the along and across-track directions is required to correct the seabed backscatter area calculations and to obtain a better estimate of the true angle of incidence at the seabed (*e.g.*, de Moustier and Alexandrou 1991; Hammerstad 2000; Hellequin *et al.,* 2003). Due to noise on individual depth values it is appropriate to determine the slope on an average number of depth values in the along-track and across-track directions (de Moustier and Alexandrou 1991). The depth data were corrected for water column and transducer face sound speed using under way temperature and targeted water column sound velocity profiles. Motion corrections were applied using the standard operating procedures of a "patch test" (Simrad 1999c). Visual inspection of the bathymetric data indicated that the applied sound speed and "patch test" corrections for no motion were adequate although due to vessel motion depth errors were evident in the outer beams, nominally greater than 60^{o} incidence. Depth outliers, usually in the near nadir region, were removed if they were greater than 3 times the standard deviation for all depth values within that ping.

The across-track slope Sat_{ij} at beam i was calculated from the depth of 5 equi-spaced beams for ping j. Beam spacing's in the along-track and across-track directions were calculated from the beam pointing angle (corrected for ray bending and vessel roll motion) and geolocation. The terrain was surveyed with the vessel travelling orthogonal to the dominant slope (typically less than 3^{o}). The along-track slope Sal_{ij} was based on the depth of 5 pings for beam i. This process results in an approximation of the macro relief in the along-track and across-track directions used to correct the seabed backscatter for incidence angle corrections. Typically small variations of slope across-track (interquartile range less than +/- 1^{o}) occurred for soft-smooth seabed reference site terrain (Fig. 4.5 b) and increased (interquartile range less than +/- 2^{o}) for hard-rough reference site terrain (Fig. 4.5 d). For both terrain types there is a wide spread of along-track slopes (Fig. 4.5 a,c) influenced by heave, pitch, roll and yaw motion correction errors. Excluding outliers the range of along-track slopes for the soft smooth terrain is typically less than +/- 2^{o} and less than +/-5^{o} for the hard rough terrain (Fig. 4.5 a,c).

Figure 4.5. Box plot of seabed slope along-track and across-track for 100 pings of a soft smooth reference site (a, b) and a hard rough reference site (c,d). The box contains the inter quartile range (50% of the data), '+' represents outliers and the vertical line the spread of the data. Beam 1 at –70°, beam 56 at 0° (nadir) and beam 111 at –70°.

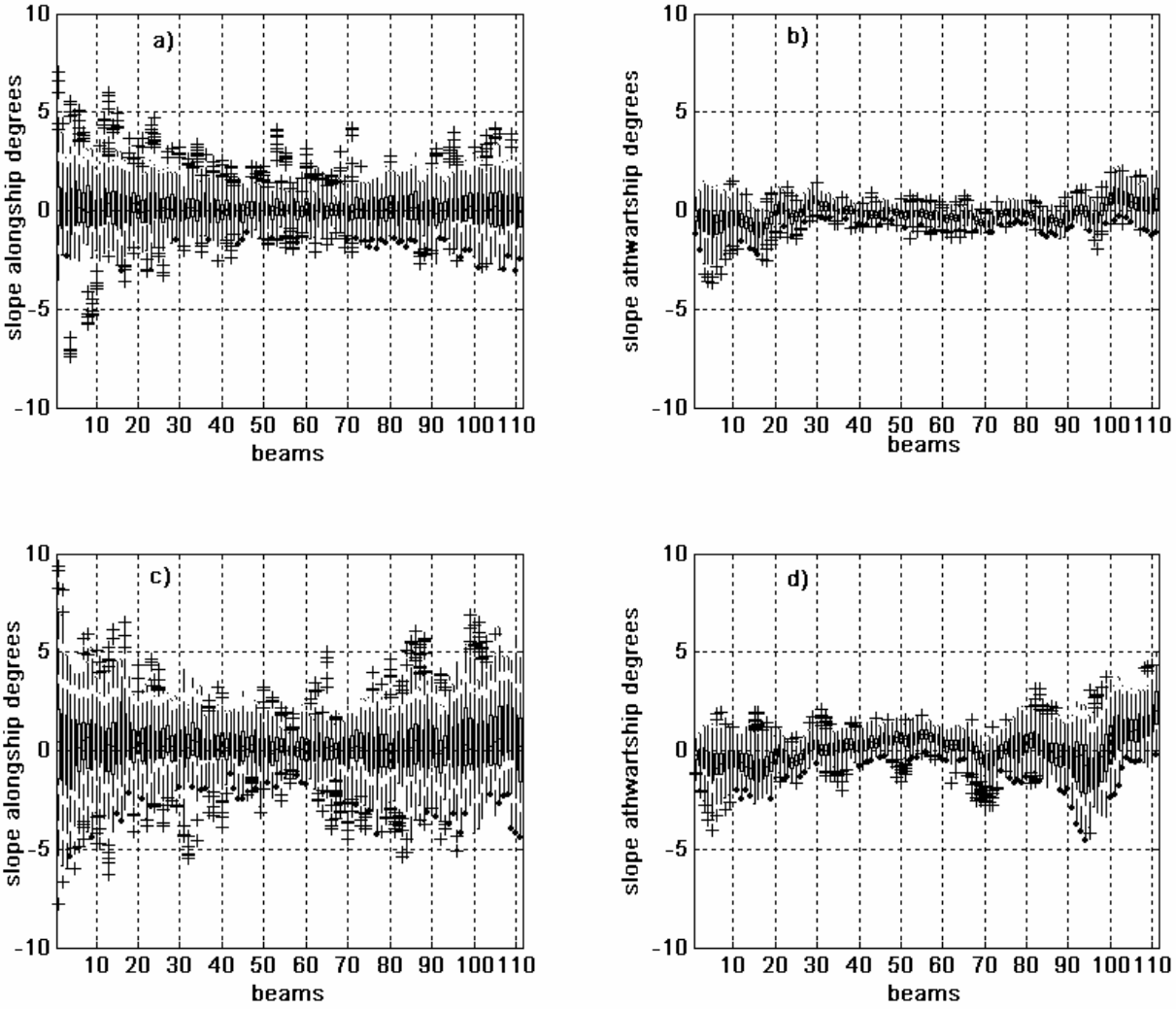

In the above analysis beam angle of the EM1002 MBS was determined based on the beam number (b_i) and the number of beams off normal when the seafloor is horizontal and flat with no vessel motion. Beam 1 at –70° incidence, beam 56 being at normal to the vessel looking directly down and beam 111 at 70° across-track to this normal (i.e. 70° incident to a flat horizontal seafloor) (Fig. 4.3). The beam angle, θ_{bi} (b_i = 1 to 111 beams), extended from the ship's downward normal following Eq.(4.1):

$$\theta_{b_i} = a\tan\left[\frac{\tan(\theta_{\max})}{\frac{N-1}{2}}(b_i - \frac{N+1}{2})\right],\ \theta_{\max} = 70^o, N = 111 \text{ beams} \qquad (4.5)$$

beams 56, 66, 76, 96 and 111 equate to transducer referenced incident angles of 0°, 26°, 45°, 63° and 70° respectively for no vessel motion. The EM1002 swath mapper appeared to be able to steer the beams consistently in the appropriate direction based on vessel motion. Figure 4.5 shows the difference in the theoretical pointing angle, Eq. 4.5, and the estimated angle based on the motion reference unit within the MBS. The highest deviation from the theoretical beam steerage angle (Eq. 4.5) is at near normal incidence mean error 0.7° and maximum 1.8°. At angles higher than 20° the deviation from the theoretical pointing angle is low, less than 0.1°. Seabed incidence angles were not adjusted by removing deviations in pointing angle although these can be seen to be very small on average at incidence angles higher than 15° or the inner 10 beams (Fig. 4.6).

Figure 4.6. Internally calculated emitted beam pointing angles for 85 pings (Fig. 4.2) incident on a horizontal flat seabed where beam 56 is at 0° and beam 111 at 70° .

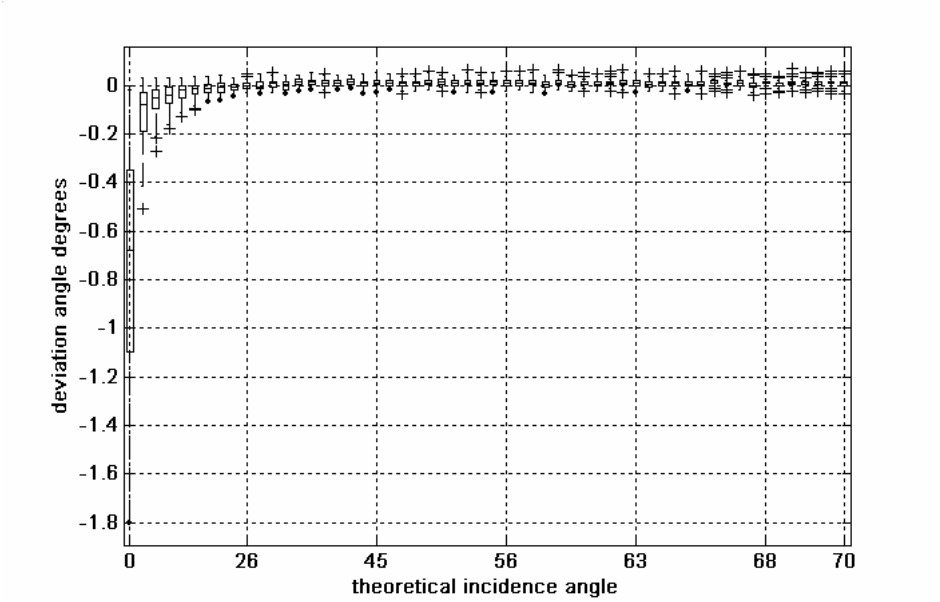

4.3.6 Seabed backscatter and spatial resolution

Seabed backscatter

The received seabed backscatter data from the EM1002 MBS (at nominally 95 kHz) in volts is band passed, envelope detected, squared and digitised at 11.973 kHz, segmented into each beam after beam forming and compensated for propagation losses. Simrad incorporates a seabed scattering theory and application that makes best use of the limited dynamic range of the electronics and printers they use (Hammerstad 1994). Simrad defines a bottom backscattering strength, BS, as the characteristic quantity for the seabed reflectivity following the sonar equation (refer to Sec. 3.3 Eq. 3.10; Hammerstad 1994). This parameter is calculated from the received echo level (EL), transmitter source level (SL), the two-way transmission loss (2TL) and the logarithm of the resolvable area A(θ_{ie}) on a horizontal flat seabed at emitted incident angle θ_{ie}, where:

$$BS(\theta_{ie}) = EL(\theta_{ie}) - SL(\theta_{ie}) + 2TL(\theta_{ie}) - 10\log_{10} A(\theta_{ie}) \quad \text{dB} \qquad (4.6)$$

The log of area A(θ_{ie}) at the centre of each beam is based on the beam geometry within the Simrad real time software and varies with seabed incidence angle, beam shape, pulse duration and range on a flat horizontal seafloor ignoring ray bending effects. Around normal incidence, the area (A_i) ensonified at the centre of each beam b_i on a flat horizontal seabed is approximated as a rectangle by (Simrad 1999c),

$$A_i = \frac{\psi_{x_i}\psi_{y_i}R_i^2}{\cos(\theta_{ie})} \quad \text{m}^2, \tag{4.7}$$

where ψ_{xi} and ψ_{yi} are the along and athwart -3 dB beam angles for beam 'i' in radians and R_i is the range in m (Fig. 3.1). As the incidence angle increases the area ensonified (A_i) at the centre of each beam changes from being beam width limited to pulse duration limited:

$$A_i = \frac{c\tau\psi_{x_i}R_i}{2\sin\theta_{ie}} \quad \text{m}^2, \tag{4.8}$$

where, c is sound speed in m.s^{-1}, τ is the pulse duration in s and θ_{ie} is the incidence angle of beam 'i' emitted from a horizontal platform (Fig. 3.1). The area A_i used in the Simrad (1999c) real time algorithm assuming a horizontal flat seabed is the minimum of Eq. (4.7) and (4.8) (Hammerstad 1994). Currently the Simrad EM1002 software only compensates for the ensonified area at the centre of each beam based on beam geometry and pulse length (Hammerstad 2000) and will be approximate for a flat horizontal seafloor. Within a beam the resolvable area on and off the centre of each beam needs to be calculated based on beam geometry, pulse lengths (Fig. 3.1) (de Moustier and Alexandrou 1991) and beam intensities to calculate an equivalent scattering area (Sec. 3.3.1).

The seabed backscatter will have both relative and absolute measurement errors. Absolute errors will be due to sonar system calibration, vessel motion and oceanic environmental conditions as well as the correction for the area ensonified based on the sonar beam pattern, seabed slope and transmission angles. The absolute level of backscatter requires correct estimation of the range compensation of absorption due to seawater (Francois and Garrison 1982) as well as the absorption due to surface bubbles (*e.g.*, Dalen and Lovik 1981). Relative changes in the backscatter level may be due to surface bubbles or depth dependent due to instrument parameters changing such as transmit power and pulse duration as well as range dependent due to incorrect assessment of absorption due to changing seawater properties. Absolute and relative changes in backscatter levels can occur with vessel motion, particularly with rate of change of pitch for multibeam systems (e.g. Stanton 1982). The following sections outline the source and magnitude of these errors.

Equivalent area estimate

The equivalent ensonified area as defined in Chapter 3 for seabed surface backscatter is the area ensonified on the seafloor that would have unity intensity over the beampattern. This is equivalent to the equivalent beam angle used in fisheries acoustics for volume scattering (MacLennan and Simmonds 1992). The equivalent seabed scattering area as a function of incidence angle is derived in Chapter 3 where at near normal incidence it is an ellipse (Eq. 3.12) and off axis a segment of an annulus approximated by a rectangle (Eq. 3.17). Figure 4.7 shows the equivalent ensonified area (Eq. 3.12 and Eq. 3.17) and the Simrad area (Eq. 4.7 and 4.8) as a function of incidence angle, depth 100 m, pulse duration 0.7 ms and EM1002 beam geometries assuming a flat horizontal seafloor (Fig. 4.7a). There is a small difference in the two ensonified area estimates that are used in the sonar equation that would affect the backscatter measurements. The highest difference (0.6 dB) occurs at less than 10^o near normal incidence and this difference reduces to -0.3 dB at 20^o and -0.35 dB at 70^o incidence (Fig. 4.7b). This backscatter measurement error will change depending on the pulse duration, range, incidence angle and beam patterns at each angle of incidence. Given the small difference between the two

estimates and without the actual calibrated beam patterns for the Simrad EM1002 no correction of the data collected has been applied for this parameter.

Figure 4.7 Estimates of the Simrad EM1002 ensonified area (a) based on Eq. 4.7 and 4.8 (dashed) and equivalent ensonified area based on Eq. 3.12 and Eq. 3.17 (solid) at 100 m depth and pulse duration 0.7 ms. Estimated seabed backscatter error, (b) between the two estimates of ensonified area in dB for incidence angles 0^o to 70^o on a flat horizontal seafloor.

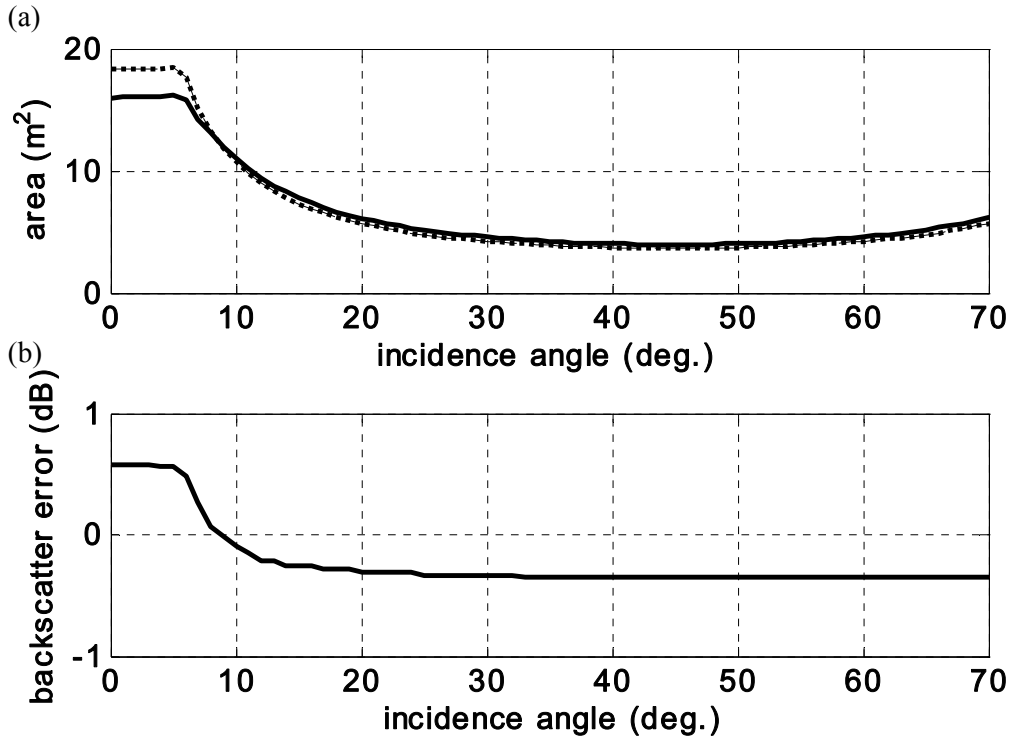

Spatial resolution

Figure 4.8 shows the area ensonified at a range of depths and pulse durations using the half power full angle beam patterns (Eq. (4.7) and Eq. (4.8)). At 100 m the area ensonified is approximately 18 m^2 on axis and varies between 4 to 6 m^2 off axis (greater than 20^o incidence) (Figs. 4.7 and 4.8). At 400 m depth the ensonification area on axis is 288 m^2 and varies between 42 – 65 m^2 off axis (greater than 20^o incidence) (Fig. 4.8). The transition between beam width limited area (Eq. 4.7) to pulse duration limited area (Eq. 4.8) occurs at 3^o, 6^o and 5^o at 50 m, 100 m and 400 m respectively (Fig. 4.8).

Figure 4.8. Simrad EM1002 seabed backscatter area (Eq. (4.7 and 4.8)) resolution at the center of each beam (A_i) on a horizontal flat seafloor for a range of incidence angles (0^o – 70^o), depths, 50 m (plus), 100 m (square) and 400 m (circle) at pulse durations of 0.2 ms, 0.7 ms and 2 ms respectively. Assumes a Simrad EM1002 with 2^o along-track and 3^o across-track conical receive beams.

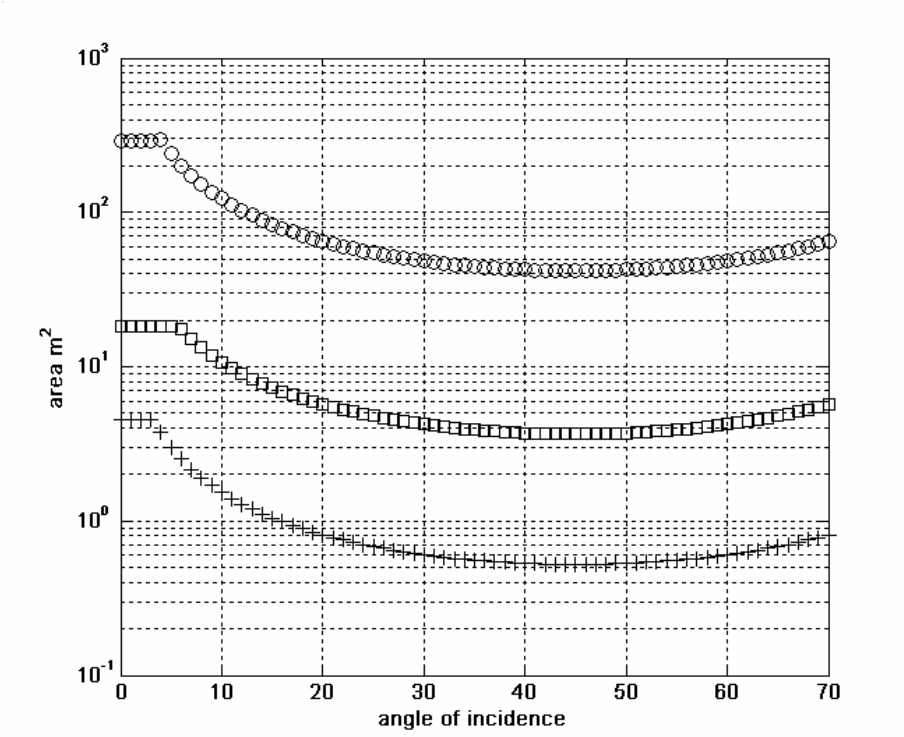

Similarly the length of the ensonified area at the beam centres on a flat horizontal seafloor is different in the along and across-track direction (Fig. 4.9). The along-track length at the beam centre (l_{x_i}) approximately corresponds to the combined transmit and received 3 dB beamwidth ψ_{xi} and range R_i :

$$l_{x_i} = \psi_{x_i} R_i \text{ m},$$

and the length in the across-track direction is approximately the minimum of

$$l_{y_i} = \frac{\psi_{y_i} R_i}{cos\theta_{ie}} \text{ m}$$

and

$$l_{y_i} = \frac{c\tau}{2\sin\theta_{ie}} \text{ m, Fig. 3.1.} \qquad (4.09)$$

These changes in sampling lengths along-track and across-track as a function of incidence angle and range will impact on the calculations of the local slope depending on the seabed topography.

Figure 4.9. Length of the ensonified region in the along-track (solid, Eq. (4.9)) and the across-track (dashed, min of Eq. (4.10 and 4.11)) directions at the beam centres for a horizontal flat seafloor at 100 m depth. Assumes a Simrad EM1002 with 2^o along-track and 3^o across-track conical receive beams and pulse duration 0.7 ms.

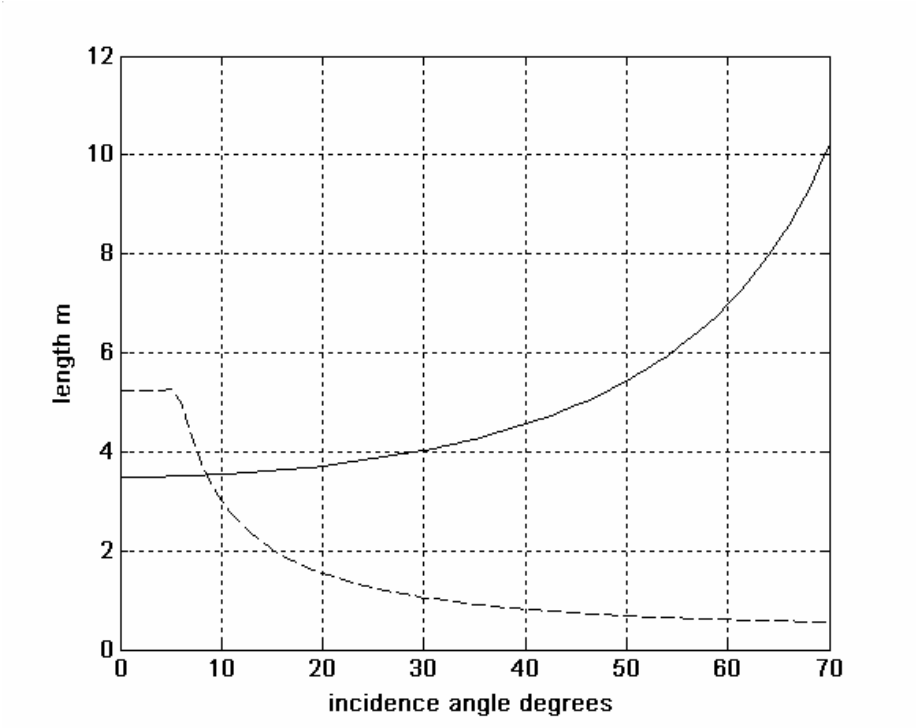

Seabed slope corrections

Across-track

It is important to distinguish between two major categories of across-track seabed slope, in terms of their influence on the area correction required. Firstly, if the seabed is across-track flat but sloping, the Simrad EM1002 MBS will treat the first return beam signal as the normal incidence beam, essentially relocating the central beam from vertical, as suits a horizontal seabed, to an off vertical orientation, normal to the across track slope. With this redefinition no change in area correction, compared with that from a horizontal seabed case, is required. Often, however, non –zero local deviations in the across track seabed slopes will be encountered. Under such conditions, variations of the area correction factors are required.

The seabed backscatter calculated from the Simrad EM1002 MBS assumes a flat seafloor (Eq. 4.8) which needs to be corrected for seabed slope (Hammerstad 1994). The real time seabed algorithms in the Simrad EM1002 calculate the area A_i compensation at the centre of each beam b_i at range R_i in metres where the minimum range R_I is assumed to be normal incidence (Eq. 4.7 and 4.8). Note that the area A_{ri} estimated at emitted angle θ_{ie} in the real time implementation of Eq. 4.7 and 4.8 in the EM1002 multibeam is approximated as the minimum of:

$$A_{ri} = \frac{c\tau\psi_{x_i} R_i}{2\left(\frac{\sqrt{R_i^2 - R_I^2}}{R_i}\right)} \text{ m}^2, \qquad (4.10)$$

and $A_{ri} = \psi_{x_i}\psi_{y_i}R_i^2$ m^2, Hammerstad (1994). (4.11)

This real time implementation of area estimation will be correct for constant across track slope where the minimum range R_I is used to determine the seabed normal incidence. The exact implementation of this algorithm in the Simrad EM1002 software is unknown as there is insufficient information in the data telegrams to calculate the exact area compensation applied for each beam.

Correction of the seabed backscatter data is required when there is a difference between the real time compensation and that calculated from the actual local seabed slope. The area A_{s_i} at beam b_i for a seafloor with across-track local slope of φ_{y_i} and small changes in along-track local slope φ_{x_i} and small angles of ψ_{x_i} is approximated using Eq. 4.7 and 4.8 by the minimum of,

$$A_{s_i} = \left| \frac{\psi_{x_i}\psi_{y_i}R_i^2}{\cos(\varphi_{x_i})\cos(\theta_{ie} - \varphi_{y_i})} \right| \text{ m}^2 \text{ and} \quad (4.12)$$

$$A_{s_i} = \left| \frac{c\tau\psi_{x_i}R_i}{2\cos(\varphi_{x_i})\sin(\theta_{ie} - \varphi_{y_i})} \right| \text{ m}^2 \text{ when } (\theta_{ie} + \varphi_{x_i} > 0) \quad (4.13)$$

for an effective incidence angle θ_{ie} emitted from a horizontal platform for beam b_i (modified from Hammerstad 1994). The area correction Λ_{Ai} in dB required on the estimated backscatter value $BS(\theta_{ie})$ (Eq. 4.6) from the real time implemented and measured local slope across-track seabed is from Eq 4.10, 4.11, 4.12 and 4.13,

$$\Lambda_{Ai} = 10\log_{10}\left(\frac{A_{si}}{A_{ri}}\right) \text{ dB}, \quad (4.14)$$

where the range to the beam centre R_i is directly measured by the MBS. Figure 4.10 shows the theoretical difference in the area compensation assuming the real time implemented area (Eq. 4.10 and 4.11) for a flat horizontal seabed and a measured local slope area (Eq. 4.12 and 4.13) difference of 0^o, 3^o and 10^o at each emitted incidence angle. The largest area correction Λ_{Ai} for a local slope difference occurs at the beamwidth and pulse duration limited area transition zones (Fig.4.8, Fig. 4.10). As the difference in real time applied and local slope increases (10^o) the correction reaches a maximum of 4.2 dB with an absolute average of 1.2 dB (Fig. 4.10). For differences in slope less that 3^o the maximum absolute compensation of the collected Simrad EM1002 data is 1.8 dB with an average of 0.4 dB. It should be noted that the theoretical correction near normal incidence shown in Figure 4.10 may be difficult to realise in practice. Near normal incidence it would be difficult to have a constant range whilst also having high changes in the angle of incidence to the seabed.

The corrected backscatter data is displayed at the seabed incidence angle after applying both the area correction (Eq. 4.14) and the difference in seabed local slope and emitted incidence angle. In this work area corrections were not applied until the difference in applied and measured seabed slope exceeded 3^o due to the difficulty in accurately measuring local slopes less than this. A local seabed slope difference of less than 3^o would nominally require a correction less than 0.4 dB which is also the minimum resolution of the EM1002 backscatter quantisation. Note that for more complex topographies the slope error as a function of incidence angle would be different to that based on the applied Simrad area using the minimum range criteria.

In this study the hard rough reference sites were based on low relief limestone outcrops where the between beam across-track slope was typically less than 3° (Fig. 4.5). The roughest training site required a seabed slope correction of peak values of 6 dB (mean 1.8 dB) for a near central beam. For this rough site 10 % of the data required a correction greater than 0.5 dB.

Figure 4.10. Area compensation (Λ_{Ai} , Eq. (4.14)) required from that implemented in the real time Simrad algorithms (A_{rti}) assuming a real time implemented incidence angle and measured local seabed incidence angle difference of 0° (solid), 3° (dash-dot) and 10° (dot) at constant range (positive starboard up). The emitted angle from the vessel ranges from -70° to 70°, assumes a Simrad EM1002 with 2° along-track and 3° across-track conical receive beams at 100 m depth and pulse duration of 0.7 mS.

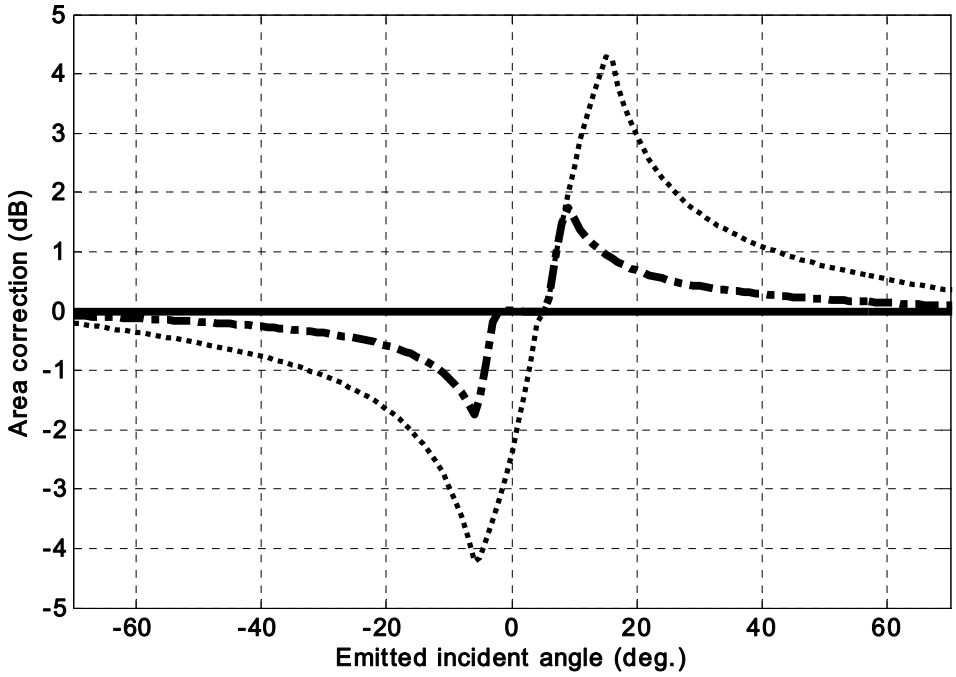

Along-track

For small changes in slope or pitch within the beam limited region in the along-track direction φ_x the area changes as a function of the inverse cosine of the slope (Eq. 4.7). As the along-track slope increases the area ensonified changes from being beam limited to pulse duration limited where based on Eq.(4.9 and 4.11) for small ψ_{x_i} the width l_{xsi} of the along-track region is approximately the minimum of,

$$l_{xsi} = \frac{\psi_{x_i} R_i}{\cos(\varphi_x)} \text{ m, and} \tag{4.15}$$

$$l_{xsi} = \frac{c\tau}{2\sin(\varphi_x)} \text{ m,} \tag{4.16}$$

at each angle of incidence. The area correction Λ_{As} in dB required on the estimated backscatter value $BS(\theta_{ie})$ (Eq. 4.6) from the assumption of a horizontal to along-track sloping seabed is from Eq (4.9, 4.15, 4.16),

$$\Lambda_{As} = 10\log(\frac{l_{x_i}}{l_{xsi}}) . \quad (4.17)$$

Corrections for along-track slope of less than +/- 5^o are negligible in the beamwidth limited region at 100 m depth, pulse duration 0.7 ms and ψ_{x_i} = 0.0349 (2^o) (Fig. 4.11). The correction for along-track slope is greater than 0.5 dB above +/- 6.5^o (Fig. 4.11). Similarly, in the pulse duration limited region the area correction would be less than 0.5 dB for slope variations along-track less than 6.5^o. In this thesis corrections for seabed backscatter in the along-track direction were not applied if the combined vector of along-track seabed slope and pitch of the vessel did not exceed 6.5^o. In the reference site analysis outlined in Chapter 6 pings with a combined pitch and slope along-track of greater than 6.5^o were excluded from the analysis.

Figure 4.11. Area correction in dB required for along-track slope change of –10^o to 10^o within the beam width limited region at 100 m depth and 0.7 ms pulse duration.

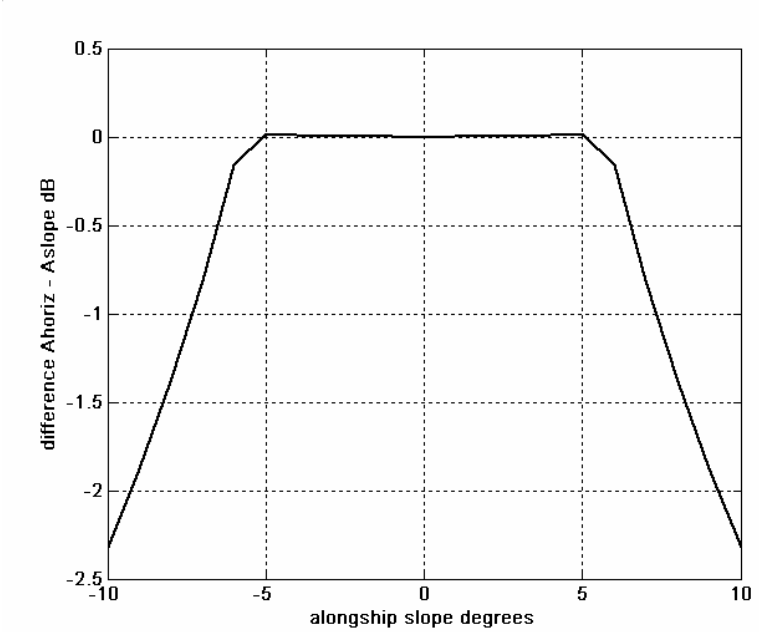

Seabed backscatter beam pattern correction

Incorrect calibration of the combined transmitter and receiver beam pattern for beam b_i needs to be corrected. Often there is a large uncertainty in the beam pattern of the transmitter across track where the intensity can vary by +/- 2 dB (Simrad data sheet EM1002). This error is often observed in the acoustic data as lines of low and high intensity parallel with the ships track when the vessel is relatively stable and the seabed is horizontal and of uniform composition (Fig. 5.8). A method of minimising this effect without detailed calibration of the beam pattern is to use a flat and homogenous training zone to calculate intensity corrections per emitted incidence angle (e.g. Hellequin *et al.,* 2003). Due to vessel motion the emitted incidence angle beam correction varies for active roll compensated multibeam sonars (e.g. Simrad EM1002) and impacts both the absolute and relative angular backscatter measurements. No correction has been applied in this work due to the variety of sea states and vessel motions encountered.

Also due to the non ideal and finite beam width/pattern of MBS beams the backscatter value at a given incidence angle can be influenced by signals off the angle of incidence (Hellequin *et al.,* 2003). This beam pattern induced change to the expected backscatter at a given incidence angle

is most noticeable near normal incidence (less than 10°) where the ensonified across-track length, l_{y_i} (Eq. 4.10), is large (Fig. 4.9) and the rate of change of backscatter to incidence angle is the highest (Ch. 3 Fig. 3.5; Hellequin *et al.,* 2003). The error predicted by Hellequin *et al.,* (2003) will depend greatly on the signal processing method employed near normal incidence and the seabed type. The Simrad EM1002 method of picking the peak digitisation point as a representative of the seabed backscatter near normal incidence would reduce this error to be less than +/- 1dB (Hellequin *et al.,* 2003, fig. 4). This error is related to the seabed type and is more significant on soft seabed types such as coarse silt and sandy mud where there is a large decline after the initial high return at normal incidence (Chapter 3 Fig. 3.5). As the same instrument was used throughout this study, backscatter variation near normal incidence will act as an absolute error but will have the same relative error for similar seabed types. No correction for this less than 1 dB error near normal incidence is carried out within this data analysis.

Sound absorption corrections

A major source of variability in relative seabed backscatter measurements can be due to differences in the applied and measured absorption during transmission through seawater. At 95 kHz the absorption of sound in seawater (Francois and Garrison 1982) varies significantly due to temperature, pressure (depth) and salinity (Fig. 4.12). A variation from 10 °C to 15 °C causes a 3 dB km^{-1} change in absorption. This 5 °C temperature range is common within the study area due to the mixing of warm East Australian current water and the colder Southern Ocean mode water.

Figure 4.12. Variation of the absorption dB km^{-1} in seawater based on Francois and Garrison (1982) at a base case of frequency 95 kHz, pH 8, temperature 15 °C, depth 0 m, and salinity 35 ppt (asterix) and variations of temperature (5 °C to 30 °C), depth (0 to 300 m) and salinity (33 to 36 ppt).

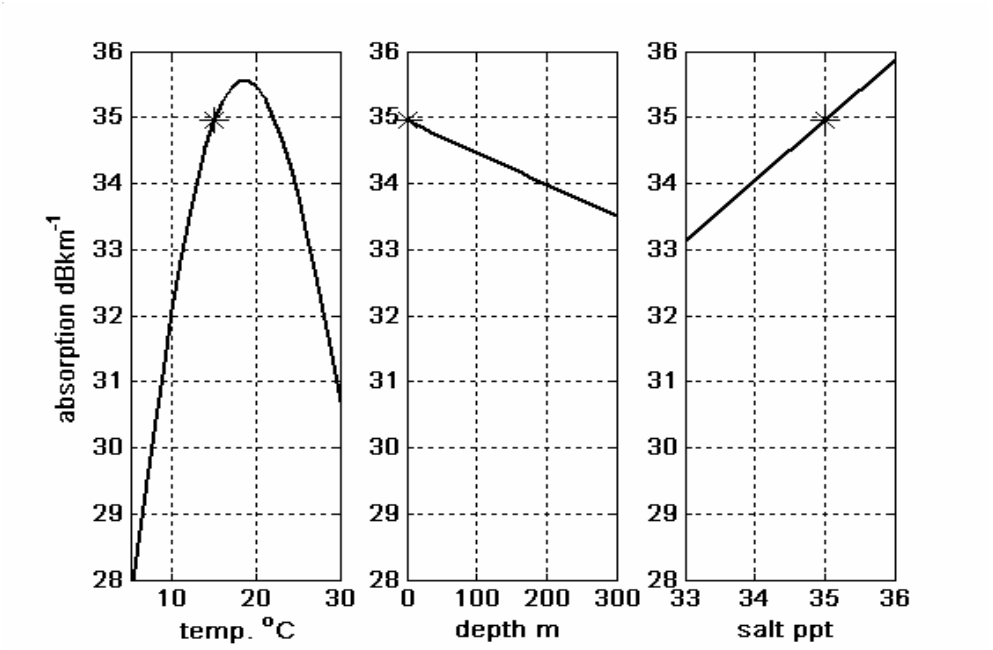

The error in measured seabed backscatter as a function of depth (D), incidence angle (θ) on a flat horizontal seafloor due to the difference in the applied and measured absorption ($\Delta_{\alpha_{set}-\alpha_{measured}}$) is,

$$Error_{\alpha} = \frac{2D}{\cos\theta}\Delta_{\alpha_{applied}-\alpha_{measured}} \text{ dB.} \quad (4.16)$$

At 200 m depth on a flat horizontal seafloor the error in the measured seabed backscatter for $\Delta_{\alpha_{set}-\alpha_{measured}}$ of 5 dB ranges from 2 dB at normal incidence to 6 dB at 70^{o} incidence (Fig. 4.13). The absorption of sound in seawater is also influenced by the present and past sea conditions as well as the vessel steaming direction due to subsurface bubbles (*e.g.* Dalen and Lovik 1981). Dalen and Lovik (1981, fig. 12) show that at 120 kHz there is a strong relationship with total attenuation and wind speed for a transducer deployed 5 m below the surface on the hull of a vessel. They estimate a total attenuation due to bubbles of 2.7 dB and 10 dB at 38 kHz and 120 kHz respectively for a wind force of 20 knots. The presence of bubble interference can be obvious in the data due to inconsistent backscatter within and between pings of very low intensity that may be associated with excessive ship motion. Micro bubbles can be present at 10 m or more below the surface and attenuate the seabed backscatter returns with no obvious deterioration to the data .

Figure 4.13. Error (dB) in the measured seabed backscatter for absorption error ($\Delta_{\alpha_{set}-\alpha_{measured}}$) of 1 dBkm^{-1} (solid), 5 dB.km^{-1} (dashed) and 10 dB.km^{-1} (dotted) at transmission angles (θ) 0^{o} to 70^{o} on a horizontal seafloor at 200 m depth (D).

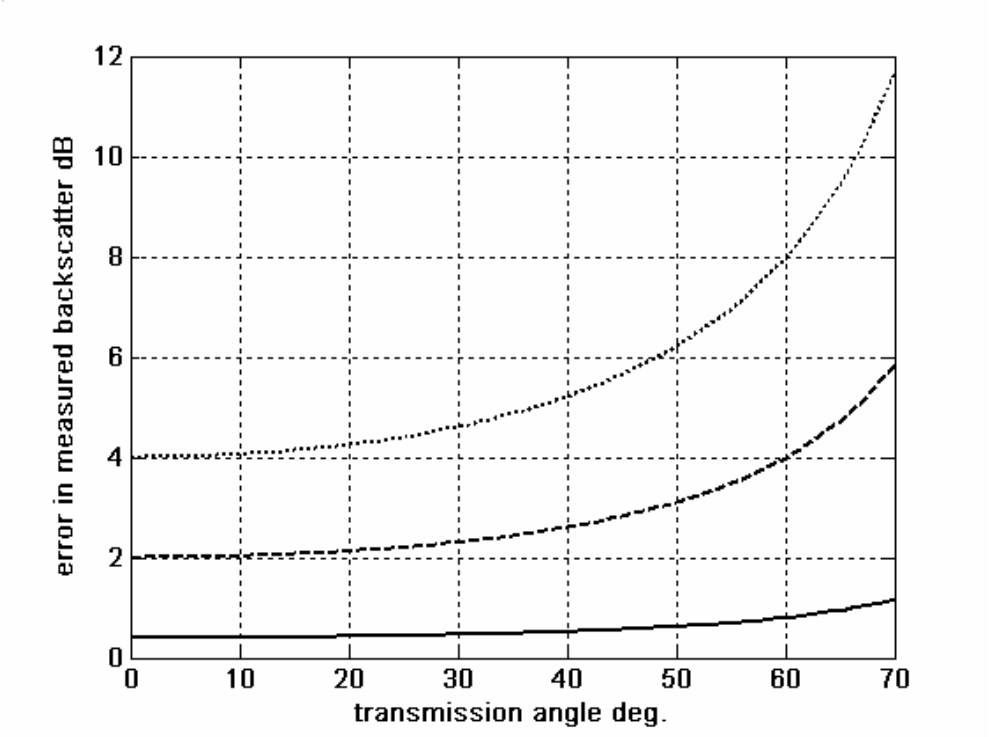

Noise effects

The EM1002 MBS backscatter and bathymetry data are affected by both instrument self-noise and environmental noise. A common and dominant noise source on ships is that due to the vessel's propeller and engine which is usually speed dependent and varies with sea state (Ron Mitson pers. comm. April 2003). A noticeable effect of vessel noise is a gradual increase in apparent seabed backscatter at deeper depths due to the time varied gain (TVG). Observations of backscatter over a gently sloping seabed showed that beyond approximately 500 m depth the recorded EM1002 backscatter gradually increased. Therefore, data collected at greater depths need ideally to be corrected for noise. No independent measure of background noise is recorded with the Simrad EM1002 data and in this analysis data deeper than 500 m are excluded. Other sources of noise can also influence the backscatter recordings at all depths (e.g. other instruments, vessel, biological and environmental). A good indicator of a noisy environment is when the bathymetric data degrades. A common effect is aeration near the transducer due to bubble sweep down causing, at its worst, complete loss of signal and, less noticeably, a slightly attenuated signal. Bubbles in the surface layers due to waves can attenuate the backscattered signal but may not degrade the bathymetry in any noticeable way.

4.4 Video system

4.4.1 Background

Remote optical observations of the seabed are carried out using light from either passive or active illumination. Passive illumination includes sunlight and bioluminescence but more commonly in deep-water active illumination systems with strobe or continuous illumination are used. The illumination range of optical images in marine environments is increased using very narrow beam artificial illumination by pulsed or continuous broadband/monochrome lasers. These systems allow the camera and light source to be closely spaced whilst still achieving a high range (attenuation lengths of 3 to 7, Jaffe *et al.,* 2001, fig. 1). Using a camera and wide light source closely spaced can achieve operating ranges of 1-2 attenuation lengths depending on water column backscatter whilst range gated and synchronous scan optical systems achieve 3-7 attenuation lengths but at much higher costs (Jaffe *et al.,* 2001, fig. 1). Due to cost and availability a simple video system with close illumination was used to observe the seafloor in this study. The objectives for seabed observations were to have continuous geolocated observations of the seafloor to describe the geomorphology, substrate and associated macro epifauna (visible by eye, 2 to 4 cm). Towing a video platform with associated acoustic geolocation beacon (USBL) close to the seafloor achieved this aim. Decoupling of the ship's motion using a two-bodied towing configuration provided stability to the imagery (Barker *et al.,* 1999, Fig. 5.1).

4.4.2 Video Equipment and Methods

The camera system utilizes two separately housed, "broadcast quality" digital Sony DVCAM format cameras; and lighting was provided by two 250 watt Deep Multi Sealites. The video system was controlled via a conductive tow cable (details in Appendix B.2). The control system enables the operator to switch the lights, lasers and cameras on and off and allow continuous monitoring of system battery voltage, pitch, roll and depth. Digital video imagery, with lasers for scaling, was collected in mono- and stereo by using one or both cameras in the array. Images were used to identify substrate type (S), geomorphology (G), faunal community group (F) and abundance of fauna (A). Fauna and geomorphology size (cm) was estimated in the X and Y planes using four (8 mW) red lasers projected into the field of view. These are arranged around the camera housing, three parallel to the focal axis and one crossing at a pre-determined

angle (Barker *et al.,* 2001). Attributes of the seabed video were scored at 1 s intervals (approx. 0.25 m) in four categories: substrate (7 types), geomorphology (10 types), fauna (10 types) and faunal abundance (3 types) (Table 2.4). These data were geo-located using the ship's GPS position and the Sonardyne tracking beacon attached to the video (Kloser *et al.,* 2001b).

4.4.3 Resolution and Categories

The video system was towed at speeds of 0.5 to 1.0 $m.s^{-1}$ and nominally 1 m above the seafloor with the camera 30^o incident to a flat seabed. The active lights illuminated an area on the seafloor described approximately by a trapezium (Fig. 4.14). A large object first scored on the periphery of illumination and sampled at 1 s intervals would be recorded 4 to 8 times in the illumination area depending on vessel towing speed. This over sampling that effectively lengthens seabed patches by 2.5 to 3.5 m was removed when patch sizes were calculated. Resolution of seabed characteristics improved as objects moved closer to the camera increasing the pixel density per unit area. In general the area viewed by the camera ranged from 4 to 7 m^2 , and varied depending on the height of the camera to the seabed (Fig. 4.14).

Figure 4.14. Illumination (plan and elevation in cm) of the seafloor with camera and light at 30^o incidence and 101 cm above the seafloor.

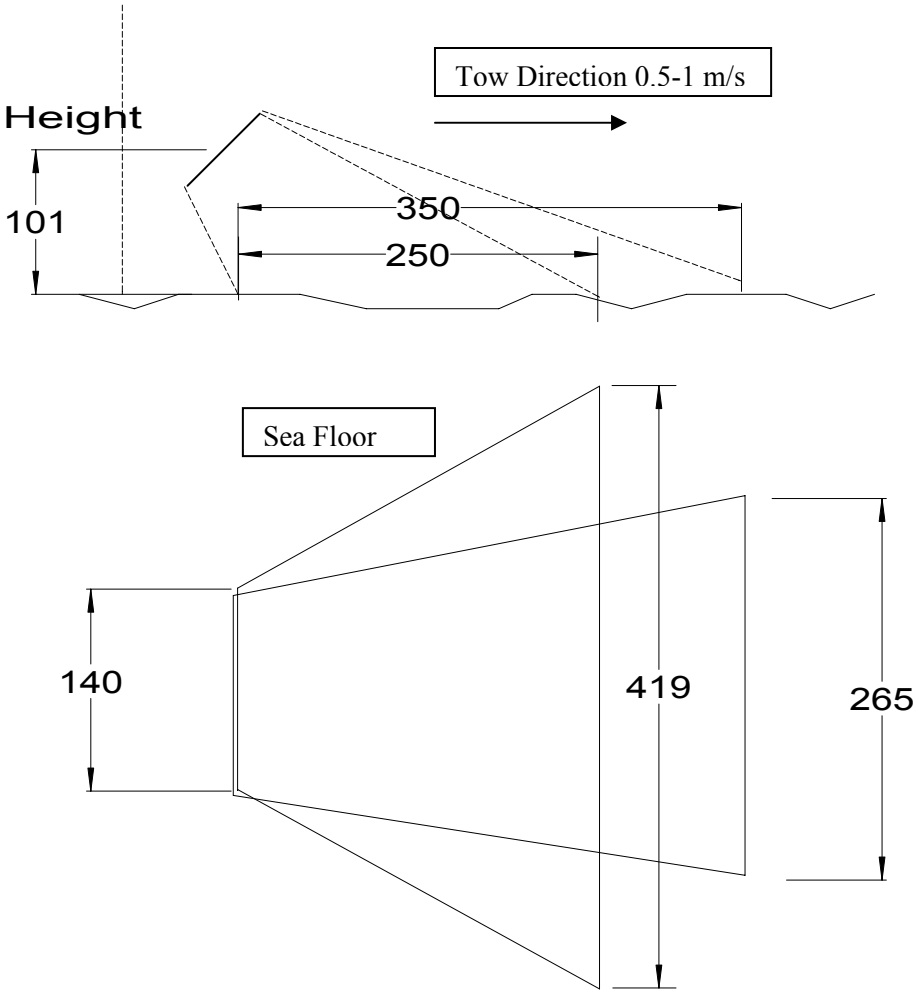

The TV display screen, CCD (charged coupled device) pixel resolution and illumination area defined the video resolution (Table 4.3). Videographic data were scored by viewing a TV-PAL monitor of 538 pixels horizontal resolution and 576 vertical active lines with a refresh rate of 25

Hz. Screen captures from the digital cameras obtained at the CCD were 752 pixels wide and 582 pixels high. From these images dimensions were measured using Optimus software and scaled by calibrated lasers (Barker *et al.,* 2001). Based on the pixel resolution measurements on objects could not be made with an accuracy of better than approximately 1 cm and in general organisms could not be identified at less than 2 to 3 cm. Due to the high sample rate of the video (25 Hz) improved resolution was possible for smaller scale features such as fine sediment clouds (Table 4.3).

Table 4.3. Resolution of the video system at center of viewing from visual viewing and digital screen captures range length 250 – 350 cm (vertical V) and center width 203 and 280 cm (horizontal H).

Image type	Pixels		Resolution cm		Comments from visual description
	H	V	H	V	
TV PAL – single frame	538	576	0.38-0.52	0.43-0.61	Can identify objects of greater than 2-3 cm close to the camera.
Continuous frame 25 Hz					Due to over sampling can observe smaller scale features and effects (i.e. sediment disturbance clouds)
Digital screen grab	752	582	0.27-0.37	0.43-0.60	Can identify objects of greater than 2 cm close to the camera

4.4.4 Geolocation of video

Accurate geolocation of the videographic data was required to correlate with the georeferenced acoustic data. A Sonardyne ultra short base line (USBL) system was used that placed a transmitter/ receiver on the camera system and a receiver/transmitter on the ship (Fig. 5.1). The accuracy of position fixes was dependent on the motion and position correction of the vessel, sound speed profile between the receiver and transmitter and the resolution of the phase measurements at the receiver (Kloser *et al.,* 2001b). The error of positioning is estimated to be 5 m at ranges of 200 m and 20 m at ranges of 1500 m when the sound velocity profile is correctly applied (Kloser *et al.,*2001b). The range to the camera system towed at 0.5 to 1 $m.s^{-1}$ was approximately 2 times the water depth. Therefore, the theoretical positioning error at 100 m and 200 m depth is less than 5 m and 10 m respectively. In practice vessel movement and incorrectly applied sound velocity profiles increased this positioning error.

4.5 Summary

This chapter outlines the acoustic and video equipment used in the field sampling to be discussed in Chapter 5 and their associated spatial scales and derived metrics. The video system operated at nominally 1 m above the seafloor with a view area of 4 to 7 m^2 and along narrow strips at 0.5 to 1 m/s covering between 0.007 $km^2\ hr^{-1}$ to 0.025 $km^2\ hr^{-1}$ independent of depth. The MBS does not view the seabed at one scale but its coverage and resolution changes with depth, pulse duration and incidence angle (range). The across-track coverage at a maximum of 140^o angular spread is 5.5 times the water depth for a flat horizontal seafloor. At 100 m depth and 5 ms^{-1} vessel speed the coverage is 9.9 $km^2\ hr^{-1}$. The resolution of the backscatter (beam intensity limited at half power levels) at 100 m depth and 0^o, 30^o, 60^o and 70^o incident to a flat seafloor is (18, 4, 4, 5.5) m^2. The backscatter resolution is reduced further according to the ensemble of along and across track values used in the algorithm.

The precision of the backscatter measurements (quantised to 0.5 dB) at a given incidence angle is dependent on the correction for ensonified area, vessel motion, seabed slope, noise and signal absorption effects as well as the power and pulse duration of the transmitter and stability of the

receiver. No independent measure of the MBS stability was carried out although it is assumed that with modern electronics this remains stable within +/- 0.5 dB throughout the two month survey. Absorption corrections due to local seawater conditions were made and remaining error is estimated to be small and less than 1 dB at maximum range of 70^{o} incidence angle (Fig. 4.13). Corrections of the Simrad EM1002 data due to angular differences less than 3^{o} between the real time applied area and the area estimated using the local slope were not implemented as the mean correction was less than 0.4 dB between –70^{o} and +70^{o} incidence (Fig. 4.10). The largest corrections for changes in slope due to a rough seabed occur at the transition zone of beam limited to pulse duration limited area ensonification (Fig. 4.10). Similarly no correction was applied for the difference in area compensation due to –3 dB beamwidth or equivalent beamwidth assumptions; this error (<0.6 dB) has its greatest impact when using the data as absolute values (Fig. 4.7). Another backscatter measurement error occurs due to intensity variations in the transmitter beam pattern (+/- 2 dB) and receiver transducer gains. If these are not correctly calibrated, lines of high and low backscatter are observed along the vessels track (Fig. 5.8). Due to vessel motion this effect will impact both the absolute and relative angular backscatter measurements. No correction has been applied in this work due to the variety of sea states and vessel motions encountered. As the EM1002 instrument was not calibrated or the beam patterns at each angle of incidence known all backscatter values presented here are relative values.

When creating a square georeferenced grid of the bathymetric and backscatter data (the most usual way to interpret the MBS data) the achievable grid size provides a guide to the available resolution, which changes as a function of depth (Table 4.2). These grid sizes assume at least two data points within a grid cell and indicate a minimum grid size requirement of 2.5 m side length at 50 m depth and 30 m at 600 m depth. At 100 m depth the minimum grid size is 5 m side length which is within the across track beamwidth resolution of the Simrad EM1002 (full angle –3 dB power levels) but would be less than the along-track resolution for incidence angles >45^{o} (Fig. 4.8). The changing shape of the sampling area (Fig. 4.7 and 4.9) due to incidence angle on the seafloor changes the resolution and correlation between grid values at these minimum grid sizes. The grid size resolution of the Simrad EM1002 MBS ranges from a couple of m to 10’s m depending on depth and that of the video is usually less that 0.1 m (0.02 m at close range) when within illumination range of the seafloor.

5 Field experiment

5.1 Introduction

A specifically acquired multibeam sonar (Simrad EM1002) and a three frequency (12, 38 and 120 kHz) normal incident echo sounder (Simrad EK500) on the 65 m research vessel *Southern Surveyor* were used in conjunction with a suite of biological and physical sampling gear (Fig. 5.1) to sample and map a range of survey areas in April-May 2000. Survey areas ranged in depth from ~12 m to ~1200 m on the continental shelf and slope in the South East Region and the Great Australian Bight (GAB) (Fig. 5.2 to 5.6; Table 5.1). In this thesis, reporting will concentrate on the Simrad EM1002 MultiBeam Sonar (MBS) data collected from 50 – 600 m depth. Full details of the voyage of Southern Surveyor 01/00, April 4 to May 21 are given in the cruise report (CMR, 2000), acoustic, biological and physical data in Kloser *et al.* (2001b) and specific geological analyses in Harris *et al.* (2000).

The survey objectives relevant to this thesis are:

- map selected areas of seabed on the continental shelf and upper slope with a MBS (Simrad EM1002) to evaluate its capability for mapping and classifying seabed types based on bathymetric and backscatter data.
- characterise the physical and biological attributes of these areas by sampling of sediments, consolidated sediments, invertebrates and fishes with a video camera, box corer, rock dredge, benthic sled and fish trawl.
- acquire water current and water column profile data for comparison with hydrodynamic climatology, and acoustic propagation calculations.
- acquire digitised acoustic data from the single-beam Simrad EK500 (12, 38 and 120 kHz).

In this chapter, the data from this field survey are treated generally and aspects of the data at several scales are discussed, but the focus here is on the utility of MBS for characterising seabed terrains and habitats at large scales (1 - 10s km). At this scale a major factor in determining the terrain is the information on seafloor morphology provided by the MBS.

5.2 Survey design

The survey design targeted biological and physical sampling based on information provided by acoustic MultiBeam Sonar (MBS) maps; survey areas included regions already known from existing data and across-shelf transects. The sampling occurred in three regions, Twofold Shelf, Coorong and Eucla (IMCRA 3.3 1998, Fig. 2.4). Within these regions survey areas represented a broad range of seabed types (based on bathymetry, geomorphology (slope and roughness), substrate type and location) and characteristic benthic fauna, and typically have high importance for fisheries (Fig. 5.2) (Bax and Williams 2001; Kloser *et al.,* 2001a). Cross-shelf coverage was completed in all regions with sampled depths approximately 50 m, 100 m, 150 m and one upper slope 200- 500 m zone (Table 5.1 and Fig. 5.3 to 5.5). Based on a historic database of existing biological and geological physical samples (Bax and Williams 2001), greater swath sampling effort occurred in two general areas of the Twofold Shelf region to provide extensive profiles of seabed habitats and associated biota from a near-shore (inner shelf) environment to the outer shelf Howe Reef and upper slope Big Horseshoe Canyon (Fig. 5.3).

The MBS mapped areas were designed to provide locations of accurately described “reference” sites for the subsequent targeted biological and physical samples (Table 5.2). The physical and biological attributes of seabed biotopes were assessed by sampling sediments, consolidated sediments, invertebrates and fishes with a box corer, rock dredge, benthic sled and fish trawl as

well as by obtaining video images. Sampling was targeted by using maps of bathymetry, bathymetry texture (shaded-bathymetry) and backscatter (centre of each beam backscatter CBB) from the EM1002 MBS produced on board (Fig. 5.6). Sampling device geolocation on the seafloor was directed using the vessel's dynamic positioning system and a Sonardyne ultra short base line (USBL) acoustic positioning system (Kloser *et al.,* 2001b). In general the geolocation of sampling gears could be positioned with respect to earth coordinates (WGS84) to within 5 to 10 m for depths less than 300 m.

Table 5.1 Areas sampled within biogeographic regions during survey SS01/00 using the Simrad EM1002 MBS showing, area, depth range, pulse length and on-board produced bathymetric grid. Regions 1, 2 and 3 are Twofold Shelf, Coorong and Eucla respectively.

Region #	Area #	Area Name	Area (km^2)	Depth range (m)	Pulse Length (μs)	Bathymetry Grid Size (m)
1	1	Disaster Bay	35.4	38 to 86	200	10 - 20
1	2	Howe Reef	144.1	95 to 140	200	20
1	3	Gabo Reef	45	114 to 120	700	20
1	4	Point Hicks	9.6	12 to 58	200	10
1	5	Broken Reef	34	112 to 116	700	20
1	6	Big Horseshoe SE	511	200 to 600	2000	20 -50
1	7	Big Horseshoe (west)	200	120 to 600	700/2000	20 - 50
2	8	Lacepede Shelf 40	3	43 to 49	200	10
2	9	Lacepede Shelf 80	19	72 to 86	200/700	20
2	10	Lacepede Shelf 120	23.3	90 to 250	700	20
3	11	GAB BPZ 50	9	50 to 60	200	10
3	12	GAB BPZ 90	24	92 to 98	200	20
3	13	GAB BPZ 140	81	130 to 160	700	20
3	14	Outside GAB BPZ 140	24	120 to 150	700	20

Table 5.2 Physical and visual operation types and frequency within survey areas during SS01/00 (Kloser *et al.*, 2001b; "S"=existing data from previous surveys, Bax and Williams [Eds] 2000). Note only invertebrates retained from the benthic sled sampling devices are shown here.

Area	Name	Sediments	Rocks	Video	Invertebrates
1	Disaster Bay	13	-	2	S
2	Howe Reef	9	4	1	S
3	Gabo Reef	8	1	1,S	1, S
4	Point Hicks	1	S	1	S
5	Broken Reef	11	1	1	1,S
6	Big Horseshoe SE	14	7	7	13
7	Big Horseshoe (west)	15	-	3	S
8	Lacepede Shelf 40	6	1	-	-
9	Lacepede Shelf 80	4	1	1	-
10	Lacepede Shelf 120	5	1	2	-
11	GAB BPZ 55	4	1	2	1
12	GAB BPZ 90	2	1	2	1
13	GAB BPZ 140	8	1	3	2
14	Outside GAB BPZ 140	2	1	1	1

Figure 5.1. The range of acoustic and ground-truth sampling gears used from Southern Surveyor during mapping survey SS01/00. For detailed specifications of the equipment refer to Kloser *et al.* (2001b).

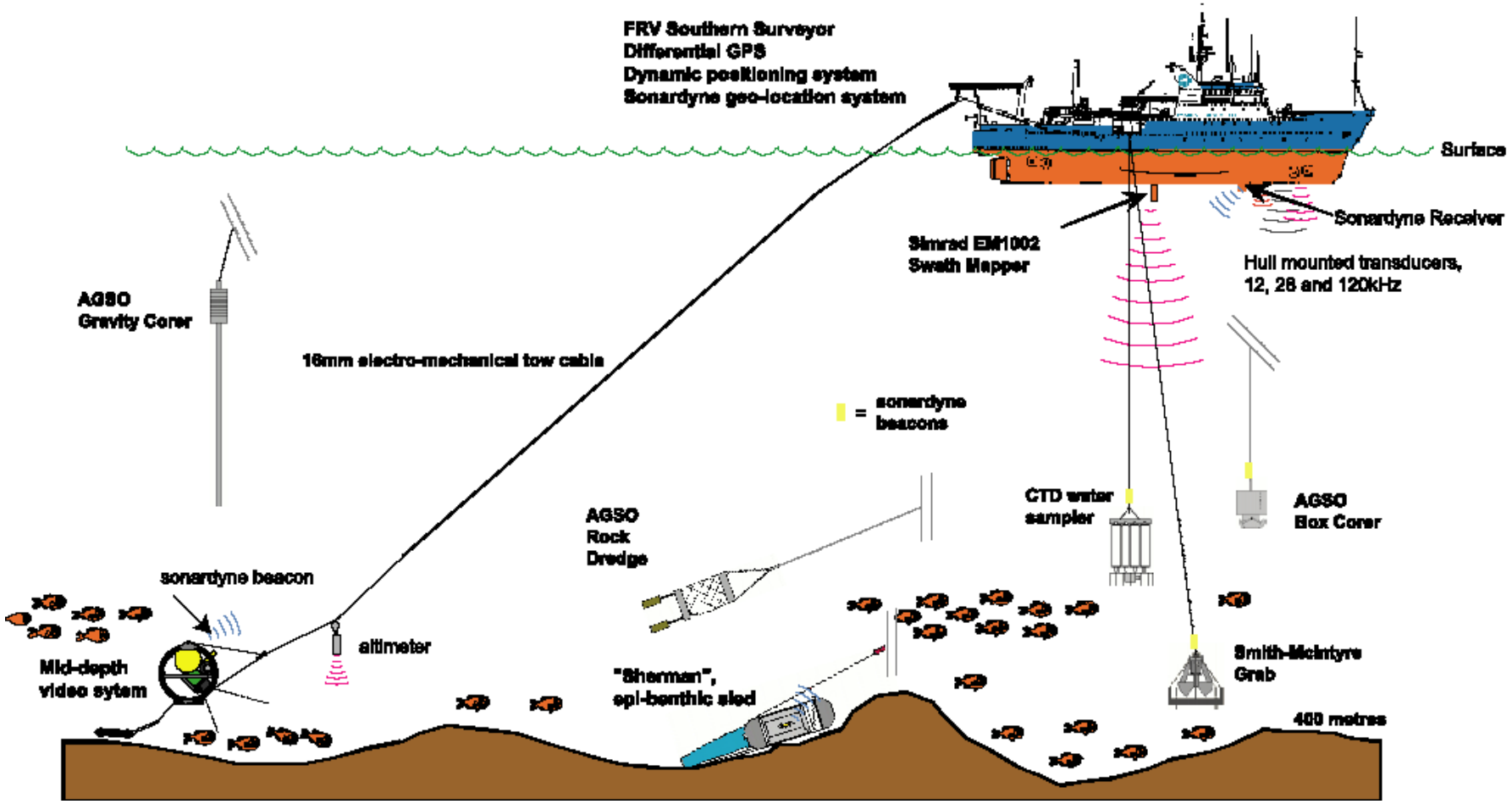

Figure 5.2 Map showing the general locations (small and large black dots) of survey areas during SS01/00 at a regional scale.

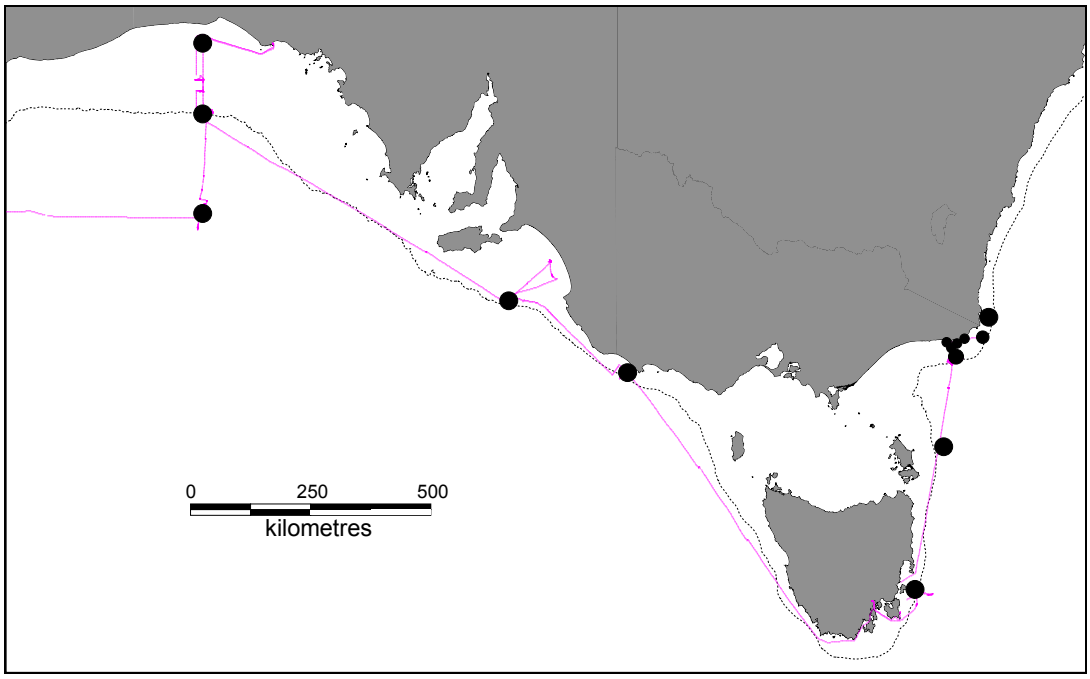

Figure 5.3 Map of MBS survey track areas mapped in the Twofold Shelf and upper slope region 1. Areas used in this analysis are named and numbered as per Table 5.1.

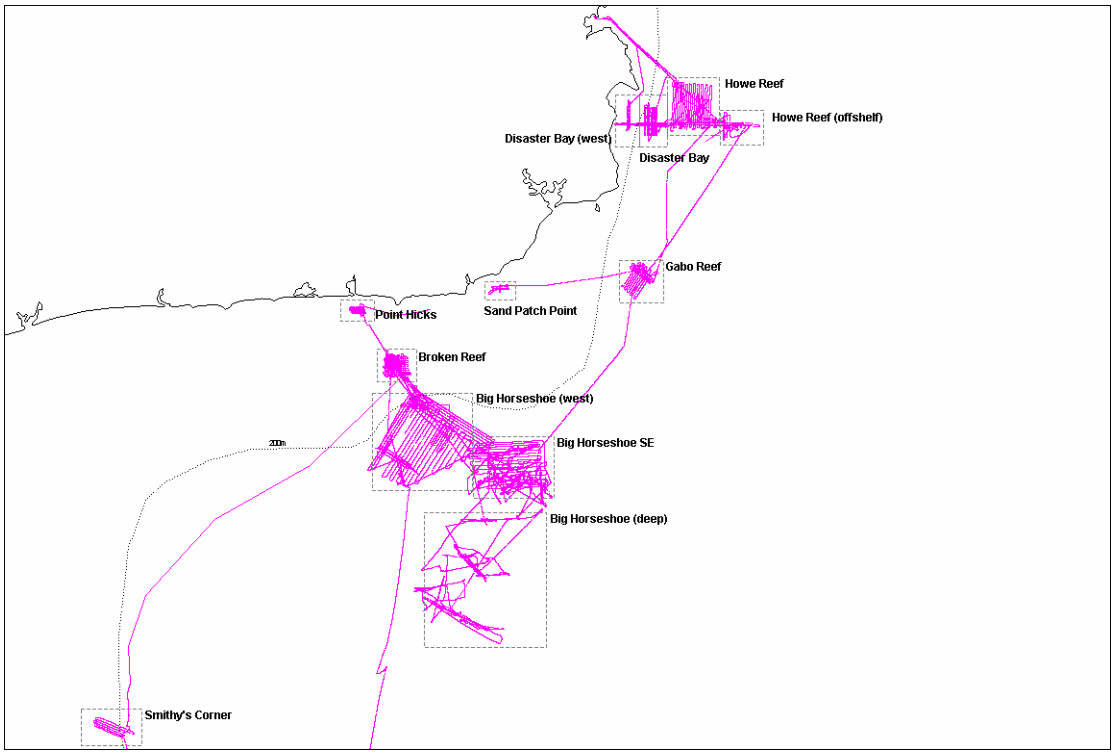

Figure 5.4 Map of MBS survey track areas mapped in the Coorong region 2. Areas are named and numbered as per Table 5.1.

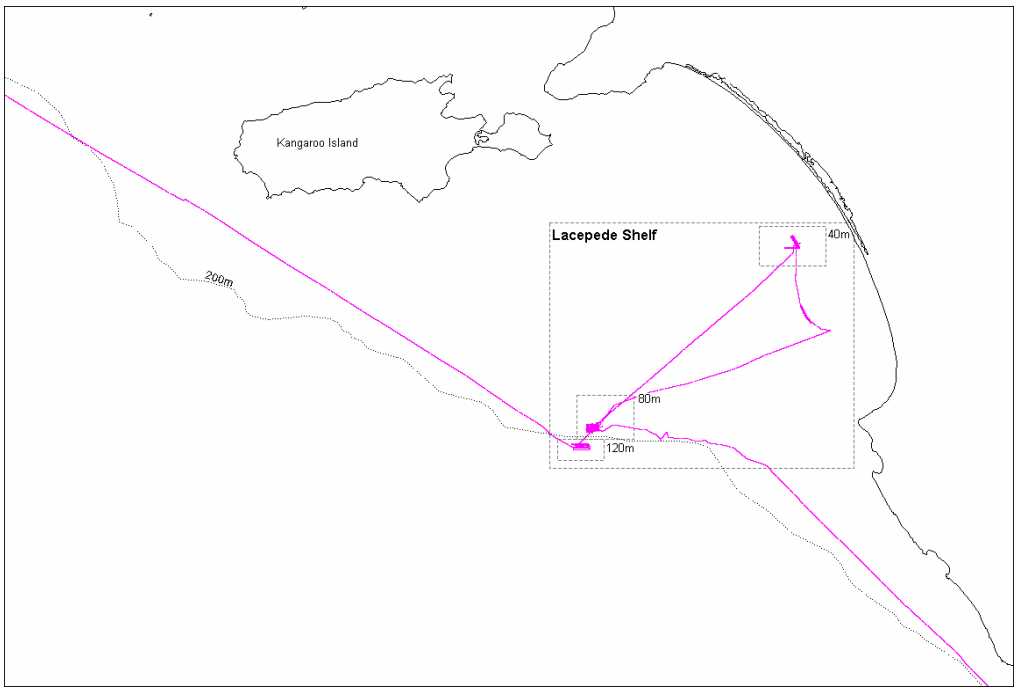

Figure 5.5 Map of MBS survey track areas mapped in the Eucla region 2. Areas are named and numbered as per Table 5.1. Also shown is the Great Australian Bight Benthic Protection Zone (GAB BPZ).

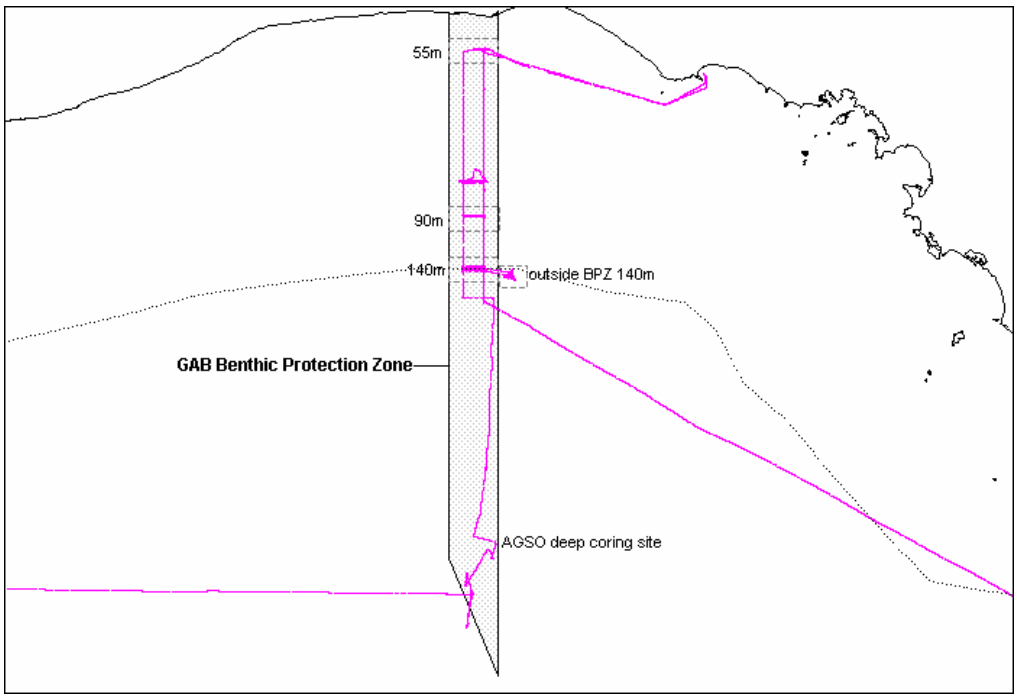

Figure 5.6 Example of MBS mapped Area 3 (Gabo Reef) showing bathymetric texture (shaded-bathymetry, 8 times vertical exaggeration), acoustic reference sites marked and associated targeted video and sediment grab/core stations.

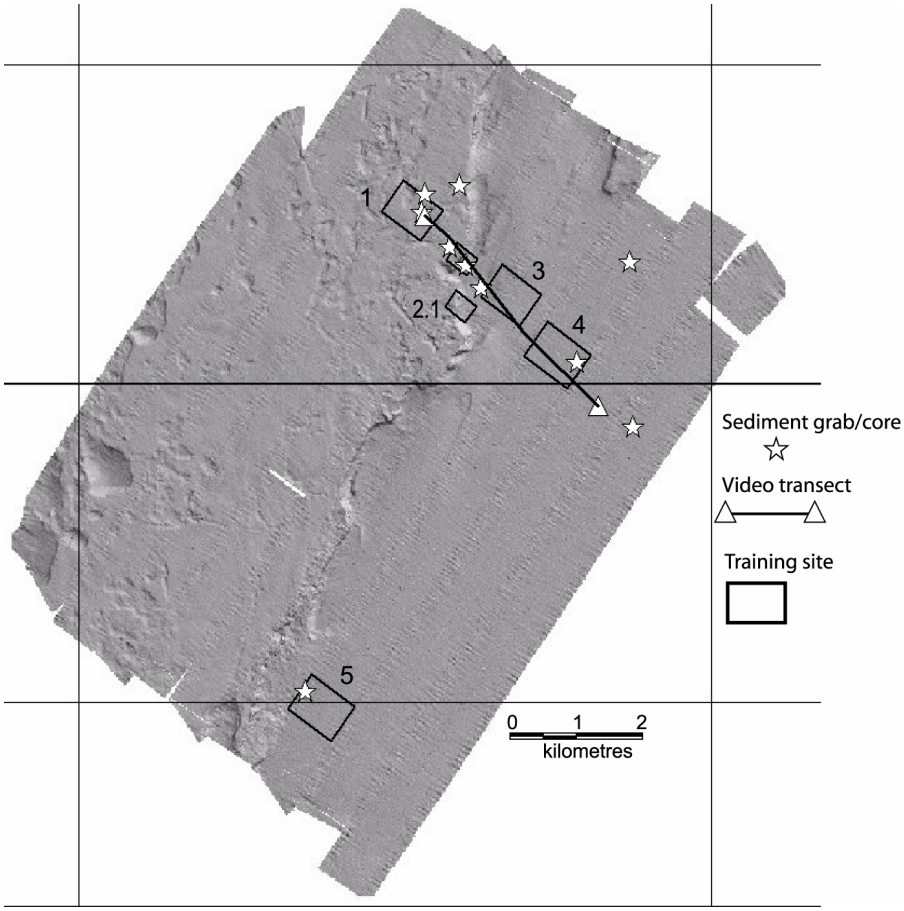

5.3 Acoustics

5.3.1 Multi-beam sonar (MBS) operation and processing

At the commencement of the survey in each area to be mapped the seawater acoustic parameters of absorption and sound speed were calculated from the formulae of Francois and Garrison (1982) and MacKenzie (1981), respectively, based upon temperature and salinity profiles obtained from the conductivity, temperature and depth (CTD) probe. The MBS mapping transect lines were in general carried out orthogonal to the seabed slope to provide as far as possible even seabed sampling width along transects. The MBS data collection system provided a helmsman display and associated software tools to set up survey transects and subsequently facilitate the accurate steaming of the vessel along the transect lines. MBS data were processed using the Simrad Neptune software to provide three data products, at 10 to 50 m grids depending on depth, of bathymetry, centre of each beam backscatter (CBB) and bathymetry texture (shaded-bathymetry). Shaded bathymetry is a virtual-illumination of a bathymetric surface using the Lambertian scattering rule $S = j\cos^2\varphi$, where S is the virtual-illumination intensity at a point, j is a background level constant and φ is the angle between the virtual-illumination source and the bathymetric surface. Bathymetric data processing on-board removed obvious depth outliers and followed standard procedures (Simrad 1999a). These three data products were inspected on board and the biophysical, geophysical and video/photographic sampling targeted at contrasting features in the imagery creating a set of reference sites (Fig. 5.6).

Scored acoustic terrain regions at megahabitat resolution (1 to 10 km) were derived from MBS maps of bathymetry, bathymetry-texture (shaded-bathymetry 8 times vertical exaggerated), seabed slope and beam centre backscatter imagery (scale –5 to –60 dB) (Fig. 5.7). The angular dependence of seabed backscatter observed in Figure 5.8a was empirically removed and represented at a reference incidence angle (40^o in this case) by averaging the across-track backscatter for 50 pings (empirically derived to maximise detail) and subtracting the mean reference incidence angle of 40^o (Fig. 5.8b, relative backscatter range set at –20 to –40 dB). The reference incidence angle of 40^o was least sensitive to the combined effects of seabed slope and incorrect sound absorption and most sensitive to changing seabed types (Chapter 4 and Chapter 6). Large transitions between ping ensembles were smoothed by linear interpolation between ensembles (using software by Caress and Chayes (1995)). This processing method highlighted irregularities in seabed backscatter where prominent south-west to north-east backscatter features become very apparent (Fig. 5.8b). Artefacts along the vessel track are caused by uneven beam compensation. Both images (Fig. 5.8a,b) are required for correct interpretation of seabed backscatter where Fig. 5.8a provides information about seabed type by the rate of change of backscatter near normal incidence and by the position of the critical angle at higher incidence angles. Based on an acoustic model, predicted backscatter as a function of incidence angles (Kloser *et al.,* 2001b) and confirmation with physical samples in the field, the scoring scheme in Table 5.3 was adopted. The methodology used is similar to that reported by Dartnell and Gardner (2004), although their focus was fine scale sedimentary facies rather than large scale (1 to 10s km) biotopes outlined here.

Figure 5.7 Example of the a) bathymetry (red 115 m to yellow 130 m), b) beam centre backscatter imagery –5 to –60 dB (black to white), c) seabed slope (yellow 0.5° to blue 10°), d) bathymetry-contrast (shaded-bathymetry 8 times vertical exaggerated) with visual megahabitat analysis of the region characterized by a low relief limestone reef (1.1 hard-rough), reef edge (1.2 hard-rough) and sediment flat of changing substrate (1.3 - 1.5 soft-smooth).

a)

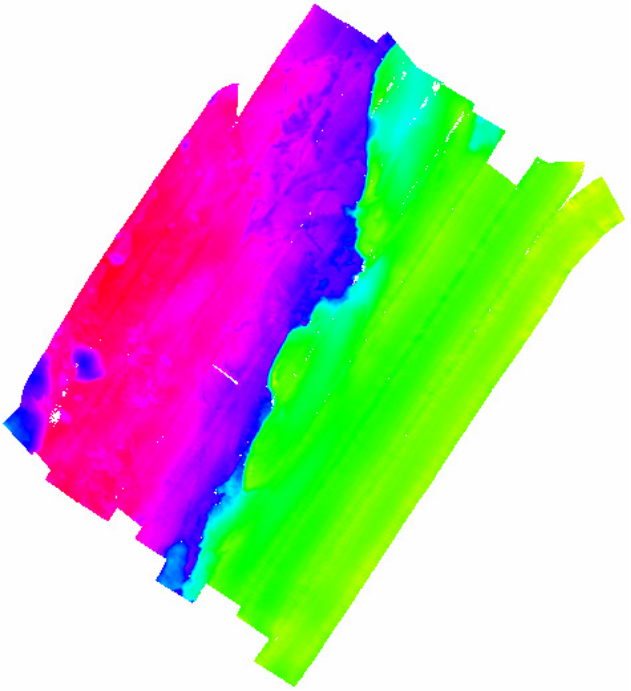

b)

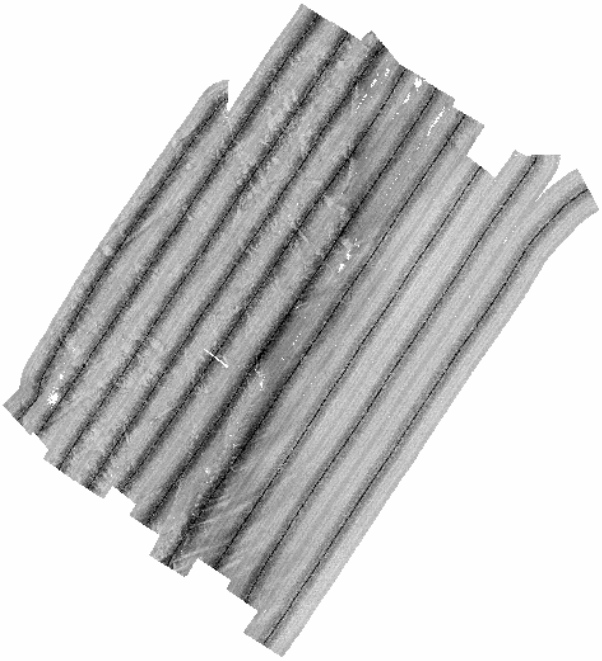

c)

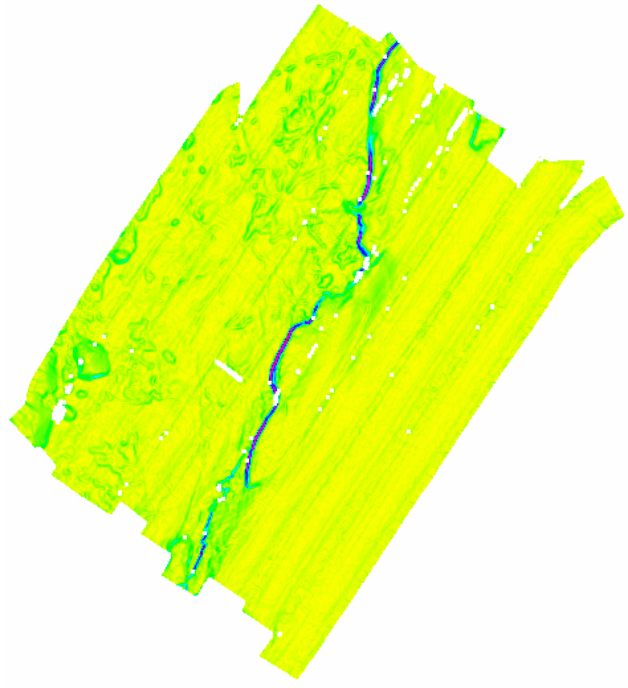

d)

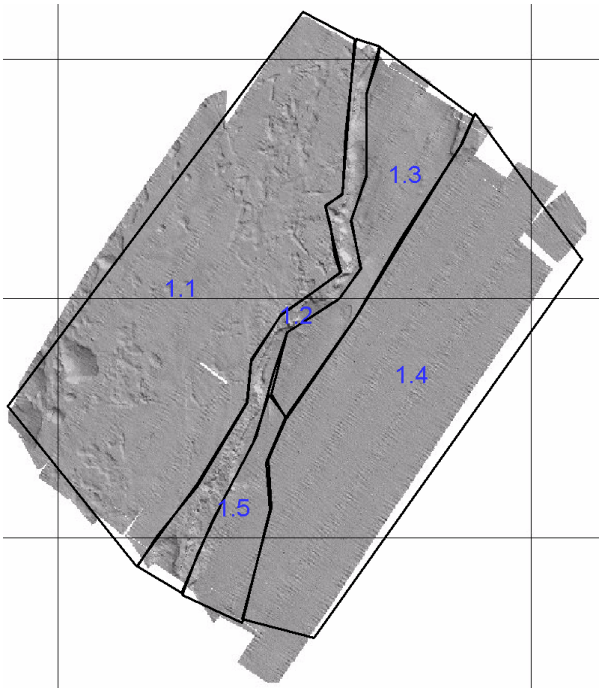

Figure 5.8 Simrad EM1002 centre beam backscatter of Gabo Reef (Fig. 4) with, a) recorded backscatter with incidence angle (scale range –5 to –60 dB) and b) removal of incidence angle backscatter dependence referenced to 40^{o} incidence angle (scale –20 to –40 dB).

a) b)

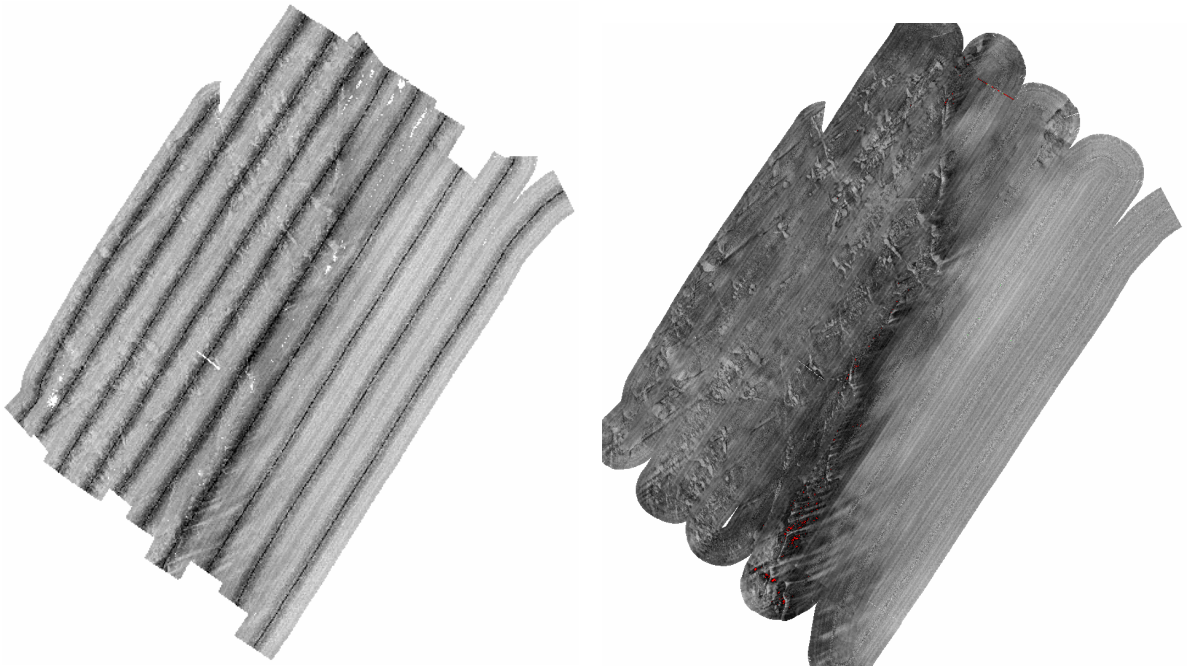

The imagery (Fig. 5.7 and 5.8) was scored against metrics of depth, bathymetry-texture, slope and backscatter strength/profile to create acoustic terrain regions (Table 5.3).

Table 5.3 Classes of depth, bathymetry-contrast, slope and backscatter attributes used to visually score benthic terrain at 1 to 10s km feature sizes in MBS maps gridded at 10 – 50 m intervals (Fig. 5.7): also shown are the inferred simplified terrain types for comparison with video terrain types.

Depth (segmented by grid size and pulse length used)	Bathymetry-contrast (sensitive to grid size, depth and illumination angle)	
1. 0-50 m (5 m grid)	1. smooth < ~ 0.5 m or 0.5% range	smooth
2. 50 -100 m (10 m grid)	2. isolated outcroppings > ~ 0.5 m or 0.5% range	rough
3. 100 - 200 m (10 m grid)	3. undulating regular > ~ 0.5 m or 0.5% range	rough
4. 200 - 600 m (50 m grid)	4. undulating irregular > ~ 0.5 m or 0.5% range	rough/hard
5. 600 – 1000 m (70 m grid)		
Slope	**Backscatter intensity and profile (uncalibrated relative intensity gauged at ~40^{o} incidence (Fig. 5.8b))**	
1. low < 1^{o}	1. uniform low (< -34 dB)	soft
2. medium (1^{o} to 3^{o})	2. uniform medium (-31 dB to -34 dB)	soft
3. high > 3^{o}	3. uniform high (>-31 dB)	hard
	4. irregular low. (< -34 dB)	soft/rough
	5. irregular med. (-31 dB to -34 dB)	hard/rough
	6. irregular high. (>-31 dB)	hard/rough

Acoustic terrain of Gabo Reef (Area 3) designated in MapInfo using the scoring based on Table 5.3 shows 5 distinct acoustic terrains (Fig. 5.7d). The reef terrain is defined by the combination of undulating irregular highly textured bathymetry (Fig. 5.7d) and the irregular medium strength backscatter profile (Fig. 5.7b). The reef edge is classified primarily using its high slope (>3^{o}, Fig. 5.7c) whilst the sediment flat has low-texture bathymetry and uniform low strength backscatter.

The visual classification approach used here was supported by metrics of the visual scoring attributes calculated on the 10 to 50 m grid bathymetry values for a subset of areas and reference sites (Table 5.4; Kloser *et al.,* 2002a; Appendix C). Kloser *et al.* (2002a) explored the use of visual and phenomenological characteristics using Triton software in the multi-beam data and compared this with single beam acoustic classification and physical and visual samples (Table 5.4). It showed that simple differentiation of low relief (< 1.0 m) limestone reef (Fig. 5.7d, terrain 1.1 and 1.2) and sediment flat (Fig. 5.7d, terrain 1.3 to 1.5) was confirmed for both the visual and phenomenological approach with low error scores (Appendix C). In this Chapter the details of the classification and associated physical and visual sampling are discussed in detail for all the areas surveyed.

Table 5.4 Summary of methods to analyse the MBS data, based on Kloser *et al.*, 2002a (Appendix C).

Method	*Inputs*	*Outputs*
Visual Classification	Bathymetry (10-50 m grid) Bathymetry-texture (shaded bathymetry vertically exaggerated 8 times) Center beam backscatter (10-50 m grid) Slope	Mega to meso acoustic terrain regions with depth, texture, slope and backscatter profile scores.
Bathymetry – metrics	10-50 m grid Bathymetry, slope, aspect, profile(rate of change of slope) and tangent	Summary metrics at mega, meso and macro resolutions (mean, std dev, skew, kurtosis)
Sidescan – backscatter metrics	Sidescan backscatter data corrected for absorption, slope and known artifacts.	Summary metrics at mega and meso resolution; (mean, 0.8 quantile mean, power spectum, contrast, std dev)

MBS performance

Throughout the survey the MBS operated at 120^{o} and 140^{o} (+/- 60^{o} to 70^{o} incident angles) swath width providing a seabed coverage of 3.5 to 5.5 times water depth respectively. The outer beams directed at 60^{o} to 70^{o} incidence highlighted motion correction errors (depth ripple) that increased in amplitude with higher vessel roll, pitch and heave motion. Depth rippling in the outer beams of up to 1 m peak to peak amplitude was clearly seen in the shaded-bathymetry maps (Fig. 5.10). The backscatter imagery was also characterised by several systematic artefacts that required correction. Obvious backscatter artefacts were observed in backscatter images due to incorrect beam amplitude compensation (along track tramlines) and incorrect absorption settings. An absorption coefficient of 35 dB km^{-1} was used for most of the voyage based on the temperature and salinity with depth profiles obtained at the start of each survey area. Errors in the measured backscatter due to incorrectly applied absorption increase with range (Fig. 4.13). Chapter 4 outlined the backscatter corrections required for ensonified area, slope and absorption and their potential magnitude. The seabed backscatter was also influenced by the background acoustic and electrical noise of the system within the environmental

conditions surveyed. The impact of background noise on the acoustic backscatter was most noticeable at depths greater than 400 m.

The EM1002 MBS was capable of recording depth data of useable quality to around 600 m (120^{o} swath) in fine sea conditions (Fig. 5.10). Generally, however, the depth limitation at 140^{o} swath was around 400 m because data quality was poor for the outer beams where the seabed was steeply sloping and when sea conditions deteriorated. In poor weather and steaming into the sea with high pitch motion, there was marked deterioration of the MBS backscatter data. At shallow depths < 200 m the bathymetric resolution of the system was sensitive to temperature profile changes within a survey area caused by refraction in the outer beams. Examples of refraction bathymetry errors were highlighted at Area 4 (Pt Hicks) where the sound speed profile was incorrect, resulting in shallower evaluated depths than actual for high incidence angles. This bathymetry error was corrected by modifying the sound speed profile in post processing (Simrad 1999a). Of greater difficulty was the correction of bathymetry where the survey moves through oceanographic temperature fronts such as at Howe Reef (Area 2). During the survey a warm water eddy was located in the Howe Reef area with a sea surface temperature difference of 1^{o} to 2^{o} and a marked thermocline at depths ranging from 40 - 80 m (Kloser *et al.,* 2001b). The eddy caused variable bathymetric changes in the high incidence angle regions from 50-70^{o} resulting in higher and lower than actual bathymetric values. To correct the data fully requires a dynamic sound speed correction profile based on the temperature field. Another error in beamforming and beam pointing is due to incorrect sound speed at the transducer face (Fig. 5.9a). The EM1002 with a rounded face will have a beamforming and beam pointing error between 60^{o} to 75^{o} emitted incidence angle (Ch. 4; MBSTC21 2000). This represents a limitation for highly accurate depth readings from MBS devices, without appropriate surface sound speed measurements and intensive sound speed profile measurements, in dynamic oceanic environments (Hughes Clark *et al.,* 2000).

Despite these limitations, the system was able to highlight small-scale seabed features such as limestone outcrops of 0.5 - 1 m or less in height at Broken Reef, Area 5 (Fig. 5.11). These limestone outcrops are generally important for supporting communities of large sponges and other attached invertebrates that provide complex habitats for fishes (Bax and Williams 2001). Also the bathymetry for Howe Reef showed the complex reef structure that has been historically difficult to interpret (Kloser *et al.,* 2001a). The MBS also revealed topographic patterns at resolutions of 100's of metres to kilometres that are not easily detected by single beam instruments. These include complex, rippled soft sediments that dominate the seabed in the Great Australian Bight Benthic Protection Zone (GABBPZ) (*e.g.* Area 14 Fig. 5.9).

Figure 5.9 Example of a) preprocessed MBS bathymetry texture (shaded-bathymetry vertical exaggeration 8 times) in the flatly sloping <1° Great Australian Bight (Area 14), depth 135-145 m, showing the depth rippling at high incidence angle (60° to 70°) on the outer beams due to vessel motion and/or incorrect surface sound speed ; b) preprocessed MBS backscatter per central beam in areas with and without large sand waves (high backscatter is black).

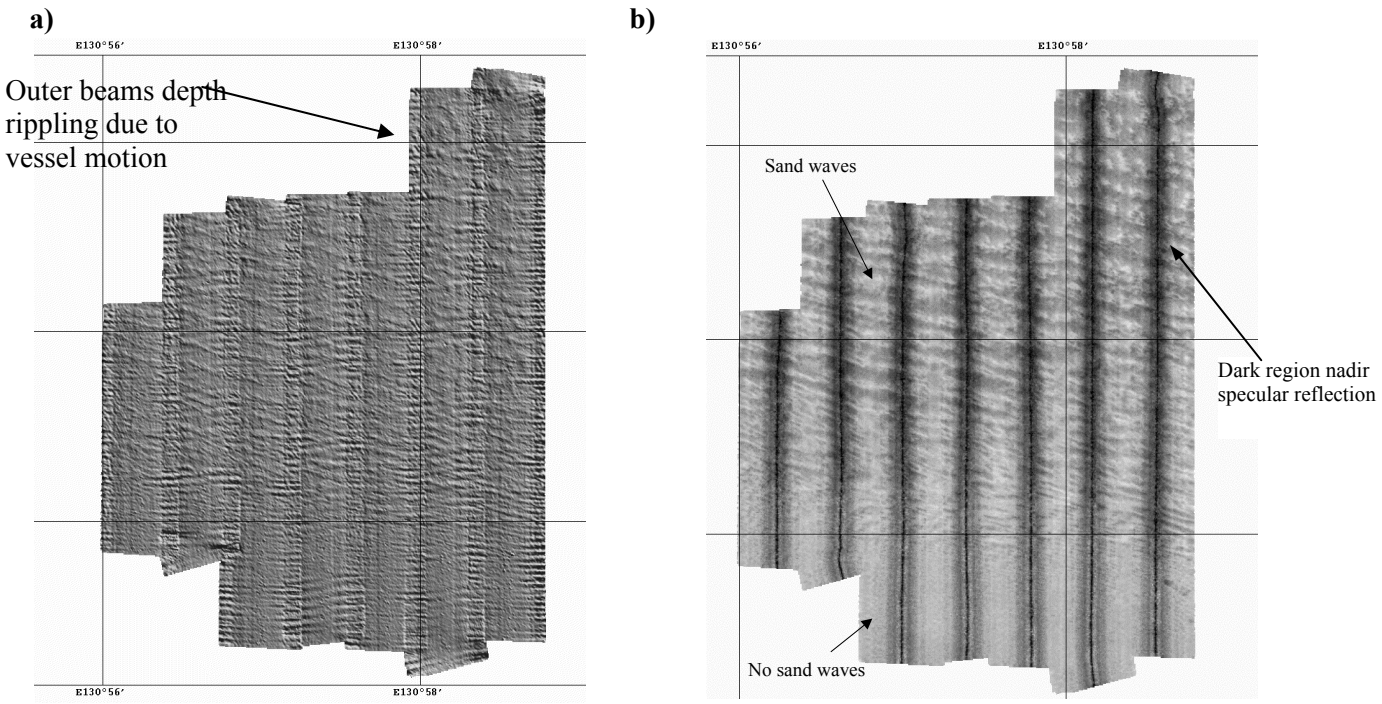

Figure 5.10 Shaded bathymetry of the Big Horseshoe (Area 6 and 7), a productive fishing ground, showing the depth limitation of the swath mapper at approximately 600 m at 120° seabed ensonification.

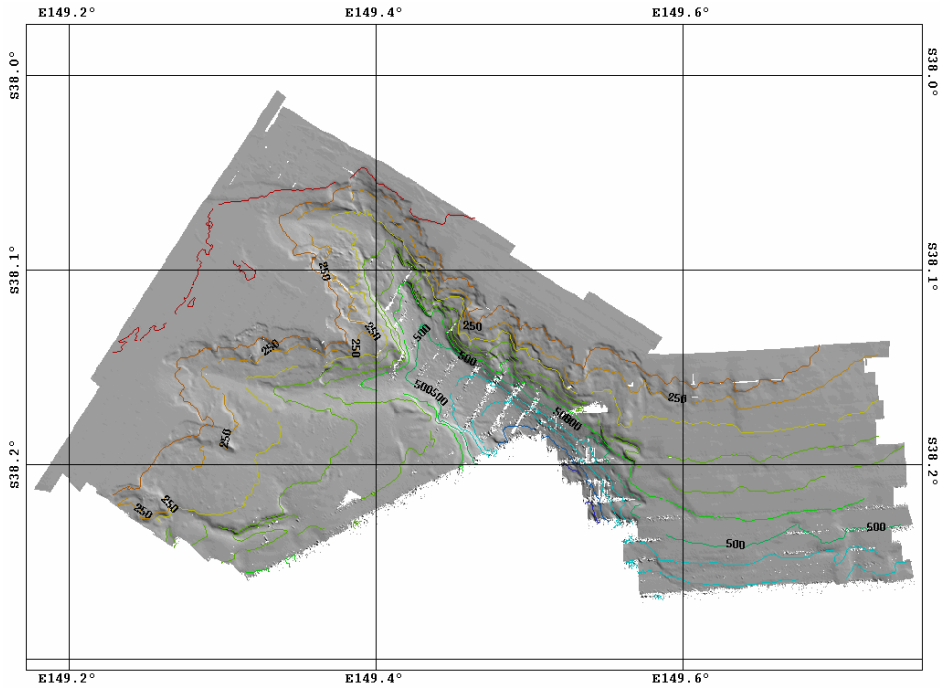

Figure 5.11. Preprocessed bathymetry texture (Sun illuminated bathymetry with 8 times height exaggeration) for Broken Reef (Area 5, depth 112 – 116 m) showing limestone outcrops of 0.5 to 1 m height. North-south lines highlight MBS artifacts due to incorrect sound speed profile or surface sound speed compensation.

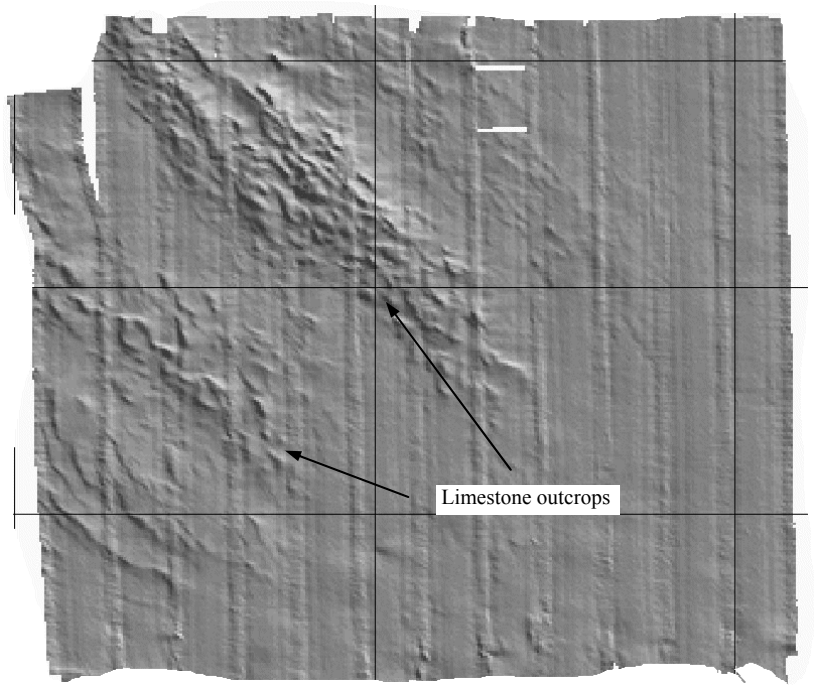

5.3.2 Single beam acoustics

Acoustic normal incident seabed and water column surveys were obtained with a Simrad EK500 echo sounder. This echo sounder has a large (160 dB) dynamic range and digitises the envelope detected seabed signals from the peak bottom signals (~20 dB re 1 m^{-1}) down to sea state or instrument noise, depending on frequency. The echo sounder was connected to three hull mounted transducers operating at 12, 38 and 120 kHz. The acoustic system was calibrated with a 42 mm tungsten carbide calibration sphere (Foote *et al.*, 1987; Simrad software version 5.3, 1996). This volume reverberation calibration technique combines the electrical and acoustic constants of the system, G_o^2 (for a given transmitter power, P_t, pulse length, τ, and band width) and the equivalent beamwidth, ψ, (provided by the transducer manufacturer) at a reference distance r_o. Sound speed, c, and absorption constant, α, are required to give range, r, independent values of the volume backscattering strength values, S_v dB (re 1 m^{-1}), based on the power received at the transducer, P_r, that is expressed in logarithmic form as:

$$S_v = 10\log(P_r) + 10\log(r^2 10^{2\alpha r}) - 10\log(\frac{P_t G_0^2 r_0^2 \lambda^2 c\tau\psi}{32\pi^2}) \text{ dB (re 1 m}^{-1}\text{).} \qquad (5.1)$$

The 38 and 120 kHz transducers were split-beam transducers and the 12 kHz transducer was a single beam. Details of the acoustic calibration constants for all three transducers are given in Table 5.5.

Table 5.5 Calibration settings for the EK500 acoustic instrument.

	Frequency		
	12 kHz	**38kHz**	**120kHz**
Absorption (dB km^{-1})	1	9	43
Pulse duration (ms)	3	1	1
Bandwidth (kHz)	1.2	3.8	1.2
Calibration constant	13.3	27.2	22.7
Beamwidth between -3dB points (degrees)	16/17.5	7.1	11.2
Equivalent beam width (dB re 1 steradian)	-13	-20.7	-18.5

Data collection and processing

Acoustic volume reverberation (S_v) data were logged continuously at three frequencies using a software package named "ECHO" (Waring *et al.*, 1994; Kloser *et al.*, 1998). The vessel's pitch/roll (at bottom detection), GPS navigation, speed and the digitised ping S_v dB (re 1 m^{-1}) data from each frequency were logged. Archived digital bottom data were quality checked using the ECHO post processing software to mask out bad data as indicated by obvious signal attenuation, usually due to strong winds and/or sea-state. This signal attenuation could be observed on the echograms by examining the loss of water column acoustic scatter as well as seabed acoustic tail scatter relative to adjacent records. Bad weather produced pronounced aeration under the vessel's hull, resulting in increased acoustic reverberation close to the transducer and a marked attenuation of the tail of the first echo and the whole second echo.

Simple indices of seabed roughness and hardness were derived from the acoustic data, by integrating the tail of the first echo and all of the first and second seabed echoes (Orlowski, 1984; Chivers *et al.*, 1990; Heald and Pace, 1996) adopting the methodology of Kloser *et al.,* (2001a). The reflected acoustic energy in the tail of the first echo, which is increasingly scattered on rougher seabed, is proposed to represent acoustic seabed roughness (Chivers *et al.,* 1990). For our depth range, D, and 1 ms pulse lengths, the angular off axis portion of the tail was summed (Eq. 5.3) between di limits d1 and d2 specified by θ_i values of 20^o-32^o from the start of the rising edge of the acoustic pulse (Eq. 5.2). The pulse offset from the bottom detection, C, was set at 1.5 meters for 38 and 120 kHz and 4.5 m for 12 kHz, where:

$$di = D(\frac{1}{\cos\theta_i} - 1) + C \qquad (5.2)$$

The entire reflected energy in the second echo, which has been reflected from the seabed twice (seabed-ship and sea water surface-seabed-ship), is used to represent acoustic hardness (Chivers *et al.,* 1990). It was defined as starting at two times the water depth (d1) and ending at two times water depth plus 20 m (d2). Several pings, p, were integrated (20-60 depending on vessel speed of 3-10 knots) to reduce between-ping variability in the backscatter returns and to standardise on a unit of length sampled, of 92.6 m (0.05 n mile):

$$\overline{S_A} = 10\log_{10}(1852^2 4\pi \frac{\sum_{p=1}^{m}(\delta d \sum_{d=d1}^{d2} 10^{\frac{Sv}{10}})}{m}) \quad \text{dB (re m}^2\text{ n.mile}^{-2}\text{).} \qquad (5.3)$$

Here S_A is the area backscatter coefficient, obtained by summing S_v between the start, d1, and stop, d2, depth range, and δd is the sampling interval. The derivation of area backscatter stems from fishery acoustic biomass studies and is used here as a relative measure of acoustic energy for volume scattering. Further details on the methodology can be found in Kloser *et al* (2001a) with units explained in MacLennan *et al.* (2002).

An example of the single beam mapping for Area 3 (Gabo Reef) at 38 kHz demonstrates that within an area the single beam systems highlight the major features observed with the MBS (Fig. 5.12) as reef and sediment flat (Fig. 5.7). Note that the second echo E2 metric that is sometimes referred to as hardness is lower on the medium porosity limestone reef than off reef at 38 kHz in this example (Kloser *et al.,* 2002a), whereas the second echo E2 metric at 12 kHz gave a higher signal on reef than off reef and the 95 kHz MBS showed higher backscatter on reef than off reef (Fig. 5.7 d). The roughness single frequency index E1 is very much greater on reef than off reef and correlates well with the MBS representation of seabed roughness at these frequencies using bathymetry (Fig. 5.7 d.). The terms second echo (E2) hardness and first echo (E1) roughness should be used with caution with single beam single frequency devices as they do not translate into physical meaning at a variety of resolutions (Kloser *et al.,* 2001a, 2002a). Details of the analysis and interpretation of the three frequency single beam data collected during the survey are outlined in Appendix C. This chapter and thesis concentrates on the MBS data collected.

Figure 5.12. Example of single beam 38 kHz backscatter: (at Gabo Reef Area 3, Fig. 5.7) a) second echo (E2) overlaid on uncorrected EM1002 backscatter and b) tail of first echo (E1) overlaid on MBS texture (sun illuminated bathymetry, 8 times vertical exaggeration). The size of the sampling dots represents the approximate 50 m sampling diameter of the single beam system (Kloser *et al.*, 2002a).

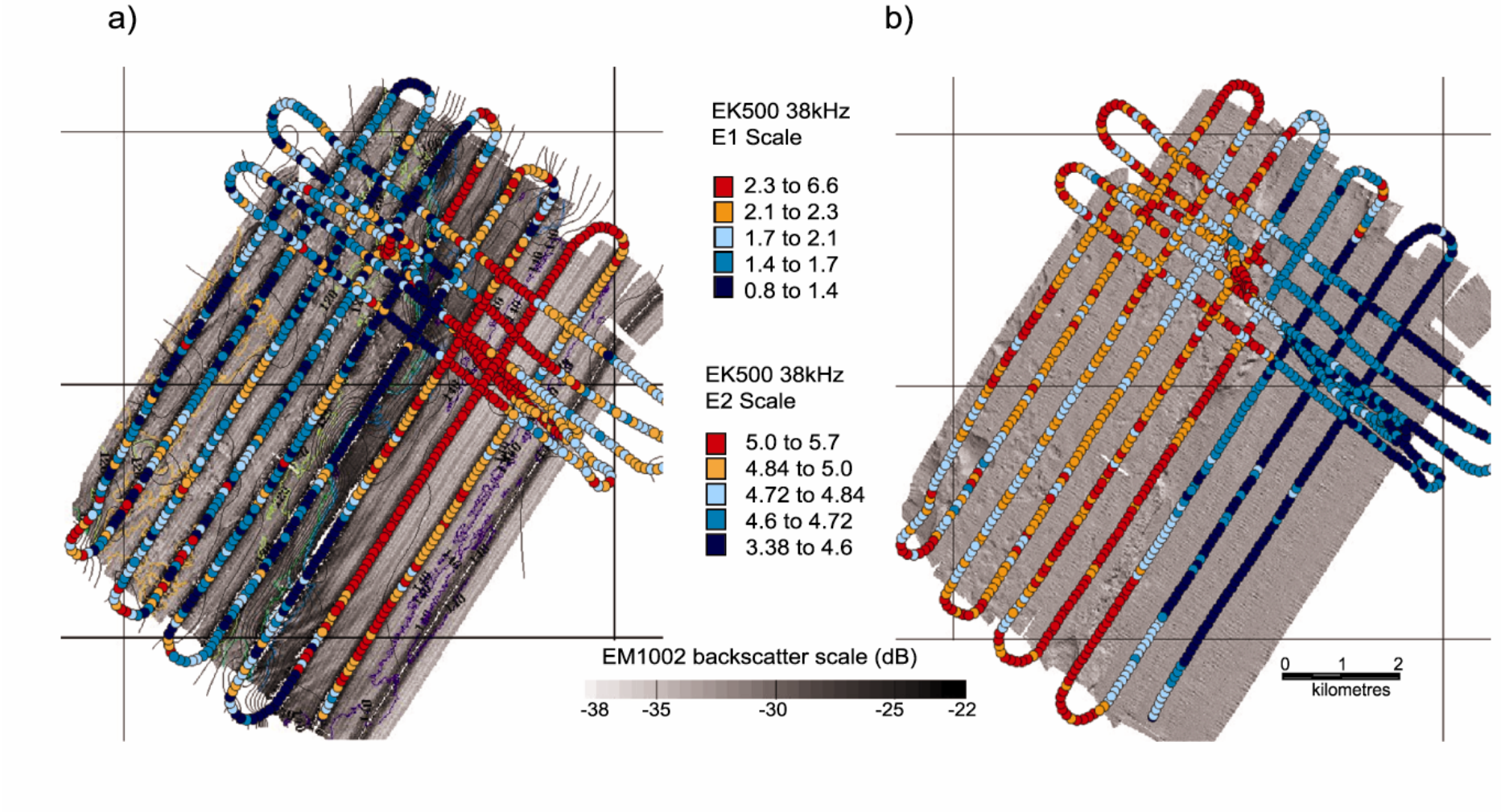

5.4 Video system

A towed mid-depth video camera was targeted on contrasting features in the swath backscatter and bathymetric images. Attributes of the seabed video were scored at 1 second intervals (approx. 0.25 m) in four categories: substrate (7 types), geomorphology (10 types), fauna (10 types) and faunal abundance (3 types) (Table 4. 3). These data were geo-located using the ship's DGPS position and the Sonardyne USBL tracking beacon attached to the video. The data were georeferenced and mapped over the MBS maps for analysis of biotope assessments (Fig. 5.13). Still images were extracted from the video and likewise georeferenced to form a reference set of characteristic habitat types within the hierarchical habitat scheme (Fig. 5.14). At a small mega habitat region of low relief limestone (Area 5, Broken Reef) a video transect highlights the patchy nature of the region and how the video data provides georeferenced habitat information (Fig 5.13; Kloser *et al.,* 2002b).

Figure 5.13. MBS backscatter referenced to 40^{o} incidence angle (high backscatter dark and prominent horizontal line normal incidence) of small feature (~4 x 4 km) showing overlay of two georeferenced and scored video transects (soft terrain classes, circles, hard terrain classes, asterisk) of varying geological and biological characteristics (Table 2.4). Geolocated sediment grab composition (pie chart) in percentage gravel (red), sand (yellow) and mud (brown). Scale of video image based on laser dots at 200 mm spacing.

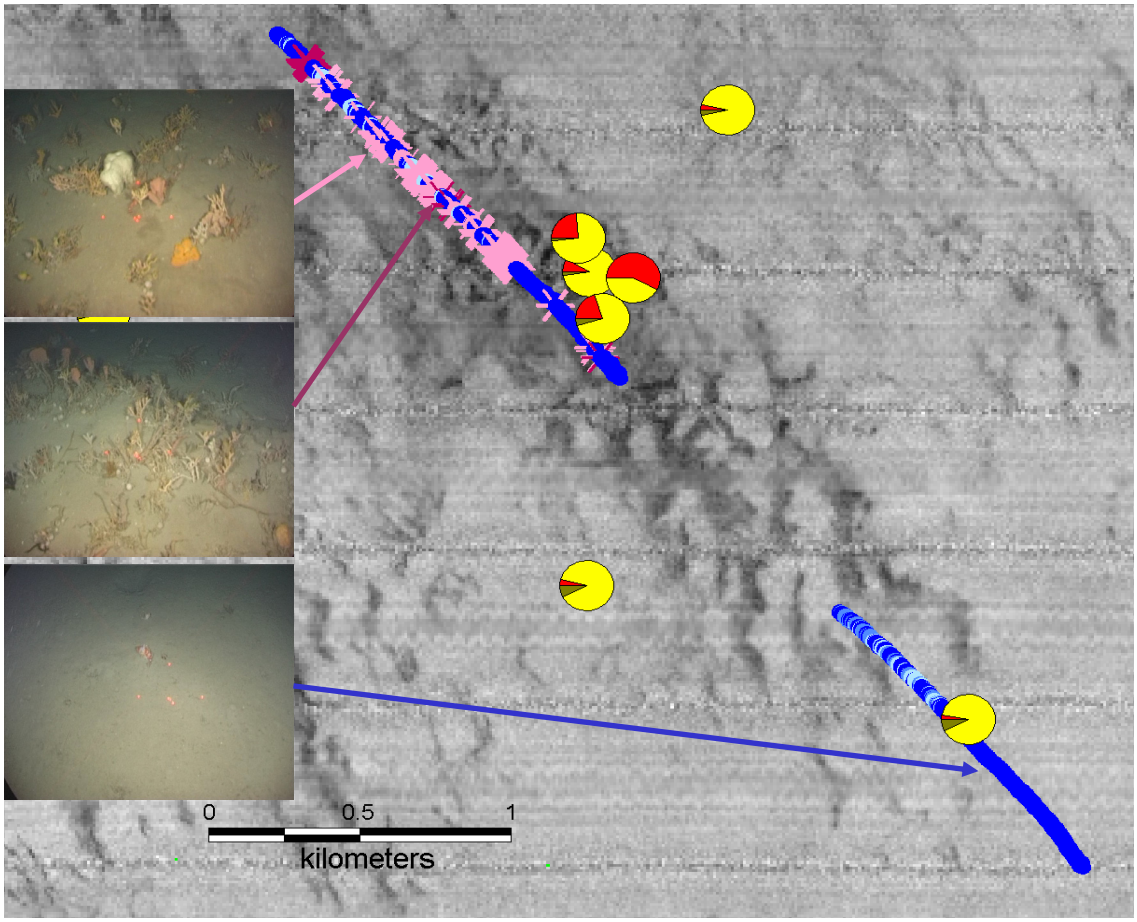

Figure 5.14 Examples of reference sit video frame grabs images for the four terrain types with depth of image shown below, laser dots at 200 mm*.

a) Soft-smooth

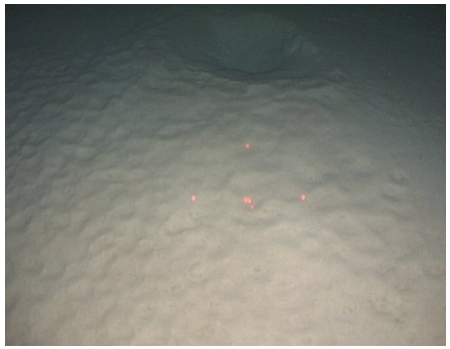

396 m

145 m

115 m

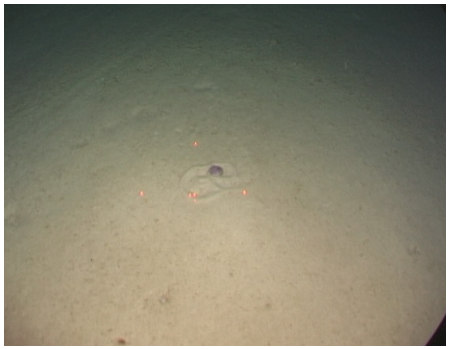

147 m

b) Soft-rough

140 m

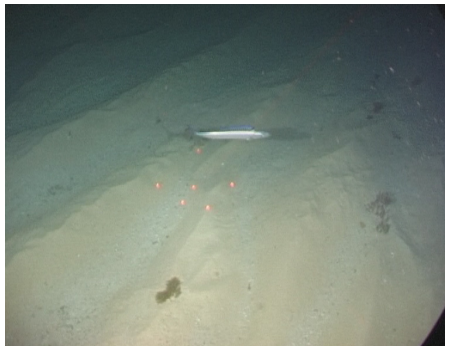

94 m

89 m

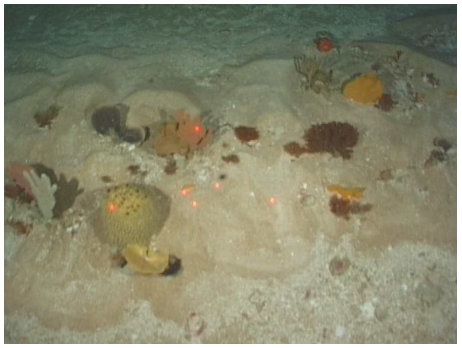

95 m

c) Hard-smooth

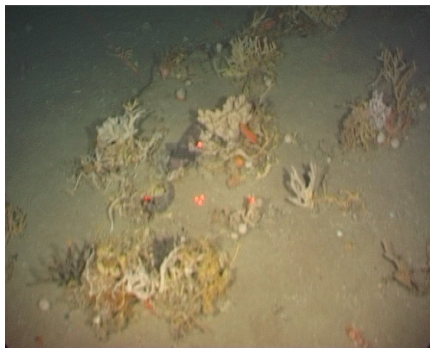

112 m

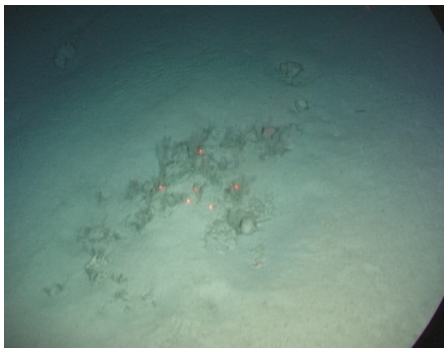

144 m

229 m

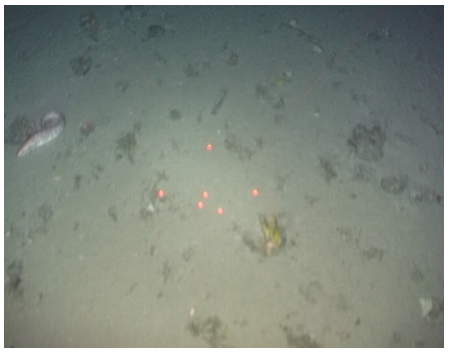

389 m

d) Hard-rough

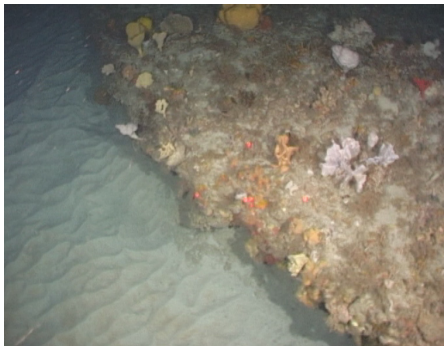

110 m

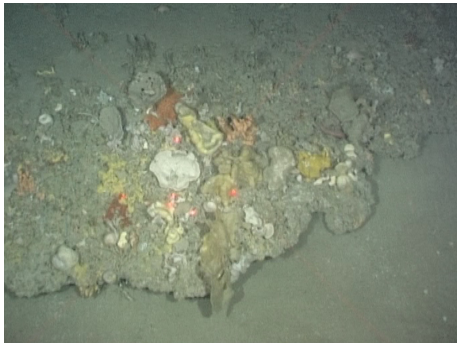

127 m

400 m

442 m

*Note triangular 4 laser dots are spaced at 200 mm in the horizontal and vertical plane, 2 crossing lasers enable distance to the seabed to be calculated.

5.5 Benthic invertebrates

Benthic invertebrates were collected using three different pieces of sampling equipment – benthic sled, demersal trawl and rock dredge. Retained specimens were removed from the gear and sorted to operational taxonomic units (OTUs) that are the lowest taxon identifiable in the field as soon as possible (refer to chapter 2). For each station, the total weight of each OTU and the number of specimens (for non-colonial animals) were recorded (Kloser *et al.,* 2001b). Selected specimens were photographed, and most of the material preserved on board using methods appropriate to each taxon. Preserved samples were sorted into major groups, then to species as far as possible. Photographed specimens were correlated to reference slides and cross-referenced. The level of identification possible varies with each major group – some groups (*e.g.,* sponges) are so poorly known that identification to species was not possible. Specimens were also forwarded to taxonomic specialists available and willing to look at material in their area for identification.

Metrics of the species and species groups identified were obtained for each acoustic terrain region using biodiversity metrics of species richness, Simpson's diversity, Shannon-Weaver diversity and evenness (Althaus *et al.,* 2004). Species were grouped according to their ecological requirements based on preferred substrate, mobility and feeding mode, into 21 functional units (FU's). Aggregating the feeding mode of active and passive filter feeders reduced the FU's to 8 levels as shown in Table 5.6.

Table 5.6. The functional unit classification scheme based on the ecological association of the species mobility, dominant feeding mode and preferred (inferred) substrate type (Althaus *et al.,* 2004).

Functional unit	Substrate and feeding mode	Example of dominant species groups
1	fixed to hard substrate, filter feeders	corallimorph anemones, barnacle (sessile/stalked), brachiopod, bryozoa (-/soft), coral (black/gold/gorgonian/colonial/solitary/octocoral), echiura, hydrocoral, hydroid, sponge (encrusting), tubeworm
2	sessile on hard substrate, filter feeders	basket-, feather-, snakestars, crinoids (stalked)
3	sessile **on/in** soft substrate filter feeders	bryozoa (vagrant), coral (seapen)
4	sessile hard substrate, scavenger	chiton
5	sessile **on/in** soft substrate, scavenger	sipuncula
6	mobile **on/in** soft substrate, scavenger	lobster (deepsea/shovelnose), mantis shrimp, squid, tusk shell
7	mobile on hard substrate, scavenger	limpet, lobster (squat), nemertea
8	mobile on soft **and** hard substrate, scavenger	amphipod, crab (hermit -deepwaer), cuttlefish, ostracod

For each acoustic terrain functional units were grouped by weight and number of individuals and expressed as g m^{-2}. Only samples obtained from a similar gear type (benthic sled) were used for this analysis. Historic data obtained from sleds in previous studies were analysed in a similar way and grouped by acoustic terrain by area as discussed in section 5.7.3.

5.6 Geological sampling

The geological characteristics of the surficial seabed were physically sampled with a variety of instruments. Surficial sediments were obtained with a Smith-McIntyre grab and box corer. The Smith-McIntyre grab retrieves approximately 0.1 m^3 of sediment per successful deployment. Box core samples were collected to obtain geoacoustic parameters such as porosity, sound speed and density. Lithology samples were collected with a rock dredge and analysed by macroscopic description (Folk 1968; Harris *et al.,* 2000). Sampling positions were merged with geolocation data from the tracking beacon used on the samplers and overlaid on MBS backscatter maps. Full details of the geological sampling are given in Harris *et al.,* (2000) and relevant details are summarised below.

For each grab and core sample the surficial depth (0-20 cm) was analysed by Geoscience Australia for grain size (percent gravel, sand and mud), total organic carbon content and calcium carbonate content. Dried sand and gravel fractions were examined under microscope and their composition and fossil content was estimated. Wet sieving was carried out using nested 2 mm and 63 μm analytical sieves. Material retained in the 2 mm sieve was *gravel*, that in the 63 μm sieve was *sand* and that collected in the beaker was *mud (*following Wentworth 1922). Gravel, sand and mud (mud fraction centrifuged at 4000 rpm) fractions were oven dried <50^{o}C and weighed to obtain the percentage of gravel, sand and mud in the sample. The calcium carbonate content of the sediment was measured using the vacuum-gasometric technique (Jones and Kaiteris 1983).

Box Core Samples

The box core samples were analysed at James Cook University using a Geotech Model 36 multi-sensor core logger (Gavin Dunbar pers. comm.). Down-core profiles of gamma- ray (sediment bulk density, ρ_s), p-wave speed, c_{sp}, and magnetic susceptibility were obtained from mini-cores removed from three box core samples in Disaster Bay (Area 1). The calculated p-wave speed through the sediment was corrected to 20^o C. Core lengths ranged from 11.5 to 20 cm and were visually inspected with grain structure/appearance logged. The grain size distribution along the core was measured at several intervals and classified into gravel, sand and mud composition.

The geoacoustic properties of sediment mass density ratio, ρ, and sound speed ratio, v, to that of seawater were calculated by:

$$\rho = \frac{\overline{\rho_s}}{\rho_w} \text{ and } v = \frac{\overline{c_{sp}}}{c_w}$$

where ρ_w and c_w were 1026 kgm^{-3} and 1512 ms^{-1} based on temperature, salinity and depth measurements at water/sediment interface in the region. These measured geoacoustic properties are compared to the predicted geoacoustic properties based on the MBS backscatter data in section 6.6.1.

5.7 Field data Summary

5.7.1 Acoustics – terrain and reference sites.

The 14 MBS surveys ranged in areas from 3 km^2 (Area 8) in shallow water to 511 km^2 (Area 6) in deep water covering a total of 1,188 km^2 (Table 5.1). The 14 surveyed areas were segmented into 80 acoustic terrains (Table 5. 7) at 1 to 10s km patch lengths defined by depth, texture, slope and backscatter metrics (Table 5.3 and Fig. 5.7 d). Within the 80 acoustic terrains, 102 sediment, 19 rock, 30 video and 24 invertebrate sampling operations were targeted (Table 5.2), forming 87 reference sites for inter comparisons of sampling devices. Figure 5.6 shows an example of a reference site. A reference site nominal area represented the width of at least half the MBS swathwidth (0^o to 70^o incidence) across-track at the depth of operation and >50 pings along-track at a vessel speed of 10 knots.

Table 5.7. MBS survey areas with number of acoustic terrain and reference sites with associated physical and visual samples.

Area	Name	Area km^2	# Acoustic Terrain	# Reference Sites	Video – hours
1	Disaster Bay	35	6	11	1.3
2	Howe Reef	144	8	5	0.4
3	Gabo Reef	45	5	6	0.7
4	Point Hicks	10	2	3	0.4
5	Broken Reef	34	8	8	1.4
6	Big Horseshoe SE	511	13	21	6.1
7	Big Horseshoe (west)	200	12	8	2.6
8	Lacepede Shelf 40	3	5	3	-
9	Lacepede Shelf 80	19	1	4	0.8
10	Lacepede Shelf 120	23	5	4	0.8
11	GAB BPZ 50	9	4	3	-
12	GAB BPZ 90	24	4	2	1.0
13	GAB BPZ 140	81	4	5	3.1
14	Outside GAB BPZ 140	24	3	4	1.4

The area of seabed sampled for each visual category of depth, texture, slope and backscatter varied with depth (Table 5.8). At shallow depths the area of seafloor sampled per unit time is limited by the MBS fixed 5.5 times depth coverage and vessel speed. For the areas sampled the texture of the seafloor as shown from the MBS data was rougher at shallow depths (70% for depths <100 m) grading to smoother at outer shelf depths (61% for depths 100 to 200 m) then rougher (67% for depths > 200 m) at upper slope depths (Table 5.9). It should be noted that the seabed will appear to be rougher at shallow depths using the MBS due to the decrease in sampling resolution with depth (Fig. 4.7). The acoustic terrains describe the general seabed topography and composition and may be related to the ecological preference of the functional units of fauna (Table 5.6).

Table 5.8. Area of acoustic terrain (km^2) at each depth stratum (m) scored for bathymetry contrast, slope and backscatter based on visual scoring of the MBS data, Table 5.3. All values rounded to nearest integer, total is sum of non-rounded values.

	Texture				Slope			Backscatter						
Depth	**1**	**2**	**3**	**4**	**1**	**2**	**3**	**1**	**2**	**3**	**4**	**5**	**6**	**Total**
0-50	6		7	10	21		3	1	5	4	0	10	3	24
50-100	41	3	10	29	83			23	25		9	7	19	83
100-200	265	39	31	159	492	2		248	8		122	116		495
200-600	32	160	83	310	78	250	258	6	347			153	80	586
Total	344	203	132	508	675	252	261	278	386	4	131	286	102	1188

Table 5.9. Distribution of visually scored acoustic terrains area (km^2) by depth for the generic seabed classes ranging from soft-smooth to hard-rough defined in Table 5.10. All values rounded to nearest integer and total is sum of non-rounded values.

Depth	Total	Soft Smooth	Soft Rough	Hard Smooth	Hard Rough
0-50	24	6	0	0	18
50-100	83	41	16	3	24
100-200	495	259	119	6	110
200-600	586	0	353	32	201

Table 5.10. Criteria for segmentation of the visual acoustic terrains scoring (Table 5.3) into generic seabed characteristics ranging from soft to hard and smooth to rough consistent with the ecological preference of functional units of fauna (Table 5.6).

	Soft-smooth	Soft-rough	Hard-smooth	Hard-rough
Texture	1	2,3,4	1	2,3,4
Slope	-	-	-	-
Backscatter	1,2,4	1,2,4	3,5,6	3,5,6

To simplify the test of faunal association with acoustic terrains into meaningful habitat preference categories the acoustic terrains can be segmented into 4 dominant classes related to seabed hardness (defined as ability for biota to attach or burrow) and roughness (Table 5.10). Using these broad categories the distribution of the acoustic terrains with depth shows that not all categories were evenly sampled with depth and terrain type (Table 5.9). In particular the hard-smooth category is underrepresented for all of the depth strata.

5.7.2 Video scoring

Throughout the survey 20 hours of video footage from 24 operations were scored and georeferenced at 1s intervals using the scheme outlined in Table 2.4 (Kloser *et al.,* 2001b). The dominant substrate types of mud and fine sediments represented 73% of the scored videos. This dominance of inferred soft substrates is reflected in the geomorphology and fauna scoring where 57% were scored as unrippled and 35% contained distinct infauna bioturbators. Typically the faunal community was present in low abundance (80%). A low abundance score occurs when less than 10% of the viewing area of the video is associated to the faunal community. Area 6 (Big Horseshoe SE) contained 6 video operations that represented 31% of the scored video data. To minimise sampling variability bias, video scores of substrate, geomorphology, fauna and faunal abundance between areas were calculated from the average of each area video scores (Table 5.11). Area averaged video data ensured even weighting of the total number of video samples between areas. Fine sediments, unrippled with either none or distinct infauna bioturbators was representative of 48% of the sampling areas. The inferred hard and very rough substrates of gravel, boulder and rock outcrop represented 16% of the scored videos. Representative reference video frame grab images of soft to hard and smooth to rough categories of seabed types were taken to link with reference sites of acoustic, geological and invertebrate sampling (Fig. 5.14). The inferred terrain-type of soft and hard will depend on the density of the material as well as the particle size and in some cases represent a mixture of categories. In this case the dominant terrain type is used and tested for consistency with the acoustic data.

Table 5.11. Classes of substrate, geomorphology and fauna used to score benthic terrains and proportions of each across the 14 study areas; also shown are the inferred dominant ecological terrain types for comparison with acoustic terrain types. All % rounded to 0.1%.

%	1. Substrate (S)	Terrain-type	%	2. Geomorphology (G)	Terrain-type
7.7	Mud	soft	50.5	Unrippled	smooth
58.6	Fine sediments	soft	4.1	Current rippled/directed scour	rough
17.9	Coarse sediments	soft	27.5	Wave rippled	rough
6.9	Gravel/pebble	hard	5.4	Highly irregular	rough
2.1	Cobble/boulder	hard	2.6	Debris flow/rubble banks	rough
0.0	Igneous/metamorphic rock	hard	9.1	Subcrop	smooth/hard
6.9	Sedimentary rock	hard	0.2	Outcrop (low <1m); no holes/cracks	rough
			0.4	Outcrop (low <1m); with holes/cracks	rough
			0.0	Outcrop (high >1m); no holes/cracks	rough
			0.3	Outcrop (high >1m); with holes/cracks	rough
%	**3. Fauna (F) (dominant faunal community)**		**%**	**4. Faunal Abundance (A)**	
22.4	None - no apparent epifauna or infauna		84.3	Low/sparse (<10%)	
12.8	Large sponges - community		13.8	Medium/intermediate (<50%)	
17.5	Small sponges - community		1.9	High/dense (>50%)	
0.3	Mixed sponges, seawhips and ascidians				
0.5	Crinoids				
0.2	Octocorals (gold corals/seawhips)				
15.6	Small encrustors/erect forms (including bryozoans)				
4.1	Sedentary: e.g. seapens				
0.7	Mobile: e.g. echinoids/holothurians/asteroids				
26.0	Distinct infauna bioturbators				

The spatial resolution of contiguous seabeds can be inferred from the video data due to its continuous recording of line data. It is assumed that the video operations were randomly distributed for a range of seabed types at various depths and biogeographic regions and there was no systematic patch shape bias (Langton *et al.,* 1995). The longest length scale in a video tow is limited to slightly less than the total length of the video record. Video records ranged

from 350 m to 2550 m (mean 1490 m; sd 690 m; n = 24) assuming a speed of 0.5 $m.s^{-1}$. The effect of including truncated contiguous seabed habitat scores at the start and end of the video transects was not significant. Truncated ends are included to ensure that long lengths of contiguous habitat are included and the video footprint (5 samples in length ~2.5 m) was removed from all contiguous length scales (see section 4.4).

Several length scales can be inferred from the data that are of relevance to the acoustic sampling. Firstly, I assume that acoustic sensing will be sensitive to the combined effects of Substrate and Geomorphology (SG) and their spatial distribution. The length scale of the contiguous combined SG score (n = 475) varied from 2.5 m to 756 m. The distribution was highly skewed to small length scales where 50% of the patch sizes were less than 18 m and 90% were less than 250 m in length (Fig. 5.15). Similarly, the contiguous length of faunal scores (n=1424), 50% were less than 10 m and 90% less than 85 m (Fig. 5.15). This implies that at fine scales the faunal community as defined here has approximately three times the spatial variability of the physical substrate (SG). The physical substrate as detected by acoustics has fine resolution variability with 50% of the patch sizes less than 18 m dominated by rough substrate types of sedimentary rock (31%). At patch sizes larger than 18 m the dominant substrates are soft mud and fine sediments (45%). No linear trend with patch size and depth was observed.

Figure 5.15. Length scales for video scores (all areas) of contiguous patches of seabed attributes, substrate and geomorphology (solid) and fauna (dashed).

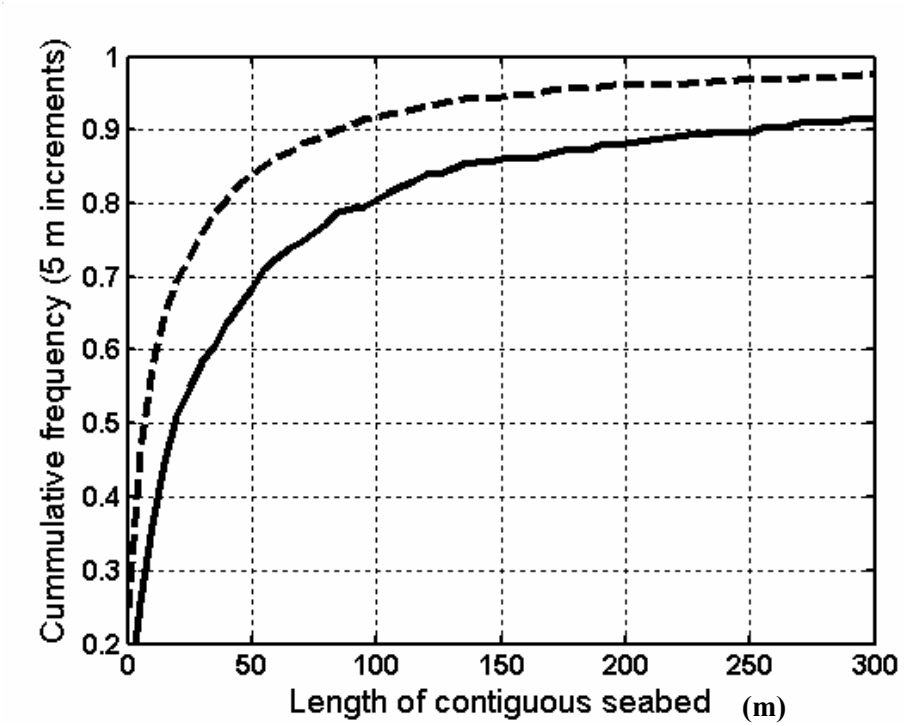

The acoustic and video scores were independently grouped into the four terrain classes of soft to hard and smooth to rough (Table 5.10 and Table 5.11) and compared in Table 5.12. Here, the segmentation of acoustic data are at patch lengths of 1 to 10 km, and this sets the scale for the comparison. Some components of the data correspond well: within the soft-smooth acoustic terrains the video scored 81% as soft-smooth (Table 5.12). This gives a high confidence in designating soft-smooth acoustic terrains. If the seabed is segmented only by soft and hard categories, 97% of the video scores are soft within a soft acoustic terrains at 1 to 10 km scale. Therefore the acoustic segmentation system developed here is in agreement with the video segmentation 97% of the time over soft seabed. However, video indicates there is also a

relatively high proportion of soft-rough substrate (16%) in soft-smooth acoustic terrains. Soft-rough acoustic terrains show less agreement with video observations, where only 29% were scored in the same class, and 70% were scored as soft-smooth. The proportion of soft-smooth seabed scored in video decreased to 49% as the seabed became harder and rougher. Hard-rough acoustic terrain is represented by a complex mosaic of all four classes, within which only 19% is observed by video to be a hard-rough seabed (Table 5.12). This result confirms the small spatial scale of variation of patchiness of seabed types observed within the video scores (Figs. 5.13 and 5.15), and indicates that the acoustic terrains of hard-rough at 1 to 10 km scale contains higher proportions of soft-smooth seabed than the actual hard-rough seabed. There were no video records from hard-smooth acoustic terrains defined at the 1 to 10 km patch length size (Table 5.9).

Table 5.12. Comparison of video terrains (% composition) of substrate and geomorphology within the acoustic terrains defined at 1-10 km scale. Each data set independently grouped into four terrain classes (see Tables 5.10 and 5.11) and two terrain classes of soft and hard terrain.

Acoustic terrain	Video records #	Video terrain composition within acoustic terrain			
		soft		hard	
		smooth	rough	smooth	rough
soft-smooth	21216	81	16	2	0
soft-rough	15560	70	29	0	1
hard-smooth	0	0	0	0	0
hard-rough	32735	49	22	10	19
soft	36776	98		2	
hard	32735	71		29	

Faunal groups were typically associated with more than one seabed type when video classes were aggregated into the four terrain types (Table 5.13). Sponge dominated communities (that made up about 30% of all faunal records, Table 5.11, faunal groups 1 and 2) were associated with all terrain types, but mostly present on hard-smooth seabed. Small encrusting and erect forms (faunal group 6, ~16% records) were strongly associated (93%) with hard-rough seabed. Sedentary filter feeders (faunal group 7) had a high affinity (96%) for soft-smooth seabed.

A higher correlation with presence/absence was found when faunal groups were segmented into simple hard or soft seabed. There are clear regions of preference where 7 out of the nine categories were associated at > 88% occurrence. Hard ground contains >97% of the faunal categories 3 to 6 whilst the soft ground contains >88% of the faunal categories 7 to 9. The separation of the faunal categories is not as distinct when splitting by smooth and rough seabed types with two faunal categories associated at greater than 87%. The small encrustors group (fauna group 6) is strongly (94%) associated with rough seabed whilst sedentary fauna (faunal group 7) is strongly (96%) associated with smooth seabed.

Table 5.13. Proportion (%) of faunal types in four terrain classes defined by video at 1-10 m feature size. Grouping of video data into terrain classes shown in Table 5.11. All values rounded to nearest integer with total the sum of non-rounded values.

Fauna Group	Soft Smooth	Soft Rough	Hard Smooth	Hard Rough	Description
#	39276	9733	4525	13307	
	%	%	%	%	
0	12	31	0	20	None - no apparent epifauna or infauna
1	8	2	46	3	Large sponges - community
2	14	9	42	10	Small sponges - community
3	0	0	2	0	Mixed sponges, seawhips and ascidians
4	0	0	8	0	Crinoids
5	1	0	0	0	Octocorals (gold corals/seawhips)
6	0	2	2	57	Small encrustors/erect forms (including bryozoans)
7	16	1	0	0	Sedentary: *e.g.* seapens
8	1	5	0	0	Mobile: *e.g.* echinoids/holothurians/asteroids
9	48	49	0	8	Distinct infauna bioturbators
Total	100	100	100	100	

The abundance (% cover) of the faunal groups on the sea floor changed depending on the seabed type and the fauna group. Significantly, higher cover (> 10% of area) of small and large sponge communities (faunal groups 1 and 2) occurs, as the seabed gets rougher and harder. When the cover exceeds 50% of the viewing area the sponge communities are only found on hard seabed. As an example, the cover of the large sponge community on hard seabed is likely to occur (70% of the time) at greater than 10% coverage and when associated with hard-rough seabed will have greater than 50% cover, 23% of the time. Likewise the small encrustor community (faunal group 6) only occurred with high cover on the hard-rough seabed.

5.7.3 Invertebrate Fauna

Analysis of faunal (invertebrate) distributional data in relation to MBS maps presented two main difficulties. The first was defining biodiversity metrics from the mix of known species and unresolved multi-species taxa (OTUs), and the mix of gear types with different collecting selectivities. Second, was that the samples taken with the most consistent sampler (the benthic sled) typically integrated over more than one seabed type, i.e. tow length was longer than the spatial scale of variation in patch size.

In total, 444 benthic invertebrate taxa from 15 phyla were identified; of these, 370 were identified as true species, while 74 OTUs represented an estimated 303 additional species (Althaus *et al.,* 2004). Comparison of catches in the different gears showed that the epibenthic sled caught most taxa, but the trawl sampled additional larger bodied and apparently sparse taxa; the rock dredge also provided additional species, and was the only tool suited to sampling the most rugged deep rocky reefs. As outlined in section 5.5 this analysis used only taxa retained in the sled catches and these were grouped into 8 functional units (FU's) according to the species' mobility, feeding mode and substrate relationship (Table 5.6). The bottom contact duration of the sled tows ranged from 800 m to 7 600 m with an average length of 2 400 m (s.d. 1 500 m), and sample weights varied widely between samples (largely due to isolated large invertebrate species; *e.g.* sponges). Samples were normalised for seabed area sampled to enable intra- and inter-area comparisons.

There were large differences in biomass density between substrate types, with higher abundances of relatively large-bodied animals (particularly sponges) on hard substrata. Within the acoustic terrains (1 to 10 km), 56% of the sessile species with a preference for soft substrate (FU 3,5), are associated to low regular backscatter (inferred soft sediment; Table 5.9). Only 7%

of sessile species with a preference for hard substrate (FU 1,2,4, Table 5.6) occur in the low regular backscatter category. As the strength and irregularity of the backscatter increase so does the proportion of sessile species associated to hard substrata (Table 5.14). The high proportion of sessile species associated to soft substrata in all acoustic backscatter categories is a result of the long integrative sampling distance of the sled combined with the fine spatial scale variation in seabed patch structure (Fig. 5.15).

Table 5.14. Proportion of soft and hard substrate preference of 5 sessile faunal groups within the 8 functional units (Table 5.6) separated into the acoustic terrains of varying backscatter and inferred hardness (Tables 5.3 and 5.10).

Acoustic backscatter class	Terrain class	Sled stations n	% FU proportion (s.d.) Soft (3,5)	Hard (1,2,4)
low	**soft**	3	56 (49)	7(8)
medium	**soft**	6	36 (32)	32 (38)
high	**hard**	-	-	-
irregular low	**soft**	-	-	-
irregular medium	**hard**	5	25 (35)	68 (32)
irregular high*	**hard**	6	38 (21)	33 (14)

* dominated by deep stations

5.7.4 Geology

Eighty successful Smith-McIntyre grabs were made across the region, with a large proportion (55%) coming from outer shelf depths (100 - 200 m). Despite this unevenness across depth, the mud fraction increased markedly with depth, increasing from 1% (n=9, s.d. 4%) to 25% (n=17, s.d. 9%) between the inner shelf and the upper slope. Both sand and gravel content decreased with depth but with high standard deviation, skewness and kurtosis indicating patchy distributions.

Table 5.15. Sediment stations mean proportion by weight of gravel, sand and mud (s.d. in brackets) for each acoustic depth class.

		% sediment composition by weight		
Depth (m)	**n**	**Gravel**	**Sand**	**Mud**
0 - 50	9	14(15)	85(15)	1(4)
50 - 100	10	6(5)	90(6)	4(7)
100 - 200	44	11(18)	83(17)	6(7)
200 - 600	17	4(6)	71(8)	25(9)

Segmenting the 80 sediment samples by the MBS backscatter features (Table 5.3) could test the hypothesis that the acoustic backscatter is a surrogate for seabed hardness (Table 5.16). There is an apparent increase in gravel content of 3% for uniform low backscatter to 33% for uniform high backscatter (Table 5.16). Therefore it appears that the dominant signal being detected by the increase in uniform backscatter at the 1 to 10s km patch length is an increase in gravel content. It should be noted that the medium backscatter score sediment samples have high standard deviations. There is no significant trend of increased gravel content with irregular backscatter of increasing intensity. There may be two explanations for this within this data set based on sample scale and sample bias. Firstly, when the backscatter is irregular it indicates variability in substrate types at fine scales. This was demonstrated at Broken Reef where the backscatter was classified as irregular medium and four sediment samples within 50 m ranged from gravel content of 8% to 58% (Fig. 5.13). Secondly, sediment grabs can only sample

unconsolidated sediments and not large rocks, boulders, clay, mud stones or solid bedrock, implying a sampling bias. At Big Horseshoe south-east (Area 6, Table 5.1) the backscatter was irregular high yet the gravel content only comprised 0 – 13% by weight in the samples. In contrast the video stations in these irregular high backscatter regions show a high proportion of mud and clay stone in rubble and boulder sizes that would contribute to the highly irregular backscatter. It is difficult to infer any rigorous relationship between trends in sediment properties based solely on sediment grab samples and acoustic backscatter at the 1 to 10s km scale without incorporating knowledge from the video scoring and rock dredge data.

Table 5.16. Sediment stations mean proportion by weight of gravel, sand and mud (s.d. in brackets) for each acoustic backscatter class (Table 5.3). All values rounded to nearest integer.

		% sediment composition by weight		
Backscatter	**n**	**Gravel**	**Sand**	**Mud**
low (soft)	17	3(3)	87(8)	10(8)
medium (soft)	12	12 (28)	71 (25)	17 (15)
high (hard)	3	33(7)	67(7)	0(0)
irregular low (soft)	18	8(12)	88(13)	5(7)
irregular medium (hard)	24	12(11)	83(12)	5(7)
irregular high (hard)	6*	5(6)	71(11)	24(13)

** dominated by deep stations*

At depths ranging from 100 to 200 m the acoustic scores of irregular bathymetry and low to high backscatter contained primarily limestone and sandstone rock types consistent with hard-rough terrain. Porosity of the rocks varied with location from low to high (Table 5.17) due to the inclusion of differing proportions of live and dead biological material (Harris *et al.,* 2000). These hard-rough platforms were a mosaic of terrain types, where the hard-rough portion could be as low as 3% (Fig. 5.13, Broken Reef), or as high as 94% (Fig. 5.7, Gabo Reef), based on video scores (Table 5.17). At the Lacepede Shelf site the low porosity limestone corresponded with highly irregular backscatter making the hard-rough characterisation of the site clear. In contrast the Howe Reef site with high porosity limestone corresponded with irregular low backscatter indicating a soft terrain but due to the irregular bathymetry is classified as hard-rough terrain (Table 5.3). The hard-rough terrain at 1 to 10s km scale was distinguished by the irregular undulations in the bathymetry and usually higher irregular acoustic backscatter (Table 5.3 and Fig. 5.7) and confirmed by video and rock dredge sampling (Table 5.17).

Table 5.17. Visual inspection of lithology (Harris *et al.,* 2000) and associated porosity from hard-rough (reef) acoustic terrains and video scoring (soft-smooth (SS), soft-rough (SR), hard-smooth (HS) and hard-rough (HR)).

Area	**Type**	**Porosity (visual inspection)**	**Video composition %**				
			#	**SS**	**SH**	**HS**	**HR**
Howe Reef	limestone	high	NA	-	-	-	-
Gabo Reef	limestone	medium	399	6	0	0	94
Broken Reef	sandstone	medium/low	3384	78	0	19	3
Lacepede Shelf 80m	limestone	low	2897	19	70	6	5

5.8 Summary

Using a simple visual classification system based on model predictions of seabed types (Chapter 3; Kloser *et al.*, 2001b), four ecologically distinct seabed types (soft-smooth, soft-rough, hard-smooth and hard-rough) were chosen to test the "at sea" MBS seabed segmentation capability at the 1 to 10s km scale. These seabed attributes have been shown to have ecological significance to the biota and management significance due to human usage of the seabed (mainly due to fishing; Bax and Williams, 2001; Kloser *et al.*, 2001a). Fine scale bathymetry (0.5 m resolution at 200 m depth) showed the outcropping and inferred sub-cropping of consolidated sediments or rocks indicative of hard rough seabed at the 1 to 10s km scale. The MBS backscatter regular progression of low, medium and high was associated to increases in gravel content. These results are expected and consistent with models of seabed scattering and supported the extrapolation of the MBS data to other regions (Chapter 3). When the backscatter was irregular a simple relationship with sediment type did not emerge although irregular low to irregular medium backscatter was associated with increases in gravel content. As the backscatter strength increases and becomes more irregular it is indicative of a patchy seabed made up of all seabed types. The best "ground truthing" data are obtained from the towed video.

Accurately georeferenced towed video data was a key data type for describing the seabed at 1 – 10 m resolution and providing reference sites within acoustic terrains. Four categories (geomorphology, substrate type, primary fauna and faunal abundance) provide coded habitat descriptions at 0.25 m intervals along narrow (2-3 m wide) transects at 100's m (Fig. 5.13). Aggregated patches (5 – 50 m in length separated by 100 – 200 m) of exposed low-relief limestone (0.5 – 1 m) and surrounding sediment plains represent a typical example of seabed on the SE Australian continental shelf and slope. The towed video transect data revealed frequently small-scale variability where 50% of seabed patch lengths were less than 20 m and the dominant faunal patch length was less than 10 m. Within the four acoustically defined terrains at 1 to 10 km size the videographic data showed there was general agreement where soft-smooth seabed contained 81% of soft-smooth video classified seabed whilst also containing 16% of the soft-rough seabed. Similarly a hard-rough acoustic terrain at 1-10s km size may contain 49% or greater of the soft-smooth seabed. When the acoustic terrain is segmented into simple soft and hard terrain the video data contained 97% soft terrain within acoustic soft terrain giving high confidence that at 1 to 10s km feature size this method is reliably detecting ecologically soft terrain. Within acoustic hard terrain the video shows high patchiness with only 29% being video hard terrain. To better define the seabed patch structure within the acoustic terrain finer scale and more quantitative analysis of the acoustic data are required (Chapter 6). Understanding patch structure and the key biotic assemblages is at the foundation of understanding the spatial and temporal dynamics of biodiversity and informing the human use of the regions such as fishing, shipping, mining and tourism (*e.g.* Hubbell, 2001).

The videography data shows that the relationship between seabed type and presence/absence of faunal groups as defined here is not unique, but general associations with high probabilities were evident. In previous studies based on photographic data general associations between sediment type and megafauna were evident (*e.g.,* Kostylev *et al.*, 2001; Edwards *et al.*, 2003). The towed video data demonstrated the highly patchy nature of the seafloor and the difficulty that single widely spaced photographs would have in describing the sediment-fauna relationship. Understanding the pattern, scale and processes of benthic systems is greatly enhanced using video data (Solan *et al.*, 2003 and references within). However, there are also several limitations of video data. Speed of collection is relatively slow and the area of seabed sampled is small, although significantly improved with laser line scan systems (Carey *et al.*, 2003). Small animals, and difficult taxonomic groups, are often poorly resolved and this limits the ability of the combination of acoustics and video to define biodiversity, and therefore to detect and monitor changes in characteristics such as species-richness or the body-sizes of

animals without further refinement (*e.g.,* calibrated paired cameras for accurate measurements, Barker *et al.*, 2001). Thus, there is a need to physically capture organisms to identify taxa and quantify biomass. Typical sled tows integrate samples over the duration of the tow and hence integrate fauna over different terrain types losing the sediment-fauna relationship. Using a camera in conjunction with the benthic sled would have improved the results discussed in this chapter.

It is highly likely that many of the terrains sampled (especially soft) were not "natural" habitats, due to cumulative impacts of trawling over many decades. This would affect the interpretation of the relationship between fauna and seabed type and, along with natural ecological processes (*e.g.,* succession, competition and community dynamics), places a temporal scale on the sampling undertaken. The functional and morphological method of characterising fauna with the video and sled sampling could be used to monitor impact on the seabed by both natural and human induced activities. The scientific reference sites created in this chapter should help form the start of long term monitoring sites of the marine benthic environments over a number of bioregions. The focus within this chapter has been understanding of the seabed at the 1 to 10s km resolution; the MBS also provides a 10s m to 1 km view of the seabed and this is explored in Chapter 6 through the use of the reference sites nested within acoustic terrains at 1 to 10s km scale. At the 10s m to 1 km patch size it is important to provide more quantitative analysis of the MBS bathymetry and backscatter explored in Chapters 6 and 7.

6 Reference site analysis

6.1 Introduction

Adopting the habitat scale terminology of Greene *et al.* (1999) discussed in Chapter 2, Chapter 5 provided an analysis of the acoustic terrain regions at the megahabitat scale (1– 10s km) and demonstrated the high degree of terrain patchiness within these acoustic terrain regions (Sec. 5.8). Terrain patchiness at mesohabitat scale (10s m to 1 km) is investigated in this chapter using reference sites (as exemplified by Fig. 5.6). Reference sites represent regions where there is coincident MBS bathymetry and seabed acoustic backscatter data and either videography or physical geological sampling or both. Line transect videography at the macrohabitat scale (1 to 10s m) is assumed to provide an unbiased measure of the terrain and epibenthic faunal communities.

Two hypotheses will be tested in this chapter.

1. At the 10s m to 1 km scale, that the MBS bathymetry and backscatter metrics can be used to determine the seabed terrain (substrate type and geomorphology) over a range of depths and between bioregions.
2. At the 10s m to 1 km scale, that the MBS bathymetry and backscatter metrics can be used to predict the dominant functional groups of the large epibenthic fauna over a range of depths and between bioregions.

6.2 Reference sites

Reference sites within an acoustic terrain represented the variability in acoustic backscatter and depth within and between sampled regions (Table 5.7). In the present work a reference site contains MBS bathymetric and seabed backscatter data from normal incidence (directly below the vessel) to maximum incidence angle (70^{o} across-track), which for a flat seafloor is a distance of 2.75 times the depth. The reference site length along the ship's track was approximately 2.75 times the water depth or at least 50 pings. The combined area of the 81 reference sites (6.1 km^2) was less than 1% of the total area (1188 km^2) sampled with the MBS. Based on 15 of the 81 reference sites within a narrow depth range (100 m to 150 m) Kloser *et al.* (2002a) demonstrated that the MBS was capable of distinguishing a simple terrain category of reef and sediment flats with 0% "cross validation" error. A low error score indicated good agreement with the reference site classifications. Validity of the error tests was visually confirmed on the data by mapping the variables on the MBS bathymetric and backscatter maps and plotting combined metrics (Appendix E; Kloser *et al.,* 2002a). MBS phenomenological metrics were obtained using Simrad (1999a) Neptune bathymetric processing and Simrad (1999b) Triton backscatter seabed classification processing. Simrad (1999b) Triton backscatter seabed classification processing software provided analysis of the acoustic backscatter, equating to a minimum classification region width of 1.73 times depth (d) across-track and length several pings (~ 10 m) along the vessel's track. Due to averaging this effectively resulted in an area 17.3d m^2. It was postulated in Kloser *et al.* (2002a) that the resolution of the seabed classification could be improved by more effective across track segmentation and including depth metrics. In section 6.7 of this chapter the statistical descriptors segment the across-track acoustic data into 6 and 10 bins.

Reference site analysis is extended in this chapter to include more sites (81) over a wider depth range (30 to 600 m) and include a comparison of the MBS backscatter measurements with a seabed model (APL94 1994; Jackson and Briggs 1992) and finer scale phenomenological metrics (*e.g.,* Huseby *et al.,* 1993). These metrics are used to investigate

the hypothesis that the terrain and the associated fauna can be described using MBS data. The test of the hypothesis uses the following steps:

1. Firstly, demonstrate that terrain types can be uniquely associated with specific acoustically derived metrics by:

- classifying sites based on fine scale video terrain metrics simplified to broad categories of seabed type that have ecological significance.
- finding reference sites that have homogeneous terrain type and explore the relationship of incidence angle with the backscatter metrics of scattered signal amplitude and its standard deviation.
- comparing the relationship of incidence angle and terrain type with a physical model (APL94 1994; Jackson and Briggs 1992) of seabed scattering.
- developing phenomenological metrics of bathymetry and backscatter at fine scale and create a georeferenced set of metrics.
- testing the reliability of these classifications using a linear discriminant cross validation error test.

2. Secondly, demonstrate that faunal communities can be associated with acoustic metrics by:

- finding a relationship between video terrain types and faunal types.
- establishing relationship between acoustics and terrain as in 1 above.
- exploring the predictive capability of the acoustics to determine faunal types.
- exploring the error of these predictions.

6.3 Videography analysis

The georeferenced video data represents the highest spatial resolution with 5-7 m^2 image area and resolution within the image typically <0.1 m to determine the seabed terrain and fauna in this thesis (Sec. 4.3). Videography data are used here to set the standard of "ground truth" for testing seabed-acoustic relationships at the reference sites. Of the 81 reference sites 62 contained video information representing 37376 scored video records or 54% of the total video data set. The videography scores of terrain (substrate plus geomorphology scores, Table 2.4) are grouped into 4 ecologically important terrain types of soft-smooth, soft-rough, hard-smooth and hard-rough (Table 5.12). The categories of soft and hard relate to the ecological ability of biological material to attach and burrow into the substrate. Hard and soft terrains are further separated into rough and smooth. Soft sediment roughness was associated with biological perturbation (*e.g.,* bioturbation) or current flow whilst harder material roughness was associated with consolidated cobble and boulders or with cracks and ledges of exposed bedrock/consolidated sediments. Roughness was quantitatively gauged within the 5 to 7 m^2 viewing area of the video along the line transects (Sec. 4.3) using 3 parallel and one crossing laser (Barker *et al.,* 2001) and knowledge of sizes of captured organisms observed on the video. The mean line transect length of 520 m (s.d.=278) assuming an average speed of 1 $m.s^{-1}$ contained on average 520 video scores per reference site. Terrain patch length was highly variable within and between reference sites and between terrain types (Fig. 6.1). Fine scale patches were evident for all terrain types, where 50% of the patch lengths were less than 58 m, 90 m, 18 m and 32 m for the soft-smooth, soft-rough, hard-smooth and hard-rough terrains respectively. The box plot of Figure 6.1 shows the median (50% of data are either lower or higher than this value) as a horizontal line and interquartile range contained within a solid box.

Figure 6.1 Box plot of contiguous terrain length (m) frequency for the soft-smooth, soft-rough, hard-smooth and hard-rough terrain types. The box contains the median (bar) and interquartile (25% to 75%) range and outliers (plus sign) being 1.5 times this range.

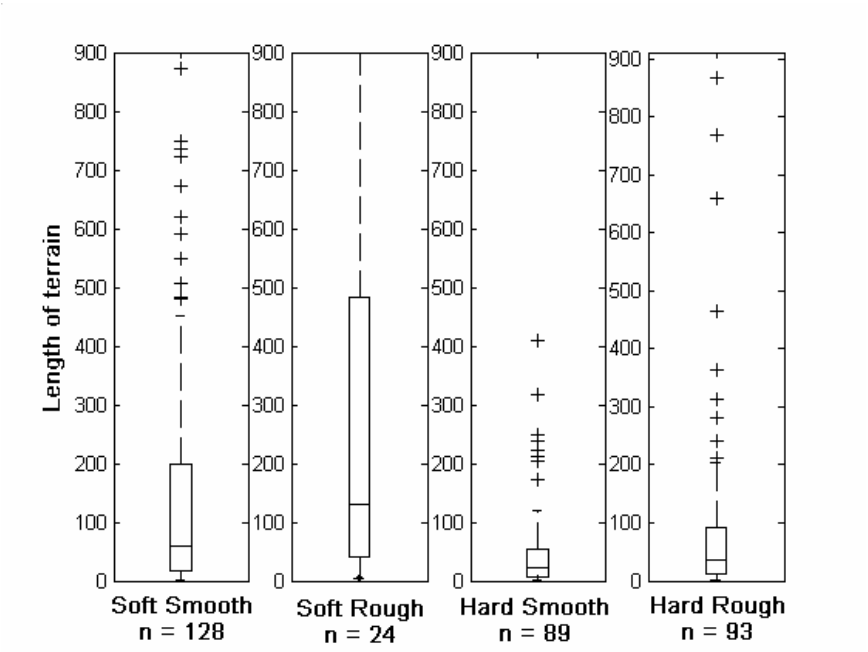

6.3.1 Segmentation into 4 ecological groups based on terrain preference

Using the video score groupings of terrain to distinguish seabed types (Table 5.11), 62 reference sites were separated into their proportions of the four terrains, 30 being homogeneous (Table 6.1). Of the homogeneous reference sites, 18 were soft-smooth, 6 soft-rough, 0 hard-smooth and 6 hard-rough (Table 6.1). A soft-smooth reference site was not considered homogeneous if the acoustics backscatter or bathymetry varied within the site based on the scoring in Table 5.3 and was not sampled by the videographic line transect. Videography scores were georeferenced over the MBS bathymetric and backscatter maps to ensure general visual correlations (Fig. 5.13).

Table 6.1. Proportional composition of reference sites designated by videography scores Table 5.11 as soft to hard and smooth to rough terrain.

Proportion of video score %	Soft Smooth	Soft Rough	Hard Smooth	Hard Rough
100	18	6	0	6
80- 99	4	4	1	5
60 -79	7	1	0	3
40- 59	4	1	5	4
20 - 39	7	0	1	5
1-19	4	1	9	11
0	18	49	46	28

Prominent changes in the terrain (geomorphological and substrate) inferred from the bathymetric and backscatter maps assisted in determining geopositioning accuracies of sampling devices (Kloser *et al.,* 2001b). The patchy nature of the terrain at the 10s m to 1 km scale is evident within the reference sites where 28 sites (45%) contained a proportion of the hard-rough terrain, but 11 of those sites contained less than 19% hard-rough video score

(Table 6.1). Hard-smooth terrain was observed at 16 sites, none homogeneous, and a high proportion (56%) occurred with less than 19% hard-smooth video score (Table 6.1). Soft-rough terrain was only observed at 13 sites (21%), 12 of those had greater than 40% soft-rough video scores with 6 homogeneous (100% soft-rough video score).

Based on the defined terrain types the presence of faunal groups 0 to 9 were distributed at varying proportions with the highest affinity (96%) being sedentary filter feeders (fauna group 7) for soft-smooth seabed (Table 6.2). The small sponge community was a widely distributed faunal group found on all terrain types, most frequently (57%) observed on hard-smooth ground and 21% also found on soft-smooth terrain when observations were weighted to ensure equal observation by terrain type then fauna group (Table 6.2).

Table 6.2 Proportion (%) of video scored fauna in the seabed terrains of Table 6.1 weighted by terrain type then fauna group. All values rounded to nearest integer, total is sum of non-rounded values.

Faunal group		Soft Smooth	Soft Rough	Hard Smooth	Hard Rough	Description
	#scores	18650	6286	4406	8034	
0	5611	18	49	1	32	None - no apparent epifauna or infauna
1	3119	20	6	64	10	Large sponges - community
2	6924	21	9	57	14	Small sponges - community
3	76	0	0	85	15	Mixed sponges, seawhips and ascidians
4	651	4	0	81	15	Crinoids
5	576	0	0	81	19	Octocorals (gold corals/seawhips)
6	4415	2	5	5	88	Small encrustors/erect forms (including bryozoans)
7	3603	96	3	0	0	Sedentary: e.g. seapens
8	618	30	62	2	6	Mobile: e.g. echinoids/holothurians/asteroids
9	11783	38	50	2*	10*	Distinct infauna bioturbators

* note this comes from SG31 and SG32 gravel terrain types in sites 1401(564), 401 (259), 402 (44), 1402(8)

Segmenting the faunal groups into hard, soft, rough or smooth terrain demonstrated higher presence/absence “preference” (association) (Table 6.3). There are clear regions of preference where hard ground contains >97% of the faunal categories 3 to 6 whilst the soft ground contains >88% of the faunal categories 7 to 9 (Table 6.3). The separation of the faunal categories is not as distinct when splitting by smooth and rough terrain types with two faunal categories separated at greater than 87% compared with 7 groups separated for the soft to hard terrain types. The small encrustors group (fauna group 6) are strongly (94%) associated with rough terrain whilst sedentary fauna (fauna group 7) are strongly (96%) associated with smooth terrain (Table 6.3).

Simple separation of soft and hard or smooth and rough terrain types shows that distinct fauna group preferences are evident and prediction (with a high probability) of distributions of faunal groups to terrain types is possible. This relationship is not unique but there are clear and highly significant (greater than 80%) relationships.

Table 6.3 Proportion of video scored faunal group in the seabed terrains soft, hard, smooth and rough weighted by terrain type then faunal type.

Faunal group	Soft	Hard	Smooth	Rough
#scores	24936	12440	23056	14320
0	67	33	19	**81**
1	26	74	**84**	16
2	30	70	**78**	22
3	0	**100**	**85**	15
4	4	**96**	**85**	15
5	0	**100**	**81**	19
6	7	**93**	6	**94**
7	**100**	0	**96**	4
8	**92**	8	32	68
9	**88**	12*	40	60

* note this comes from SG31 and SG32 gravel terrain types in sites 1401(564), 401 (259), 402 (44), 1402(8)

Faunal group presence varied with terrain type as well as the abundance (% cover) within and between terrain types (Table 6.4). Significantly, higher covers (> 10% of area) of small and large sponge communities (Faunal groups 1 and 2) occur as the terrain gets rougher and harder. Only on hard terrain are sponge communities found with cover exceeding 50%. Likewise the small encrustor community (Faunal group 6) only occurred with high cover on the hard-rough terrain (Table 6.4).

Table 6.4 Proportion of video scored fauna where the cover is greater than 10% or greater than 50% (in brackets) for the seabed terrains of soft-smooth, soft-rough, hard-smooth and hard-rough.

Faunal group	Soft-Smooth	Soft-Rough	Hard-Smooth	Hard-Rough
0				
1		17	77 (4)	63 (23)
2		10	75 (17)	51 (13)
3				100
4			0.37 (4)	
5				
6				27
7	1			
8				
9	12 (4)	87 (21)		10

The videography data shows that there is a relationship between terrain types and faunal group presence/absence and proportion abundance/cover at high probabilities of association. Therefore, establishing a link between the video terrain classification of soft, hard, smooth and rough and the MBS acoustic data will provide an important prediction capability for the preferred association and abundance of faunal groups. As an example, the large sponge community found on all terrain types is 74% more likely to be found on hard than soft terrain. Also, the cover of the large sponge community on hard terrain is likely to occur (70% of the time) at greater than 10% coverage and when associated with hard-rough terrain will have greater than 50% cover, 23% of the time.

6.4 Physical sampling

6.4.1 Surficial Sediments

Physical sampling of the surficial sediments and lithology was carried out at 41 reference sites. Within the homogeneous sites sediment samples showed that the soft-smooth sites contained 13% (n=11, s.d. =8%) mud whereas the soft-rough sites contained 1% mud (n=5, s.d. = 2%) (Table 6.5). These surficial sediment samples support the separation of videographic scores into soft-smooth and soft-rough categories. It is expected (hypothesised) that for rougher soft ground the current is stronger and smaller particles are removed (discussed in chapter 2), consistent with the above observation. The hard-rough sediment sites contained a higher gravel content (9%, n=3, s.d.=4%), but the result is inconclusive due to the difficulty of sampling hard sites with the sediment grab. Hard-rough surfaces such as boulders and consolidated rock outcrops are difficult to sample with a sediment grab and samples may be significantly biased. Many (28, Table 6.1) of the reference sites contained a mosaic of terrain types ranging from hard-rough to soft-smooth but were classified as hard rough at the acoustic terrain scale (1 to 10s km). This mosaic of terrain types is demonstrated by the repeat sampling within a Broken Reef reference site (#5.03). Three sediment grabs within tens of meters yielded samples ranging from gravel dominant to fine sand dominant. This fine scale variability is consistent with the patchy nature of the seabed observed using the video (Fig. 6.1). No correlation of sediment grain size with depth was noted in the sediment samples within homogeneous sites, with the sparse samples obtained.

Table 6.5 Sediment composition, percentage gravel (G%), sand (S%) and mud (M%) with associated standard deviation (s.d.) with the video scored homogeneous reference sites outlined in Table 6.1.

Homogeneous score of reference sites	sites/ samples	Gravel G% (s.d.)	Sand S% (s.d.)	Mud M% (s.d.)
Soft-smooth	18/11	3(1)	84(7)	13(8)
Soft-rough	6/5	9(8)	89(8)	1(2)
Hard-smooth	0/0	-	-	-
Hard-rough*	6/3	9(4)	90(4)	1(1)

* sediment samples of hard rough sites are not representative of the sites hardness due to inability of the Smith McIntyre grab to sample hard or large particles.

The sediment sampling provides a clear separation of terrains classified as soft-smooth and soft-rough based on the percentage composition of mud and gravel. Hard-smooth and hard-rough terrains were not adequately sampled with the sediment grab used in this study.

6.4.2 Lithology

The lithology within hard reference sites was inferred from visually inspected material retained in targeted rock dredges (Harris *et al.,* 2000). Accurately directing rock dredges to obtain material within the reference site boundaries was difficult. At depths ranging from 100 to 200 m the lithology consisted of limestone and sandstone and is inferred as being representative of the acoustic terrain of the hard-rough reef sites. Porosity of the lithologies varied with reef location from low to high (Table 6.6) due to the inclusion of biological material (Harris *et al.,* 2000). The reefs at 1-10 km feature resolution were distinguished based on the irregular undulations in the bathymetry and usually higher irregular acoustic reflectivity (Table 5.3 and Fig. 5.7). These reef platforms were a mosaic of seabed terrains,

where the hard-rough portion could be as low as 6 %, Broken Reef, or as high as 99 %, Lacepede Shelf, based on videography (Table 6.6).

Table 6.6 Visual inspection of lithology (Harris *et al.*, 2000) and associated porosity from hard rough (reef) acoustic terrain and video scoring (soft-smooth (SS), soft-rough (SR), hard-smooth (HS) and hard-rough (HR)).

Area	Lithology sample #	Type	Porosity (relative values)	Reference site #	Video composition			
					SS	SH	HS	HR
Howe Reef	139	limestone	High	2.03	**			
Gabo Reef	143	limestone	Medium	3.01	NA			
Broken Reef	218	sandstone	Medium/low	5.03	94	0	5	6
*Lacepede Shelf 80m	292	limestone	Low	9.01	0	0	3	99

* pulse length different due to shallower depth **not scored due to poor visibility but general description possible

6.5 Multi Beam Sonar (MBS) reference site analysis

Georeferenced videography data and physical samples within reference sites were used to explore multi-beam sonar (MBS) acoustic data relationships within and between terrain types. The acoustic backscatter data has been pre-processed as outlined in Chapter 4 to represent a relative depth compensated seabed backscatter value in dB. Seabed backscatter values were corrected for sound absorption and the across-track seabed slope obtained by averaging 5 eqi-spaced depth values (Ch. 4). Due to residual pitch, roll and heave depth errors these slope measurements were variable. Maximum error was associated with higher incidence angles (Fig. 4.5b). To reduce the effect of fine scale slope measurement error only seabed slopes measuring greater than 3^o were compensated. A slope correction of less than 3^o has a mean error less than 0.4 dB (Fig. 4.10). No pitch correction was applied but this effect was reduced by only accepting pings where the pitch was less than 4^o due to vessel motion and the along-track data were obtained along depth contours to reduce along-track seabed slope. Pitch correction error is small when the combined vessel pitch and seabed slope along-track incident angle is less than 7.5^o near normal incidence (Fig. 4.11).

Two simple metrics of the centre of each beam backscatter (BS_{bci}) expressed in dB, its mean and standard deviation for 'n' pings as a function of incidence angle were calculated for each swath transect within a reference site. The mean and standard deviation of the backscatter were calculated for each incidence angle step based on centre of each beam backscatter values expressed in linear terms (bs_{bci}) for n pings within the training site.

$$\text{mean } \overline{bs_{bc_i}} = \frac{1}{n}\sum_{j=1}^{n} 10^{\frac{BS_{bc_{ij}}}{10}},$$

$$\text{log mean } \overline{BS_{bc_i}} = 10\log_{10}(\overline{bs_{bc_i}}), \qquad 6.1$$

$$\text{with standard deviation } SD = 10\log_{10}\left(\left(\frac{1}{n-1}\sum_{j=1}^{n}(bs_{bc_{ij}} - \overline{bs_{bc_i}})^2\right)^{\frac{1}{2}}\right) \qquad 6.2$$

Figure 6.2 shows the seabed backscatter as a function of incidence angle corrected for local slope on a flat seafloor for a homogeneous soft-smooth and hard-rough reference site. At normal incidence (0^o) there is high backscatter for both the terrain types. As the incidence

angle increases the soft-smooth terrain backscatter decreases at a faster rate than the hard-rough terrain site. At 14^{o} incidence it is possible to separate the two seabed types backscatter (75% of the inter-ping variation) using the underlying box plot equivalent to a student-t test. The backscatter separation between the two terrains increases with incidence angle to a maximum of 13 dB at 68^{o}. The incidence angle box plot, where 50% of the backscatter (in dB) data are contained with the box, describes the sample variability associated for each terrain with incidence angle (Fig. 6.2). High variation between pings is observed near normal incidence and decreases as the beam angle increases. The backscatter with incidence angle variability is generally smaller for the soft-smooth terrain.

Of note is the correlation of underlying highs and lows between the two terrain profiles (Fig. 6.2). These common variations between two very different seabed types indicate a possible instrument calibration variation between beams of +/- 2 dB. This consistent variation when the vessel has minimal roll between beams is also observed in the average of 11 soft-smooth sites and 15 hard-rough sites (Fig. 6.3).

Figure 6.2 Variation in relative seabed backscatter (dB) for two reference sites >50 pings one side of the swath width, soft-smooth (lower) and hard-rough (upper) for seabed incidence angles of 0 to 70 degrees. Box plot shows variation of site backscatter dB with median and inter quartile (25% to 75%) range of dB values, solid line is linear mean of backscatter.

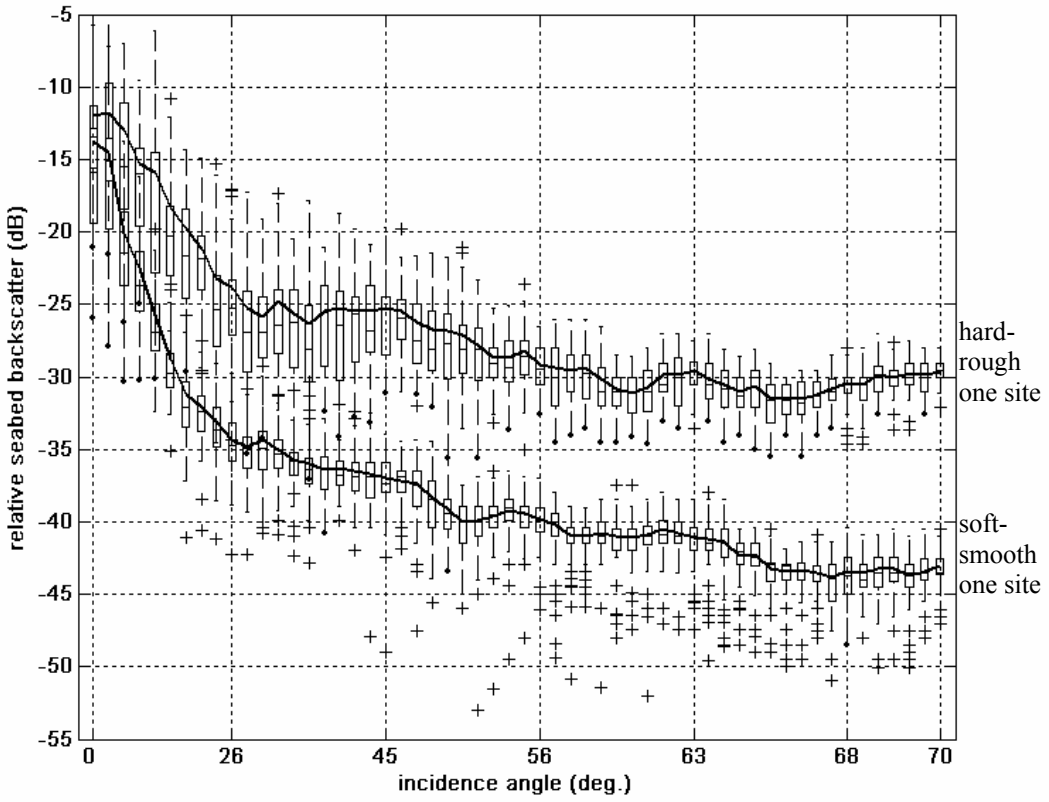

To explore the change in reflectivity with seabed incidence angle (0^o to 70^o degrees incidence) between a number of sites, 11 homogeneous soft-smooth reference sites and 15 heterogeneous hard-rough sites were established. The hard-rough sites were assigned based on a homogeneous videographic score or heterogeneous terrain designated as reef based on acoustic terrain scores of bathymetry and backscatter metrics (Table 5.9). There is a clear separation (5 dB at incidence angles > 16^o) between soft-smooth and hard-rough sites using the relationship between backscatter and incidence angle (Fig. 6.3). The relative seabed backscatter separation of the profiles decreases from 5 dB to 0 dB for incident angles 16^o to 0^o. Similarly, the standard deviations of backscatter for the mean soft-smooth and hard-rough sites are separated by 0.5 to 1 dB for incident angles greater than 16^o (Fig. 6.4). The variation between sites is very low (0.25 dB interquartile range) for the soft-smooth sites and very much higher (0.5 to 1dB interquartile range) for the hard-rough sites (Fig. 6.4). At incident angles less than 16^o the difference in standard deviation of backscatter decreases from 0.5 dB to 0.1 dB (Fig. 6.4). Based on these sites the MBS is able to separate sites using either backscatter or standard deviation of backscatter for incident angles greater than 16^o. For incident angles less than 16^o both the backscatter and standard deviation of backscatter converge and would not be as informative in separating these seabed terrains.

Of note is the steep decline in relative seabed backscatter from normal to 51^o incidence then uniform to slightly increasing backscatter at higher incidence angles for both soft-smooth and rough hard terrain types (Fig. 6.3). This increasing backscatter at high incidence angles contrasts with model predictions (Fig. 3.3) and could be due to three dominant factors. Firstly, there could be an error in the beam pattern calibration or absorption coefficient applied to the outer sectors (51^o to 70^o incidence) of the swath mapper that are operating at a different frequency. Secondly, there may be an effect of the critical angle where there is an increase in backscatter due to seabed sound speed properties (Ch. 3). Thirdly, there may be contamination from the second seabed echo that has been reflected from the seabed to surface and then seabed and arrives on a flat seafloor at the receiver at 60^o incidence angle. Others have observed elevated backscatter at high incidence angles in experimental data at the same or lower frequency range 35 – 100 kHz (Jackson and Briggs 1992 fig.10b, Williams *et al.,* 2002 fig.7). Backscatter predictions using a poroelastic model based on Biot theory and an "effective density" fluid model derived from Biot theory also predict an increase in backscatter due to surface roughness near the critical angle (Williams *et al.,* 2002 fig. 4). Given that there is elevated backscatter for several seabed types over a range of depths (lessens effect of 2^{nd} seabed echo), it is more likely that the consistent elevated backscatter is due to beam pattern calibration errors that are correlated between 15 hard-rough and 11 soft-smooth sites collected with minimal vessel roll (Figure 6.3).

Figure 6.3 Variation of relative seabed backscatter between sites for 11 soft-smooth (solid mean) and 15 hard-rough sites (dotted mean) according to seabed incidence angle. Box plot shows variation of site means (dB) with median and inter quartile (25% to 75%) range.

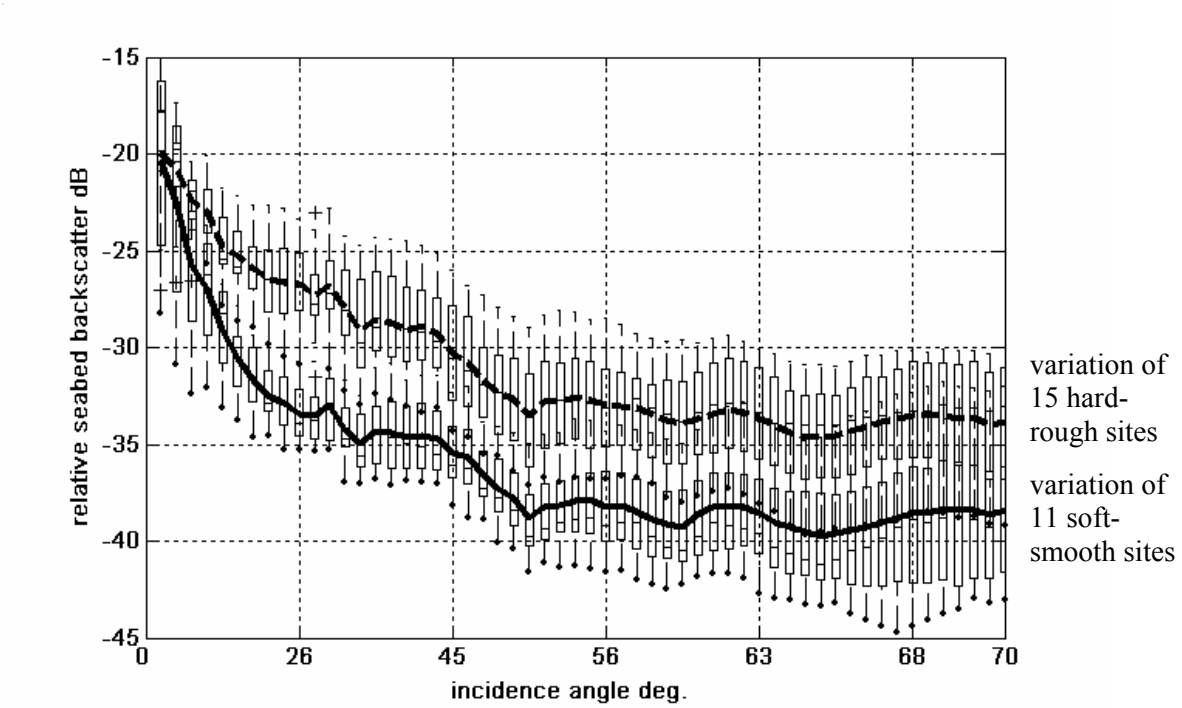

Figure 6.4 Variation of mean relative standard deviation of backscatter for 11 soft-smooth (dotted mean) and 15 hard-rough sites (solid mean) according to seabed incidence angle where 0^{o} is normal to the seabed. Box plot shows variation of site standard deviation means with median and inter quartile (25% to 75%) range.

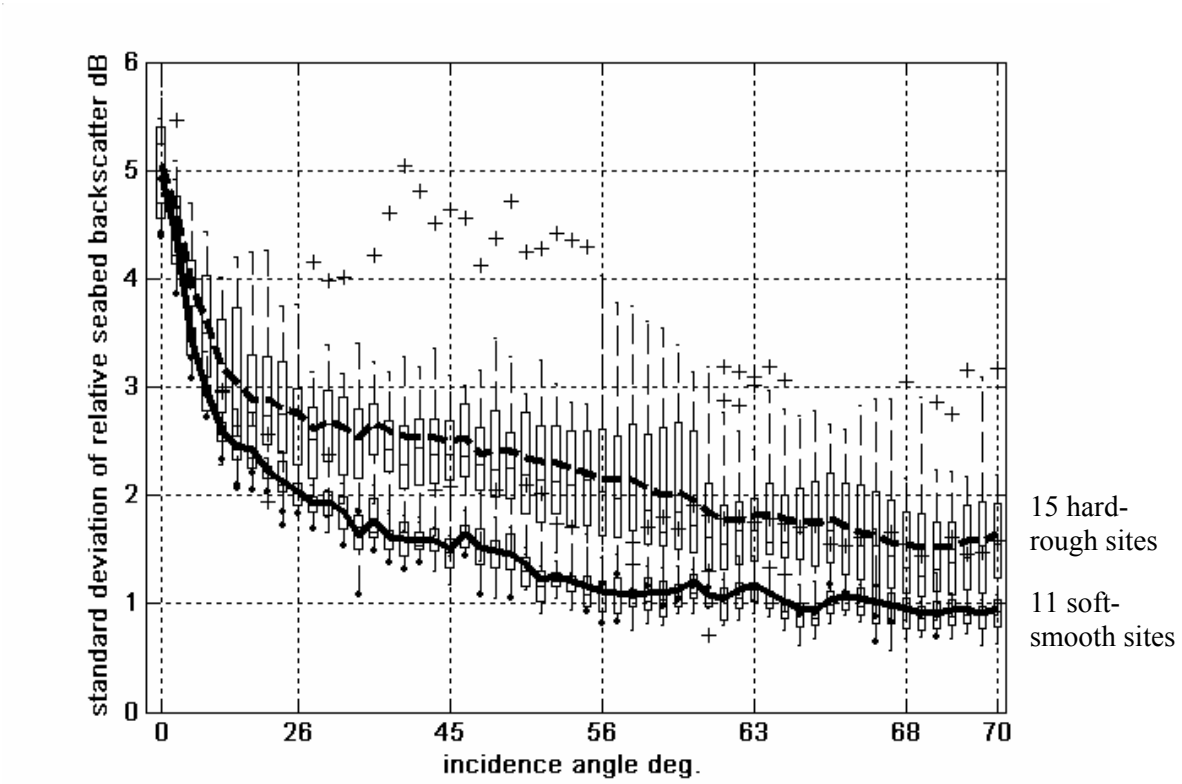

6.5.1 Soft-smooth sites

Of the 18 sites classified as soft-smooth by video, 6 occurred in less than 100 m depth, 7 were from 100 to 200 m depth and 5 were greater than 200 m depth; ten of these sites were sampled for sediments. MBS backscatter site data where sediment samples contained <10% mud fraction were visually separate (box plot) than reference sites having > 10% mud (Fig. 6.5a). The separation of the MBS mean backscatter interquartile range increases with incidence angle giving higher discriminatory power between % composition mud sites (Fig. 6.5a). Of note was a decreased near normal incident backscatter of 8 dB grading to 0 dB at 20^{o} incident between six shallow sites (50-100m) and 8 deeper sites (100-200 m). No instrument artefact due to pulse length or power was uncovered and a comparison of hard-rough sites for similar depth ranges did not show a similar pattern (Fig. 6.7a). The difference may be due to changes in sediment layer depth and changes in porosity leading to lower reflection coefficient and higher attenuation within the sediment.

The variation of MBS backscatter standard deviation for the soft-smooth reference sites is similar (overlapping interquartile ranges) for <10% and >10% mud sites (Fig. 6.5b). There is high (5dB) variation at normal incidence reducing rapidly to 2.5 dB (16^{o}) and then reducing gradually to 1dB at 70^{o} incidence. The similarity of the standard deviation of backscatter for the different mud composition soft-smooth sites is important for between terrain discrimination. Two sites with similarly low backscatter standard deviation incident angle profiles could be distinguished using the mean backscatter to incident angle relationship having in this case a mud composition <10% or >10%. Figure 6.4 shows that if two terrain types have the same relative seabed backscatter it may be possible to separate them into soft-smooth and hard-rough using the backscatter standard deviation.

Figure 6.5 Variation of backscatter mean (a) and standard deviation (b) for soft-smooth reference sites, 4 with mud composition < 10 % (solid mean) and 6 with mud > 10% (dashed mean). Box plot shows variation of site mean and standard deviation means with median and inter quartile (25% to 75%) range.

a) **b)**

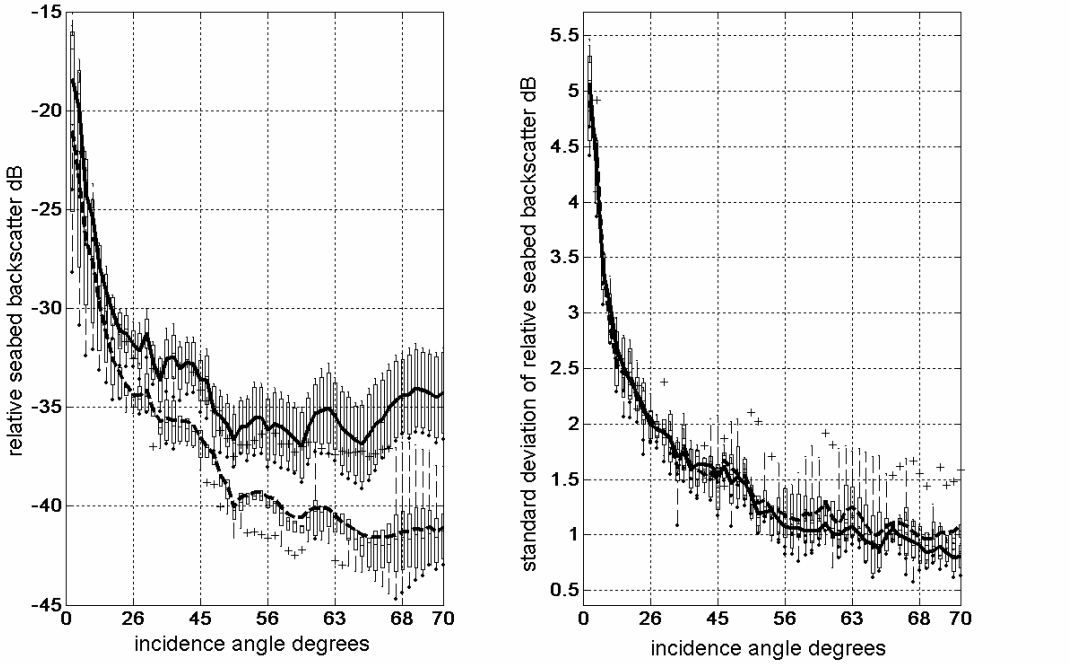

6.5.2 Soft-rough site

Of the six homogeneous soft-rough reference sites, two contained corrupted acoustic data due to deeper depths or poor weather and three sites within a similar region contained videography data that could not be adequately georeferenced. Analysis is therefore restricted to a single homogeneous reference site, depth 138 m, large scale slope less than 1^{o} with a sediment sample dominated by sand (90% sand, 6% gravel and 4% mud). The mean seabed backscatter with incidence angle for the soft-rough site is similar in amplitude variation to the mean of the soft-smooth sites and much lower in amplitude than the hard-rough sites (Fig. 6.6 a). This contrasts with the standard deviation of backscatter being similar to soft-smooth sites when incidence angles are less than 36^{o} and higher at incidence angles greater than 36^{o} (Fig. 6.6 b).

Figure 6.6 Comparison of the a) mean and b) standard deviation of relative seabed backscatter of a soft-rough site (solid) with 11 soft-smooth sites (dash-dot) and 15 hard-rough sites (dashed).

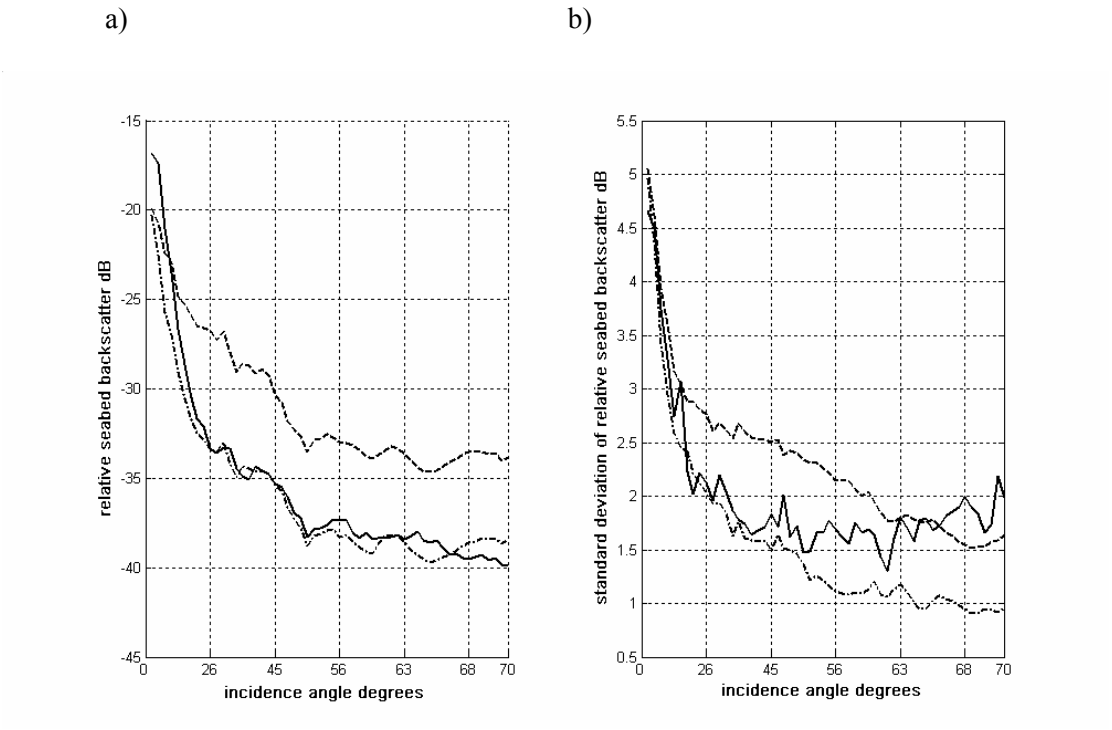

It is not possible to separate the soft-smooth and soft-rough sites based on the mean of the backscatter with incidence angle relationship (Fig. 6.6 a). The standard deviation of backscatter could be used to differentiate the sites but only at high (~44^{o}) incidence angles. The georeferenced time series of acoustic backscatter for the soft-rough site has a regular undulating pattern distinctly different from the uniform soft-smooth terrain. Phenomenological statistics using GLCM and a power spectrum metric will be used to describe these features in Chapter 6.7.

6.5.3 Hard-rough sites

The videographic data classified 6 hard-rough reference sites as being homogeneous (Table 6.1). These sites did not include reference sites within acoustic terrains known from both lithology and bathymetry to be limestone/sandstone reefs (Table 6.6). These reef reference sites varied in the proportion of hard rough terrain characteristics from 5 to 99 % (Table 6.6). A reference site was classified as hard-rough when 5% of the video score was hard-rough terrain and the reference site was within a hard-rough acoustic terrain (Table 5.9). This increased the number of available hard-rough sites from 5 to 7 in the 50 to 100 m depth range and from 1 to 8 in the 100 to 200 m depth range. The relationship of the mean backscatter with incident angle from the 50 to 100 m and 100 to 200 m hard-rough sites were very similar with overlapping interquartile ranges (Fig. 6.7 a). Soft-smooth sites in contrast had a high difference in mean backscatter at low incidence angle (<16^{o}) between the same depth ranges as discussed previously. Based on the standard deviation of relative backscatter the 100 – 200 m hard-rough sites were 1 dB higher between 40^{o} to 60^{o} incidence and greater than 0.3 dB higher between 26^{o} to 70^{o} than the 50 to 100 m sites (Fig. 6.7 b). The macro roughness as observed with the bathymetry indicated that the deeper sites were rougher although no quantitative metrics were obtained using the videographic data.

Figure 6.7 Variation of mean backscatter (a) and its standard deviation (b) for 15 hard-rough reference sites (solid), 7 within 30 to 100 m depth (dotted), 8 within 100 to 200 m depth (dashed) according to incidence angle. Box plot shows variation of between site means and standard deviation with median and inter quartile (25% to 75%) range.

a) **b)**

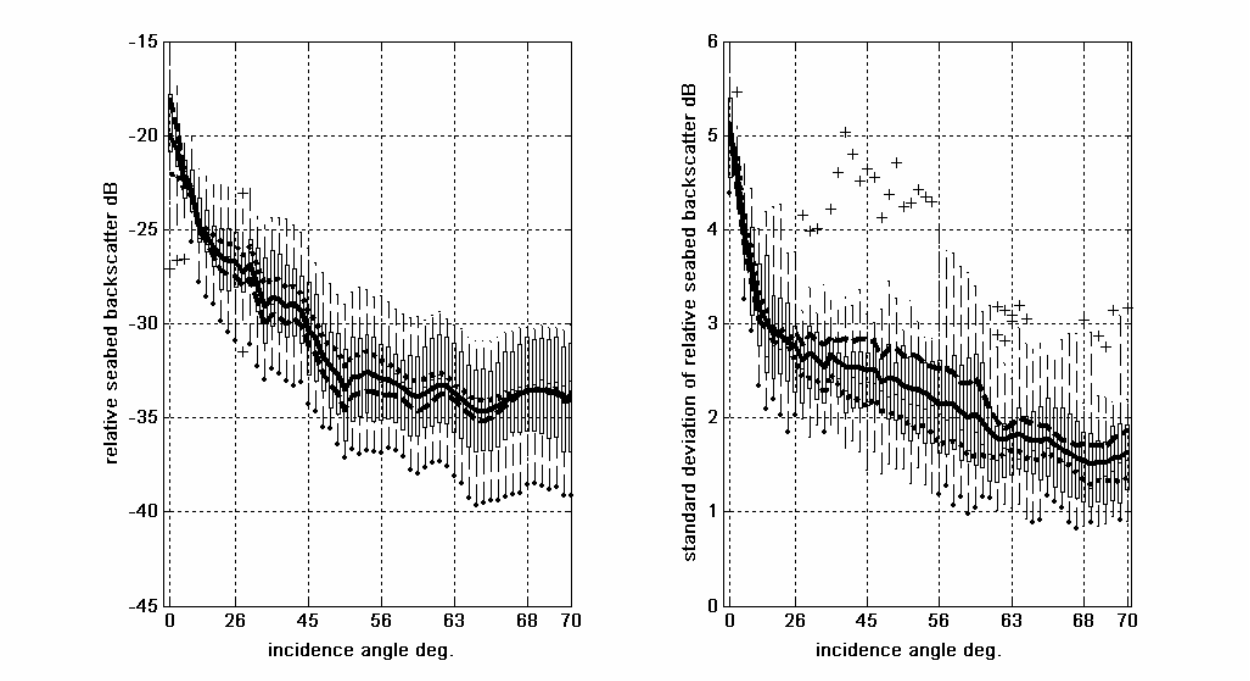

6.5.4 Patchy hard-rough sites (Reef)

Based on acoustic terrains, lithology and available video data 4 sites were designated as being hard-rough reef sites (Table 6.6). The acoustic terrains designation of reef was determined predominantly by the undulating bathymetry. These reef reference sites had a mean relative backscatter that could be similar (at lower end of interquartile range) to soft-smooth reference sites where the mud content was less than 10% (Fig.6.8 a). The similarity increased at higher incidence angles (Fig. 6.8 a). Reef site mean standard deviation was consistently higher (0.5 to 1 dB) between 14^o to 60^o than the soft smooth sites of <10% and >10% mud (Fig. 6.8 b). Both the mean and standard deviation could be used to separate the soft-smooth and hard-rough sites within 14^o to 60^o incidence.

Figure 6.8 Variation of mean backscatter (a) and its standard deviation (b) for 5 reef reference sites (solid mean) and soft-smooth reference sites (Fig. 6.5) with mud composition < 10 % (dashed mean) and 6 with mud > 10% (dotted mean) according to incident angle. Box plot shows variation between sites with median and inter quartile (25% to 75%) range.

a) **b)**

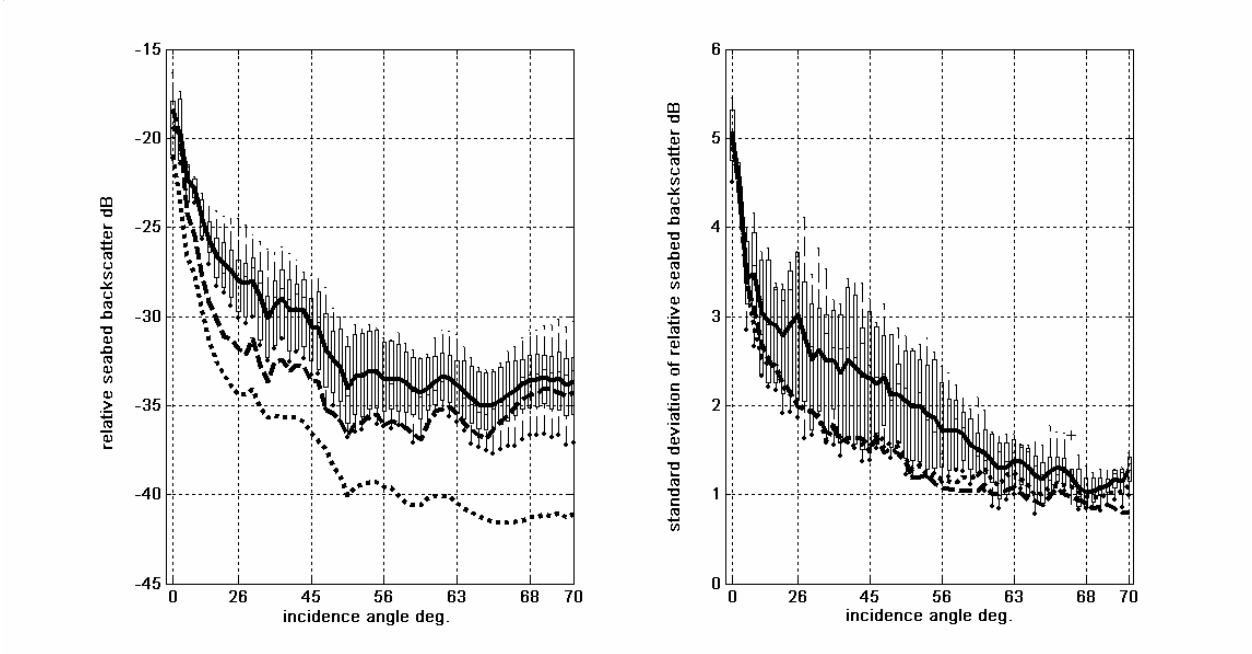

In summary this section has shown that by using two simple metrics of the MBS backscatter, being the mean of a number of pings at a given incidence angle and its standard deviation, it is possible to differentiate between soft-smooth and hard-rough sites. It is also possible using the mean backscatter to distinguish between changes in the percentage composition of mud for the sites surveyed. This ability to distinguish between terrain types is not uniform across the range of seabed incident angle. Clearly the results show that at near normal incidence ($<16^o$) there is little discrimination provided by the relative seabed backscatter mean or its standard deviation metric. To improve the discrimination between and within the terrains for incident angles 16^o to 70^o it is necessary to have both the mean and standard deviation. Within this range certain incidence angles on particular terrains will provide better separation of the relative seabed mean of backscatter and its standard deviation.

6.6 Model based classification using APL94 model

Based on the theory of acoustic scattering presented in Chapter 3 and the APL94 (1994) seabed scattering model the geoacoustic properties of the seabed can be evaluated by solving the inverse problem using the MBS backscatter mean. A 12 dB amplitude shift of the MBS backscatter data was needed to maximise the fit of the data to the APL94 model minimising the Kolmogorov-Smirnov (KS) statistic (mean= 0.38, s.d.=0.08, n=75). The nature of the large discrepancy between the relative MBS backscatter and the APL94 model is unknown but consistent across all sites. This difference may be a combination of model error, calibration uncertainty and calculation of the equivalent ensonified area (Figure 4.7). To investigate these differences detailed knowledge of the Simrad EM1002 pre-processing algorithms are required but was not available. After the MBS values were all adjusted by 12 dB there remained significant differences between the APL94 model and the mean soft-smooth and hard-rough terrain types (Fig. 6.9). Firstly, at high incidence angles ($>55^o$) the

model shows a decreasing backscatter whereas the backscatter data for both terrain types increases (Fig. 6.9). This increasing backscatter is likely due to the critical angle that is predicted to occur within this range of incidence angles for sandy sediment sound velocities (Ch.3). Secondly, the hard-rough sites are within the APL94 (1994) model prediction profiles of medium to coarse sand and higher backscatter is expected given the hard-rough terrain features.

Figure 6.9 APL94 model predictions (adjusted by –12 dB) of typical seabed types ranging from rock to clay terrains assuming geoacoustic properties in Table 3.2 at 0° to 70° incident to the seafloor, and mean backscatter for soft-smooth (dotted) and hard-rough (solid) reference sites (Fig. 6.3).

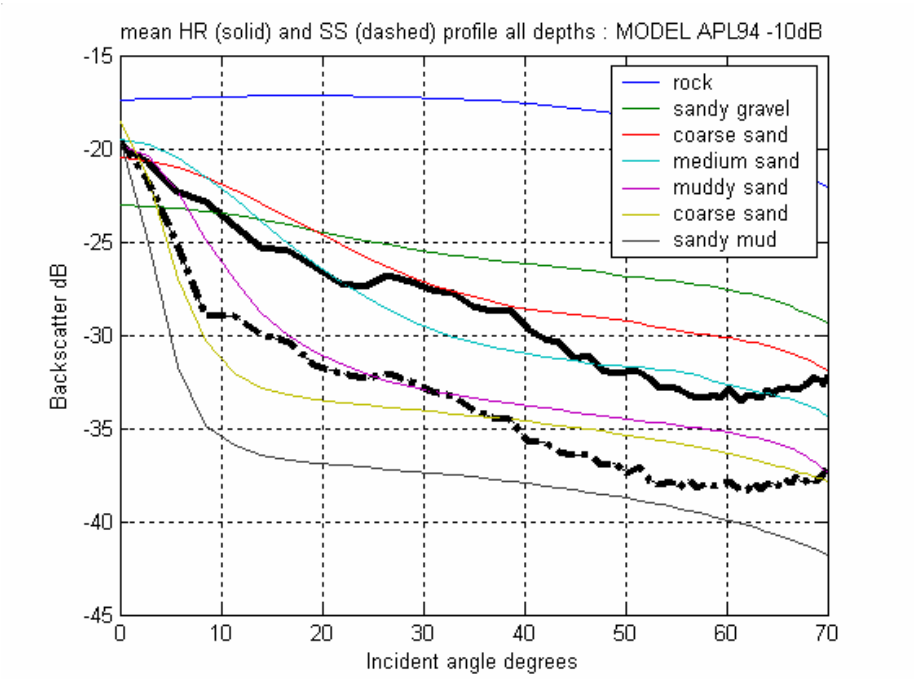

In this section the homogeneous site MBS backscatter data as a function of incidence angle is compared to the APL94 model by considering two questions. Firstly, what is the robustness of separating the soft and hard sites using the APL94 model? Secondly, by solving the inverse problem, do the derived geoacoustic properties agree with the videographic and physical sampling for separation within and between soft-smooth and hard-rough sites? To fit the MBS backscatter data to the APL94 model two fitting procedures were used. Firstly, the MBS data were separated into the model seabed types (Table 3.2) using the KS test to select the best fit. Secondly, a simulated annealing fitting procedure optimised the geoacoustic parameters for the best KS test fit constrained by the limits of the geoacoustic parameters (Table 3.3). It was observed that model parameter predictions based on simulated annealing varied greatly for sites of similar profiles and were sensitive to the absolute backscatter level of the MBS.

6.6.1 Soft-smooth sites

MBS backscatter data for 11 soft-smooth sites, depth 50 to 200 m, that contained sediment samples (Table 6.7) were fitted to the APL94 (1994) model using the lowest KS test for historic geoacoustic values (Table 3.2) and simulated annealing. Similar fitting was obtained when using the historic values (Table 3.2) (KS mean=0.24, s.d.=0.09, n=11) or simulated annealing (KS mean=0.17, s.d.=0.04,n=11), where KS fit statistics of 1 is poor and 0 is good (Fig. 6.10). The fitting of the APL94 model data was highly dependant on incidence angle, where the fit was poor (error 3 to 15 dB) at near nadir 0° to 28° incidence and good (~less

than 2 dB) between 30° to 65° incidence and slightly poorer fit for incidence angles > 65° (Fig. 6.10).

Table 6.7. Prediction of sediment size (in phi units) based on model values (Table 3.2) and minimum Kolmogorov-Smirnov (KS) fit to 11 homogeneous soft-smooth terrain reference sites with measured sediment composition (gravel, G, sand, S, mud, M).

Site #	Predicted Mean Grain Size (phi)		Measured Sediment composition % dry weight			Depth
		KS fit	M	S	G	m
1.05	5.5	0.27	30	67	3	73
13.01	5.5	0.32	19	78	3	144
13.02	5.5	0.32	14	85	1	144
1.06	5	0.39	17	82	1	112
1.07	5	0.34	16	82	2	89
1.08	5	0.21	15	83	2	87
5.07	3	0.13	9	88	3	89
14.03	2.5	0.18	11	86	3	150
1.09	2.5	0.14	5	90	5	90
3.05	1.5	0.21	3	92	5	135
3.05	1	0.14	3	92	5	135

The predicted seabed phi size from the APL94 (1994) model using the best fit to the historic geoacoustic seabed properties (Table 3.2) followed the general trend in grain size of the homogeneous soft-smooth sites (Table 6.7). Significantly as the mud fraction increased the predicted grain size decreased (higher phi size) ($R^2 = 0.54$, n = 11).

Figure 6.10 Box plot of difference in mean backscatter data at each incidence angle to that predicted by the APL94 (1994) seabed backscattering model from 11 soft-smooth reference sites (50 to 200 m depth) using two methods of fitting; a) using simulated annealing, b) best fit to historic geoacoustic values (Table 3.2).

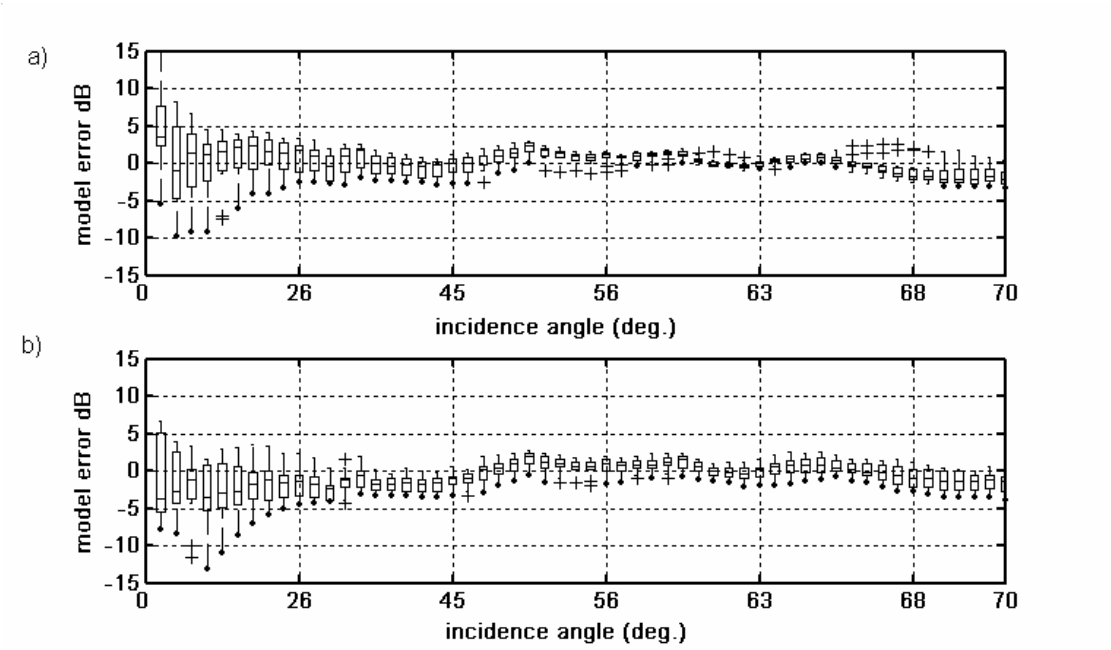

Higher mud compositions in sediment samples were commonly associated with higher predicted phi sizes (i.e. smaller grained sediments Table 6.7). Similarly higher gravel content was associated with lower phi sizes (i.e. larger grains Fig. 6.11), although there is a high degree of variability when including all reference sites (Fig. 6.11).

Figure 6.11. Predicted sediment size (phi) based on model values (Table 3.2) and minimum Kolmogorov-Smirnov test fit to 36 reference sites with sediment composition of gravel (o) and mud (*), dry weight fraction (%).

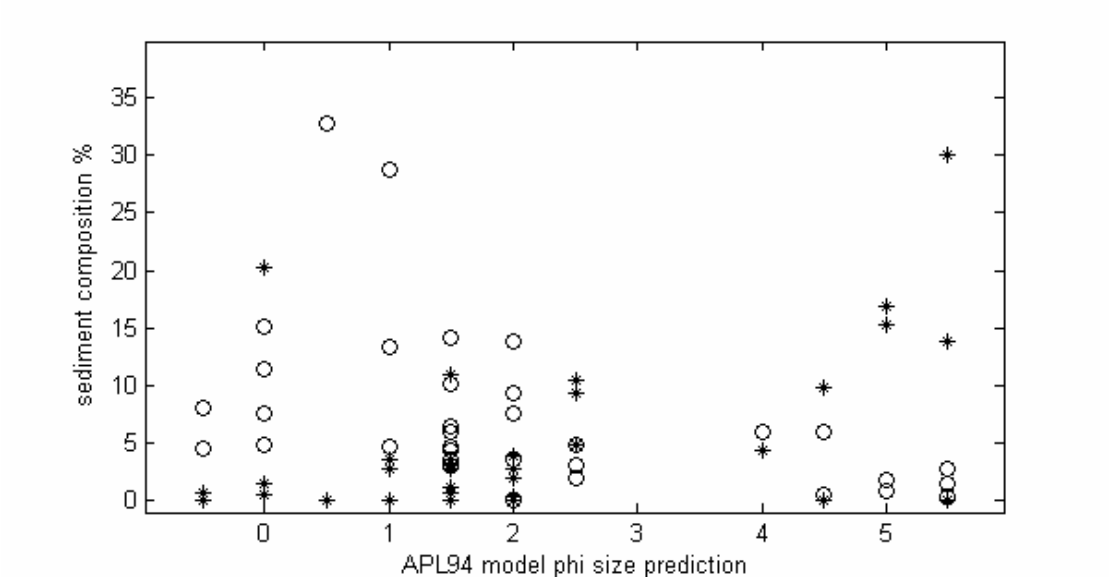

Some of the variability observed is due to the inhomogeneity of the hard-rough reference sites (Table 6.1). Repeat samples (3) of sediments at a reference site showed that sediment composition varied by 8 to 58 % for gravel and 0 to 5 % for mud within 50 m. The acoustic data for the reference site was averaged for 50 pings being 50 m and 100 m wide.

Physical sampling at two homogeneous soft-smooth sites using a box core provided material for independent geoacoustic measurements (Table 6.8). The density-ratio and sound-speed-ratio were calculated from the sediment bulk density and p-wave velocity respectively (Sec.5.7).

Table 6.8 Geoacoustic properties of density ratio and sound speed ratio of two soft smooth sites based on box core samples.

Reference Site #	Core #	Core depth (cm)	Seabed depth (m)	G %	S %	M %	Density ratio	Sound speed ratio	Description
1.05	bc19	20.5	73	3	67	30	1.657	1.030	Stratified from muddy sand (0-5 cm) to coarse sand (14-20.5 cm) good bulk density and P-wave velocity readings from 8 - 20 cm
1.06	bc14	11.5 to 20	85	2	77	21	1.608	1.035	Stratified from muddy sand (0-5cm) to coarse sand at 11.5 cm. Good bulk density and P-wave velocity readings from 12 to 20 cm which is inconsistent with depth of core

The bulk density ratio (1.608 and 1.657) for the stratified sediment types is within the expected range (1.339 to 2.231) of sediments ranging from muddy sand to coarse sand based on historic data (Table 3.2). In contrast the sound speed ratio, 1.03 and 1.035 of the sediments

is 5% lower than the expected range, 1.08 to 1.2503 (Table 3.2). Using simulated annealing the predicted bulk density ratio (1.16 and 1.295) and sound speed ratio (0.849 and 0.894) for reference sites 1.05 and 1.06 are very much lower than the measured values (Table 6.8) and well outside the historic values (Table 3.2).

6.6.2 Soft-rough site

Based on model values the soft-rough site was predicted (KS test = 0.2) to have a phi size of 4, equivalent to a sediment composition of clayey sand and associated very low roughness metrics (spectral exponent, 3.25 and spectral strength, 0.001119) (Table 3.2). These spectral roughness values equate to a 2 cm rms height difference at 1 m (Fig. 6.12), assuming a power law and isotropy (Sec. 3.5). The video data does not support the low roughness predicted for the site where the peak to peak heights were approximately 25 cm (~9 cm rms). Also, a sediment sample at the site contained high sand and gravel content (90% sand, 6% gravel and 4% mud) and would have a lower phi size (~1.5) than the phi size of 4 predicted using the APL94 model. Simulated annealing predictions (KS test = 0.11) of seabed roughness metrics, spectral exponent (2.62) and spectral strength (0.5617) were very much higher than the model default historic roughness values (Table 3.2). Simulated annealing roughness values predict a height difference of 14 cm rms or 40 cm pk-pk at a distance of 1 m (Fig. 6.12). These are similar to the peak to peak heights estimated using laser measure from the videographic data.

Figure 6.12 Prediction of surface roughness assuming power law relief spectrum and isotropy for a soft-rough site using model values (solid) (Table 3.2) and simulated annealing (dotted).

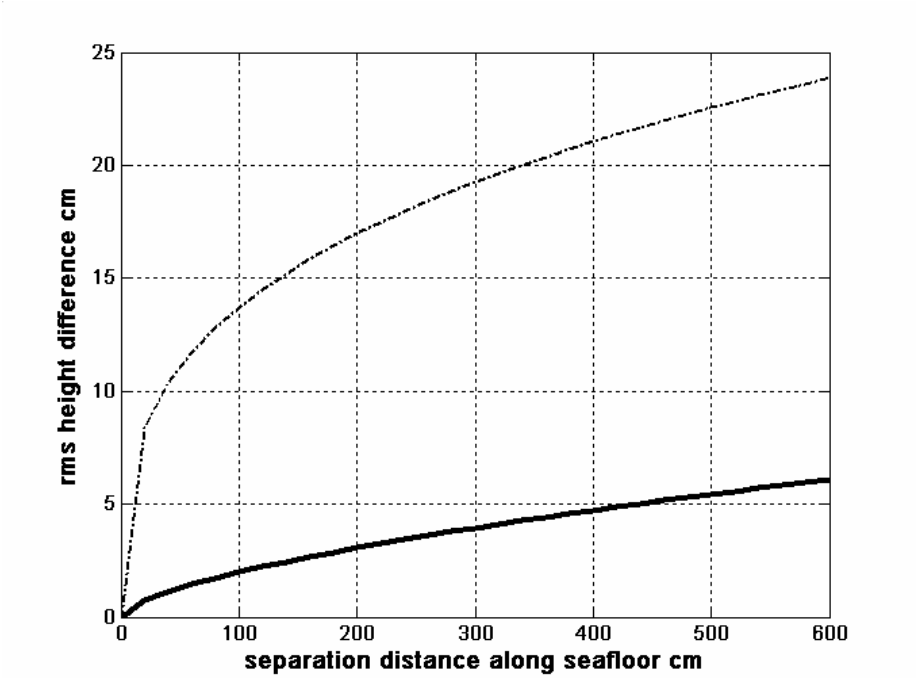

6.6.3 Hard-rough sites

Fourteen hard-rough sites were assigned if greater than 5% of the video score indicated it was hard-rough and the site occurred within a megascale hard-rough acoustic terrain (Table 5.9). The KS fit test to the APL94 model using historic geoacoustic values (Table 3.2) (KS=0.18, s.d.=0.05, n=14) and simulated annealing (KS =0.14, s.d.=0.04, n=14) showed a similar trend to the soft smooth sites (Fig. 6.10). The predicted mean sediment size of rough-hard sites (mean phi size= 0.9, s.d.= 1.7) was significantly larger than the soft-smooth sites (mean phi

size= 3.8, s.d.=1.2, n=11). The difference in the means (2.9 phi size) was significant at the 0.05 confidence level (Student t= 5.1, d.f = 24) assuming that the distributions are normal. Similarly the spectral strength of the seabed is inferred to be rougher for larger sediment sizes using the historic geoacoustic values in Table3.2 (Fig. 6.13).

Figure 6.13 Model predicted a) mean sediment grain size (phi) and b) spectral strength based on model values (Table 3.2) for the 11 soft smooth and 14 hard rough reference sites 50 – 200m depth.

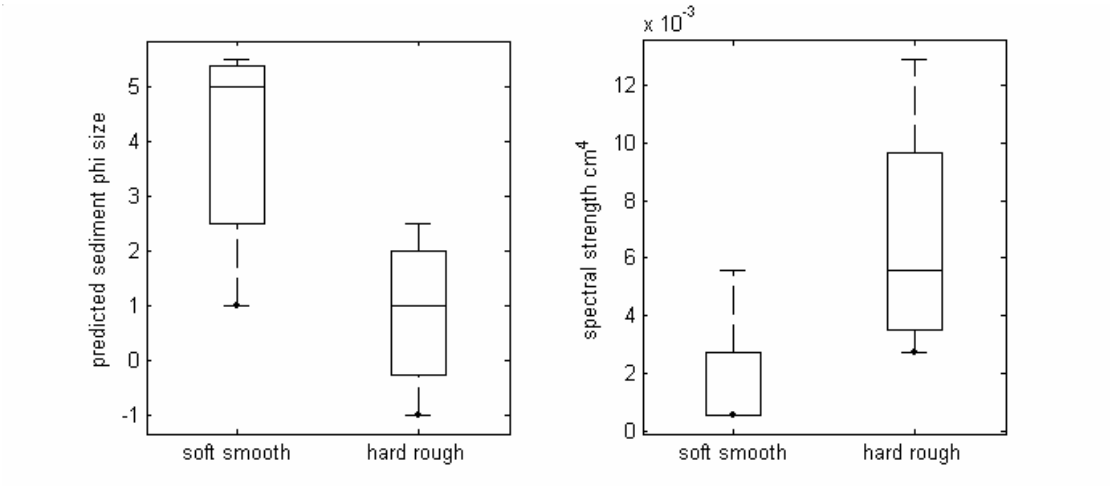

The ability of the APL 94 (1994) model to predict roughness of the seafloor using simulated annealing for soft-smooth and rough-hard terrains was investigated based on the recommended general limits of the geoacoustic parameters (Table 3.3). Large values of spectral exponent and spectral strength were observed for both soft-smooth and hard-rough seabed terrains (Fig. 6.14). These were orders of magnitude higher than those of historic spectral exponent values for similar seabed types (Fig. 6.13). The roughness parameters of spectral exponent and spectral strength (Student t=-1.56 and t=-0.7, d.f.=24 respectively) could not separate the soft-smooth and hard –rough sites at the 0.05 confidence level assuming an underlying normal distribution.

Figure 6.14. Box plot of APL94 (1994) model predicted roughness values a) spectral exponent and b) spectral strength for soft smooth and hard rough reference sites using simulated annealing with general limits specified in Table 3.3.

a) **b)**

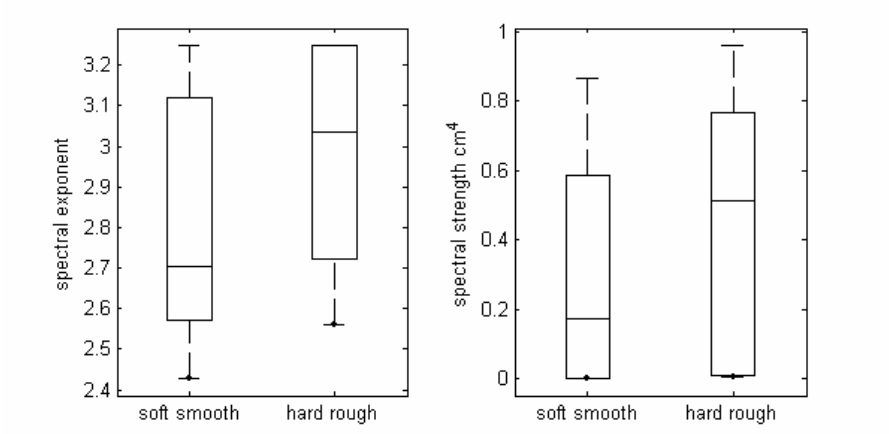

Using the inverse of the APL94 (1994) model, sediment grain size can be reasonably predicted for soft-smooth sediments whilst the roughness of the seafloor is poorly predicted. This can be demonstrated with a simple example comparing a known low porosity hard-rough reef site (site 2.03, Table 6.6) with a soft-smooth sediment-flat site (site 3.05, Table 6.7). The predicted sediment-flat-site grain size (phi size 1 to 1.5) is larger with higher spectral roughness than the reef site (phi size range 1.5 to 2). Spectral roughness assuming a power law and isotropy (Sec. 3.5) predicts that the soft-smooth sediment-flat site rms height difference across the seafloor is either higher or lower than the reef site dependent on sampling directions (Fig. 6.15). The two sites are very different based on video data; the reef site having low porosity limestone either as subcrops or outcrops (Table 6.6). The video measured roughness at the east-west soft-smooth site was very much less than that predicted 17.5 cm rms or 50 cm peak to peak over a 1 m separation distance (Fig. 6.15). It should be noted that the two sites are reliably separated using the backscatter standard deviation (Fig. 6.4). The prediction of geoacoustic properties using the simulated annealing approach outlined here does not appear to be producing reliable or realistic values. There may be an improvement to the model predictions of geoacoustic parameters if beam pattern artefacts are removed. Due to vessel motion a consistent method to remove these artefacts was not successful. The cumulative whole of incidence angle profile was used in the KS test to determine the profile of best fit and minimise sensitivity to within profile beam pattern artefacts.

Figure 6.15 Simulated annealing APL94 (1994) model prediction of surface roughness assuming power law relief spectrum and isotropy for two reference sites; soft-smooth (o) and reef (*) with orthogonal sampling, north-south (solid) and east-west (dotted).

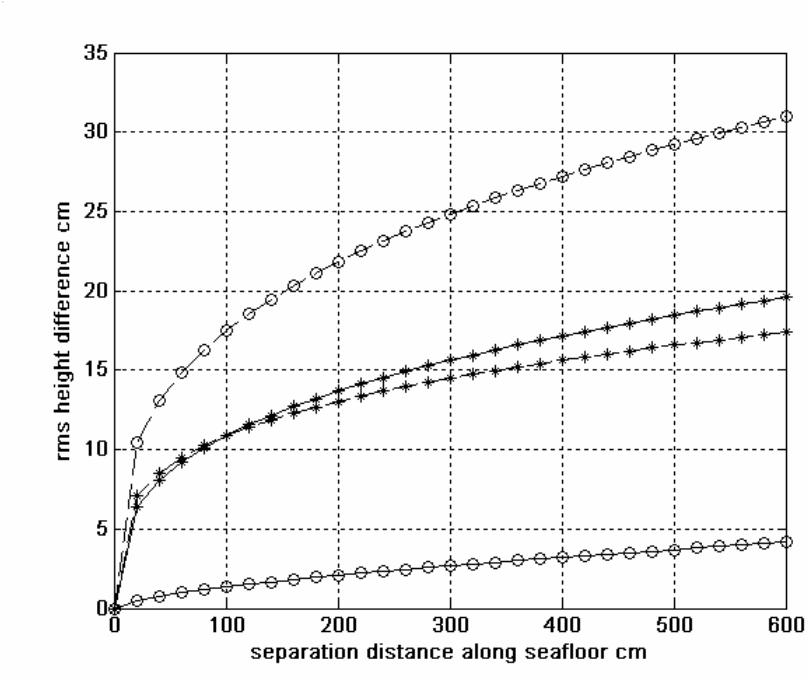

6.7. Statistical descriptors for seabed segmentation

Based on the analysis of the seabed backscatter for the reference sites and knowledge of the APL94 (1994) model a segmented (by ensonified incident angle) statistical classification of the backscatter is proposed. A model based classifier based entirely on the mean backscatter is by itself insufficient to segment the seafloor into terrain types (Sec. 6.6). Using the

backscatter standard deviation provided enhanced discriminatory power for certain seabed types but only within certain ensonified incidence angles (Sec. 6.5).

Of note is that most sites represented a mosaic of seabed types at fine spatial scales where 50% of the variability occurs at length scales between 18 m to 90 m (Fig. 6.1). Using a phenomenological approach it is possible to extract out features in the backscatter and bathymetry data that could provide better discrimination at a finer scale. Previous methods required the entire half swath width (2.75 times water depth) from normal to maximum (70^o) ensonified incidence angle. Phenomenological properties defined in Section 3.8 for the acoustic backscatter, spectral, grey level concurrence matrix (GLCM), mean backscatter, standard deviation of backscatter and quantile of the backscatter were derived from the data for selected incidence angles and ensemble of pings. In addition metrics from the depth data were calculated based on the mean and its standard deviation, slope and its standard deviation. The mean depth was not used in the subsequent classification systems due to it being included in the higher level separation of acoustic terrains at the megahabitat scale.

The scale of the metrics extracted from the MBS data was preset to take advantage of the difference in response over the backscatter profile and ensure even sampling areas. Two levels of segmenting the across-track data, 6 and 10 segments, were explored (Table 6.9). Using the Simrad EM1002 MBS (111 beams at 140 degrees swath) at equidistance spacing the across-track sampling distance per sector is 1.1 times depth and 0.5 times depth for the 6 and 10 sectors respectively (Table 6.9). The across-track sampling area for echostatistics is very much smaller than 6 and 10 segment sizes (Sec. 4.2.2). The sampling length along-track is defined by the beamwidth of the swath system that increases with depth and the vessel speed and ping rate (Sec. 4.2.2). To avoid correlative sampling the segmentation of the data along-track for a horizontal flat seafloor should be larger than the width, l_i , ensonified by the along-track beam width, ψ_i , (0.044 radians for EM1002) at incident angle, θ_i ;

$$l_i = \frac{\psi_i d}{\cos(\theta_i)} \text{ m following Eq. 4.16.} \qquad (6.3)$$

For incident angles, θ, 0^o to 70^o assuming a flat seafloor the width of the ensonified area, l_i , at depth, d, ranges from 0.044d to 0.129d .

The predicted along-track sampling ranges from 4 to 374 m for depths 50 to 600 m and ping ensembles of 4, 8 16 and 32 (Table 6.10). At a 4 ping ensemble there will be overlap of sampling from adjacent sectors when the incidence angle exceeds 55^o (Sec. 4.2.2). To ensure even sampling both along-track and across-track 25 pings are required for the 10 sector subdivision or 52 pings for the 6 sector case, assuming a ship speed of 10 knots and maximum ping rate (Table 6.10).

Table 6.9. The effective sampling distance of segmenting the across-track ensonification of the MBS backscatter data assuming 111 equidistant spaced beams into 5 and 10 segments for a flat horizontal seafloor. Note the centre beam (angle 0) is replicated in adjacent segments.

segment	6 segments		Across-track Distance Factor of seabed depth	10 segments		Across-track Distance Factor of seabed depth
	beams	angles		beams	angles	
1	22	-71 to 61	1.10d	11	-71 to –67	0.55d
2	23	-60 to –30	1.15d	11	-66 to –60	0.51d
3	11	-29 to 0	0.55d	11	-59 to –49	0.51d
4	11	0 to 29	0.55d	11	-48 to –30	0.53d
5	23	30 to 60	1.15d	12	-29 to 0	0.55d
6	22	61 to 71	1.10d	12	0 to 29	0.55d
7				11	30 to 48	0.53d
8				11	49 to 59	0.51d
9				11	60 to 66	0.51d
10				11	67 to 71	0.55d

Table 6.10. The effective sampling distances of segmenting the along and across track ensonification of the MBS backscatter data assuming a swath sampling of 140 degrees and speed of 10 knots for various depths.

Depth (m)	Across-track distance (m) Segmentation of swath		Along-track distance (m) pings			
	6*	10	4	8	16	32
50	52	25	4	8	16	31
100	105	50	8	16	31	62
200	210	100	16	31	62	125
400	420	200	31	62	125	249
600	630	300	47	94	187	374

* the inner sector is only half of the outer sectors.

Eleven parameters were derived from the MBS at ensemble spatial resolutions of 6 and 10 sectors across-track and 4, 8, 16 and 32 pings along track (Table 6.11). Acknowledging the poor discrimination of the central portion of the beam to discriminate terrain types (Sec. 6.5.2) a parameter that looked at the ratio of the central beam backscatter to adjacent sectors, ’bps’, was derived (Table 6.11). This ‘bps’ parameter gives a relative gradient across the incident angles to estimate the seabed composition in the central sector based on information in other sectors.

Table 6.11. Parameters derived from the MBS backscatter and depth used in the phenomenological segmentation of the seafloor (described in Sec. 3.8).

Parameter	Description
mn	Mean ensemble of backscatter amplitude.
q8	80% quantile.
sd	Standard deviation of backscatter amplitude.
bps	Ratio of central mean backscatter to adjacent sectors
df3	Power spectrum of backscatter
ddf3	Power spectrum of depth data
co	Contrast of GLCM
en	Entropy of GLCM
dsd	Standard deviation of depth
ssd	Standard deviation of slope
smn	Mean slope

To test the correlation of the parameters within terrain types and the importance of parameters in detecting differences between terrain types, four reference regions were established. The reference regions represented homogeneous ecological terrain types of soft-smooth, soft-hard, hard-smooth and hard-rough. It was not possible to find a site that contained 100 % hard-smooth videographic score. Therefore, subsets of a site were extracted that demonstrated by video analysis 100 % hard smooth terrain type in each sector. The correlation, 'corr', of a parameter, i, to parameter, j, within a terrain type can be measured based on the covariance matrix, 'cov' (Matlab 6.5).

$$corr = \frac{\mathrm{cov}(i,j)}{\mathrm{cov}(i,i)\,\mathrm{cov}(j,j)}. \qquad (6.4)$$

The correlation between parameters for the 4 ecological terrain types shows that many parameters are correlated with correlation coefficients greater than 0.5 and less than -0.5 (Table 6.12). The standard deviation of backscatter (sd) metric gave the highest number of correlations across all seabed types. Therefore, there is significant amount of redundant information in the parameters. The least correlated parameters with the seabed terrain types are those that deal with spectral characteristics (ddf3 and df3) (Table 6.12).

Table 6.12. Number of times the correlation between parameters within the 4 ecological terrain types is greater than 0.5 or less that –0.5.

	Number of parameter correlations greater than 0.5 and less than -0.5.			
Parameter	**site 1 SS**	**site 2 SR**	**site 3 HS**	**site 4 HR**
'bps'	0	3	4	3
'co'	2	3	5	1
'ddf3'	0	0	0	0
'df3'	0	0	0	0
'dsd'	0	1	1	1
'en'	2	2	4	1
'mn'	2	2	5	3
'q8'	2	2	5	3
'sd'	4	4	5	3
'smn'	0	0	0	1
'ssd'	0	1	1	2

The ability for a parameter to detect differences between the four ecological terrain types was gauged by a separation metric. All the parameters were normalised by their standard deviation prior to measurement of the separation metric. Several measures of separation between parameters can be used ranging from Euclidian to Mahalanobis distance metrics. The Mahalanobis distance metric was chosen here as it has the advantage of including both the mean separation of the variables and the variability around the mean using the covariance matrix. It is assumed that a Mahalanobis distance of 5 or greater represents a significant separation distance (Huseby *et al.,* 1993). The mean backscatter, 0.8 quantile and standard deviation provided the best separation parameters for incidence angles of 30^{o} and higher (sectors 1,2,5 and 6) (Table 6.13). At incidence angles less than 30^{o} the "between segments" (s34) parameters of mean backscatter, 'bps', and frequency,'df3', provide the best discrimination of terrain types (Table 6.13). For the terrain types selected the depth metrics of standard deviation of depth and slope were important in all sectors but the mean slope provided no discriminatory power at the defined Mahalanobis separation metric of 5 (Table 6.13).

Table 6.13 Number of times the Mahalanobis distance between the four ecological terrain types for a given parameter was greater than 5 for the 6 segments (1 to 6) combined by common incidence angles 1&6, 2&5, and 3&4 for the 4 ping ensemble (Table 6.9).

	Number of times Mahalanobis distance was greater than 5 between the 4 ecological terrain types for the 6 sectors.			
Parameter	**1&6**	**2&5**	**3&4**	**ALL**
mn	6	5	0	11
q8	6	5	0	11
sd	5	5	0	10
bps	4	3	3	10
df3	0	2	4	6
co	1	1	2	4
en	3	2	0	5
ssd	2	1	1	4
dsd	1	1	1	3
ddf3	1	0	0	1
smn	0	0	0	0
Total	28	25	11	

Figure 6.16 shows the between terrains Mahalanobis distance metric and the importance of different incident angle segments ranked by Table 6.13. Frequency, 'df3', and GLCM contrast, 'co', parameters have very high separation distances for some sectors and specific sites (Fig.6.16). The frequency parameter is the dominant distance metric for incidence angles less than 30^{o} whilst the contrast, 'co', metric is important for the reference sites selected and incidence angles greater than 60^{o}.

Figure 6.16 Mahalanobis distance measure of separation between the four ecological terrain types. The 6 sectors are grouped by the three similar incident angle segments, S16 (incidence angles from 61^o to 71^o), S25(incidence angles from 30^o to 60^o) and S34 (incidence angles from 0^o to 29^o).

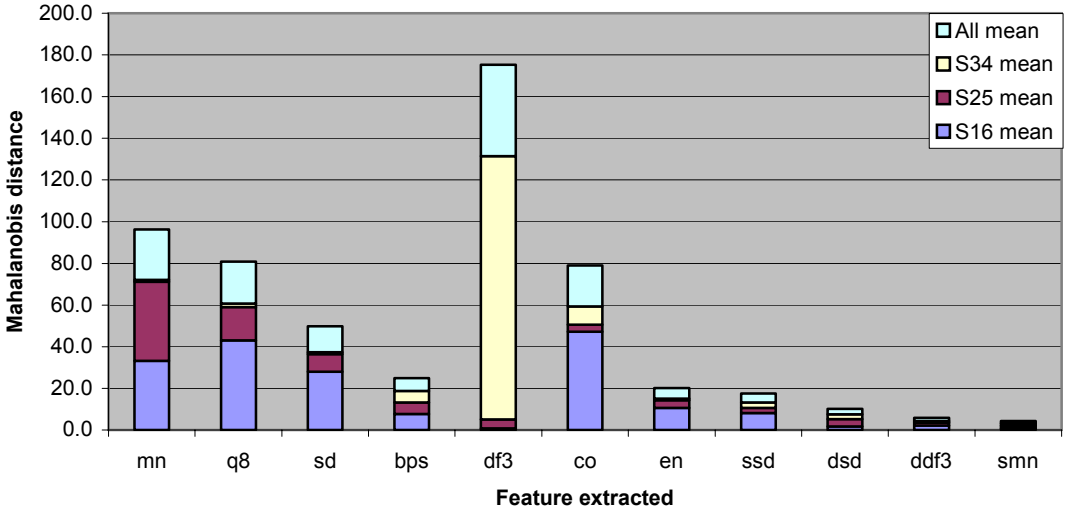

The four ecological terrain types were classified using the reference sites and linear discriminant analysis with a Mahalanobis distance metric. Reference site prediction error was based on the cross-validation-error scores (Matlab 6.5); where each site observation is systematically dropped from the site list and the excluded observation classified using a linear discriminant function. A low error score indicated good agreement with the reference site classifications (Table 6.14). The effect of including the between segment mean backscatter ratio parameter, 'bps', reduced the cross validation error for incidence angles less than 30^o from 32 % error to 4 % error. Validity of error tests was visually confirmed on the data by mapping the variables on the MBS maps of bathymetry and backscatter and plotting the combined metrics.

Table 6.14 Cross validation error for the four ecological terrain types using the 6 beam segments with and without the cross segment mean backscatter 'bps' metric.

Segments	No 'bps' error %	With 'bps' error %
16	2	2
25	7	7
34	32	4
Total error	**14%**	**4%**

Classification of a region was performed using discriminant analysis and a linear separation metric based on the reference site data for each of the four terrain types (Matlab 6.5). This classification method provides a consistent approach to compare inclusion and exclusion of parameters in the classification process (Fig. 6.17).

Figure 6.17. Classification of a complex reference site seabed slope less than 2° using four ecological terrain types, 6 sectors and 4 ping ensemble as training sites, a) not using and b) using between sector information parameter, 'bps', with scored video transect overlaid. Terrain type key, soft-smooth blue, soft-rough green and hard-smooth, brown.

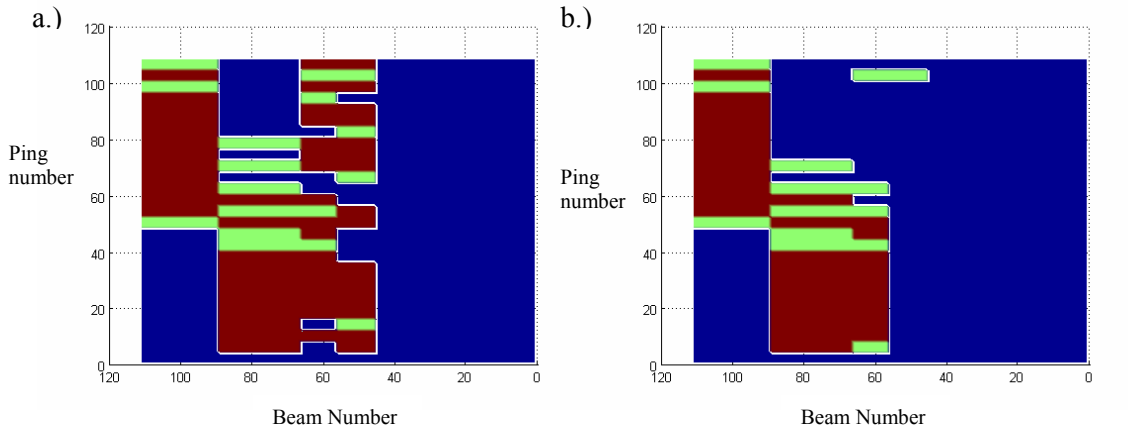

It was possible to improve the classification of the complex region of backscatter and bathymetry providing better spatial resolution using 10 segments; lowering the overall cross validation error in the linear discriminate analysis to 3% for all segments combined (Fig. 6.18).

Figure 6.18. Classification of a complex reference site seabed slope less than 2° using four ecological terrain training types, 10 sectors and 4 ping ensembles using all parameters with scored video transect overlaid. Terrain type key, soft-smooth blue, soft-rough green and hard-smooth, brown.

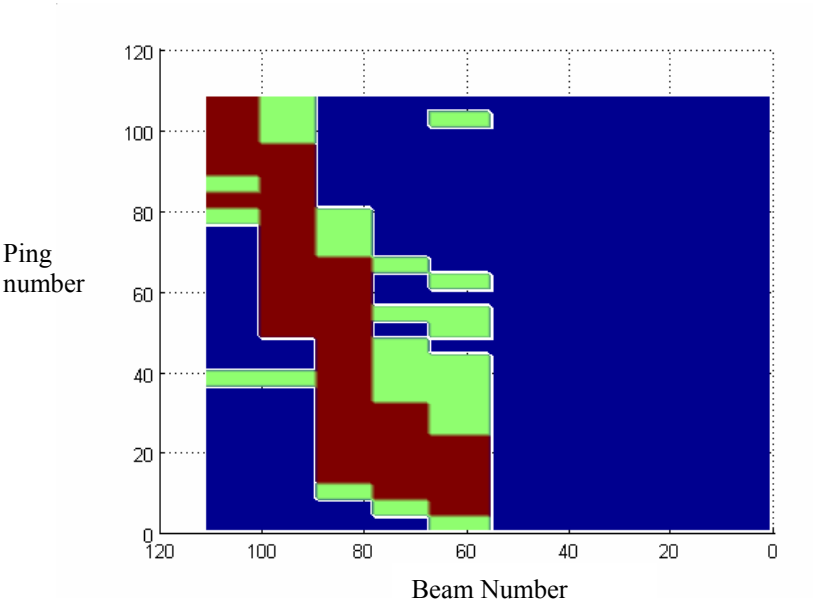

In summary, using phenomenological statistics it is possible to segment the seabed into terrain types at fine resolution to at least 10 segments across the MBS swath profile and equivalent and often finer along track segments depending on vessel speed. Performance of metrics shows that the frequency metric 'df3' is important near normal incidence compared with the mean and standard deviation of backscatter. The GLCM contrast metric is important at higher incidence angles for certain terrain types. The reliability of predicting terrain types

produces low error scores (less than 4%, Table 6.14) when the between sector backscatter metric,'bps', is used.

6.8 Incidence angle referenced backscatter

The phenomenological analysis of the acoustic data showed that the mean backscatter was the most important metric for separating the four ecological terrain types off normal incidence (Table 6.13) and that many of the other metrics were highly correlated with the mean backscatter (Table 6.12). At high incidence angles (greater than 10^o) the mean backscatter could reliably distinguish video soft from video hard seabed sites (Fig. 6.3). This associates well with the fauna analysis that showed the strongest fauna association discrimination between video soft and hard terrain. Removal of the generic incidence angle to backscatter profile by an ensemble ping average and referencing the backscatter to a set incidence angle provides a relative mean backscatter seabed plot that, off normal incidence, should reliably distinguish soft from hard seabed terrain (Fig. 5.8). The choice of reference angle needs to maximise the within site separation as well as being minimally sensitive to slope correction and absorption errors (Fig. 4.7, 4.10 and 4.13). Incidence angles between 30^o and 50^o are suitable and based on the maximum separation of seabed types in the APL94 (1994) model (Fig. 6.9) and maximum separation of the backscatter standard deviation (Fig. 6.4), 40^o incidence represents a suitable choice at this frequency and for the seabed types encountered. Based on the reference sites in Figure 6.3 a 40^o referenced incidence angle backscatter profile shows the discrimination achieved (Fig. 6.19). Note at near normal incidence the greater overlap of the distributions indicating poorer discrimination.

Figure 6.19. Comparison of the acoustically hard (solid) and soft (dashed) reference seabed types shown in Figure 6.3 referenced to 40^o incidence angle. Box plot shows variation of site means (dB) with median and inter quartile (25% to 75%) range.

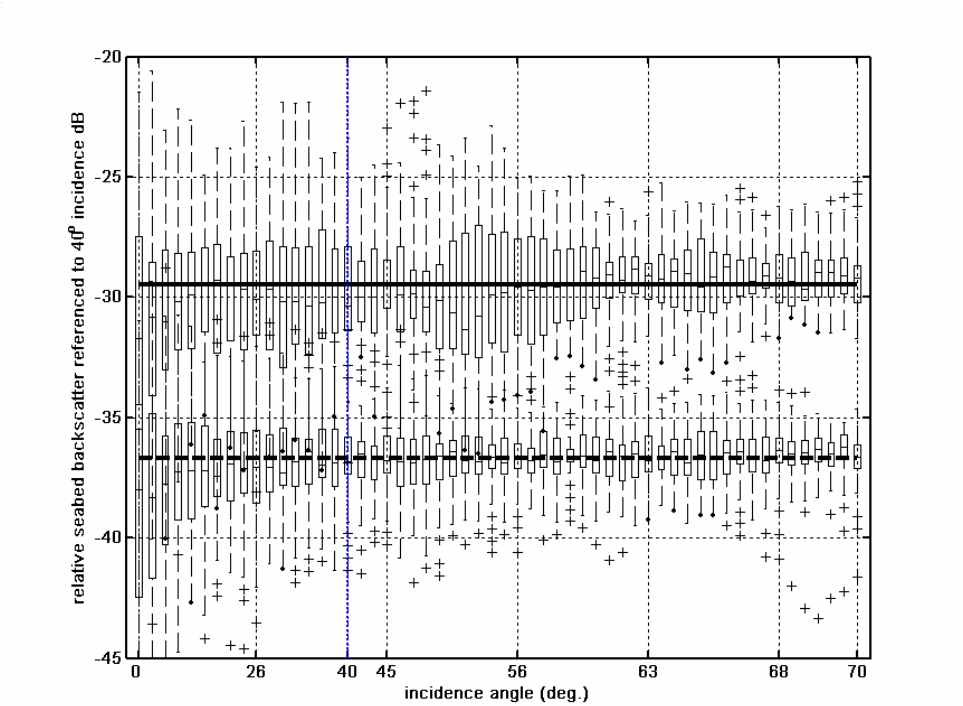

6.9 Summary

This chapter has developed a link between the terrain characteristics of soft to hard and smooth to rough observed by the video and the MBS metrics derived from bathymetry and backscatter at the mesohabitat scale. Videography data showed that the seabed terrain was patchy where 50% of patch lengths were less than 18 to 90 m using the soft, hard, smooth and rough categories. Using video scored data 18 soft-smooth, 6 soft-rough and 6 hard-rough sites were established that were assumed to be homogeneous over the MBS incident angles of 0 to 70^{o}. No homogeneous hard-smooth sites were found. For the homogeneous sites sediment sampling showed there was a clear grain size differentiation between soft-smooth and soft-rough terrain types based on the composition of mud and gravel (Table 6.5). Sediment sampling of hard sites was not conclusive due to the inability of the sediment grab to penetrate or retain rock material. Lithology sampling carried out with a rock dredge supported the characterisation of the hard-rough sites containing limestone and sandstone of varying porosity.

Using the MBS relative seabed backscatter, mean and standard deviation, clear differences were observed between homogeneous soft-smooth and heterogeneous hard-rough sites. Rough sites could be distinguished using the higher standard deviation for a large number of beams. The ability to separate rougher sites was not uniform for all beams; near normal incidence ($<16^{o}$) there was insufficient difference in the standard deviation of backscatter to separate the terrain types. The backscatter standard deviation was similar for all soft-smooth sites independent of mud composition whereas it was possible to separate soft-smooth sites by mud fraction using the mean of the relative seabed backscatter as a function of incident angle.

It is also possible to predict the relative grain size between soft-smooth terrains by fitting the MBS backscatter data to the APL94 (1994) model using well constrained historic geoacoustic values. Predicting specific geoacoustic properties using geoacoustic values with general limits using the inverse of the seabed backscatter model by simulated annealing did not provide consistent results. Large variations in predicted geoacoustic values were observed for density, sound speed, spectral strength and spectral exponent that were not supported by physical or visual sampling. To interpret the seabed backscatter using the APL94 model the whole incident angle range from 0^{o} to 70^{o} was used. Finer resolution interpretation was not investigated; a phenomenological statistical approach was favoured.

Building on the knowledge of the MBS metrics for homogeneous soft-smooth and heterogeneous hard-rough reference sites a segmented phenomenological approach using both bathymetric and backscatter statistics was derived. The MBS ensonification width was segmented into 10 regions and reference metrics derived for each segment. Using this method a resolution of 0.55 times depth was achieved. This is 3 times finer than the currently used commercial segmentation method (Simrad 1999b). Error scores for the discrimination between terrain sites were 4%. Improved characterisation (from 32% error to 4% error) near normal incidence was achieved using a between segment backscatter metric. Finer resolution may be possible using extra segments or using the side scan data incorporating the backscatter data in-between the centre of the beams. The mean of the backscatter is the most dominant discriminator and the performance of an incidence angle referenced backscatter transformation is explored in more detail in Chapter 7.

This chapter has established that it is possible to separate the terrain reliably into 4 classes of soft-smooth, soft-rough, hard-smooth and hard-rough using phenomenological statistics. Terrain sampling resolution occurs at 0.55 times depth across track (assuming a flat seafloor) and at finer resolution along track depending on the ping rate and beam width. Therefore the hypothesis is supported that the MBS can determine the simple terrain types identified over a

range of depths and between the bioregions sampled with a high degree of confidence at mesohabitat scales (10's m to 1km).

The four broad terrain classifications were hypothesised to be ecologically important for biological communities at the mesohabitat scale. Using the videographic data faunal groups showed distinct preferred presence/absence patterns between terrain types. The separation of soft and hard terrains indicated that nine out of the 10 faunal groups were present in either terrain at frequencies greater than 70%. Smooth to rough terrains showed a faunal community presence of greater than 70% for eight out of the ten faunal groups. The selectivity of fauna to soft-smooth sites showed a strong preference for only one fauna type (Sedentary *e.g.*, seapens) at 96% whereas 3 faunal groups preferred hard-smooth terrain at higher than 80% preference. Simple separation of terrain into hard and soft provided the best segmentation of fauna group presence using the faunal categories described. The density of faunal groups within and between terrains varies markedly (Table 6.4). Segmentation of the terrain into soft-hard and smooth-rough provides a means to predict fauna group presence and estimated density.

A link between the terrain type identified by video and the MBS has been established and a weaker link was been established between the simple terrain types of soft and hard and faunal groups for 70% association for 80% of the faunal groups providing strong support for the hypothesis linking terrain and faunal communities. This chapter concludes that the null hypothesis that there is no link between terrain type and MBS metrics is rejected at the mesohabitat scale. Chapter 7 explores the link between faunal groups and terrain types in more detail using the incidence angle referenced backscatter.

7 Acoustic interpreted maps for a region

7.1 Introduction

Based on the previous chapters, it is possible using the MBS data and associated physical and visual sampling to create maps of the seabed that are nested in a hierarchy of spatial habitat units proposed for Australia's marine jurisdiction (Fig. 1.1; NOO 2002). The sizes of spatial areas and their needs for spatial management were outlined in Table 2.2. Based on the classification scheme (Table 2.2) this chapter examines the largest surveyed region (Horseshoe Canyon 711 km^2; Area 6 and 7 Table 5.2, also known as Everard Canyon (Conolly 1968)) which ranges from 120 m to 600 m depth and the ability to map or estimate the biotopes of this region using acoustic and video measures as surrogates. The Horseshoe Canyon region identified is also an active demersal fishing area where the seabed has been modified over time by bottom contact fishing. The extent that this may effect the estimate of biotopes for the region is also explored.

The general approach to mapping habitats presented here is as follows:

1. The survey area is placed in context at a regional scale of 100s km using historic information from existing geological, oceanographic and biological knowledge. Here the seabed is separated into depth units such as slope, shelf and abyss and regional units based on oceanographic conditions and known fish biogeography (IMCRA 3.3 1998).

2. At the 1 to 10s km and larger feature size the MBS data are used to distinguish the major geomorphological units based on the substrate and morphology of the seafloor which include canyons, sediment plains, ridges etc.

3. At the 10s m to 1 km feature size the combined substrate, geomorphology and dominant faunal composition is identified based on a combination of MBS and video data.

4. At the 0.1 to 10s m feature size detailed information about the sessile biota and its interaction with the substrate and other biota is identified using video. At this feature size it is possible to identify impacts and monitor/identify temporal changes for monitoring.

This thesis has so far examined mapping of the seabed primarily at the 10s m to 10s km scale. Chapter 5 established that visual semi-quantitative acoustic descriptors based on depth and backscatter metrics could be used to distinguish seabed types in 1 km to 10 km patches. Within these patches the dominant terrain types (soft, hard, smooth and rough) could be described and they were often a mosaic of terrain types (Table 5.12). In particular terrain patches were often less than 20 m length and the dominant faunal groups less than 10 m length. The finest resolving size of the video sampling used here was a patch area of 4 to 7 m^2 and patch lengths of 2.5 to 3.5 m (Fig. 4.15). The video can resolve at much finer scales for individual species and substrate type to sizes less than 0.1 m. Using the combined MBS metrics of bathymetry and backscatter, Chapter 6 explored a quantitative description of the seafloor terrain based on a set of homogeneous reference sites. Using phenomenological metrics a resolution of terrain patches within the MBS backscatter was possible when aggregating the data at patch lengths of 0.55 times depth across-track and 0.1 to 0.6 times depth along track. The phenomenological metrics used in Chapter 6 were highly correlated with each other and the mean relative amplitude backscatter referenced to 40^o was shown to provide good discrimination of soft and hard seabed types relevant for associated fauna at the reference sites. In this chapter the backscatter metric of mean amplitude within a 30 m grid

cell (ensuring more than one backscatter value within a grid cell for depth range 200 to 600 m) that is referenced to a common incidence angle of 40^{o} is used in conjunction with bathymetric metrics (*e.g.*, slope). This ensures that there is a common sampling area at all depths but a 30 m grid square at shallow depths (150 m) will be a mean of many more samples than a corresponding 30 m grid square at 600 m depth.

7.2 Horseshoe Canyon example

The study area of Horseshoe Canyon (Everard Canyon) was selected as it represents a complex range of terrain types and has importance to local fisheries (Bax and Williams 2001). A potentially high human impact from fishing includes a high concentration of demersal trawl fishing, and an increasing and expanding use of fixed gears (traps, bottom long lines and set nets). For example, increased trawl effort in the 200 – 600 m depth range between 1995 to 1999 represented a repeated impact 7 times higher than in the 0 - 200 m depth range (Larcombe *et al.,* 2001). Increased and expanded targeting of specific habitats in depths to 500 m using fixed gears has had the effect of moving effort for some species from relatively flat trawl grounds to harder and rougher substrate types (Williams *et al.*, 2004). To ensure long term sustainability of the fisheries within this canyon and the associated upper slope region (200 to 600 m depth) spatial closures have been proposed. Understanding the seabed and the biota within this canyon therefore has current management importance for both sustainable fisheries and conservation of biodiversity.

7.2.1 Regional setting

100s km features

Based on a compilation of available bathymetric data the major geomorphic units (based on IHO, 2001) around Australia were described (Harris *et al.,* 2002, table 2.3). Within the South East Australian Marine Planning Region the major geomorphic units are shown in Figure 2.5 and bathymetry in Figure 7.1 highlighting the Horseshoe Canyon study site.

Figure 7.1 Location of study site within the Bass Canyon and Twofold shelf province on the east coast of Australia (Harris *et al.*, 2002).

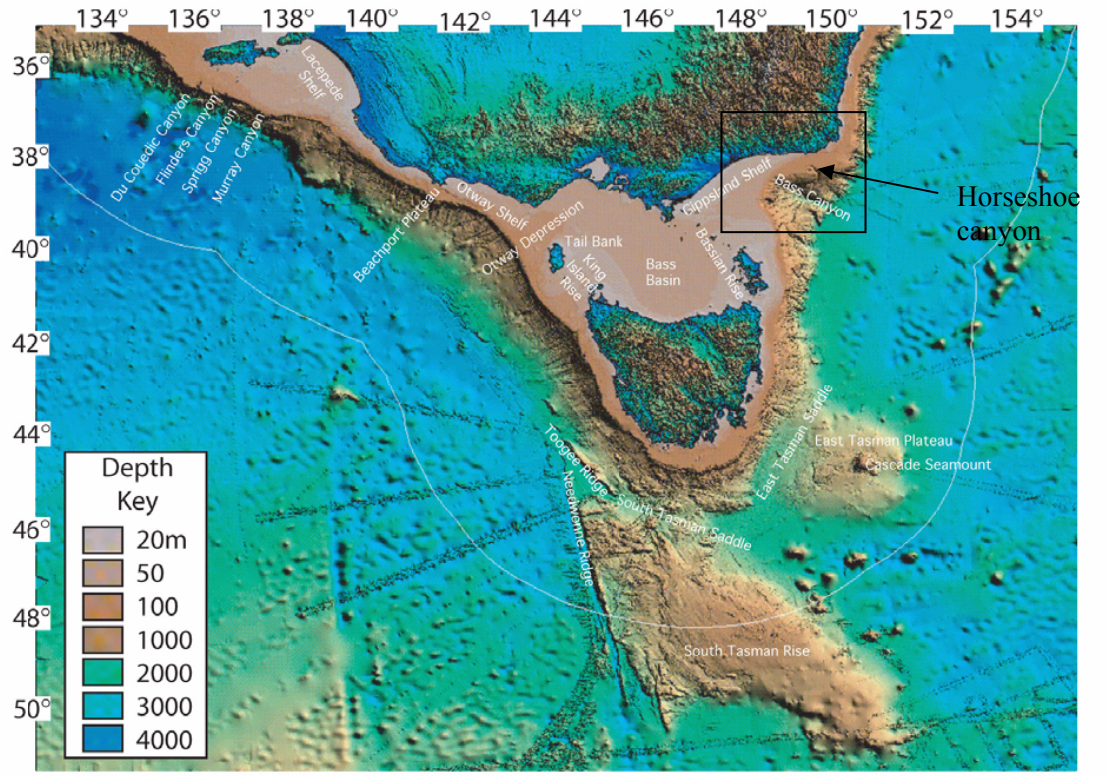

Using existing geological, oceanographic and biological data (inshore species 0 to 200 m) the Horseshoe Canyon study site lies within the Twofold shelf province (Fig. 2.4; IMCRA 3.3 1998). This province is characterised by *" Submaximally exposed coastline with long sandy beaches broken by rocky headlands and numerous coastal lagoons. Moderate tidal range ~ 2 m. Mean annual sea-surface temperature reflects the influence of warmer waters brought into Bass Strait by the East Australian Current. Variable wave energy."* (sic. IMCRA 3.3 1998). The geomorphology within the Twofold shelf region is characterised by sediment mosaics, low relief sandstone/limestones outcrops, high relief limestone banks with cliffs and inshore granite banks termed reefs on nautical charts (fig.3, Bax and Williams 2001). Acoustic single beam echo sounder data at depths from 30 to 200 m delineated the major features (Kloser *et al.,* 2001a). Off the shelf at depths greater than 500 m interpretations of the geological and tectonic elements have been assisted by detailed bathymetric MBS's and seismic profiles (Hill *et al.*, 1998; Hill *et al.,* 2001). This margin off Gippsland is dominated by a large embayment 100 km across and floored by an ESE-tending chasm, the Bass Canyon, which is 60 km long and 10-15 km wide. The canyon has cut down into the margin and is bounded by very steep walls 1000 m high. Sediment from the shelf is channelled into the entrance of Bass Canyon by three major, deeply-incised tributary canyons and a number of smaller ones (Hill *et al., 2*001). At its north-eastern extent the Horseshoe Canyon (Everard Canyon) feeds into the Bass Canyon (Fig. 7.2).

Figure 7.2 Detailed bathymetry of the Bass Canyon using historic data from deep water MBS surveys (Hill *et al.*, 2001, fig. B2) with Horseshoe Canyon study site marked.

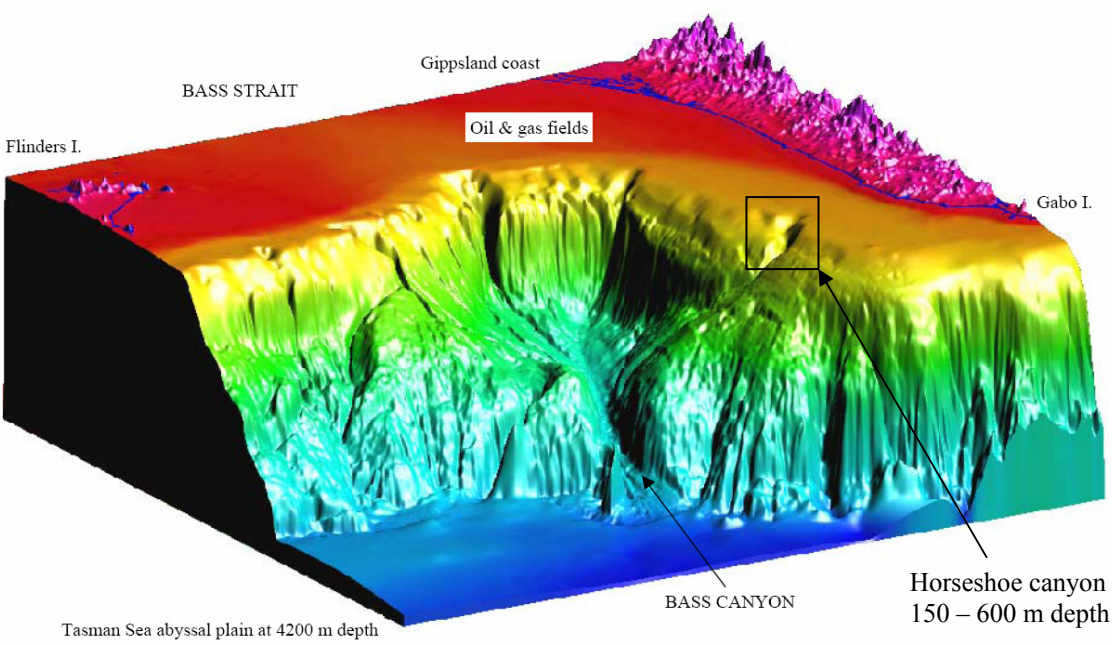

10 to 100 km features

This chapter focuses on the Horseshoe Canyon (Fig. 7.3) and the MBS data from the Simrad EM1002 and associated physical and optical sampling carried out in April to May 2000 (Kloser *et al.,* 2001b).

Figure 7.3. Bathymetric data from the Simrad EM1002 of Horseshoe Canyon, illumination 20° elevation, 35° azimuth, depth 130 m (brown) to 600 m (blue).

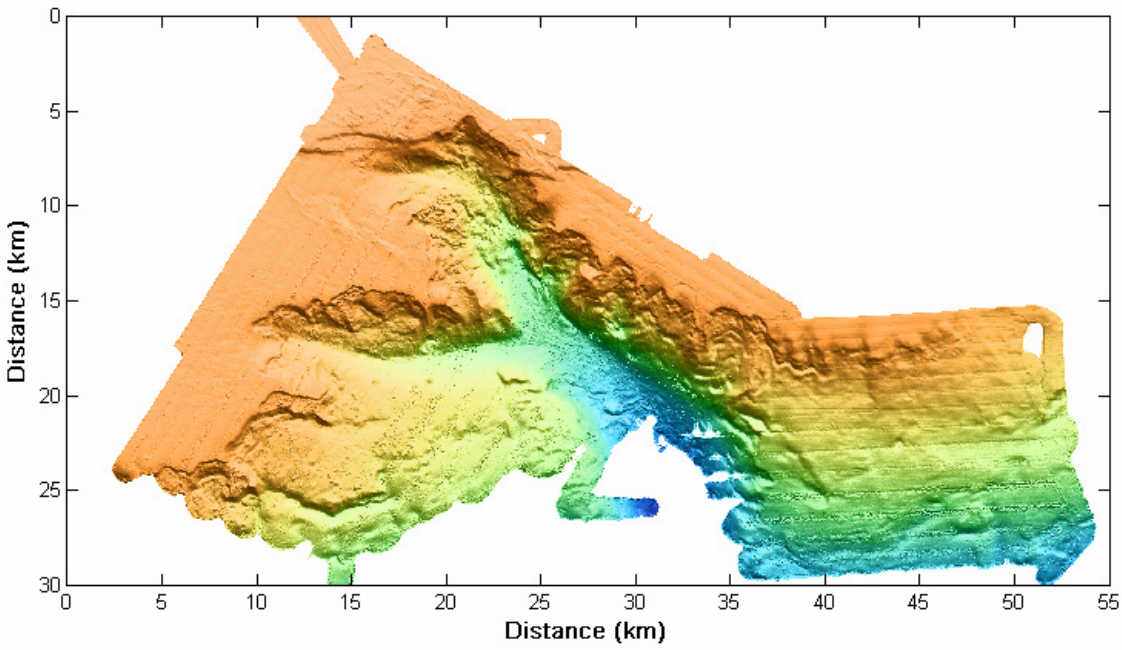

Figure 7.4 Direction and relative amplitude of a.) surface (20 m) currents shown with arrows recorded during the mapping of the canyon. Note the circulatory nature of the currents over the canyon with minimal current in the centre and higher currents over shallow water (Kloser *et al.*, 2001b), b.) lantern fish (*Lampanyctodes hectoris*) aggregated in the canyon, recorded with a 38 kHz echo sounder.

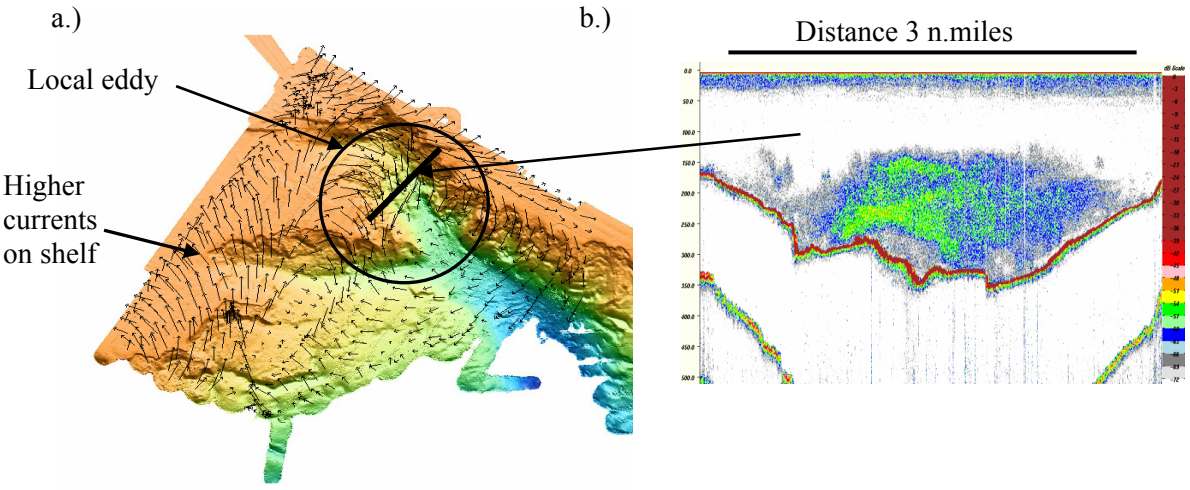

The current within the region was measured in April 2000 with a vessel mounted 150 kHz RDI ADCP (Kloser *et al.,* 2001b). Due to the bathymetric features the predominant northerly current formed an eddy within the canyon during the time of the survey (Fig. 7.4a). This eddy was also associated to a highly aggregated school of small (5 to 7 cm) lantern fish (*Lampanyctodes hectoris*) which extended throughout the canyon (Fig. 7.4b; Kloser *et al.,* 2001b). Therefore the canyon feature is demonstrated to represent an important feature for changing current circulation and in this instance a region where large schools of lantern fish aggregate. At the scale of 10 to 100 km the feature represents an important ecological unit.

7.2.2 Horseshoe Canyon 1 to 10 km features

Using semi quantitative bathymetry, backscatter and slope metrics at a 30 m square grid the visual characteristics as outlined in Chapter 5 were used to segment the region into 25 terrain areas. At the 1 to 10 km feature size 4 outer shelf, 3 shelf break, 11 slope and 7 canyon areas were defined (Fig. 7.5). It should be noted that boundaries were often not distinct with a grading of the depth, slope and backscatter variable from one area to another (Figs. 7.5. 7.6 and 7.7). The visual subdivision helps characterise the dominant qualities and fuzzy borders between terrain types at the 1 to 10 km feature size.

Figure 7.5 Bathymetry of Horseshoe Canyon ranging from 150 m depth (brown) to 600 m depth (aqua) with illumination elevation (20^o), azimuth (35^o), depth 130 m (brown). Segmentation of the region based on visual classification of bathymetry, slope, shaded bathymetry and backscatter into 25 acoustic terrain types as outlined in Chapter 5 Table 5.3. Boxed region (dashed) detailed in Figure 7.12.

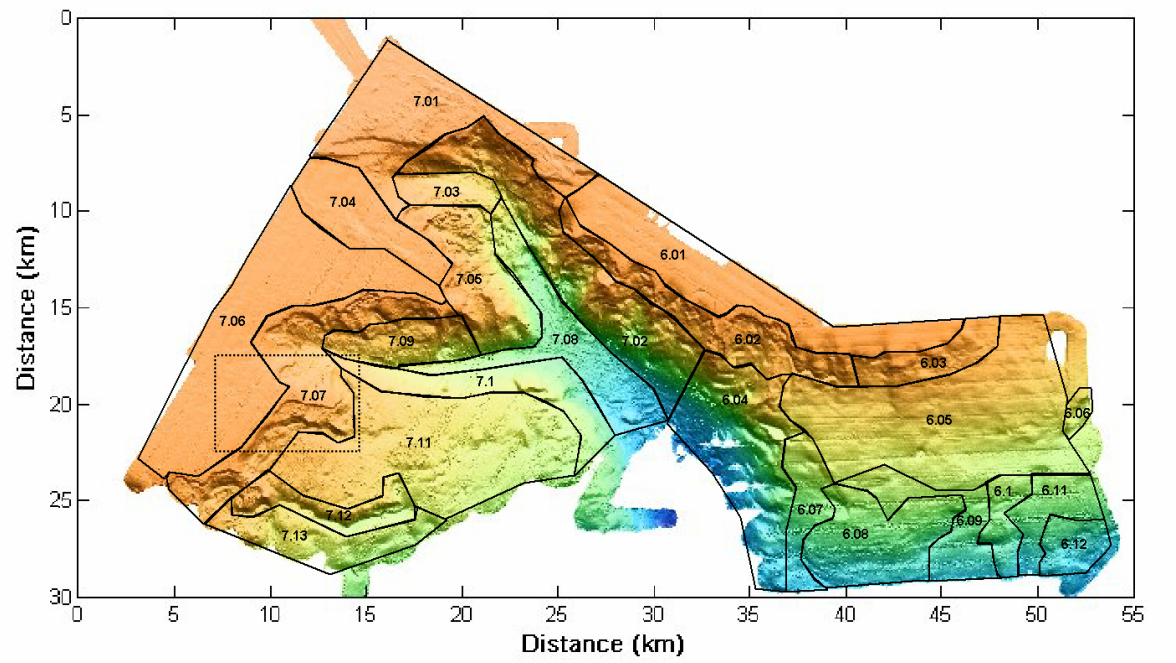

Figure 7.6 Slope derived from the MBS bathymetry (30 m grid) and segmented into 4 slope classes being, 0^o to 3^o (white to blue), 3^o to 5^o (aqua), 5^o to 10^o (yellow) and greater than 10^o (red).

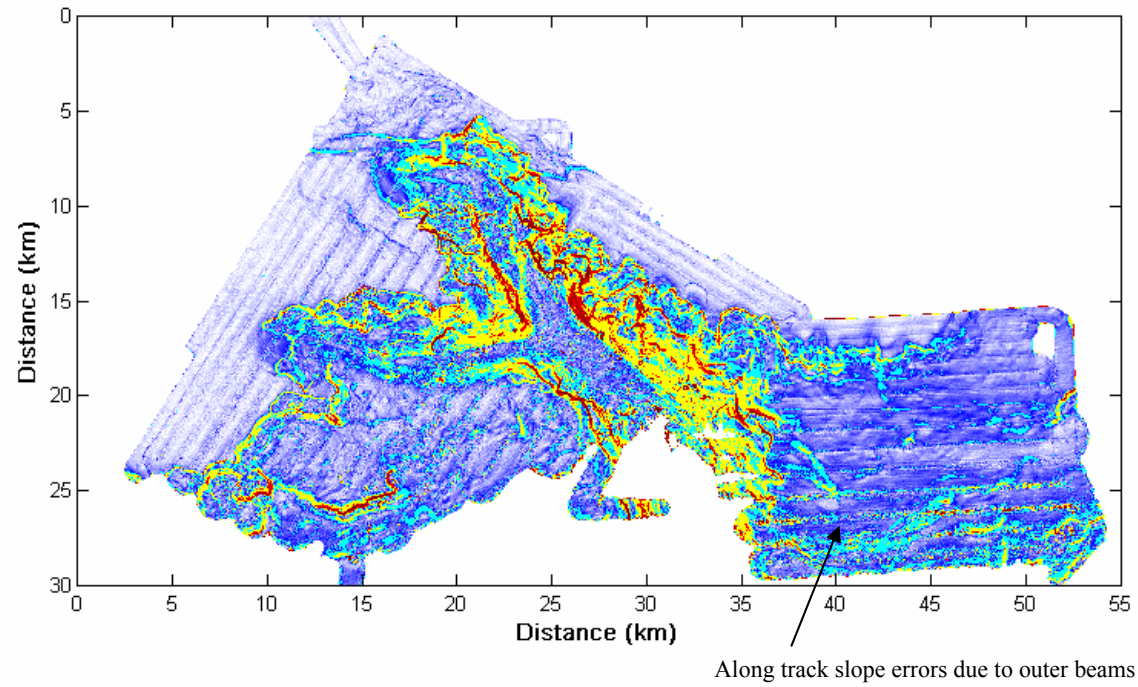

Figure 7.7 Relative backscatter (dB, 30 m grid), a.), referenced to 40° incidence angle – 40 to –20 dB (white to black); b.), segmented by soft (blue) < -33.5 dB, transition (cyan) -33.5 dB to -31 dB, hard (red) > -31 dB terrain (Table 7.1). Backscatter at depths greater than 550 m removed due to increased noise interference.

a.)

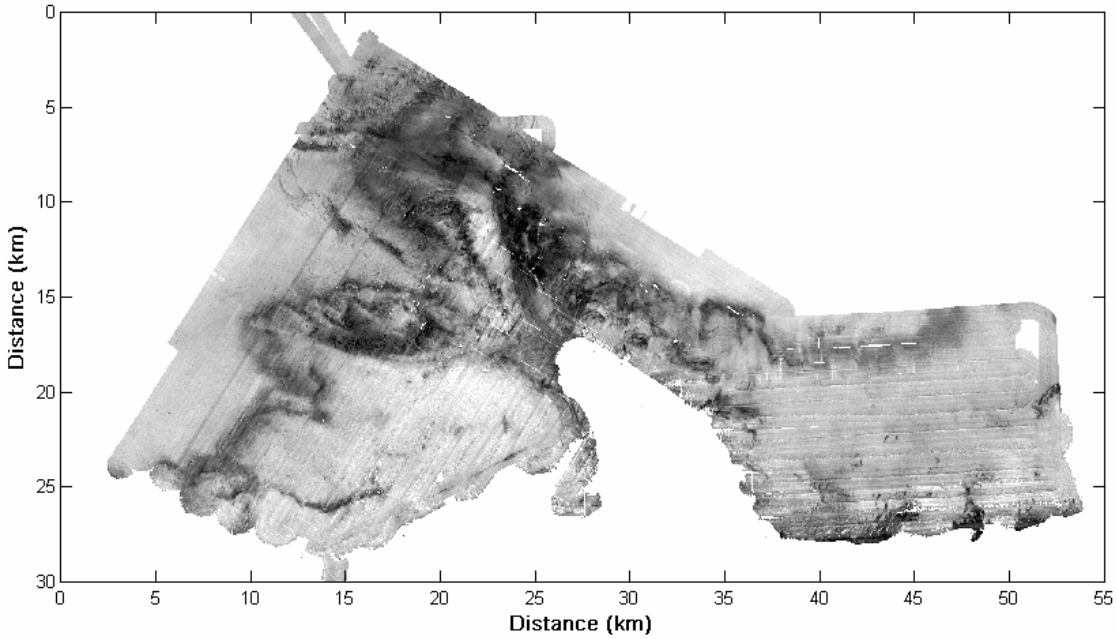

b.)

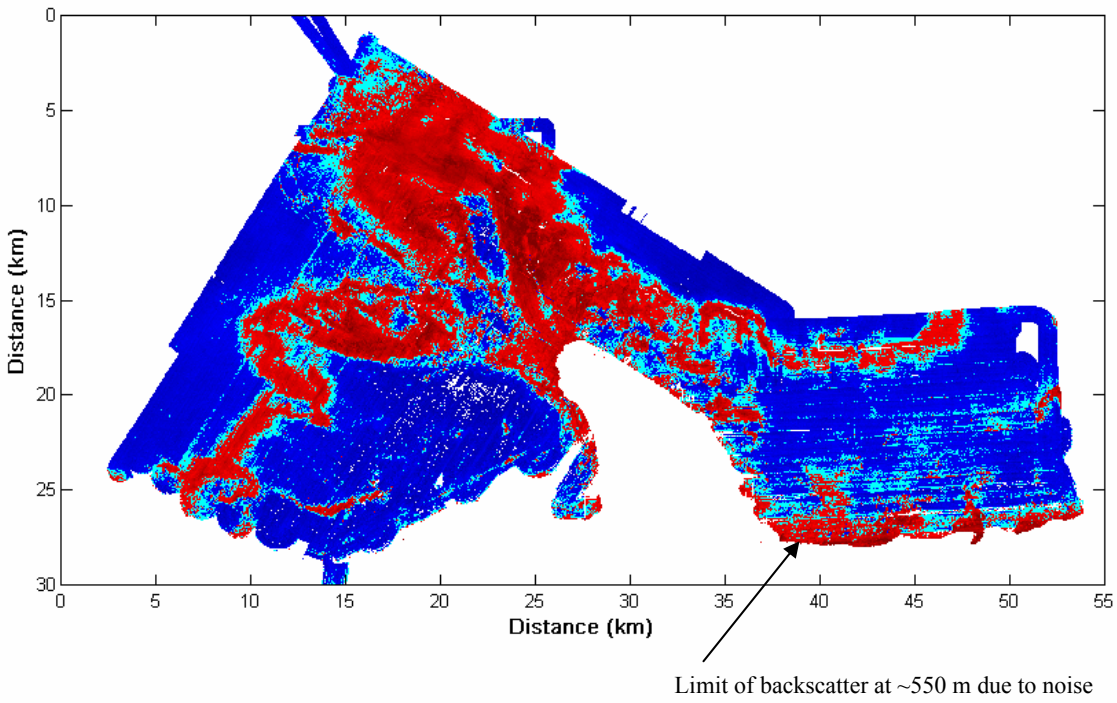

Table 7.1 shows the probability of a site being hard or soft based on echo amplitude based on the reference site analysis of Chapter 6 and the nominal reference backscatter angle of 40°. The amplitude range in Table 7.1 with associated colour range was applied to the backscatter in Figure 7.7a (Fig. 7.7b). Using a simple metric of soft and hard as defined by the reference sites described in Chapter 6 it is possible to predict hard sites as having a mean backscatter of higher than –31 dB and soft sites as having a backscatter value less than –33.5 dB. Within the amplitude range of –33.5 to –31 dB the seabed has a 36% probability of being hard or 64% being soft based on the proportion classification of the 15 hard and 11 soft reference sites (Table 7.1).

Table 7.1 Probability % of seabed being classified as hard or soft based on the mean amplitude of 26 reference sites referenced to 40° incidence angle Figure 6.3.

	reference site class		backscatter
# sites	15	11	
amplitude range	hard	soft	colour
dB	%	%	
> -31	80	0	red
-33.5 to -31	20	36	aqua
<-33.5	0	64	blue

As the slope of the seabed increases so does the backscatter as referenced to 40° incidence angle (Fig. 7.8). An acoustically soft seabed (<-33.5 dB @ 40° incidence) has 90% of slope values less than 4° whilst an acoustically hard seabed (>-31 dB @ 40° incidence) has 90% of slope values less than 11°. The error in relative seabed backscatter for across track seabed slope at 40° reference is less than 0.3 dB for acoustically soft terrain and less than 0.7 dB for acoustically hard terrain for 90% of the values (Fig. 4.10).

Figure 7.8 Cumulative probability of slope derived from an acoustically soft seabed (solid) and an acoustically hard seabed (dashed).

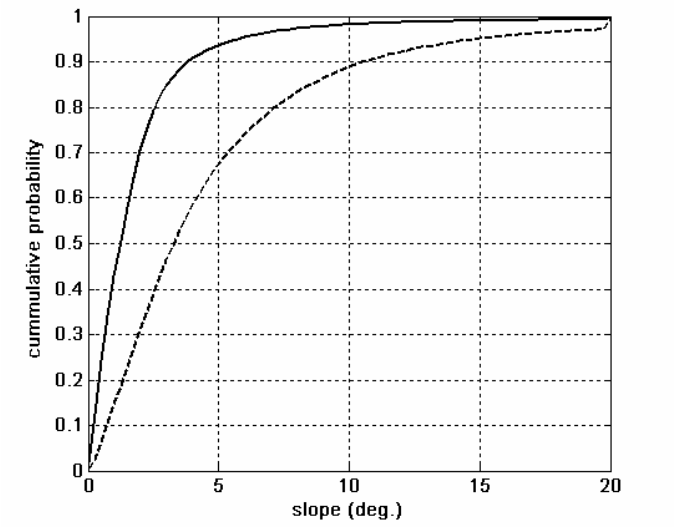

Table 7.2. Summary of the 25 acoustic terrain types for the Horseshoe Canyon (Fig. 7.5 for key) based on the backscatter, bathymetry and slope metrics of mean (m) standard deviation (s.d.) and kurtosis (k) with a description of major features (Kloser *et al.*, 2001b). Predominantly soft acoustic terrain highlighted in italic bold.

Acoustic terrain		Geomorphic description	Depth (m)			Slope (degrees)			Backscatter (dB)			Terrain description
#	type		m	s.d.	k	m	s.d.	k	m	s.d.	k	
7.03	Hard	Canyon	-281	37	2.4	2.9	2.4	45.0	-27.2	2.6	3.6	head of canyon 1 moderate slope
7.05	Hard	Canyon	-299	84	2.5	6.5	5.6	20.3	-29.1	3.9	2.7	south west canyon 1 wall steep slopes
7.09	Hard	Canyon	-310	47	2.8	4.4	3.9	45.4	-27.4	3.4	2.7	north canyon 2 wall moderate slopes
7.02	Hard	Canyon	-327	115	2.8	7.5	6.5	26.8	-27.0	3.0	2.8	north east canyon 1 wall steep slopes
7.1	Hard	Canyon	-413	74	2.2	5.3	5.2	21.1	-33.2	4.2	2.4	south canyon 2 wall moderate to steep slopes
6.04	Hard	Canyon	-505	129	2.0	7.6	8.0	23.9	-27.2	6.2	3.4	east canyon 1 wall high slopes
7.08	Hard	Canyon	-519	83	2.2	5.5	8.2	22.0	-27.4	5.6	2.6	canyon floor
7.01	Hard	outer shelf	-138	18	4.9	1.2	1.1	19.1	-29.2	2.9	2.4	low relief limestone outcrops
7.04	Hard	outer shelf	-156	5	4.4	0.8	0.8	79.0	-32.2	2.7	3.4	low relief limestone outcrops
7.06	***Soft***	***outer shelf***	***-157***	***6***	***2.4***	***0.6***	***0.5***	***40.8***	***-35.2***	***1.6***	***7.0***	***uniform low slope and low backscatter***
6.01	***Soft***	***outer shelf***	***-164***	***10***	***3.4***	***0.8***	***0.7***	***48.7***	***-35.3***	***2.4***	***3.9***	***uniform low slope and low backscatter and***
7.07	Hard	shelf break	-213	31	2.2	3.4	2.9	17.3	-29.7	2.6	2.8	shelf break west end steep slopes high backscatter
6.02	Hard	shelf break	-216	35	2.1	3.9	2.8	5.1	-30.0	2.8	2.6	shelf break ne end high slopes high backscatter
6.03	Hard	shelf break	-224	20	2.3	2.4	1.3	8.7	-31.1	2.0	3.2	shelf break n end moderate slopes high backscatter
7.12	Hard	upper slope	-331	57	2.0	5.6	5.7	18.2	-33.3	3.5	2.7	ridge high backscatter
6.05	***Soft***	***upper slope***	***-334***	***52***	***2.0***	***1.8***	***0.9***	***69.2***	***-34.8***	***1.4***	***6.1***	***slightly sloping sediment plain***
7.11	***Soft***	***upper slope***	***-344***	***49***	***2.0***	***2.4***	***3.6***	***72.6***	***-36.7***	***1.7***	***4.4***	***slightly sloping low backscatter***
7.13	***Soft***	***upper slope***	***-374***	***50***	***2.3***	***3.5***	***4.4***	***58.1***	***-35.6***	***2.3***	***7.0***	***moderately sloping low backscatter***
6.06	Hard	upper slope	-377	26	1.8	3.6	3.2	8.0	-31.2	3.3	2.6	ridge high backscatter
6.07	***Soft***	***upper slope***	***-482***	***80***	***2.1***	***4.1***	***6.3***	***36.7***	***-31.7***	***5.0***	***3.2***	***moderately sloping low backscatter***
6.09	***Soft***	***upper slope***	***-495***	***71***	***1.5***	***3.5***	***5.2***	***48.2***	***-31.2***	***3.5***	***2.6***	***moderately sloping low backscatter***
6.11	***Soft***	***upper slope***	***-499***	***49***	***3.3***	***3.7***	***6.0***	***46.8***	***-32.9***	***3.8***	***3.8***	***moderately sloping low backscatter***
6.1	Hard	upper slope	-499	54	1.9	3.7	3.9	59.7	-28.5	5.0	1.9	moderately sloping irregular high backscatter
6.08	Hard	upper slope	-519	54	1.9	3.7	4.1	55.3	-28.2	4.2	2.3	moderately sloping irregular high backscatter
6.12	Hard	upper slope	-575	37	2.1	5.4	6.9	21.2	-24.8	4.1	2.6	moderately sloping irregular high backscatter

Figure 7.9. Location of, a.), sediment grab samples as percentage by weight of sand (yellow), mud (brown) and gravel (red) and, b.), video terrain type of soft-smooth (orange), soft-rough (yellow), hard-smooth (pink), hard-rough (red), c.), video terrain type of soft (blue) and hard (red). Relative backscatter (30 m grid) referenced to 40^{o} incidence angle white to black (-40 to –20 dB).

a.)

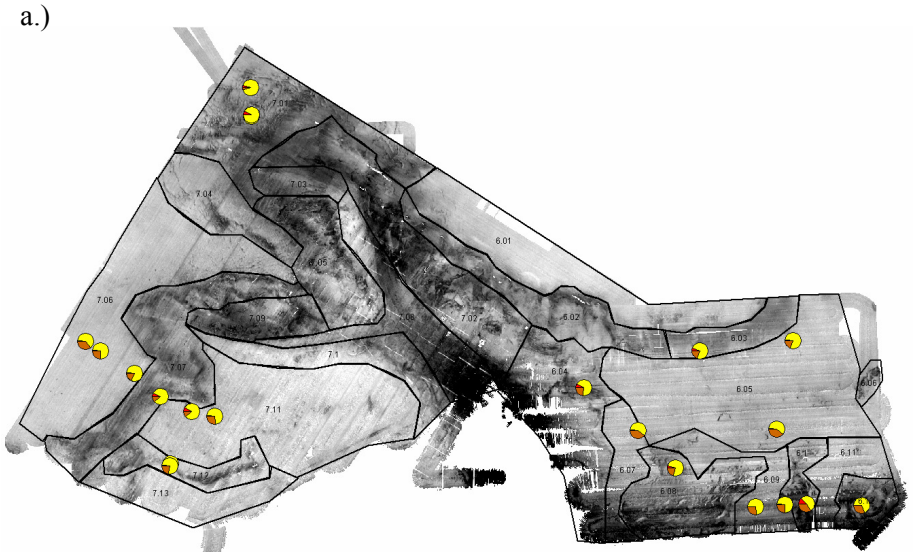

b.)

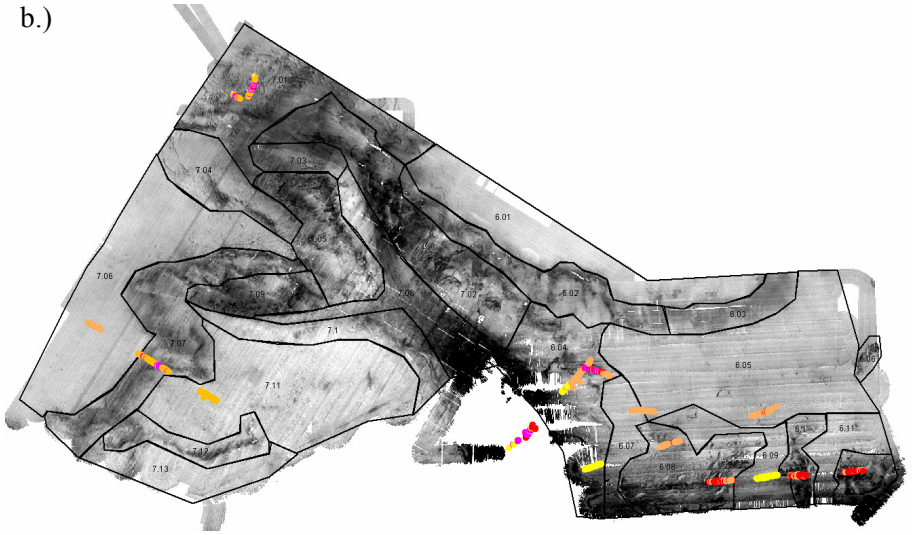

c.)

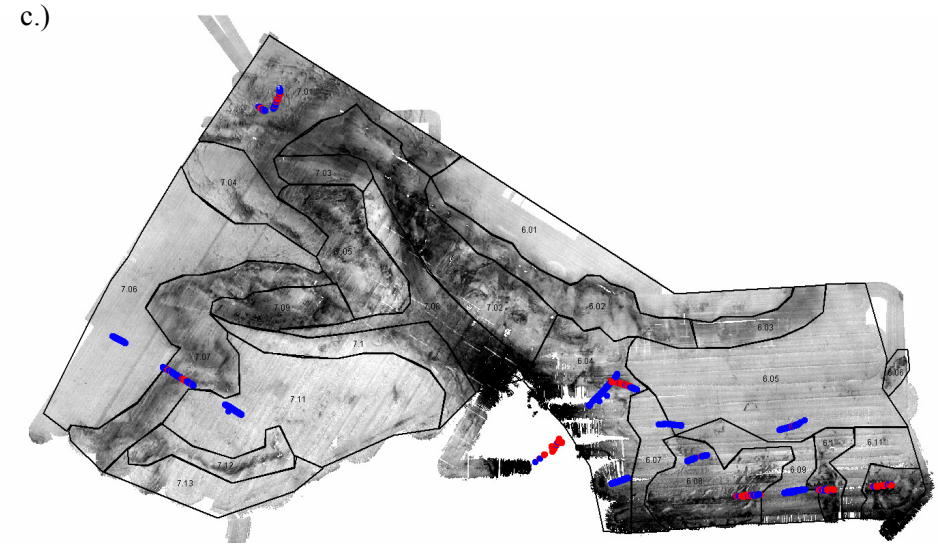

At 1 to 10s km feature size the visual segmentation (Ch. 5 Table 5.3) of the terrain by acoustic depth, slope and backscatter shows the relationship with quantitative metrics (Table 7.2) and visual correlations of bathymetry, slope and backscatter (Figs. 7. 5, 7.6 and 7.7 respectively). Within the 25 acoustic terrain areas, 20 sediment grabs, and 9 video operations (32796 one second video scores) were targeted (Fig. 7.9). The video classified soft and hard terrain and associated fauna type was segmented into the acoustic terrain types of soft and hard (Table 7.3). At the 1 to 10s km patch size the video terrain classes show that for five acoustic scored soft terrains the video proportion of soft is higher than 97%. When the acoustic terrain is classified as hard the video scored terrain contains a high (25% to 75%) proportion of video soft terrain (Table 7.3). The high proportion of video soft terrain within acoustic hard terrain is also reflected in the typical faunal types that inhabit the acoustic hard terrain. When the video terrain is soft faunal classes of bioturbators, octocorals and sedentary (faunal class 9, 7 and 5 respectively) are found with 100% dominance (Table 7.4) and this is also the case when the acoustic terrain is classified as soft at the 1 to 10 km feature size (Table 7.3). The video hard terrain is dominated (greater than 98%) by large sponges, a mix of sponges, seawhips and ascidians and small encrusters (faunal types 1, 3 and 6; Table 7.4). The hard acoustic terrain contains these faunal types in high proportion but also contain a high proportion (43%) of typical soft terrain types (e.g., bioturbators) due to the high proportion of video soft terrain (Table 7.3).

Table 7.3 Proportion of video terrain class of soft and hard and video faunal classes as defined in Table 2.4 segmented by the acoustic terrain type areas shown in Table 7.2 and Fig. 7.5. Soft acoustic terrain and predicted soft fauna type in italic bold.

Acoustic terrain		Video classification terrain %			Fauna type %									
#	type	#	soft	hard	0	1	2	3	4	***5***	6	***7***	8	***9***
6.04	hard	7047	69	31	6	6	24	0	0	***0***	2	***14***	5	***43***
6.05	***soft***	***2555***	***98***	***2***	***0***	***0***	***0***	***0***	***0***	***0***	***2***	***80***	***3***	***15***
6.07	***soft***	***1179***	***100***	***0***	***0***	***0***	***0***	***0***	***0***	***0***	***0***	***99***	***0***	***1***
6.08	hard	3741	55	45	1	0	0	0	0	***0***	44	***0***	3	***52***
6.09	***soft***	***2200***	***97***	***3***	***0***	***0***	***0***	***0***	***0***	***0***	***3***	***0***	***6***	***91***
6.1	hard	2330	34	66	0	0	0	0	0	***0***	65	***0***	0	***35***
6.12	hard	2942	25	75	0	0	0	0	0	***0***	73	***0***	3	***24***
7.01	hard	4418	65	35	35	7	58	0	0	***0***	0	***0***	0	***0***
7.06	***soft***	***1458***	***100***	***0***	***65***	***0***	***0***	***0***	***2***	***0***	***0***	***25***	***8***	***0***
7.07	hard	2374	75	25	7	0	6	2	21	***0***	0	***60***	2	***1***
7.11	***soft***	***1420***	***100***	***0***	***1***	***0***	***0***	***0***	***0***	***14***	***0***	***5***	***2***	***79***

Table 7.4 Proportion of video classified fauna (Table 2.4) segmented into the video terrain types of soft and hard defined by the substrate and geomorphology classes (Table 2.4). Predicted soft fauna type highlighted in bold italic.

		Video classes		
		video terrain %		
fauna	#	soft	hard	Fauna description
0	3104	97	3	None - no apparent epifauna or infauna
1	764	0	100	Large sponges - community
2	4414	32	68	Small sponges - community
3	58	0	100	Mixed sponges, seawhips and ascidians
4	536	25	75	Crinoids
5	***200***	***100***	***0***	Octocorals (gold corals/seawhips)
6	5526	2	98	Small encrustors/erect forms (including bryozoans)
7	***6123***	***100***	***0***	Sedentary: *e.g.* seapens
8	923	94	6	Mobile: *e.g.* echinoids/holothurians/asteroids
9	***10016***	***100***	***0***	Distinct infauna bioturbators

At the 1 to 10s km feature size the geomorphology and acoustic visual and quantitative metrics are used to segment the seabed into terrain types. These terrain types can be segmented into simple acoustic soft and hard terrain where acoustic soft terrain correlates well with video soft terrain (greater than 98%). The prediction of faunal types within the acoustic soft terrain type is consistent with video faunal scores for soft terrain. Within acoustic hard terrain there is a high proportion of video soft terrain and a mixture of both soft and hard faunal types at the 1 to 10 km feature size. This mixture of video soft and hard terrain types within acoustic hard terrain at the 1 to 10 km scale is reflected in the proportions of soft and hard faunal types within the region at 1 to 10 km scale.

7.2.3 Horseshoe Canyon 10s m to 1 km features

The correlation of the 32796 video scores segmented into video soft and hard terrain types with the relative backscatter (referenced to 40^{o} incidence angle), depth and slope metrics is 0.7, –0.2 and 0.3 respectively at a grid size of 30 m. Backscatter is highly correlated (0.7) with video terrain and this relationship is illustrated in Figure 7.10a. Within acoustic classified soft terrain the proportion of video classified soft terrain is 100% for backscatter values less than -34 dB and decreases as video classified hard terrain is encountered (Fig. 7.10 b, blue dashed line). In acoustic classified hard terrain the video classified hard terrain the seabed backscatter cumulative probability increases from 10% at–32 dB to 100% at –20 dB. The video classified soft terrain within the acoustic classified hard terrain has a backscatter mode of –30 dB compared with a backscatter mode of -36 dB in the acoustic classified soft terrain (Fig. 7.10 a). Due to the 30 m backscatter grid size (area 900 m^2) and the video viewing area of 5 to 7 m^2 there is potential that backscatter values of soft and hard are influenced by the patch size of the soft and hard terrain encountered.

Figure 7.10 Relative backscatter (grid 30 m) referenced to 40° incidence angle for video classified terrain type of soft (dashed) and hard (solid) within acoustic classified terrain of soft (blue) and hard (red), a.), occurrence and b.), relative proportion in 2 dB bins.

a.) b.)

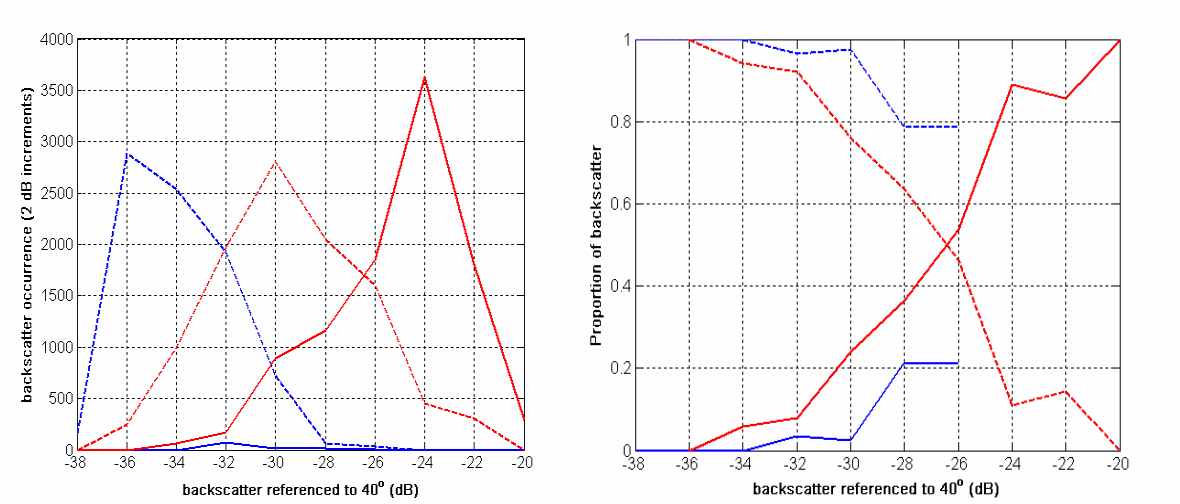

The patch length of video soft and hard terrain within the acoustic hard terrain is similar where 50% of patch lengths are less than 30 m (Fig. 7.11b). In comparison the acoustic soft terrain contains long patches of video soft (50% greater than 500 m) and short lengths of video rough (50% less than 30 m) terrain (Fig. 7.11b). The video soft and hard terrain patch length structure within acoustic soft and hard terrain for the Horseshoe Canyon region is similar when all 14 regions are combined (Fig. 7.11a). This high proportion of patch lengths less than 30 m is potentially a major explanation of the merging of soft and hard video terrain types across backscatter values (Fig. 7.10).

Figure 7.11. Contiguous patch length of video terrain, soft (dashed) and hard (solid) within acoustic terrain of soft (blue) and hard (red) for a.), all regions and b.), the Big Horseshoe region (areas 6 and 7).

a.) b.)

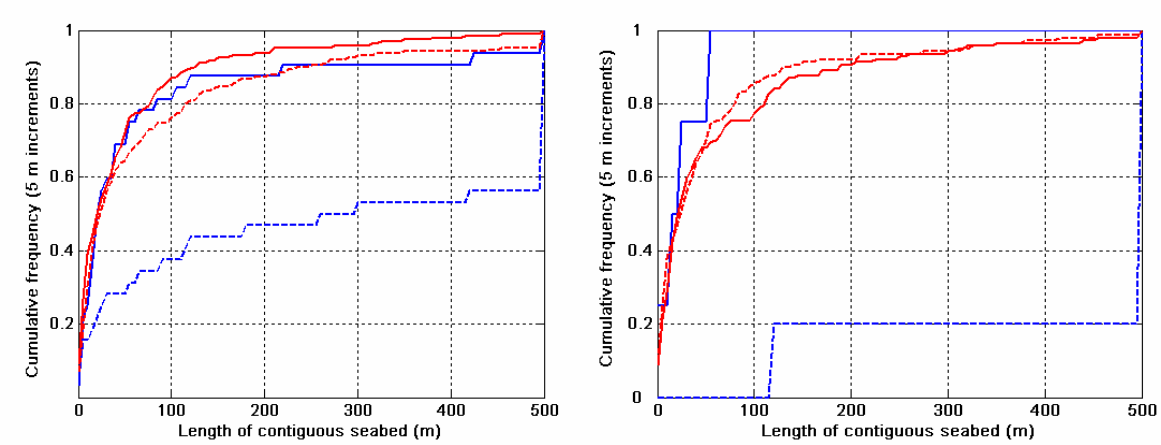

The 10 faunal classes of the 32796 video records are correlated with depth, slope and backscatter at 0.6, -0.1 and -0.2 respectively; depth and backscatter are not correlated (-0.3) and backscatter and slope are not correlated (0.3). Depth is correlated (0.6) with the faunal classes defined in Table 2.4 and is an important metric to stratify the fauna encountered here. In the Horseshoe Canyon acoustic soft terrain the faunal patch lengths are very short with 50% being less than 20 m (Fig. 7.12b) whereas the video soft terrain has patch length 50% of which are greater than 500 m (Fig. 7.11b). When considering all the video data (65975 scores) for all regions (14) the video soft terrain fauna (50% less than 20 m) has smaller patch sizes than the video hard terrain fauna (50% less than 50 m) (Fig. 7.11). Therefore to correctly characterise the fauna within acoustic soft terrain a sample size of less than 10 m is required to achieve the Nyquist sampling criteria for 50% of the fauna patch lengths observed by video.

Figure 7.12. Contiguous patch length of video fauna in video soft (dashed) and hard (solid) terrain within acoustic terrain of soft (blue) and hard (red) for a.), all regions and b.), the Big Horseshoe region (areas 6 and 7).

a.) b.)

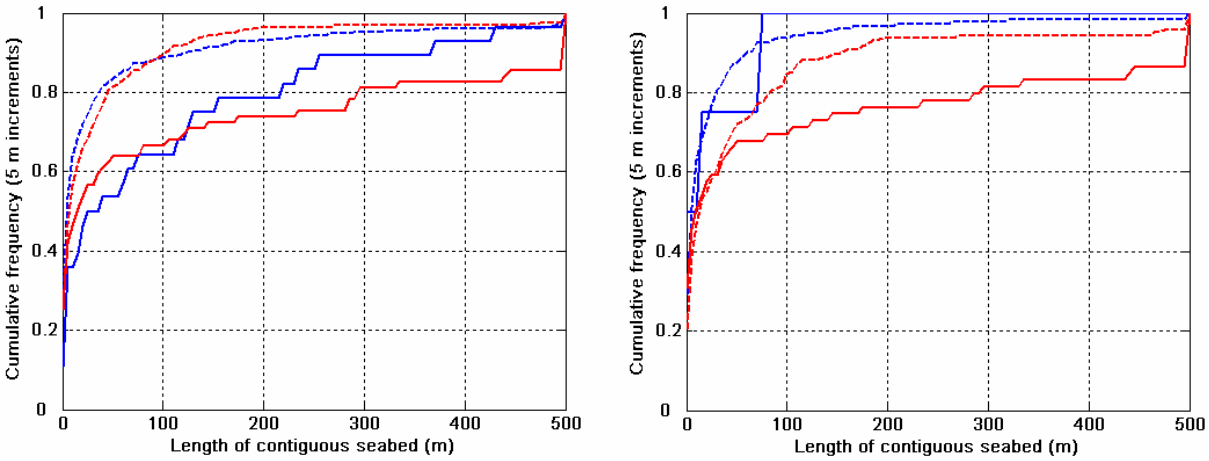

Despite the difference in the acoustic and video sampling size some general fauna to backscatter trends emerge where faunal types 9, 5 and 7 are associated with low backscatter and types 1, 2, 3, 4 and 6 associated with high backscatter (Fig. 7.13).

Figure 7.13. The cumulative video classified fauna of types 0 to 9 (Table 2.4) associated with increasing values of backscatter where soft type fauna are associated with lower backscatter (dashed) and hard associated fauna associated with high backscatter (solid) and no affinity dotted.

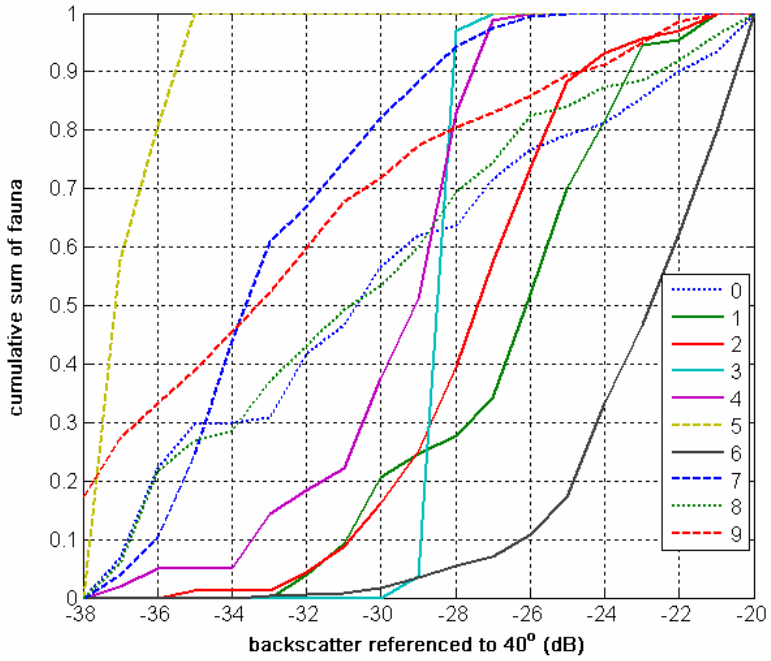

Figure 7.14 illustrates the terrain and faunal features at the 10s m to 1 km feature size in the south-west section of the Horseshoe Canyon (Fig. 7.5). The boundaries of the acoustic terrain areas 7.06, 7.07 and 7.11 show good visual agreement with the detailed slope and backscatter metrics (Fig. 7.14). At the reference sites of 5, 6 and 7 hard terrain shown as red in the video record (Fig. 7.14) is also associated with a stalked crinoid (*Metacinus cyaneus*).

Crinoids are passive filter feeders and are the least understood of the living echinoderms yet their skeletal remains are among the most abundant and important fossils. Crinoids were major carbonate producing organisms during the Paleozoic and Mesozoic periods over a wide range of depths (Ausich 1998). Stalked crinoids are now predominantly found at depths greater than 100 m and a similar species (*Metacinus rotundus)* has a dispersive larval stage (Nakano *et al.,* 2003). The stalked crinoids commonly have an encrusting holdfast system that can attach to hard substrate but the isocrinids have hook like cirri along the stalk allowing the crinoid to release its hold and crawl with its arms (Ausich 1998). Images of the stalked crinoid (*Metacinus rotundus)* observed in reference sites 5 and 7 (Fig. 7.15) show the distinctive crown and stalk of the animal that gives it the common name of "sea lily". The crown faces towards the current to passively filter food of particle sizes of ranges commonly 50 to 400 µm (Ausich 1998).

Figure 7.14. Section of the Horseshoe Canyon (Fig. 7.5, 30 m grid) showing the, a.), slope (details Fig. 7.6), b.), backscatter (details Fig. 7.7a) and c.) segmented backscatter into soft and hard terrain (details Fig. 7.7b) with sediment grab samples (pie charts, gravel (red), sand (yellow) and mud (brown)) and video classified terrain into soft (blue) and hard (red) terrain. Reference sites 4, 5, 6, 7, 8 are shown within terrain areas 7.06, 7.07 and 7.11.

a.)

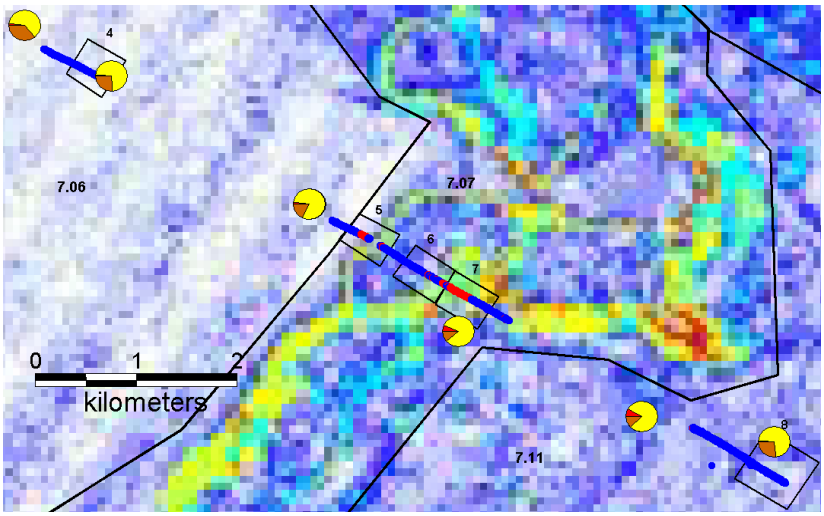

b.)

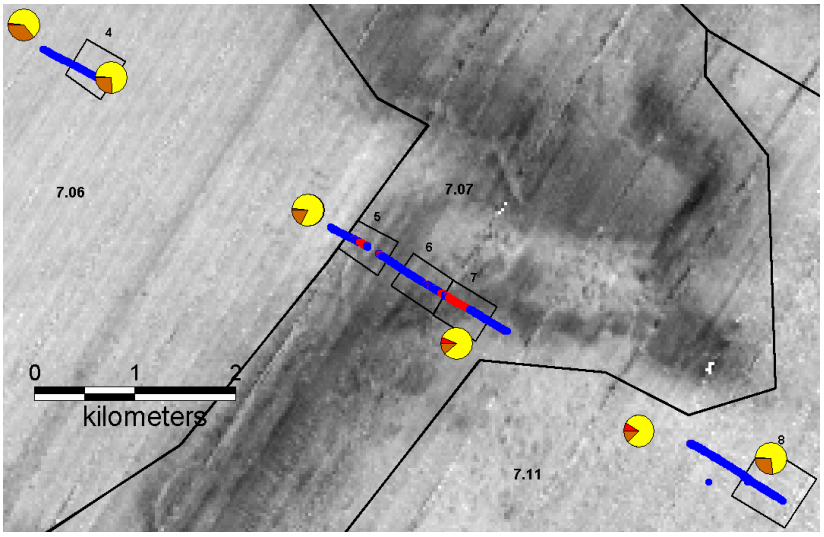

c.)

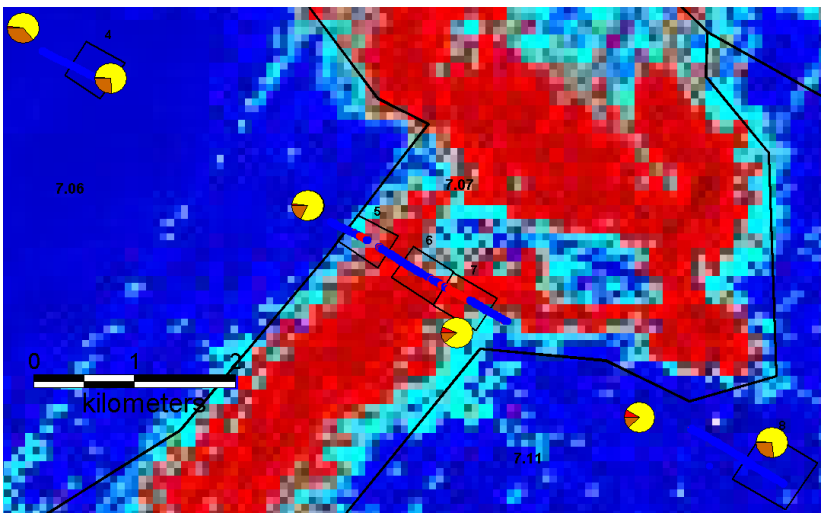

Figure 7.15 Example images of the stalked crinoid (*Metacinus rotundus)* observed in a.) reference site, 5 at 185 m depth and b.), reference site 7 at 229 m depth (Fig. 7.14).

a.)

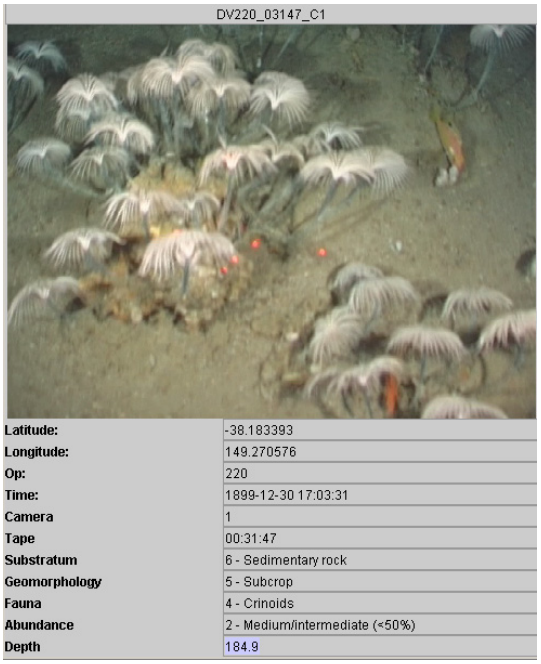

Latitude:	-38.183393
Longitude:	149.270576
Op:	220
Time:	1899-12-30 17:03:31
Camera	1
Tape	00:31:47
Substratum	6 - Sedimentary rock
Geomorphology	5 - Subcrop
Fauna	4 - Crinoids
Abundance	2 - Medium/intermediate (<50%)
Depth	184.9

b.)

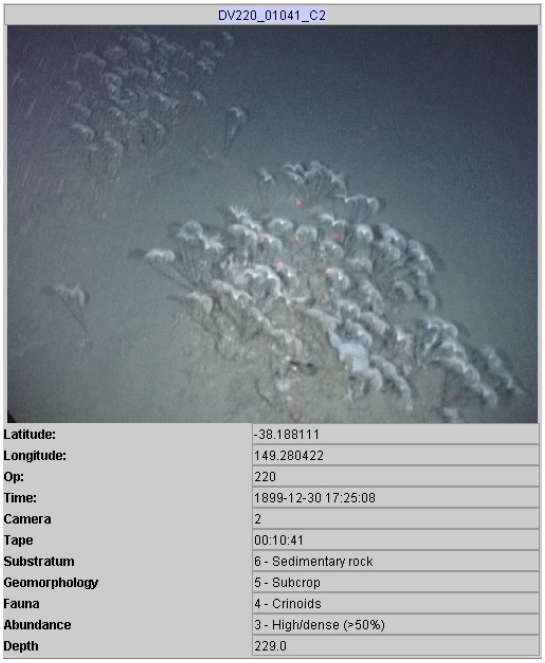

Latitude:	-38.188111
Longitude:	149.280422
Op:	220
Time:	1899-12-30 17:25:08
Camera	2
Tape	00:10:41
Substratum	6 - Sedimentary rock
Geomorphology	5 - Subcrop
Fauna	4 - Crinoids
Abundance	3 - High/dense (>50%)
Depth	229.0

Within this data set 75% of the 738 observations of crinoids (fauna type 4) occurred between depths of 167 m to 222 m, slopes of 2.2^{o} to 14^{o} and backscatter values of –29.7 dB to –26.0 dB (Fig. 7.16a). This agrees well with the species parameters where it needs hard substrate for attachment (greater than –31 dB is classed as hard acoustic terrain); is a tall (30 - 50 cm) passive filter feeder preferring conditions of enhanced currents which would be typically found on the shelf break in this region (typified by higher slopes).

The potential proportional surveyed area of habitat for crinoids over the 90th and 50th percentile range of observations based on acoustic backscatter, slope and depth within the canyon region is 6.7% and 1.3% respectively (Fig. 7.17). When the cover of crinoids in the video viewing area was estimated to be greater than 10% (159 scores, Fig. 7.16b) the potential habitat area was 4.4% to 0.8% for the 90th percentile and 50th percentile range of observations respectively. This highlights the highly selective range of preferred potential terrain for this species and if this terrain can be easily modified or the species removed due to bottom contact fishing, then the persistence of the species in this region would be threatened.

Figure 7.16. Relationship of video classified fauna type 4 (crinoids, 738 scores) with MBS variables of depth, slope and backscatter at 30 m grid for a.), all records and b.) where the cover was greater than 10% of the viewing area (159 scores).

a.) b.)

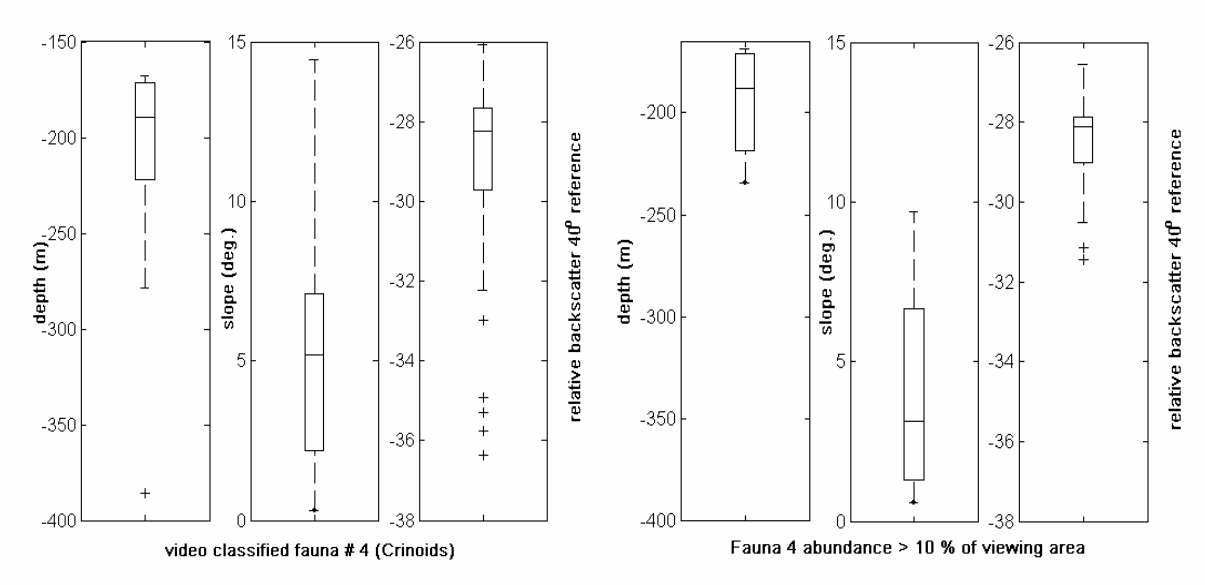

Figure 7.17. Potential distribution of the fauna category 4 (Crinoids) based on the 90th percentile (green) and the 50th percentile (red) range for the entire MBS data set (blue).

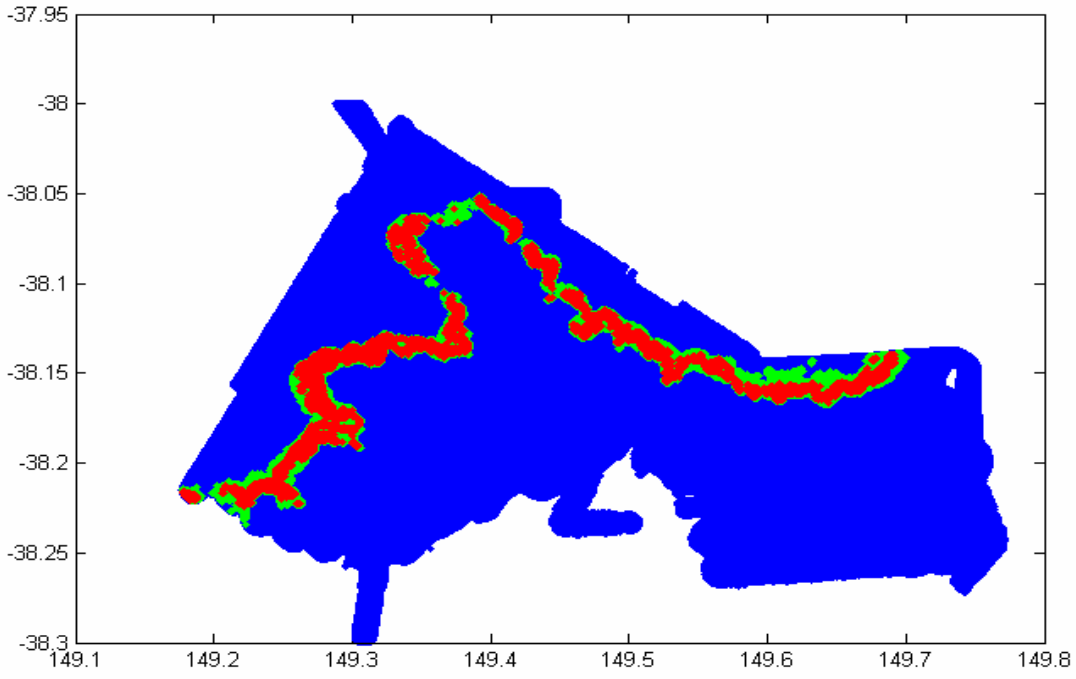

7.2.4 0.1 to 10 m resolution, fine scale video

At the 0.1 to 10 m resolution scale the video data are important to classify the fine scale substrate, geomorphology and fauna of the seabed. With accurate geolocation it is possible to create scientific reference sites that can be used for future monitoring of both natural and human induced changes. The geolocation was measured with an ultra short base line acoustic tracking system estimated to have a positioning error of 3-4 % of range (Kloser *et al.*, 2001b). This represents a limiting factor for accurate repositioning of the camera system. Despite this limitation it appears possible to observe impacts of fish trawling and predict changes in the seabed and its fauna at the scale of 10s m (Williams *et al.,* 2004). The video system can also observe dynamics and give insights into behaviour of animals (e.g. feeding mode of crinoids, Fig. 7.15).

Identifying consolidated sediment or partially buried hard substrate (subcrop) with video data is problematic and can lead to a potential bias when used as "ground truth" for interpreting acoustic data. The video provides images of the surface of the seafloor and based on clues within the video record the probable substrate may be inferred. Indicators in the video images that are typically used to detect the presence of a hard substrate are attached fauna, no soft terrain associated fauna (e.g. bioturbation, Fig. 7.13) and the association in sequence of video images. With no obvious hard substrate fauna the potential for misclassification of hard substrate is greatest when there is an overlay of a thin veneer of fine sediments. In reviewing a section of scored video it is possible to highlight regions where the surface substrate is scored as fine sediments, unrippled, but the actual biological substrate is composed of a fine-grained sediment covered subcrop, indicative of partially buried consolidated sediment or bedrock.

The hypothesis that video classified mud or fine sediments, unrippled with no bioturbated fauna may be misclassified is explored using the acoustic backscatter data as a proxy for hard terrain. There were 2885 records (8.8% of video records) scored as video soft when the acoustic backscatter was greater than –31 dB. It is possible that a proportion of these observations are actually hard substrate (being due to subcrops of consolidated sediments or rocks). This potential misclassification of the substrate and geomorphology by video is illustrated with the crinoid fauna and scientific reference sites 5, 6 and 7 (Fig. 7.14c). The video classifies the terrain as predominately soft whilst the acoustic backscatter strength indicates it is predominately hard. Note that the acoustic system depending on frequency penetrates thin sediment layers as discussed in Chapter 3. A detailed review of the video through this section showed signs of fauna and morphology that support the acoustic definition of the terrain. Therefore using a combination of video scores and acoustic metrics a more reliable interpretation of the seabed type can be obtained. Care needs to be taken when interpreting video as "ground truth" for subcrops (consolidated sediments or rocks) terrain types.

The probability of finding certain faunal functional groups on consolidated and unconsolidated sediment may depend on natural and anthropogenic induced changes. It is highly likely that we were not sampling unmodified biotopes due to cumulative impacts by trawling over many decades. This would affect the interpretation of the relationship between sediment, fauna and terrain and, along with natural variation (*e.g.* succession, competition and community dynamics), places a temporal constraint on the sampling undertaken. The functional and morphological method of characterising fauna from the video could be used to monitor changes in seabed due to both natural processes and human activities. As an example, large erect sessile fauna (*e.g.* crinoids and sponges) may be removed during bottom contact fishing whilst smaller sessile organisms remain, and this can be detected using video (Pitcher *et al.,* 1997, 2000; Sainsbury *et al.,* 1997).

7.2.5 Demersal fishing activity

Using the Australian South East Fisheries database of fishing effort recorded from fishers log books, it is possible to explore the targeting of specific terrain types using demersal fishing gears. Fishers record the vessel position as the gear enters the water and when it is hauled on deck at 0.01^{o} resolution (approximately 1.1 km) although some fishers record the time and position that the fishing gear contacts and leaves the seabed. Fishers can also incorrectly enter coordinates of demersal trawls that are entirely in the wrong position, very long or very short. To accurately locate the demersal trawl seabed contact position requires correction of the layback from the vessel and identifying when the trawl was in contact with the seabed. The layback position of the demersal trawl is related to the warp out, vessel heading, water depth, vessel speed, currents and wind speed. Therefore estimating the exact bottom contact position for each trawl is a non-trivial task. To simplify the task it is assumed that trawls greater than 40 km (less than 5% of records) are not targeted and probably misreported. It is assumed that the mid point of the trawl indicates the terrain being targeted and systematic errors of recording due to changes in the definition of the start and end of the trawl will average out. These simplifying assumptions were tested by visual analysis of individual trawl shots plotted on the region and supported by visual correlations. Fishers' log book data prior to 1997 were not considered because the georeferenced resolution decreased due to log book resolution being at 0.1^{o} (Mike Fuller pers. comms. 2004). Logbook data from Commonwealth fisheries are confidential and the Australian Fisheries Management Authority (AFMA) has an operating rule of only presenting data aggregated from five or more vessels to protect vessel anonymity and 'secret fishing locations (Larcombe *et al.,* 2001). To conform to this rule no figures of the analysis are presented.

Between 1997 and 2004, 4265 demersal trawls were targeted with a trawl centre point in the region bounded by polygons 6.01 to 6.12 and 7.01 to 7.14 (Fig. 7.5). Of these trawls 63% of trawl centres were in polygon areas designated as acoustic soft terrain and 37% in acoustic hard terrain. Considerable demersal trawl activity (1578 shots from 1997 to 2004) occurred in regions designated as acoustic hard and this activity changes yearly. From the data available it appears that new acoustic hard regions are being targeted over time. Acoustic hard terrain area 6.04 was only lightly fished in 1997 to 2002 and fishing effort appears to have increased in 2003 and 2004 but concentrated in the shallower northern part of this region. In the hard region where crinoids were observed by video (area 7.07) the fishing effort was higher in 1997 to 2001 and reduced between 2002 and 2004. The direction of the trawls shows that fishing is primarily carried out along depth contours. Demersal trawls on acoustic soft terrain (2687 shots from 1997 to 2004) were primarily focused on the deeper regions (300 – 450 m) with trawls generally following the depth contours. This analysis highlights that demersal trawling is occurring in both acoustic soft and hard terrain types and that this trawling effort may have modified the distribution and abundance of fauna observed by video in April of 2000. The degree to which the fauna has changed on these seabed types due to demersal trawling and the ability of the deep sea fauna to regenerate is poorly known.

Using the video data at the scientific reference sites it should be possible to monitor the changes in faunal groups, abundance and sizes of the dominant erect fauna (Kloser *et al.,* 2001b). This requires finer scale measurements using the video system and requires higher resolution sampling and correction for range and angle using stereo cameras and or laser scaling (*e.g.,* Barker *et al.*, 2001).

7.3 Summary

Based on an overarching classification scheme the MBS data were placed in a regional context at the 100s km scale using historic knowledge. The MBS provides detailed information at the 1 to 10s km scale using simple metrics of depth, slope and backscatter. The acoustic backscatter has been referenced to 40^{o} incidence angle to provide the best discrimination between seabed types and to reduce the sensitivity to variations in seabed slope, absorption and background noise. Using a simple backscatter amplitude segmentation criterion based on reference sites of known acoustic hard and soft seabed types, the visual segmentation of the Horseshoe region at 1 to 10s km scale was supported with quantitative metrics.

The acoustic soft terrain regions were observed to be 98% video soft terrain giving high confidence in identifying soft terrain from acoustics at the 1 to 10s km scale. Within acoustic soft terrain a distinctive faunal group was dominant although it is recognised that the faunal distribution observed may have been modified due to demersal trawling. The acoustic hard terrain at 1 to 10s km scale contained a high proportion of video soft terrain. This high proportion of video soft terrain also increased the proportion of soft terrain faunal types occurring within acoustic hard terrain.

The patch lengths of terrain types appeared to be a major influence on the backscatter strength within acoustic hard terrain. In acoustic hard terrain, small patches of video soft terrain were observed, 50% with patch lengths less than 30 m and not resolvable on the 30 m square grid used. Therefore acoustic backscatter from a video soft patch of seabed would be influenced with surrounding hard seabed increasing the backscatter. Within acoustic soft terrain at the 1 to 10s km size the video soft patches were longer, 50% being greater than 500 m in length.

Using the MBS metrics it is possible to explore the potential terrain suitable for a species within the region. In this instance the distinctive stalked crinoid species (*Metacinus rotundus)* has an apparent preferred habitat identified by depth, slope and backscatter strength. Using these metrics the potential distribution of the species in the wider region can be estimated. This preliminary distribution map could be further refined with other physical and biological variables, such as nutrient availability, temperature, salinity, current stress, aspect and inferred larval distribution. Using these metrics it would be possible to predict the wider potential terrain where this species could exist. Thus it would be possible to use the MBS data to explore where a marine protected area or fisheries closure could be placed to include suitable terrain for this species.

8 Summary and Discussion

8.1 Exploratory seabed biotope surveys in deep water

For most of the Australian deepwater marine jurisdiction greater than 100 m depth, we have poorly defined bathymetry and even poorer characterisation of the seabed substrate, geomorphology and associated fauna. This thesis has outlined a general approach for characterising the seabed as follows:

1. The survey area is placed in context at a regional scale (100s km) using historic geological, oceanographic and biological knowledge. Here the seabed is separated into depth units such as slope, shelf and abyss and regional units based on oceanographic conditions and distributions of fauna (IMCRA 1998).

2. At the 1 to 10s km feature size and larger, the MBS data are used to distinguish the major geomorphological units based on the morphology and substrate of the seafloor; these include canyons, sediment plains, ridges, sand waves etc.

3. At the 10s m to 1 km feature size, the combined substrate, geomorphology and dominant sessile macrofauna composition is identified.

4. At the 0.1 to 10s m feature size, detailed information about the biota and its association with the substrate and other biota is identified. At this feature size and smaller it is possible to identify seabed changes relevant to individual species due to natural or anthropogenic effects.

Based on the MBS and video in-water remote sensing tools with limited geological and biological physical sampling, a simplified protocol to carry out exploratory surveys addressing points 2, 3 and 4 above has been established.

8.1.1 Terrain features 1 to 10s km

One need for seabed mapping is at the 1 to 10s km feature size which, in deepwater, is the length scale used to define boundaries on maps for management purposes (*e.g.,* MPAs and fisheries spatial closure zones). The detailed bathymetric data from the MBS, at square grid cells of 4 to 42 m depending on depth, seabed slope and MBS incidence angle (Table 8.1 and Chapter 4), can provide detailed boundaries of rough seabed structures such as elevated limestone/sandstone banks (important habitats for fishes, Williams *et al.,* 2004) and clearly delineate other important seabed features such as large patches of sand waves and canyons at 1 to 10s km scale (*e.g.,* Fig. 5.7 to 5.11 and Fig. 7.3). Therefore the bathymetric data from the MBS, alone, are sufficient to delineate a number of important geomorphic features (*e.g.,* Todd *et al.*, 1999; Gardner *et al.*, 2003). Fine scale bathymetry (0.5 m resolution at 200 m depth) showed the outcropping and inferred sub-cropping of consolidated sediments or rocks indicative of hard-rough terrain at the 1 to 10s km scale. It should be noted that a classification bias of acoustic rough terrain occurs with increasing depth due to the decreased horizontal and vertical resolution of the acoustic system (Table 8.1). The towed video transect data revealed frequent small-scale variability where 50% of terrain patch lengths were less than 20 m and the dominant faunal patch length was less than 10 m. At this scale the MBS is unable to detect the terrain patch structures at depths beyond ~200 m assuming at least 2 samples within the square grid cells are required (Table 8.1).

Measurements of seabed echo return time to estimate depth from multibeam sonars have both relative and absolute errors that are well documented (Simrad 1999; Mitchell 1996; Calder

and Mayer 2003). Backscatter measurements from the seabed using these MBSs are less well documented and the accuracy and precision of such measurements for a range of incident angles is often ill defined. Instrument calibration for transmit power, pulse length, beam pattern and receiver stability for individual beams is also not standardised. Methods of calibration are possible with calibrated spheres and instrument system tests but are not often implemented by users or manufacturers. Maintaining accuracy of the data subject to vessel motion and aeration is also required. This thesis has outlined the corrections to acoustic backscatter measurements required to address issues of ensonified area, water column absorption, seabed slope and background noise. Due to uncertainty in the calibration and the exact pre-processing algorithms used within the Simrad EM1002 the backscatter measurements reported here can only be presented as relative.

Table 8.1. Theoretical depth data densities on a horizontal flat seafloor based on a Simrad EM1002 (2^o conical 111 beams) and Simrad EM300 (1^o conical 132 beams) equispaced covering 140^o and surveying at a speed of 5 ms^{-1} (ignoring attitude and refraction effects). Minimum square grid size requiring at least 2 depth samples within a grid cell.

Depth	Beam spacing			Approximate minimum square grid size m	
m	Along-track m	Across-track m			
		EM1002	EM300	EM1002	EM300
50	1.0	2.5	NA	3	NA
100	1.9	5.0	4.2	5	4
200	3.9	10.0	8.4	10	8
400	7.8	20.0	16.8	20	17
600	11.7	30.0	25.2	30	25
1000	19.5	NA	41.9	NA	42

These relative MBS backscatter to incident angle profiles from selected homogeneous sites were consistent with a simple backscatter model including both surface and volume scattering from the seafloor over a range of depths (60 m to 400 m). At normal incidence stronger backscatter returns are observed that decrease with incidence angle at a rate consistent with roughness and hardness attributes of the seabed (Fig. 6.2). To remove this backscatter to incidence angle profile, for visualisation and to provide incident angle independent metrics, a reference incidence angle between 30^o and 40^o is used. The reference incidence angle of 40^o is chosen in this thesis due to its minimisation of backscatter corrections, better differentiation of model seabed types and region of reduced backscatter standard deviation (Chapter 4). The incident angle referenced backscatter maps (Fig. 5.8 and Fig. 7.7) results in a loss of seabed terrain characterisation information, in particular the rate of decrease of backscatter near normal incidence (0^o to 30^o), and effects of the critical angle at incidence angles from ~50^o to 70^o. Using the seabed backscatter referenced to 40^o incidence angle, hard and soft seabed segmentation procedure was established based on well-described reference sites. Models of different seabed types, measured backscatter to incident angle profiles from homogeneous reference sites and minimisation of backscatter corrections support the selection of reference incidence angles between 30^o and 40^o.

A simplified visual analysis of the MBS metrics of bathymetry and relative intensity of backscatter, combined into soft, hard, smooth and rough terrain, was investigated at the 1 to 10s km scale. The video data confirmed that acoustically defined soft terrain was predominantly video soft, 98% of the time, whilst the acoustic hard terrain at the 1 to 10s km

scale contained 29% video hard and 71% video soft terrain (Chapter 5). Video transects highlight the small scale patches that exist in hard terrain and that hard terrain defined by acoustics at 1 to 10s km contains a high proportion of video soft terrain patches. There was little agreement between the video classified rough terrain types and the acoustically classified rough; it appears that the video and acoustic systems are observing different roughness characters at different scales. Sand waves of 2 m peak to trough height and a 30 m wavelength, detected with the MBS, will not be easily detected with a towed video observing 5 to 7 m^2 of seafloor. Also it was difficult to establish a simple relationship between sediment grain size and MBS backscatter composition because of the inability of the sediment sample to characterise hard-rough (*e.g.* rocky or boulder) terrain. Within homogeneous reference sites there was good agreement between grain size and low backscatter soft acoustic terrain. As the backscattering strength increases and becomes more irregular it is indicative of a patchy seabed terrain made up of all terrain types. This was demonstrated in one region where four sediment grabs within 10s m ranged from gravel dominant to sand dominant. In such cases the best "ground truthing" data are obtained from the towed video.

8.1.2 Terrain features 10s m to 1 km

To better define the 10s m to 1 km terrain patch structure within the acoustic backscatter data, more quantitative analysis of the acoustic data were investigated. The analysis compared the georeferenced video and physical data at a range of incidence angles at well described homogeneous and heterogeneous reference sites with models of seabed backscatter (*e.g.,* Jackson and Briggs 1992) and phenomenological characters in the backscatter data (*e.g.,* Huseby *et al.,* 1993). Based on the well described reference sites it was possible to separate hard-rough from soft-smooth ecological terrain types using the magnitude of the echo amplitude and its standard deviation for incidence angles higher than 16^o (Chapter 6). Soft-smooth sites could also be separated into high and low mud fraction using the mean echo amplitude at incidence angles higher than 26^o. Using both the mean echo amplitude and its standard deviation at a range of incidence angles hard-rough, soft-smooth and soft-rough sites could be separated at incidence angles higher than 16^o, 26^o and 44^o respectively. Comparison of level shifted (12 dB) seabed backscatter data from reference site with the model (APL94 1994) also reliably separated soft-smooth sites from hard-rough sites (Chapter 6, 6.13). A level shift of 12 dB of all incidence angle data were required to best match model and experimental data (Ch. 6). It was not possible to predict actual geoacoustic properties by inverting the model for the reference sites encountered in this study with the simulated annealing method used. A major limitation of the above analysis was the need to use the entire incident angle range from 0^o to 70^o which is unable to resolve the fine scale patchiness of the terrain at the 10s m scale in water depths greater than 100 m. Phenomenological characters of the backscatter data showed that the 4 ecological seabed types within the reference sites could be distinguished with a cross validation error of 4% for 10 incident angle segments (Chapter 6, Table 6.14). Many of the extracted features were correlated with the mean of the backscatter and its standard deviation at incidence angles higher than 30^o. In the near normal incidence region the "power spectrum" and "ratio of mean backscatter between sectors" metrics provided the highest discriminatory information gauged by the Mahalanobis distance metric. Of note was the use of the backscatter metric referenced to 40^o incidence angle to reliably separate ecologically hard from soft terrain. The simplicity (easy to understand processing method) and robustness (easy to map and identify errors) of this metric makes it a very useful parameter. From the analyses presented in Chapter 6, the null hypothesis that there was no link between ecological terrain types and MBS backscatter metrics is rejected. The video data also demonstrated a link between the 4 ecological terrain types and the faunal types at high probabilities of association.

8.1.3 Terrain features 0.1 to 10 m

In previous studies based on photographic/video data general associations between sediment type and megafauna were evident (*e.g.,* Kostylev *et al*., 2001; Edwards *et al.*, 2003). In this study the video data show that video terrain type is not a completely reliable predictor of the presence/absence of faunal groups, but some general associations with high probabilities are evident. The towed video data demonstrated the highly patchy nature of the seafloor and the difficulty that single widely spaced photographs would have in describing the sediment fauna relationship. Understanding the pattern, scale and processes of benthic systems is greatly enhanced using video data (Solan *et al.*, 2003 and references therein). However, there are also several limitations of video data. Speed of collection is relatively slow and the area of seabed sampled is small, although significantly improved with laser line scan systems (Carey *et al*., 2003). The video hard-smooth subcrop class is difficult to classify reliably and was usually inferred by the type of fauna present. A combined use of the acoustic backscatter and video is being explored to reduce this inconsistency in future surveys (Chapter 7). Small animals, and difficult taxonomic groups, are often poorly resolved. This limits the capacity of the combination of acoustics and video to define biodiversity, and therefore to detect and monitor changes in characteristics such as species-richness or the body-sizes of animals without further refinement (*e.g.,* calibrated paired cameras for accurate measurements and higher resolution video systems, Barker *et al.*, 2001). Thus, there is a need to physically capture organisms to identify taxa and measure biomass. Typical sled tows integrate samples over the duration of the tow and hence integrate fauna over different terrain types, obscuring the sediment-fauna relationship. Using a camera in conjunction with the benthic sled would have improved the results obtained in this study.

It is highly likely that within the soft and hard seabed terrains at the 1 to 10s km feature size we were not sampling "natural" habitats due to cumulative impacts of trawling over many decades. This would affect the interpretation of the relationship between sediment fauna and terrain and, along with natural variation (*e.g.,* succession, competition and community dynamics), places a temporal constraint on the sampling undertaken. The functional and morphological method of characterising fauna from the video and sled sampling could be used to monitor changes in seabed due to both natural processes and human activities. As an example, large erect sessile fauna (*e.g.,* sponges) may be removed during bottom contact fishing whilst smaller sessile organisms remain, and this can be detected using video (Pitcher *et al.,* 1997, 2000; Sainsbury *et al.,* 1997). The scientific reference sites created in this study should provide a basis of a system of long term benthic monitoring sites over a number of bioregions.

The acoustic data at broad scale can be used to identify generic geomorphic and substrate features that may act as surrogates for ecological variables relevant to management. An example of this surrogacy is that the detailed bathymetry provided by the MBS enabled us to define at 1 to 10s km scale major geomorphic features including canyons, elevated limestone reef (Fig. 5), broken limestone reef and sand waves at resolutions of 0.5 m in height or 0.5% of range. Within the 1 to 10s km regions it was possible to detect ledges that were indicative of enhanced attached megafauna using the derivative of depth (slope). In particular, within the Big Horseshoe (also known as Everard Canyon) the shelf edge was characterised by an unusual benthic megafaunal assemblage dominated by an apparently uncommon stalked crinoid. Using a combination of bathymetry, slope and backscatter the preferred terrain for this species could be identified (Chapter 7, Fig. 7.17).

8.2 National scale seabed biotope mapping needs in deep water

It was been demonstrated in this thesis that maps of bathymetry and backscatter in deep water (100 to 1500 m) can be used to characterise the seabed terrain at a number of spatial scales suitable to management needs (Ch. 2). Based in part on this work a Simrad EM300 multibeam sonar was subsequently purchased to target the 100 to 1500 m depth range to evaluate the ecological characteristics of the seafloor. The instrument selected required narrow beams and well described collection of the seabed backscatter. The Simrad EM300 purchased for the Research vessel *Southern Surveyor* has higher resolution and forms more beams than the Simrad EM1002 used in this study (Table 8.1).

An immediate need for the MBS is illustrated by the identification of the 'Zeehan' draft candidate MPA off western Tasmania in Australia's SEMR during 2004. It is composed of three separate areas, of which the largest area runs from the continental shelf (in approximately 100 m depth) to abyssal depths (greater than 3000 m), and the section running across the offshore fishing grounds of the shelf edge and slope (Fig. 8.1). Specifications for designing the SE MPAs include a requirement that each MPA bounds two complete submarine canyons. Pre-existing coarse resolution scientific bathymetry data provided the basis for estimating canyon positions and indicated that the MPA boundary included one canyon and parts of three others (Fig. 8.1a). A multibeam bathymetry map (surveyed in April 2004) of the real structure of canyons over the slope region shows that four canyons, one large and three small, are bounded by the MPA (Fig. 8.1b, c, untextured regions at the deep and shallow margins have no multibeam coverage). Two of the three "canyons" identified from the pre-existing bathymetry data have negligible presence on the slope. Pre-existing bathymetric data predicted the larger canyons well, but missed or mis-identified smaller canyons that have more impact at upper slope depths where narrow bands of unique biodiversity are located.

Figure 8.1 Example of the EM300 MBS bathymetry and improved knowledge from the outer shelf upper slope: (a) image from previous information with canyons marked (Harris *et al*., 2002); (b) the extra detail of the topography provided with the MBS; proposed marine protected area boundary in red. (c) map of the bathymetry joined with deeper water Simrad EM12 MBS data showing the outer shelf and the continental slope of the region.

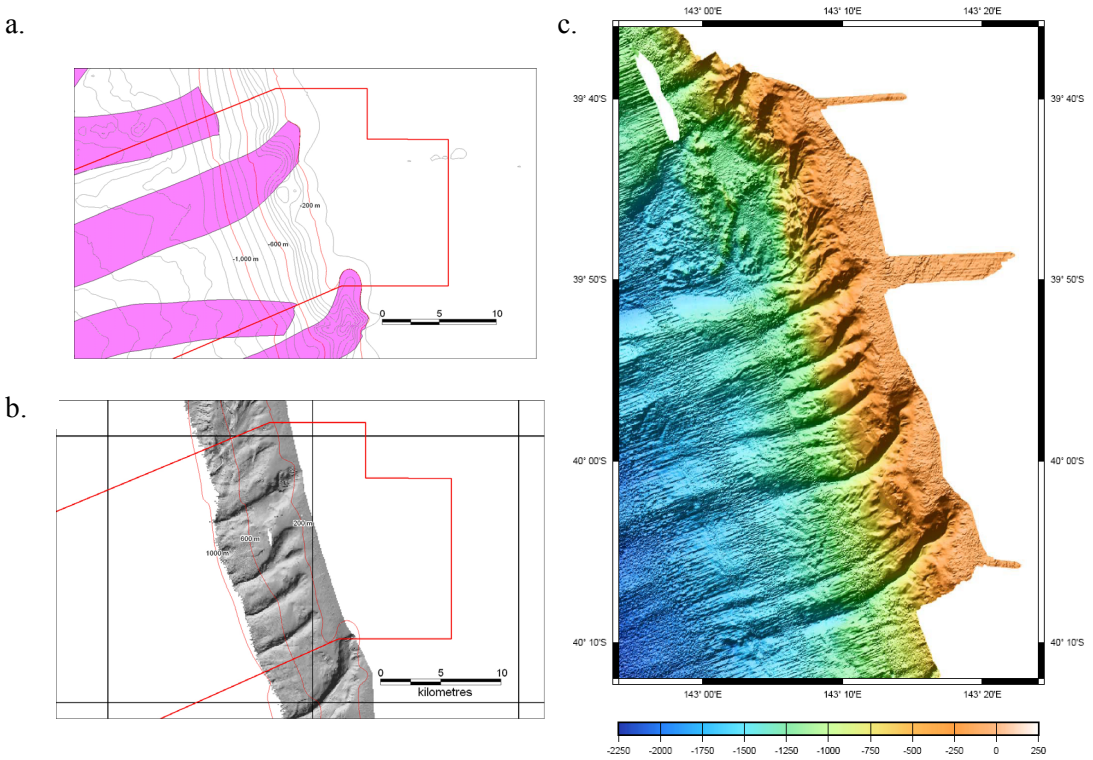

8.3 Mapping Australia's marine regions

The Australian marine environment is approximately 16 M km^2 of which 6.4 M km^2 around the Australian coast has been segmented into 7 "Large Marine Domains" for operational management purposes (Chapter 2). These domains correspond to regional scale patterns in the fauna and physical and chemical environment that have developed over eons (IMCRA 3.3, 1998). The area and slope of each depth stratum within each domain was calculated based on a compiled bathymetric grid at 0.01^o resolution (Geoscience Australia, 2004).

The survey days required to provide 100% swath mapping coverage for 25 to 5000 m depths using a Simrad EM300 MBS are estimated based on the typical angular coverage obtained during recent voyages and 10 knots vessel speed (Table 8.2). To achieve full coverage in shallow water (less than 150 m) would take considerable effort with estimates of between 375 to 5582 days per Large Marine Domain (LMD) (Table 8.2) and may be of questionable value with better return on targeted coverage in areas of highest need or alternative sampling designs that cover less than 100% of the area. In the 150 to 1000 m depth range (of greatest interest to marine resource managers due to its unique biodiversity, small seabed area and concentration of bottom contact fishing), the time required to survey the LMDs is well within current sea going capacities of 29 to 289 survey days per annum (Table 8.2). The 150 to 1000 m depth range of the entire SEMR could be surveyed with a MBS in 57 days, larger regions such as NWS and the NE would take considerably longer, 289 and 271 days respectively.

Table 8.2. Approximate time in days to provide 100% multibeam cover using a Simrad EM300 multibeam sonar operating at 5 ms^{-1} from 25 m to 6000 m depths for each Australian Large Marine Domain excluding islands and Antarctic territory.

EM300		Survey Days @ 10 knots for each Large Marine Domain						
Depth range m	Angular coverage	SE	S	W	NW	N	NE	E
25 - 150	130°	1473	2425	479	2090	5582	1799	375
150-1000	130° - 120°	57	92	86	289	29	271	41
1000-6000	120° – 15°	806	720	397	296	0	432	400
	Total Area							
	1000 km^2	1160	1090	529	894	808	1261	652

The minimum theoretical bathymetric grid size for the EM300 MBS operated at 10 knots and 140° seabed ensonification over a horizontal flat seafloor is 4 m at 100 m depth increasing to 25 m at 600 m depth (Table 8.1). In practice, due to vessel motion and slower ping rates the grid sizes are increased giving lower resolution. The resolution of the multibeam system also depends on the finite beam width of the beams that will smooth rough surfaces. In a large proportion of the Australian Marine Jurisdictional area the bathymetry is poorly understood and soundings are sparse. The resolution obtained with the EM300 multibeam sonar is compared with previous historic data with a high density of historic soundings that included single beam and deeper water swath maps at >1000 m, beyond the shelf break (Fig. 8.1). The historic data were compiled to aid the design of marine protected areas and integrated all available bathymetric data; an analysis of slopes ("drainage") enabled a coarse identification of geomorphological features such as submarine canyons (Harris *et al.*, 2002, Fig. 8.1 A). A MBS bathymetric map of the region showed far more detail and provided accurate information on the location of the canyon features that had been used to situate the MPA (Fig. 8.1B). The MBS survey from 150 to 1000 m was carried out in 10 hrs and when joined with deeper water Simrad EM12 data provides a detailed view of the continental slope (Fig. 8.1C).

Based on typical survey conditions, the entire outer shelf and upper slope region (150 to 1000 m depth) of the South-East Marine region (SEMR) could be mapped with a MBS in 57 days. Such a survey would provide a much needed management and scientific input at the100s km regional scale but also detailed data at the 1 to 10s km scale. The importance of reconnaissance survey using acoustic or optical sampling prior to physical sampling is well supported (Solan *et al.*, 2003). Clearly with the tools currently available there is a strong case to systematically sample the outer shelf and upper slope of the Australian Marine Jurisdiction. This seabed region is a major source of fish for domestic markets and as a result is subject to the highest repeated fishing impact in the SEMR. Australia is currently establishing a network of offshore marine protected areas that, as exemplified above, needs an understanding of the seascape at the 1 to 10s km scale. A simple first step would be the accurate location and size of geomorphic features such as canyons and elevated limestone reefs, which can be obtained directly from the MBS bathymetry. At the next level, the backscatter, with minimal processing to correct for sound propagation and seabed slope, could be used to distinguish soft from hard seabed terrain. This thesis has shown that at this level there are distinct biological community preferences and that the biodiversity within each terrain class is likely to be distinctly different. Based on our existing knowledge and the recent installation of a mid-depth MBS (Simrad EM300) on the national research vessel, a national survey strategy would include:

1) Systematic MBS mapping of the outer continental shelf and upper slope (150 to 1000 m depths) of the Australian Marine Jurisdictional area as a priority zone.

2) Classification and segmentation of the acoustic data into terrain types based on bathymetry and backscatter, representing terrain at 1 to 10s km scale.
3) Targeted, georeferenced sampling with physical and visual tools in regions of highest priority, determined by human impacts or predicted biodiversity values.
4) Establishment of scientific reference sites for monitoring natural and human induced changes in areas with high management relevance.

Appendix A

References

Alexandrou , D.and Pantzartzis, D. 1993. A methodology for Acoustic Seafloor Classification. IEEE Journal of Ocean Engineering, 18(2): 81-86.

Alexandrou, D., de Moustier, C., and Haralabus, G. 1992. Evaluation and verification of bottom acoustic reverberation statistics predicted by the point scattering model. The Journal of the Acoustical Society of America, 91(3): 1403-1413.

Althaus, F., Williams, A., Gowlett- Holmes, K., Furlani, D. and Kloser, R. J. 2004. Patterns of Diversity and Community Composition on the Shelf and Slope of the Southeast Region: Benthic invertebrate and demersal fish catch data from OP2000-SE02 and SEF Ecosystem projects. Technical annex to "Final Report on Project OP2000-SE02" to the National Oceans Office.

APL94-Applied Physics Laboratory. 1994. High frequency ocean environmental acoustic model handbook APL-UW TR 9407. Applied Physics Laboratory Technical report (University of Washington).

Ausich, W.I. 1998. Early phylogeny and subclass division of the Crinoidea. Journal of Paleontology, 72: 499-510.

Barker, B.A.J., Helmond, I., Bax, N.J., Williams, A., Davenport, S. and Wadley, V.A. 1999. A vessel-towed camera platform for surveying seafloor habitats of the continental shelf. Continental Shelf Research, 19: 1161-1170.

Barker, B.A.J., Davis, D.L. and Smith, G.P. 2001. The Calibration of Laser-referenced Underwater Cameras For Quantitative Assessment of Marine Resources. Proceeding MTS/IEEE Oceans2001.

Bax, N.J. and Williams, A., [Eds.]. 2000. Habitat and fisheries productivity in the South East Fishery. Final report to the Fisheries Research and Development Corporation, Project 94/040. CSIRO Marine Research (Hobart).

Bax, N.J. and Williams, A. 2001. Seabed habitat on the southeast Australian continental shelf – context, vulnerability and monitoring: Marine and Freshwater Research, 52: 491-512.

Begon, M., Harper, J.L., and Townsend, C.R. 1996. Ecology: individuals, populations and communities, 3rd edn. Blackwell Science, Cambridge.

Brekhovskikh, L.M. and Lysanov, Y.P. 1991. Fundamentals of Ocean Acoustics. 2nd edition. Springer-Verlag, Berlin, 270pp.

Bruce, B.D., Condie, S. A. and Sutton, C. A. 2001, Larval distribution of blue grenadier (*Macruronous novaezelandiae* Hector) in south-eastern Australia: further evidence for a second spawning area. Marine and Freshwater Research, 52: 603-610.

Buckingham, M. J. 1997. Theory of acoustic attenuation, dispersion, and pulse propagation in unconsolidated granular materials including marine sediments. The Journal of the Acoustical Society of America, 102 (5): 2579-2596.

Calder, B. R., and Mayer, L. 2003. Automatic Processing of High-Rate, High-Density Multibeam Echosounder Data. Geochemical, Geophysical and Geosystems (*G3*), 10.1029/ 2002GC000486, 4(6)3.

Canepa, G., Bergem, O. and Pace, N. P. 2003. A new algorithm for automatic processing of bathymetric data. IEEE Journal of oceanic Engineering, 28(1): 62-77.

Caress, D.W. and Chayes, D.N. 1995. New software for processing sidescan data from sidecan-capable multibeam sonars. Oceans 95 MTS/IEEE, Challenges of our changing global environment, October 9-12, San Diego, California, USA, pp. 997-1000.

Carey, D.A., Rhoads, D.C., and Hecker, B. 2003. Use of laser line scan for assessment of response of benthic habitats for demersal fish to seafloor disturbance. Journal of Experimental Marine Biology and Ecology, 285-286: 435-452.

Chivers, R.C., Emerson, N. and Burns D.R. 1990. New acoustic processing for underway surveying. Hydrological Journal, 56**:** 9-17.

Chotiros, N.P. 1995. Biot model of sound propagation in water-saturated sand. Journal of the Acoustical Society of America, 97(1): 199-214.

Clay, C. S. and Medwin, H. 1977. Acoustical Oceanography: Principles and Applications. John Wiley and Sons: NewYork USA.

CMR, 2000, Cruise Report: CSIRO *Southern Surveyor* 01/00. April 4 – May 21 2000. CSIRO Marine Research (Hobart.)

Collins, W., Gregory, R., and Anderson, J. 1996. A digital approach to seabed classification. Sea Technology August, 83-87.

Condie, S. A., Loneragan, N. R., and Die, D. J. 1999. Modelling the recruitment of tiger prawns (Penaeus esclentus and P. semisulcatus) to nursery grounds in the Gulf of Carpentaria, northern Australia: implications for assessing stock recruitment relationships. Marine Ecological Progress Series 178: 55-68.

Conolly, J.R. 1968. Submarine canyons of the continental margin, east Bass Strait (Australia). Marine Geology, 6: 449-461.

Dalen, J., and Lovik, A. 1981. The influence of wind-induced bubbles on echo integration surveys. Journal of the Acoustical Society of America, 69: 1653-1659.

de Moustier, C. 1986. Beyond bathymetry: Mapping acoustic backscattering from the deep seafloor with Sea Beam. Journal of the Acoustical Society of America, 79(2), 316-331.

de Moustier, C. and Alexandrou, D. 1991. Angular dependence of 12 kHz seafloor acoustic backscatter. Journal of the Acoustical Society of America, 90(1): 522-531.

Dartnell, P., and Gardner, J.V. 2004. Predicting seafloor facies from multibeam bathymetry and backscatter data. Photometric engineering and remote sensing, 70(9): 1081-1091.

Denbigh, P. N. 1989. Swath bathymetry: Principles of operation and an analysis of errors. IEEE Journal of oceanic engineering, 14(4).

Edwards, B.D., Dartnell, P. and Chezar, H. 2003. Characterizing benthic substratums of Santa Monica Bay with seafloor photography and multibeam sonar imagery. Marine Environmental Research, 56: 47-66.

Elton, C. 1927. Animal Ecology. Sedgewick & Jackson, London 96p.

Fisher, F. H. and Simmons, V. P. 1977. Sound absorption in sea water. The Journal of the Acoustical Society of America, 62: 558-564.

Fofonoff, P. and Millard, R.C. Jr. 1983. Algorithms for computation of fundamental properties of seawater, 1983. _UNESCO Technical Papers in Marine Science, 44: 53 pp.

Folk, R.L. 1954. The distinction between grain size and mineral composition in sedimentary-rock nomenclature, Journal of Geology 62: 344-359.

Folk, R.L. 1968. Petrology of sedimentary Rocks. Austin, Texas, Hemphill.

Foote, K. G., Knudsen, H. P., Vestnes, G., McLennan, D. N., and Simmonds, E. J. 1987. Calibration of Acoustic Instruments for Fish Density Estimation: A Practical Guide. Cooperative Research Report International Council for the Exploration of the Sea , 69.

Francois, R. E. and Garrison, G. R. 1982. Sound absorption based on ocean measurements. Part II:Boric acid contribution and equation for total absorption. The Journal of the Acoustical Society of America, 72: 1879-1890.

Frisk. G.V. 1994. Ocean and Seabed Acoustics: A theory of wave propogation. Prentice Hall: Englewood Cliffs, NJ, USA.)

Gardner, J.V., Dartnell, P., Mayer, L.A., and Hughes Clarke, J.E. 2003. Geomorphology, acoustic backscatter, and process in Santa Monica Bay from multibeam mapping. Marine Environmental Research, 56: 15-46.

Gensane, M. 1989. A statistical study of acoustic signals backscattered from the sea bottom. IEEE Journal of Oceanic Engineering, 14: 84-93.

Geoscience Australia 2004 . Geoscience Australia bathymetry data set at 0.1^{o} resolution. Geoscience Australia, Canberra, Australia.

Goff, J.A., Swift, D.J.P., Duncan, C.S., Mayer, L.A., and Hughes-Clarke, J. 1999. High-resolution swath sonar investigation of sand ridge, dune and ribbon morphology in the offshore environment of the New Jersey margin. Marine Geology, 161: 307-337.

Greene, H.G., Yoklavich, M.M., Starr, R.M., O'Connell, V.E., Wakefield, W.W., Sullivan, D.E., McRea, J.E. Jr., and Cailliet, G.M. 1999. A classification scheme for deep seafloor habitats. Oceanologica Acta, 22: 663-678.

Gunderson, L. H., Holling, C. S., Light, S. S. 1995. Barriers and bridges to the renewal of ecosystems and institutions. New York, Columbia University Press.

Hamilton, E.L. 1972. Compressional-wave attenuation in marine sediments. Geophysics, 37(4): 620-646.

Hamilton, E. L. and Bachman, R.T. 1982. Sound velocity and related proporties of marine sediments. Journal of the Acoustical Society of America, 72(6): 1891-1904.

Hammerstad, E. 1994. Backscattering and sonar image reflectivity. EM 12/950/1000 Technical Note. Kongsberg Horton Norway12pp.

Hammerstad, E. 2000. Backscattering and seabed image reflectivity. EM Technical Note Kongsberg Horton Norway 6pp.

Harris, P., Radke, B., Smith, A., Glen, K., Rollet, N., Exon N. and Passlow V. 2000. Marine geological data collected during *Southern Surveyor* voyage 01/00: eastern Bass Strait and Great Australian Bight - AGSO research cruise number 224. Australian Geological Survey Organisation, v. 2000/43.

Harris, P., Heap, A., Passlow, V., Sbaffi, L., Fellows, M., Porter-Smith, R., Buchanan, C., and Daniell, J. 2002. Geomorphic Features of the Continental Margin of Australia, Report to the National Oceans Office on the production of a consistent, high-quality bathymetric data grid and definition and description of geomorphic units for Australia's EEZ Seabed Mapping and Characterisation Project Team: Petroleum and Marine Division, Geoscience Australia, GPO Box 378, Canberra, ACT 2601.

Heald, G.J. and Pace, N.G. 1996. An analysis of the 1st and 2nd backscatter for seabed classification. In 'Proceedings of the 3rd European Conference on Underwater Acoustics, 24-28 June 1996'. vol. II, pp. 649-654.

Hellequin, L., Boucher, J. and Lurton, X. 2003. Processing of high frequency multibeam echo sounder data for seafloor characterisation. IEEE Journal of Oceanic Engineering, 28(1): 78-89.

Hill ,P.J., Exon, N.F., and Keene, J.B. 1998. The continental margin off east Tasmania and Gipplsland: structure and development using new multibeam sonar data. Exploration Geophysics. 29, 410-419.

Hill, P., Rollet, N. and Symonds, P. 2001. Seafloor mapping of the South-east Marine Region and adjacent waters. AUSTREA final report: Lord Howe Island,south-east Australian margin (includes Tasmania and South Tasman Rise) and central Great Australian Bight. Canberra: Australian Geological Survey Organisation, Record 2001/08.

Holling, C.S. 1992. Cross-scale morphology, geometry and dynamics of ecosystems. Ecological Monographs, 62: 447-502.

Hubbell, S.P. 2001. The unified neutral theory of biodiversity and biogeography. Monograpghs in population biology. Princeton University Press, Princeton, NJ.

Hughes-Clark, J.E.H., Mayer, L.A., Mitchell, N.C., Godin, A. and Costello, G. 1993. Processing and interpretation of 95 kHz backscatter data from shallow-water multibeam sonars. IEEE II 437-442.

Hughes-Clark, J.E., Gardner, J.E., Torresan and Mayer, L.A. 1998. The limits of spatial resolution achievable using a 30 kHz multibeam sonar: model predictions and field results. Proceedings Oceans 1998 Nice vol3.

Hughes-Clark, J.E., Lamplugh, M. and Kammerer, E. 2000. Integration of near-continuous sound speed profile information. Proceedings Canadian Hydrographic Conference Montreal, May 2000.

Huseby, R.B., Milvang, O., Solberg, A.S. and Bjerde, K.W. 1993. Seabed classification from multibeam echosounder data using statistical methods. In Oceans '93. Volume III. New York: IEEE. 229-233.

Hutchinson, G.E. 1958. Homage to Santa Rosalia or why are there so many kinds of animals? Am Nat 93:145–1.

ICES. 2007. Acoustic seabed classification of marine physical and biological landscapes. ICES Cooperative Research Report No. 286. 183 pp.

IHO. 2001. Standardization of Undersea Feature Names: Guidelines Proposal form Terminology. International Hydrographic Organisation and International Oceanographic Commission, Monaco. 40pp.

IMCRA 3.3. 1998. Interim Marine and Coastal Regionalisation for Australia: an ecosystem-based classification for marine and coastal environments. Version 3.3. Environment Australia, Commonwealth Department of the Environment (Canberra).

Inman, D.I. 1952. Measures for describing the size distribution of sediments. Journal of sedimentary petrology, 22(3): 125-145.

Ishimaru,A. 1978. Wave propagation and scattering in random media. Volume 2: multiple scattering, turbulence, rough surfaces, and remote sensing. Academic; New York, NY (USA), 572 pp.

Ivakin, A.N. and Lysanov, Yu. P. 1988. Determination of the structure of marine sediments from acoustic sensing data. Soviet physics – acoustics, 34(1): 114.

Ivakin, A.N. and Jackson, D.R. 1998. Effects of shear elasticity on sea bed scattering: Numerical examples. Journal of the Acoustical Society of America, 103(1): 346-354.

Jackson, D. R., Winebrenner, D. P., and Ishimaru, A. 1986. Application of the composite roughness model to high-frequency bottom backscattering. The Journal of the Acoustical Society of America, 79(5): 1410-1422.

Jackson, D.R. and Ivakin, A.N. 1998. Scattering from elastic sea beds: First-order theory. Journal of the Acoustical Society of America, 103(1): 336-345.

Jackson, D.R., and Briggs, K.B. 1992. High-frequency bottom backscattering: roughness versus sediment volume scattering. The Journal of the Acoustical Society Of America, 92(2): 962-977.

Jaffe, J.S., Moore, K.D., McLean, J. and Strand, M.P. 2001. Underwater Optical Imaging: Status and Prospects. Oceanology, 14(3): 64-75.

Jones, G.A. and Kaiteris, P. 1983. A vacuum-gasometric technique for rapid and precise analysis of calcium carbonate in sediments and soils. Journal of Sedimentary Petrology, 53(2): 655-660.

Jones, C.D and Jackson, D.R. 2001. Small Perturbation Method of High-Frequency Bistatic Volume Scattering from Marine Sediments. IEEE Journal of Oceanic Engineering, 26(1): 84-93.

Kloser, R. J., Sakov, P. V., Waring, J. R. Ryan, T. E. and Gordon, S. R. 1998. Development of software for use in multi-frequency acoustic biomass assessments and ecological studies, Fisheries Research and Development Corporation T93/2, 74pp, ISBN 0 643 06192 4.

Kleinrock, M.C., Hey, R.N., and Theberge, Jr. A.E. 1992. Practical geological comparison of some seafloor survey instruments. Reophysical Research Letters, 19(13): 1407-1410.

Kloser, R.J., Bax, N.J. Ryan, T.E. Williams A. and Barker B.A. 2001a. Remote sensing of seabed types-development and application of normal incident acoustic techniques and associated ground truthing. Marine and Freshwater Research, 52: 475-89.

Kloser, R.J., Williams, A. and Butler, A. 2001b. Acoustic, biological and physical data for seabed characterisation. Report to the National Oceans Office, Progress Report 2 of Project OP2000-SE02, April 2001. CSIRO Marine Research Hobart, pp 332.

Kloser, R.J., Keith, G., Ryan, T., Williams, A. and Penrose, J. 2002a. Seabed biotope characterisation in deep water – initial evaluation of single and multi-beam acoustics. In Proceedings of the 6th European Conference in Underwater Acoustics, Gdansk 2002, Stepenowski, A. Ed, pp 81-88.

Kloser, R.J., Williams, A. and Butler, A. 2002b. Exploratory Surveys of seabed habitat in Australia's deep ocean using remote sensing- needs and realities. In Proceedings of the ICES Document CM 2002/K:06.

Kloser, R.J., Williams, A. and Butler A. 2004. Marine biological and resource surveys South East Region: Assessment of Acoustic mapping of seabed habitats. Report to the National Oceans Office. Final report of project OP2000-SE02, March 2004. CSIRO Marine Research, pp 26.

Kostylev, V.E., Todd, B.J., Fader, G.B.J., Courtney, R.C., Cameron G.D.M. and Pickrill, R.A. 2001. Benthic habitat mapping on the Scotian Shelf based on multibeam bathymetry, surficial geology and sea floor photographs. Marine Ecology - Progress Series, 219: 121-137.

Krause, D.C. and Menard, H.W. 1965. Depth distribution and bathymetric classification of some sea-floor profiles. Marine geology, 3: 169-193.

Krumbein, W.C., 1936. Application of logarithmic moments to size frequency distribution of sediments. Journal of Sedimentary Petrology, 6: 35-47.

Langton, R.W., Auster, P.J., and Schneider D.C. 1995. A spatial and temporal perspective on research and management of groundfish in the northwest Atlantic. Reviews in Fisheries Science, 3: 201-229.

Larcombe, J.W.P., McLoughlin, K.J., Tilzey, R.D.J. 2001. Trawl operations in the South East Fishery, Australia: spatial distribution and intensity: Marine & Freshwater Research, 52: 419-430.

Lewis, M. 1999. CSIRO-SEBS (Seamount, Epibenthic Sampler), a new epibenthic sled for sampling seamounts and other rough terrain. Deep-Sea Research Part 1, 46: 1101-1107.

Lyons, A.P. and Abraham, D.A. 1999. Statistical characterization of high-frequency shallow-water seafloor backscatter. Journal of the Acoustical Society of America, 106(3): 1037-1315.

MacKenzie, K.V. 1981. A nine-term equation for sound speed in the oceans. Journal of the Acoustical Society of America, 70: 807-812.

MacLennan, D.N., and Simmonds, E.J. 1992. Fisheries acoustics. Fish and Fisheries Series No. 5. Chapman and Hall. London. 325 pp.

MacLennan, D.N., Fernandes, P.G. and Dalen, J. 2002. A consistent approach to definitions and symbols in fisheries acoustics. ICES Journal of Marine Science, 59: 365-369.

Mann, K.H. and Lazier, J.R.N. 1996. Dynamics of marine ecosystems: biological-physical interactions in the oceans. 2nd ed. Cambridge: Blackwell Science. 394pp.

MBSTC21. 2000. Fourth Asia-Pacific coastal multibeam sonar training course. Ed. Hughes Clark, J. de Moustier, C. Mayer, L. and Wells, D. Course notes, Cairns, Australia August, 2000.

Matsumoto, H., Dziak, R.P., and Fox, C.G. 1993. Estimation of seafloor microtopographic roughness through modeling of acoustic backscatter data recorded by multibeam sonar system. Journal of the Acoustical Society of America, 94(5): 2776-2787.

Mitchell, N.C. and Clark, J.E. 1994. Classification of seafloor geology using multibeam sonar data from the Scotian Shelf. Marine Geology, 121: 143-160.

Mitchell, N.C. 1996. Processing and analysis of Simrad multibeam sonar data. Marine Geophysical Research, 18(6): 729-739.

Nakano, H., Hibino, T., Oji, T., Hara, Y., and Amemiya, S. 2003. Larval stages of a living sea lily (stalked crinoid echinoderm). Nature , 421(9): 158-160.

Neshyba, S. 1987. Oceanography: Perspectives on a fluid earth. John Wiley And Sons: New York, NY (USA): 528 pp.

NOO. 2002. National Oceans Office. Ecosystems – Nature's diversity. South-east Regional Marine Plan Assessment Reports. National Oceans Office, Hobart, Australia.

Ogilvy, J. A. 1992. Theory of wave scattering from random rough surface. IOP Publishing: London GB.

Orlowski, A. 1984. Application of multiple echoes energy measurements for evaluation of sea-bed type. Oceanologia, 19: 61-78.

Pace, N.G. and Dyer, C.M. 1979. Machine classification of sedimentary sea bottoms. IEEE Transactions on geoscience electronics, 17(3): 52-56.

Pace, N.G. and Gao, H. 1988. Swathe Seabed Classification. IEEE Journal of Oceanic Engineering, 13: 83-90.

Pierce, J.W., and Graus, R.R., 1981. Use and misuse of the Phi-Scale: Discussion. Journal of Sediment Petrology, 51: 1348-1350.

Pitcher, C.R., Burridge, C.Y., Wassenberg, T.J., Poiner, I.R. 1997. The effects of prawn trawl fisheries on GBR seabed habitats. p. 107–123. In The Great Barrier Reef, science, use and management: a national conference: proceedings. Vol. 1. (Great Barrier Reef Marine Park Authority: Townsville).

Pitcher, C. R., Poiner, I. R., Hill, B. J., and C. Y. Burridge. 2000. Implications of the effects of trawling on sessile megazoobenthos on a tropical shelf in northeastern Australia. ICES Journal of Marine Science, 57: 1359–1368.

Pouliquen, E. and Lyons, A.P. 2002. Backscattering from bioturbated sediments at very high frequency. IEEE Journal of Oceanic Engineering, 27(3): 388-402.

Preston, J.M., Christney, A.C., Bloomer, S.F. and Beaudet, I. L. 2003. Seabed classification of multibeam sonar images. MTS 0-933957-28-9, 8pp.

Raven, P.H. and Johnson, G.B. 1986. Biology, Times Mirror/Mosby College Publishing, USA .

Rayleigh, J.W.S.L. 1945. Theory of sound, volume 2 chapter 13, p 89-96. Dover publications. Original edition 1878.

Roff, J.C. and Taylor, M.E. 2000. National frameworks for marine conservation -- a hierarchical geophysical approach. Aquatic Conservation: Marine and Freshwater Ecosystems, 10: 209-223.

Sainsbury, K.J., Campbell, R., Lindholm, R., Whitelaw, A.W. 1997. Experimental management of an Australian multispecies fishery: examining the possibility of trawl induced habitat modification. In: Pikitch EK. Huppert DD and Sissenwine MP (eds). Global trends: fisheries management. American Fisheries Society, Bethesda, Maryland, p. 107-112.

Seibold, E. and Berger, W.H. 1996. The sea floor: an introduction to marine geology. 3rd ed. Berlin: Springer-Verlag. 356pp.

Simrad 1999a. Triton seafloor classification, instruction manual. Kongsberg, Horton, Norway.

Simrad 1999b. Neptune, operators manual. Kongsberg, Horton, Norway.

Simrad 1999c. Operator Manual EM1002 Multibeam echosounder-160977B. Kongsberg, Horton, Norway.

Snelgrove, P.V.R., and Butman, C.A. 1994. Animal-sediment relationships revisited: cause versus effect. Oceanography and Marine Biology: An annual review, 32: 111-177.

Solan, M., Germano, J.D., Rhoads, D.C., Smith, C., Michaud, E., Parry, D., Wenzhoefer, F., Kennedy, B., Henriques, C., Battle, E., Carey, D., Iocco, L., Valente, R., Watson, J. and Rosenberg, R. 2003. Towards a greater understanding of pattern, scale and process in marine benthic systems: a picture is worth a thousand worms. Journal of Experimental Marine Biology and Ecology, 285-286: 313-338.

Stanic, S. and Kennedy, E. 1992. Fluctuations of high-frequency shallow-water seafloor reverberation. Journal of the Acoustical Society of America, 91(4): 1967-1973.

Stanton, T.K. 1982. Effects of transducer motion on echo-integration techniques. Journal of the Acoustical Society of America, 72: 947-949.

Stanton, T. K. 1985a. Seafloor classification using sonar echo statistics. Proceedings of the Institute of Acoustics, 7: 35-48.

Stanton, T.K. 1985b. Echo fluctuations from the rough seafloor: Predictions based on acoustically measured microrelief properties. Journal of the Acoustical Society of America, 78(2): 715-721.

Sternlicht, D.D. 1999. High frequency acoustic remote sensing of seafloor characteristics. PhD dissertation University of California, San Diego.

Sternlicht, D.D. and de Moustier, C.P. 2003. Time-dependent seafloor acoustic backscattering (10-100 kHz). Journal of the Acoustical Society of America, 114(5): 2709-2725.

Stewart, R.A., and Chotiros, N.P. 1992. Estimation of sediment volume scattering cross section and absorption loss coefficient. Journal of the Acoustical Society of America, 91(6): 3242-3247.

Stewart, W. K., Chu, D., Malik, S., Lerner, S., and Singh, H. 1994a. Quantitative seafloor characterization using a bathymetric sidescan sonar. IEEE Journal of Oceanic Engineering, 19(4): 599-610.

Stewart, W. K., Jiang, M. and Marra, M. 1994b. A neural network approach to classification of sidescan sonar imagery from a midocean ridge area. IEEE Journal of Oceanic Engineering, 19(2): 214-24.

Todd, B.J. Faber, G.B.J. Courtney R.C. and Pickrill R.A. 1999. Quaternary geology and surficial sediment processes, Browns Bank, Scotian Shelf, based on multibeam bathymetry. Marine Geology, 162: 165-214.

Urick, R. J. 1983. Principles of underwater sound. New York, McGraw-Hill, 423 p., ISBN: 0070660875.

Waring, J.R., Kloser, R.J., and Pauly, T. 1994. Echo – Managing Fisheries Acoustic Data. In 'Proceedings of the International Conference on Underwater Acoustics University of New South Wales, Dec. 1994'. pp.22-24.

Wentworth, C.K. 1922. A scale grade and class terms for clastic sediments. The Journal of Geology, 30(5): 377-392.

Wildish, D. and Kristmanson, D. 1997. Benthic suspension feeders. Cambridge University Press, New York, NY (USA), 409 pp.

Williams, A., Kloser, R.J., and Barker, B. 2004. Mapping, understanding and managing fishery habitat: a case study of the commercial pink ling (*Genypterus blacodes*: Ophidiidae) off SE Australia. Proceedings of the ICES Annual Science Meeting, Vigo, Spain, 2004.

Williams, K.L., Jackson, D.R., Thorson, E.I., Tang, D., and Briggs, K.B. 2002. Acoustic backscattering experiments in a well characterized sand sediment: Data/model comparison using sediment fluid and biot models. IEEE Journal of Oceanic Engineering, 27(3): 376-387.

Appendix B

Equipment description (extracted from Kloser *et al.*, 2001)

B.1 Swath mapping system

Figure B.1. A schematic diagram of the swath mapping system.

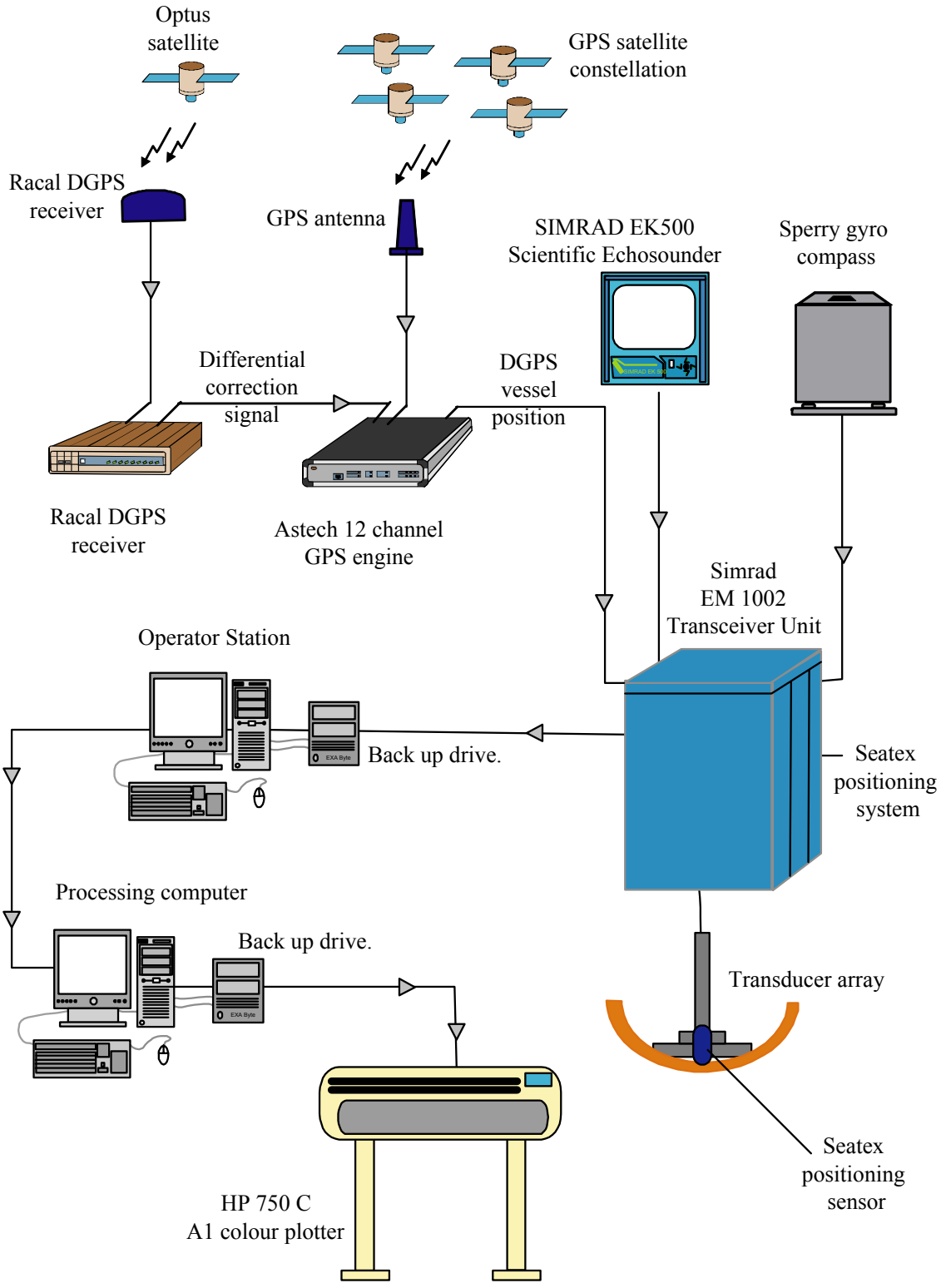

Specifications

Manufacturer:	Kongsberg Simrad
Model:	EM 1002
Frequency:	95kHz
Maximum ping rate:	>10 Hz
Beamwidth:	2x2°
Beam Spacing:	Equidistant and equiangle
Coverage sector:	up to 150°
Depth range from transducers:	2 to 1000 metres
Depth resolution:	2, 4 or 8 cm
Pulse Lengths:	0.2, 0.7 and 2 ms
Range sampling rate:	9 kHz (8 cm)
Beam-forming method:	phase interpolate
Tranceiver Unit:	
Serial Interfaces for:	Positioning systems
	Attitude (pitch, roll, heave)
	Heading
	Clock
	Datum Heights
Special Interfaces:	Trigger input/output
	Clock synchronisation
Supply Voltage:	115 or 230 Vac 50/60 Hz

Features of the swath mapping system

The Simrad EM1002 is a phase interpolated beam-forming swath mapper using a rounded head to reduce sound velocity beam forming errors. It forms 111 beams that are effectively 2 by 2 degrees per beam. The seabed depth per beam is calculated using an amplitude or phase algorithm depending on the angle of incidence. A value of mean backscatter per beam is calculated and side-scan values are collected by digitisation along the beam with 1-40 samples collected for each beam. The beams are electronically controlled for roll stabilisation.

For this survey the system was operated in an equidistant mode to give even sampling across the seafloor. The swath width was set to 140 degrees with pulse lengths varying with depth: 0.2 ms^{-1} at 0-100 m, 0.7 ms^{-1} at 100-200 m and 2 ms^{-1} for 200-600 m.

B.2 Camera system (video)

Figure B.2 The Mid-Depth Stereo Video system being retrieved on the RV Southern Surveyor. The cameras are shown in the central housings and the six lasers for the scaling system can be seen in the mounting block of the camera housings.

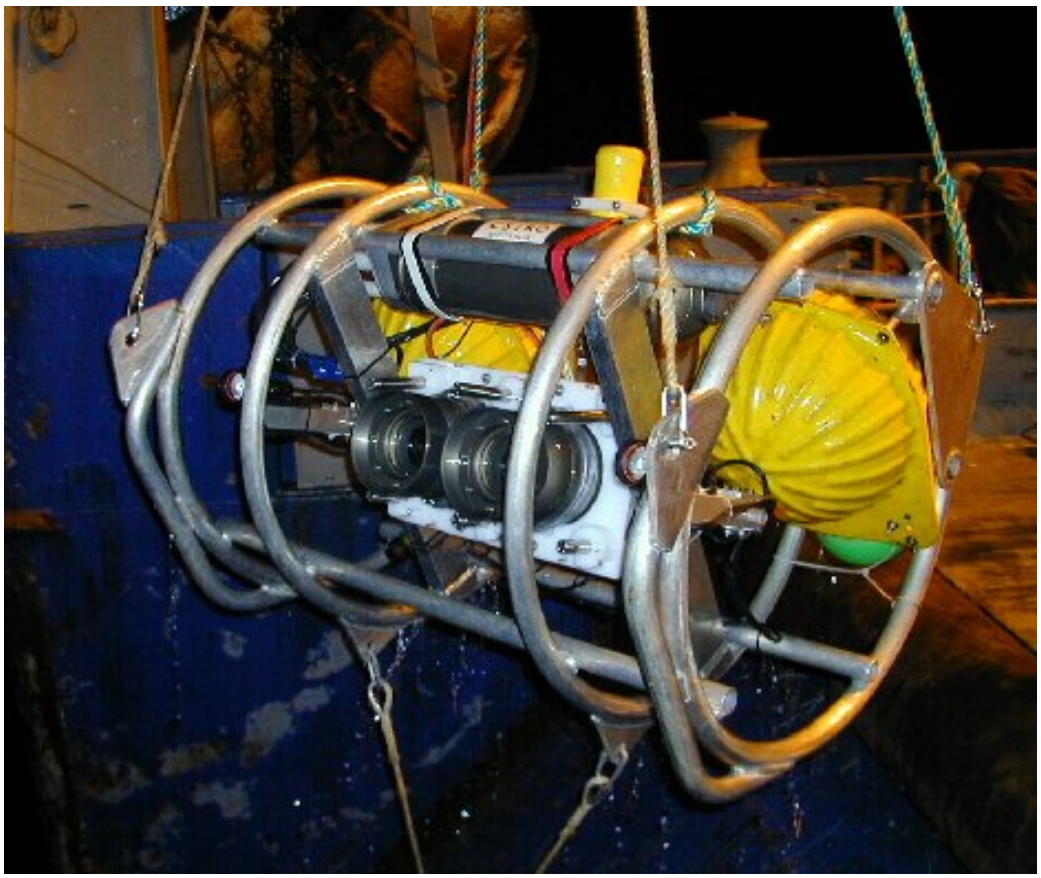

Specifications of current system

Maximum operating depth:	2000 meters
Video cameras:	Sony DSR-PD100T DVCam digital video
Recording time:	80 minutes mono, 40 minute stereo
Other features:	Laser measure scaling system
	2x250 watt lighting powered from surface via cable
	Real-time frame grabs (at 7 second intervals) sent to ship
	Open ocean capability
	Self-regulating system to keep camera at a constant height off seafloor

Features of the video system.

The mid-depth video system (Figure B.2) is fully controllable from the surface. The lights and lasers can be switched on and off as can the cameras. The cameras can either record

simultaneously to give stereo footage, or sequentially to double the recording time and hence area covered. The communications package gives us a constant readout of the tape counter and battery voltages as well as depth, water temperature, height above bottom, pitch and roll of the camera frame. Thus the entire system can be monitored and controlled from the surface via the tow cable (Figure B.3).

Figure B.3 A schematic diagram of the tow configuration and control systems needed for the Mid Depth video system.

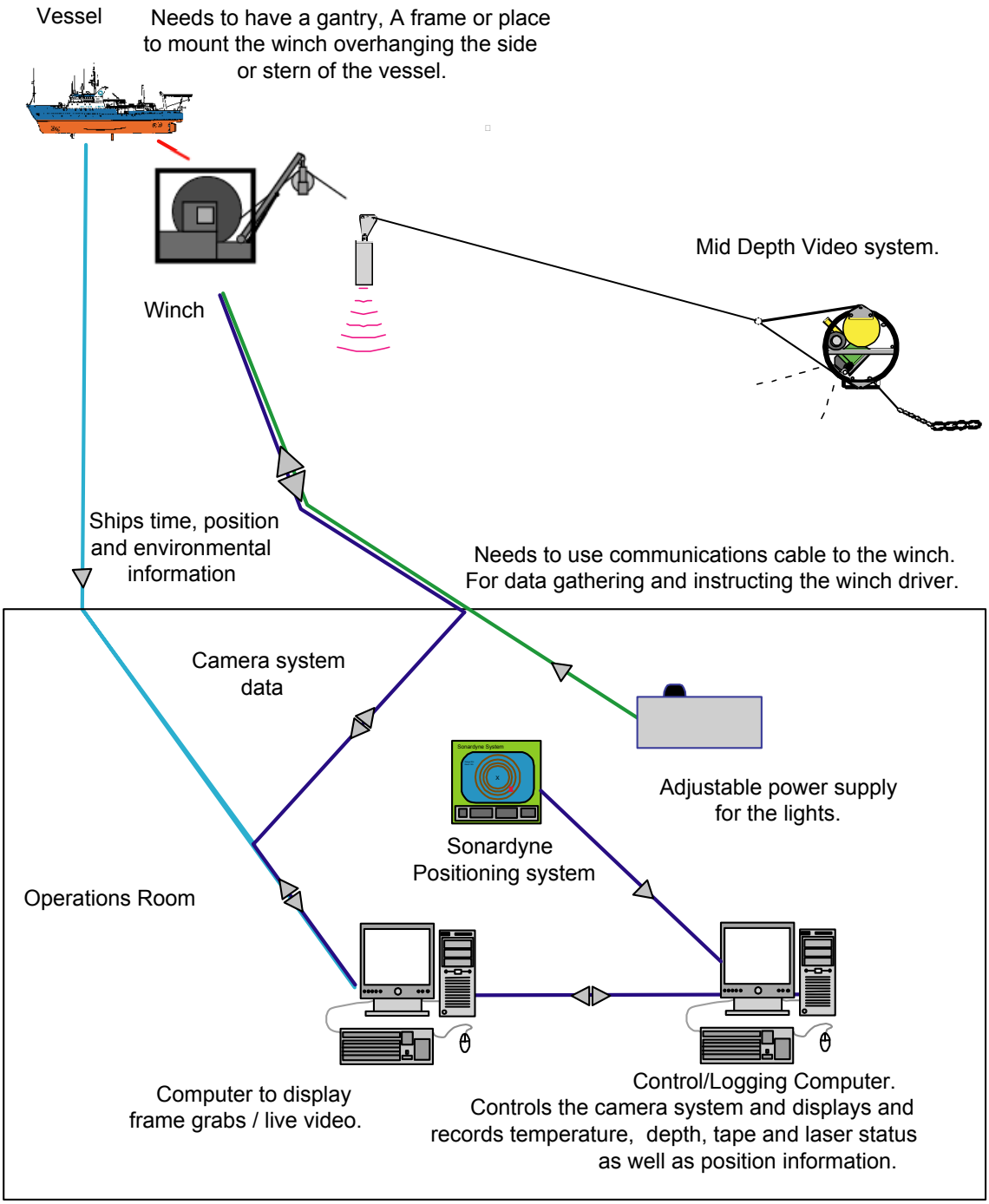

B.3 Tracking system for position fixing of towed gears

Figure B.4 General system overview with the components that constitute the system.

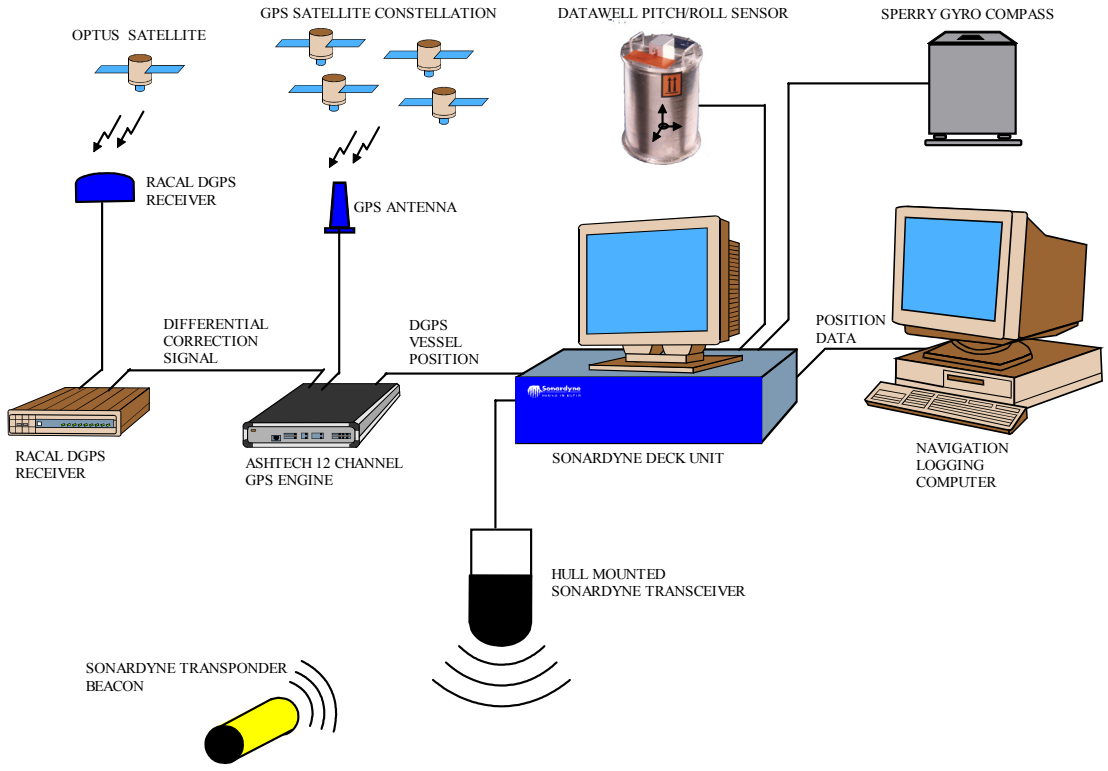

Features of the position fixing system

Acoustic beacons (Figure B.4) are attached to towed instruments (MUFTI towed body, grabs, epibenthic sleds, MIDOC, video and stills cameras) to give high accuracy position fixes for the instrument relative to the vessel. A hull mounted transceiver transmits an interrogation pulse in all directions from beneath the ship. A beacon in the water will send a reply that the hull transducer detects and uses to determine the direction, inclination and distance to the beacon. Using this data we can calculate the latitude and longitude of the beacon's position. This system is essential for accurately geo-locating our equipment in the water column or on the seafloor and is used when-ever possible

B.4 Epibenthic sled

Figure B.5 "Sherman" the epibenthic sled, front view, on the back deck of the RV *Southern Surveyor*.

Specifications

Manufacturer:	CSIRO Marine Research
Model:	Sherman
Weight:	1,200 kg
Main Use:	Sampling the epibenthos (invertebrates)
Mouth Area:	120cm x 50cm
Construction:	Steel Plate (up to 12mm thick)
Target substrate:	Seamounts and reefs
Cod end material:	30mm streatched mesh knotless nylon (2mm twine size)
Cod end size:	Mouth area 0.5 m^2, 3.5m in length
Chafing mat:	Conveyor belt section
Protective Bag for cod end:	50mm diamond mesh using 1.6mm wire

Features of the epibenthic sled "Sherman"

Sherman (Figure B.5) is an epibenthic sled designed to sample on any terrain, but particularly rough seamounts and reefs. The sled is constructed out of steel plate of 12 mm thickness in the runners and 10mm in the box with specially designed cutting bars that collect large pieces of biota, and excellent rock samples at times. The tow bridle system along with the solid construction allows Sherman to work in very demanding terrains (Lewis, 1999). The bridle system uses lifting chain (high tensile tested chain) of 10 and 13 mm thickness and tows from the back of the sled with the 13mm galvanised chains around the runners giving the angle of attack to the bottom. This bridle system allows for a 4 stage break-away system that has proven very reliable to date.

B.5 Smith-McIntyre grab

Figure B.6 The Smith-McIntyre grab being retrieved over the side of the RV *Southern Surveyor*.

Specifications

Manufacturer:	CSIRO Marine Research
Weight:	100 kg
Main Use:	Sediment sampling
Mouth Area:	32cm X 38cm
Construction:	Stainless steel
Target substrate:	Fine to medium grain sediment

Features of the Smith-McIntyre Grab

The Smith-McIntyre Grab (Figure B.6) can collect a core of sediment approximately 320 mm x 380 mm x 200 mm deep. The grab is loaded at the surface by compressing the springs and setting the jaws in the open position. The grab is automatically triggered upon landing. When triggered the grab is driven into the sediment by the preloaded springs and it's own inertia upon landing. When retrieved, the jaws close collecting a relatively undisturbed core of sediment. The Smith-McIntyre grab proves to be relatively reliable, returning a good volume of sediment from suitable bottom types.

B.6 Box corer

Figure B.7 The small box corer being deployed off the RV *Southern Surveyor*.

Specifications

Dimensions:	150mm X 150mm X 200mm
Construction:	Stainless Steel with a perspex liner
Weight:	40Kg
Main Use:	Collecting relatively undisturbed cores of soft sediment

Features of the box corer

The Australian Geological Survey Organisation (AGSO) provided a small box corer (Figure B.7) for sampling softer sediment. The box section was a 150mm square and used a perspex liner to enable the collection of undisturbed cores. The box corer was driven into the sediment by its own weight and as the weight came off the cable the release pin activated. As the corer was retrieved the jaws closed and cut the core free. The box corer was intended to be used to collect undisturbed sections of sediment for acoustic analysis, as well as faunal and grain size analysis. The device did not perform as well as hoped and the Smith-McIntyre grab was used for collecting these samples.

B.7 Rock dredge

Figure B.8 The AGSO rock dredge and catch on the back deck of the RV *Southern Surveyor*.

Specifications

Mouth Area:	027 m^2, 890mm X 305mm
Construction:	Galvanised steel, 12mm in mouth section
Weak link:	Adjustable shear pin from 1 – 9 tonnes
Weight:	100kg
Pipe dredges:	2 X 200mm diameter and 500mm long
Sample bag construction:	Chain mesh using 6mm galvanised chain
Bag size:	890mm x 305mm x 1000mm
Mesh size:	70mm square
Main use:	Collecting rocks, sediment and invertebrates

Features of the Rock Dredge

The rock dredge (Figure B.8) used on this trip was borrowed from AGSO. The dredge had an adjustable weak link (shear pin) system on the towing bridle (1-9 t). The mouth of the dredge was constructed from 12mm thick galvanised steel with a mouth area of 890 mm x 305 mm or 0.27 m^2. The chain bag consists of 6mm galvanised chain forming a square mesh with 70 mm sides. Attached at the end of the mesh bag is a plate to which the safety chain and two pipe dredges, each approximately 200 mm in diameter and 500 mm long, are attached. The chain bag proved to be very resilient and successful at collecting larger invertebrates as well as rocks. The AGSO rock dredge was attached to the trawl warp with a swivel of 5 tonne safe working load to minimise twisting and consequent damage to the warp.

Appendix C

Proceedings of the Sixth European Conference on Underwater Acoustics, Stepnowski, A. Ed., Gdansk, June 2002: 81-88 p.

Seabed biotope characterisation in deep water – initial evaluation of single and multi-beam acoustics

R. J. Kloser[a], G. Keith[a], T. Ryan[a], A. Williams[a] and J. Penrose[b]

[a]*CSIRO Marine Research, GPO Box 1538 Hobart Tas. 7001 Australia, e-mail: rudy.kloser@csiro.au*
[b]*Curtin University of Technology Perth WA*

Summary

Mapping seabed biotopes or their surrogates is a fundamental first step in understanding the nature of the seabed. We outline our methodology for initial evaluation of commercial single and multi-beam acoustic systems to characterise the surficial geological and biological attributes of the seabed in water depths > 50 m. A Simrad EM1002 swath mapper and EK500 echosounder at 12, 38 and 120 kHz were used to map selected sites on the shelf and upper slope. At each site the geo-referenced biophysical, geophysical and video sampling was targeted on contrasting features in the swath mapped bathymetry and backscatter imagery. These physically and visually described seabed sites are compared to commercially implemented seabed classification methods for simple differentiation of low relief (< 1.0 m) limestone reef and sediment flat mesohabitats. The video data highlighted the patchy nature of the reef structures that exist as 5 to 20 m patches at intervals of 200 m. The 'Triton' swath mapping seabed classification software reliably differentiated the reef with 0 % error rate, but was sensitive to pulse length changes. Also, it needed large training sites, therefore reducing its spatial resolution, due to across beam averaging. The single beam first echo tail, E1, and second echo, E2, integration methods produced error rates of 21 to 35 % for single frequencies and 17% when combining the 12 and 38 kHz frequencies. Within a region all single frequencies provided good discrimination of major seabed morphology. High resolution depth data from the swath mapper using slope and profile metrics performed reliably at 0 to 20 % error rates. The information contained in the hi-resolution swath bathymetry and backscatter maps goes well beyond simple mesohabitat scale (~10s m to 1km) differentiation. It may also be used to infer geological, biological and oceanographic processes at a variety of spatial scales that will form the basis of our ongoing analyses.

1. Introduction

Australia is custodian to a large marine jurisdiction with associated seabed habitats that need to be managed for multiple use purposes. To map seabed habitats of the whole Australian Marine Jurisdiction (AMJ) will require the development of surrogates due to the large region and difficulty/expense of sampling the marine environment. These seabed surrogates will need to describe the geological and biological features (biotopes) and be able to detect changes in them that are of management significance.

Acoustic methods of sensing the water column and seabed habitats provide a potential method for developing these surrogates when used in conjunction with direct capture and visual sampling methods. Simple normal incident single and multi-frequency acoustic methods provide a useful sampling tool to map the seabed seascape in terms of broad scale bathymetry and seabed hardness and roughness on flat seabeds with associated ground truthing [eg 1,2]. To improve seabed sampling resolution, depth resolution and account for seabed slope, multi-beam acoustic systems are being used.

Multi-beam swath acoustic systems provide detailed bathymetry along the line of the vessels track with swath widths of 2 to 10 times water depth as well as producing detailed backscatter maps of the seabed. The vessel mounted

backscatter maps have lower resolution than those produced by towed sidescan instruments but due to beam forming, multi-beams can correct for seabed slope and geo-reference the backscatter. Investigations using multi-beam backscatter maps to date have concentrated on geological mapping, (eg [3]) and only recently habitat mapping [4]. What is less certain is the ability of the bathymetry and associated backscatter data to be used as a surrogate for habitat maps of a given region and across regions to determine the level of physical and visual sampling required.

In this paper we provide our initial assessment methodology for commercially implemented seabed segmentation methods (RoxAnn/EchoPlus and Simrad Triton) using single and multi-beam acoustic technology and their ability to distinguish specific seabed training sites over several regions. The training sites are described using sediment/lithology and video sampling and are nested within acoustic facies regions based on visually scored swath mapped backscatter and bathymetric regions at a mesohabitat scale of 10's m to kilometre [5].

2. Equipment and Methods

A 111 beam 95kHz (nominally) swath mapper (Simrad EM1002) and three frequency (12, 38 and 120 kHz) normal incident echo sounder (Simrad EK500, version 5.3) were used to map various regions (50 – 1500 m depth) in the south-east of Australia. The regions were chosen based on historic knowledge as having high importance for fisheries and physical characteristics of depth, seabed morphology (slope and roughness), sediment type, lithology, latitude and longitude [6]. We present our initial analysis from 4 regions with areas ranging from 30 to 60 km^2.

At the commencement of each survey region the seawater propagation parameters of absorption and sound velocity were calculated based upon temperature and salinity profiles obtained from a CTD. The swath survey bathymetry was processed using the Simrad Neptune software to provide three data products, at 10 to 20 m grids, of bathymetry, backscatter and sun illuminated imagery. These three data products were visually inspected on board and the biophysical, geophysical and video/photographic sampling targeted at contrasting features in the imagery creating a set of reference or training sites. The precise location of the direct sampling devices used the vessels dynamic positioning system and a Sonardyne USBL. In general the location of sampling gears could be directed to within 5 to 10 m for depths less than 300 m, Fig. 1.

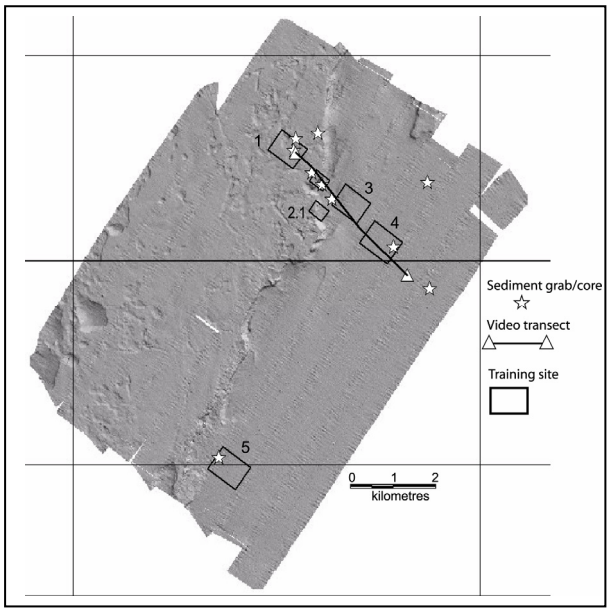

Figure 1 Sun illuminated bathymetry, 8 times vertical exaggerated of Gabo Reef with acoustic training sites marked and associated video and sediment grab/core stations

Acoustic facies regions at mesohabitat scale (10's m to km) in the swath bathymetry, 8 times vertical exaggeration bathymetry, slope and backscatter were designated in MapInfo using a visual scoring based on Table I.

Table I Preliminary acoustic facies scores for swath mapping based on depth, texture, slope and backscatter attributes at 10 – 20 m grid intervals.

Depth (pulse length)	**Texture (t)**
1. 0-50 m	1. smooth < 0.5 m
2. 50 -100 m	2. isolated outcroppings > 0.5 m
3. 100 - 200 m	3. undulating regular > 0.5 m
4. 200 - 500 m	4. undulating irregular > 0.5 m
5. 500 - 1000 m	
Slope (s)	**Backscatter profile (b) (-22 to –55 dB)**
1. low < 1 deg	1. uniform low
2. medium > 1 and < 3	2. uniform medium
3. high > 3	3. uniform high
	4. irregular low.
	5. irregular med.
	6. irregular high.

Metrics of the visual scoring attributes were calculated on the 10 to 20 m grid bathymetry values for each training site region. The metrics for slope, aspect, profile and tangent were extracted and summaries of mean, std, skewness and kurtosis calculated, using GRASS, (http://grass.itc.it). Only

swath angles less than 60° were processed due to outer beam ripples [6]. Profile and tangent metrics are the curvatures in the direction of steepest slope and in the direction of the contour tangent respectively. The maps of slope and profile were visually of greatest benefit in interpreting seabed morphology and edge features.

The sidescan backscatter data from the EM1002 were corrected by removing beam pointing tramlines, Lamberts law and centre beam smoothing (Simrad bottom backscatter modifiers [7]) using modified MB systems software [8] and processed using Simrad Triton seabed classification software version 1.6 [9]. Triton extracts 5 statistical features of the aggregated across track sidescan data (4 bins across track, beams 0-20, 21-55, 56-89, 90-110) and several pings. The extracted statistical features are 0.8 quantile, Pace (power spectrum), contrast, mean value and standard deviation. These statistical features form a five-dimensional vector that is georeferenced and using Bayes classification produce maps based on two or three (selected by visual inspection) of the five vectors. Problems with the performance of the EM1002 during the survey with both backscatter and bathymetry limited the analysis to swath widths less than 60 degrees [6].

Calibrated acoustic single beam 12, 38 and 120 kHz ping based volume reverberation (Sv) data were logged, quality assured and processed using a software package named 'ECHO'. Simple metrics were derived from the data, by integrating the tail of the first echo, E1, and all of the second seabed echo, E2 [1,2]. For our depth range and 1 mS pulse lengths, the angular off axis portion of the tail integrated, di, was between, θi, values of 20-30 degrees from the start of the rising edge of the acoustic pulse. The pulse offset was set at 1.5 meters for 38 and 120 kHz and 4.5 m for 12 kHz, where:

$$di = bottom\_depth * (\frac{1}{Cos\,\theta i} - 1) + pulse\_offset$$

The second echo was integrated at two times the water depth (d1) and ending at two times water depth plus 20 m (d2). Several pings, p, were integrated (nominally 20 pings at vessel speed of 10 knots) to reduce between-ping variability in the backscatter returns and to standardise on a unit of length sampled, 92.6 m (0.05 n.mile):

$$\overline{s_A} = 10\log_{10}(1852^2 4\pi \frac{\sum_{p=1}^{m}(\delta d \sum_{d=d1}^{d2} 10^{\frac{Sv_{dp}}{10}})}{m}) \text{ dB re } m^2 \text{ n mile}^{-2}$$

Where S_A is the area backscatter coefficient, integrated between the start, d1, and stop, d2, depth, and δd is the acoustic sampling interval.

Combined frequency acoustic metrics were obtained by calculating the first principle component of the standardised E1 and E2 values [10]. This method is used to explore the added information in the separate acoustic, tail of first and second echo, metrics when combining frequencies.

The physical sampling of the geological and biological characteristics were carried out with a variety of instruments. Surficial sediments were obtained with a Smith-McIntyre grab and lithology samples were collected with a rock dredge. Video footage were obtained with a vertical drop and towed video platform. The video imagery was used to characterise the biological communities and geomorphology. Details of the collection instruments and sampling and analysis protocols are reported for geology [11] and biology and video [2]. The video data contained four scored attributes at 1 second intervals (approx. every 0.25 m): substratum (S), geomorphology (G), fauna (F) (community groups) and abundance (A), Table II.

At each training site metrics were obtained from;

- Single beam three frequencies
- Multi-beam bathymetry
- Triton seabed software
- Visual scoring of swath bathymetry and backscatter.

These metrics were compared to the geophysical and biophysical video scoring, sediments and lithology, from the training sites. The data from the single and swath backscatter were evaluated on the ability to distinguish mesohabitat scale features defined as reef and sediment flats using linear discriminate analysis and a Mahalanobis distance metric. Training site prediction error was based on the cross-validation-error scores, S-plus ver 6.0. Where each site observation is systematically dropped from the site list and the linear discriminate function estimated and the excluded observation classified. A low error score indicated

good agreement with the training site classifications. Validity of error tests were visually confirmed on the data by mapping the variables on the swath maps and plotting the combined metrics.

Table II Attributes of seabed habitats recorded during simple analysis of image data

	1. Substratum (S)		2. Geomorphology (G)
0	Mud	0	Unrippled
1	Fine sediments	1	Current rippled/directed scour
2	Coarse sediments	2	Wave rippled
3	Gravel/pebble	3	Highly irregular
4	Cobble/boulder	4	Debris flow/rubble banks
5	Igneous/metamorphic rock	5	Subcrop
6	Sedimentary rock	6	Outcrop (low <1m); no holes/cracks
		7	Outcrop (low <1m); with holes/cracks
		8	Outcrop (high >1m); no holes/cracks
		9	Outcrop (high >1m); with holes/cracks
	3. Fauna (F)		4. Abundance (A)
0	None - no apparent epifauna or infauna	1	Low/sparse (<10%)
1	Gardens – large sponges	2	Medium/intermediate (<50%)
2	Gardens - small sponges	3	High/dense (>50%)
3	Gardens - mixed (sponges, seawhips, ascidians)		
4	Crinoids		
5	Octocorals (gold corals/seawhips)		
6	Small encrustors/erect forms (including bryozoans)		
7	Sedentary: e.g. seapens		
8	Mobile: e.g. echinoids/holothurians/asteroids		
9	Distinct infauna bioturbators		

The area of seafloor ensonified and viewed from the various sampling methods limits the direct comparison between devices. The swath mapper was operated at 10 knots in an equidistant mode to give even sampling of depth at the 111 beam centres across the seafloor with a swath width of 140° and pulse length of 0.7 ms. Surveying in 100 m depth, 2 pings per second and at 10 knots the beam pointing centres are spaced 5 m apart athwart ship and 2.5 m along ship. This represents the effective horizontal resolution of the system. The depth resolution was variable due to outer beam ripples and heave error but visually precise to +/- 0.25 m locally around any given feature. The area ensonified for sidescan backscatter on the seafloor assuming a flat seabed and horizontal platform is defined as:

$A = 10\log_{10} \psi_x \psi_y R^2$ around normal incidence, and

$A = 10\log_{10} \frac{c\tau\psi_x R}{2\sin\theta}$ elsewhere.

Here, c is sound speed in m/s, τ is the pulse length in s, ψ_x and ψ_y are the along and athwart 3 dB beamwidths in radians, θ is the angle of incidence and R is slant range in m. The normal incident area as a function of seabed depth, D, is valid until the bottom incident angle is larger than the largest angle from the following:

$$\cos\theta_{l1} = (1 + \frac{c\tau}{2D})^{-1}$$

$$\sin\theta_{l2} = -\frac{\psi_x D}{c\tau} + \sqrt{\left(\frac{\psi_x D}{c\tau}\right) + 1}$$

At 100 m depth the sidescan ensonification area is approximately 10 m^2 on axis and varies between 4 to 6 m^2 off axis.

The single beam ensonified area for seabed classification for the tail of the first echo is approximately an annulus from the start integration angle of θ_1 (20°) to θ_2 (30°) off normal incidence. The second echo has a less well defined ensonification area but we assume that it is represented by a circle that the sounder beamwidth would describe at 3 times water depth [12]. At 100 m depth the first echo is approximately defined by an annulus of start diameter 35 m and end diameter 54 m, area 1280 m^2. The second echo has an effective sampling diameter of 80, 37 and 52 m and areas of 4900, 1058 and 2164 m^2 for the 12, 38 and 120 kHz frequency beam patterns respectively.

3. Results

The 15 training sites from the 4 regions, depths 90 to 140 m, are grouped into two mesohabitats of limestone reef (r) and sediment flats (sf), Table III. The reefs consist of high to medium porosity limestone with isolated outcroppings > 0.5m height grading to undulating irregular > 1 m height. A reef ledge site represented a 5-15 m drop with slopes at >5 degrees. The sediment flats of < 0.5 degree slope consisted of sediments ranging from dominant gravel through to muddy sand.

Table III Summary of training sites nested within swath facies regions and mesohabitat class of reef (r) and sediment flat (sf). The swath backscatter and bathymetry 10/20 m grid maps are scored for texture (t), slope (s) and backscatter (b) (Table I) and dominant sediment and

lithology characteristic.

Training Site	Meso-habitat	Swath Facies t,s,b.	Dominant sediment/lithology
1	r	415	medium porosity limestone
2.1	r	436	reef edge limestone
3	sf	113	gravel
4	sf	112	sand
5	sf	115	sandy gravel
6	r	425	medium porosity limestone
7	r	414	medium porosity limestone
7.1	r	414	medium porosity limestone
8	sf	115	sand
8.1	sf	115	sand
9	sf	112	sand
10.1	sf	112	sandy gravel
10.2	sf	112	sandy gravel
11	r	414	high porosity limestone
12	sf	112	sandy gravel
13	r	414	high porosity limestone
14	sf	112	sand
15	sf	111	muddy sandy

The substratum, geomorphology and fauna based on the video scoring shows that the training sites are heterogeneous on the reef (site 6) and reef edge and more homogeneous off the reef (site 9), Table IV. The video scores confirm the substratum and geomorphology associated to the training sites based on swath bathymetry visual scoring. Of note is the small difference (6 to 7 %) between what is defined as reef (6) and sediment flat (9) and represents the patchy scales (5 – 20 m) of the reef. The sediment flats are characterised by fine sediments (9) with dominantly small sponge gardens to coarse sediments (3) with dominantly small encrusters.

Table IV Video scoring showing combination scores (% > 0.5%) for substratum (S), geomorphology (G) and fauna (F) for reef edge (2), reef (1,6) and sediment flat (3,9) training sites, based on Table II where an SGF score of 100 is equivalent to, fine sediments, unrippled and no apparent epifauna and infauna. Reef scores in italic.

(S.G.) substratum and geomorphology score							
site	**10**	**20**	***65***	***66***	***67***	***69***	**Length m**
1r	6	0	*94*	*0*	*0*	*0*	200
2r	37	0	*54*	*0*	*0*	*9*	340
3sf	24	76	*0*	*0*	*0*	*0*	200
6r	93	0	*5*	*1*	*1*	*0*	500
9sf	100	0	*0*	*0*	*0*	*0*	400

(S.G.F.) substratum, geomorphology and fauna score										
	100	**102**	**202**	**206**	**208**	***651***	***652***	***661***	***671***	***691***
1r	6	0	0	0	0	*91*	*3*	*0*	*0*	*0*
2r	36	0	0	0	0	*54*	*0*	*0*	*1*	*9*
3sf	10	14	2	73	1	*0*	*0*	*0*	*0*	*0*
6r	0	94	0	0	0	*5*	*0*	*1*	*0*	*0*
9sf	0	100	0	0	0	*0*	*0*	*0*	*0*	*0*

The sediment characteristics of percentage gravel, sand, mud, total organic carbon and calcium carbonate for sand and mud proved to be a poor discriminator of reef mesohabitat, combined cross validation error rate of 0.43. The mean phi sediment size from the training sites shows that for reef site 6, multiple sediment grabs (3) within tens

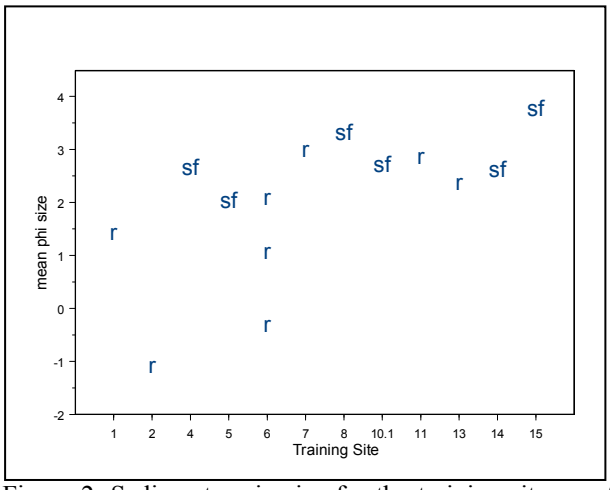

Figure 2. Sediment grain size for the training sites, reef (r) and sediment flat (sf) in phi units with larger grains representing smaller phi sizes. Site six has multiple samples.

of meters can yield a variety of sediment sizes ranging from gravel dominant to fine sand, Fig. 2. This is consisted with the patchy nature of the seabed observed using the video for site 6, Table IV.

The cross validation error for the single and swath frequency highlight the limitations of the single beam system and the frequency dependence of classification. The combined single beam error 21% and 35% for discriminating reef and sediment flats of the 12 and 38 kHz frequencies respectively demonstrates that the 12 kHz is marginally better for discriminating the reef and sediment flat characteristics for this training set, Fig. 3. Combined single frequencies 12 and 38 kHz improved the cross classification error (0.14). The E1 and E2 metrics for the 120 kHz frequency were not available for all training sites and regions due to acoustic and electrical interference. An example of the mapping for a single region for the 38 kHz demonstrates that within a region the single beam systems highlight the on reef and sediment flat features, Fig. 4. Note that the E2 metric that is sometimes referred to as hardness is lower on reef than off reef. The Triton echo statistics combined cross classification error from the 5 metrics of the sidescan backscatter was 0 %. This increases to 24 % error rate when combining 0.2 and 0.7 pulse length data.

The depth data from the swath mapper for slope and profile metrics were used to describe the reef and sediment flat features of the training sites. The cross validation error rates varied between 0 – 20 % dependant on the covariance model assumed in the linear discriminate model. This demonstrates that a fine scale seabed depth metric is a reliable classifier of mesohabitat scale features as defined here.

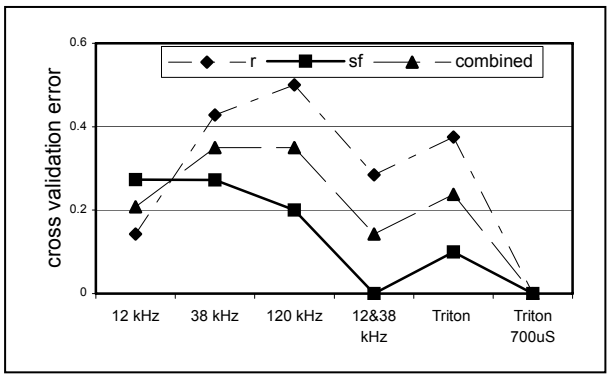

Figure 3 Cross classification error rate for estimating reef (r) and sediment flats (sf) and combined error for the single frequencies 12, 38 and 120 kHz and combined frequencies and swath Triton software with mixed pulse lengths (Triton) and single pulse length Triton 700uS.

4. Discussion

Georeferenced video data (recorded at a very fine spatial scale) shows that a patchy distribution of substratra and epifauna (at scales of ~5-200 m) underlies the classification of biotopes in our training sites. One characteristic type of deep water reefs in our study region is aggregated patches of outcropping low relief limestone (with its associated fauna) as seen at reef site 6. Many individual patches are low-relief (0.5 to 1 m in height) about 100- 200 m apart and 5 to 50 m in length. These reef features are surrogates for the

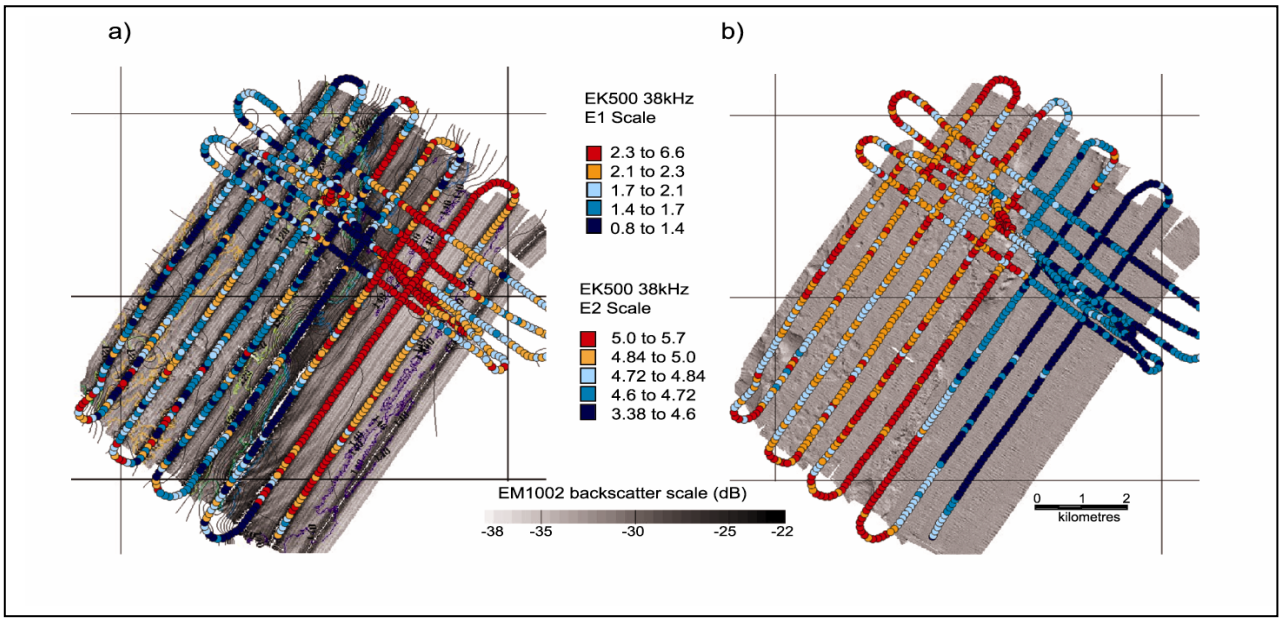

Figure 4. Swath map EM1002 and single 38 kHz products of a) uncorrected EM1002 backscatter for Gabo Reef with second echo (E2 Hardness?) overlaid and b) sun illuminated bathymetry, 8 times vertical exaggeration, with tail of first echo (E1 roughness?) overlaid. The size of the sampling dots represents the approximate 50 m sampling diameter of the single beam system.

distributions of epifaunal communities at the mesohabitat (10's m to 1 km) scale.

It is therefore not surprising that sediment grain size represents a poor discriminator of these heterogeneous reef sites, classification error rates of approximately 50%. The variability of the sediment grabs for reef site 6 is a good indicator of the reef habitat but requires high sampling rates and costly vessel time. Therefore training sites could not simply be labelled with rock/gravel/sand/mud descriptions for the scales of observations.

The visual scoring of the swath bathymetry and uncorrected backscatter proved to be adequate for mesohabitat scale region delineation. The classifications are supported by the video and bathymetric metrics of slope and profile with 0 to 20% cross validation error rates. We are encouraged to extend this visual classification method to more sites and introduce more supportive quantitative bathymetry and backscatter metrics. Visual scoring of the swath data has the added ability to operate at a variety of scales in the classification process.

Simrad Triton swath backscatter metrics could discriminate the simple on reef and off reef features with 0% error rates. Nonetheless, limitations due to sensitivities to pulse length, swath angle and associated energy level changes are evident. The aggregation of a quarter swath width, 173 m at 100 m depth, and several pings, 10 m, limits its spatial resolution to an area of approximately 1700 m^2. The Triton classification could be improved by adding depth metrics in the algorithm or in post processing. In our case the Triton software could not operate beyond 60 degrees due to an unresolved error in the sidescan data.

The single beam systems provided useful information but with higher error rates at single frequencies. The terms second echo hardness and first echo roughness should be used with caution with single beam single frequency devices as they do not translate into physical meaning at a variety of scales. For example the limestone reef at site 1 the 12 kHz gave a higher second echo signal between on reef and sediment flats whereas the reverse occurred at 38 kHz, Fig. 3. The scale of sampling with the E1 and E2 metrics are 2 orders of magnitude higher than the swath mappers and the video sampling devices. This changing scale introduces resolution and classification problems with patchy changes in seabed types.

The swath mapper bathymetry and backscatter maps by themselves are an insightful and cost-effective method for understanding seabed structure and identifying or inferring underling geological and oceanographic processes that are of significance for the distribution of biological communities. The information content contained in the bathymetry and sidescan data is largely untapped by current processing methods. The scale discussion here is restricted to 10s m to km's but finer resolution information in the swath and video data will be further explored for biotic assemblages. This will be best achieved by combining a variety of information including high resolution bathymetry and backscatter along with physical and visual sampling and other environmental variables such as current.

Acknowledgement

We would like to thank the Australian National Oceans Office and CSIRO Marine Research for funding this research. We would also like to thank Dr Alan Butler the co-biological investigators on the project, and to Bruce Barker for analysis of the video data.

References

[1] R.C. Chivers, N. Emerson, and D.R. Burns: New acoustic processing for underway surveying. *Hydrological Journal* **56,** (1990) pp 9-17.

[2] R.J. Kloser, N.J. Bax, T.E. Ryan, A. Williams and B.A. Barker: Remote sensing of seabed types-development and application of normal incident acoustic techniques and associated ground truthing. *Marine and Freshwater Research*. **52** (2001) pp475-89

[3] B.J. Todd, G.B.J. Faber, R.C. Courtney and R.A. Pickrill: Quaternary geology and surficial sediment processes, Browns Bank, Scotian Shelf, based on multibeam bathymetry. *Marine Geology* **162**, (1999). pp 165-214.

[4] V.E. Kostylev, B.J. Todd, G.B.J. Fader, R.C. Courtney, G.D.M. Cameron and R.A. Pickrill: Benthic habitat mapping on the Scotian Shelf based on multibeam bathymetry, surficial geology and sea floor photographs. *Marine Ecology - Progress Series,* **219** (2001) pp 121-137

[5] H.G. Greene, M.M. Yoklavich, R.M. Starr, V.E. O'Connell, W.W. Wakefield, D.E. Sullivan, J.E. Jr. McRea and G.M. Cailliet: A classification scheme for deep seafloor habitats. *Oceanologica Acta* **22**, (1999), pp 663-678.

[6] R.J. Kloser, A. Williams and A. Butler: Acoustic, biological and physical data for seabed characterisation. Report to the National Oceans

Office, Progress Report 2 of Project OP2000-SE02, April 2001. CSIRO Marine Research Hobart. (2001) pp 332.

[7] E. Hammerstadt: Backscatering and Sonar Image Reflectivity, Simrad EM 12/950/1000 Technical Note April 15th (1994),pp 12.

[8] D.W. Caress and D.N. Chayes: New software for processing sidescan data from sidecan-capable multibeam sonars *Oceans 95 MTS/IEEE, Challenges of our changing global environment, October 9-12, San Diego* , (1995) *pp.997-1000 , California, USA. Proceedings Volume 2. Washington, D.C.: The Marine Technology Society, pp.692-1385.*

[9] Simrad Triton: Triton seafloor classification, Instruction manual. Kongsberg Simrad (1999).

[10] P.J.W Siwabessy, J.D. Penrose, D.R. Fox, and R.J. Kloser: Bottom classification in the continental shelf: a case study for the North-west and South-east shelf of Australia. In 'Proceedings of the Australian Acoustical Society Nov. 2000, Perth (2000) pp. 265-270

[11] P. Harris, B. Radke, A. Smith, K. Glen, N. Rollet, N. Exon and V. Passlow: Marine geological data collected during *Southern Surveyor* voyage 01/00: eastern Bass Strait and Great Australian Bight - AGSO research cruise number 224. Australian Geological Survey Organisation **43** (2000).

[12] G.J. Heald and N.G. Pace. An analysis of the 1st and 2nd backscatter for seabed classification. *Proc. 3rd European Conference on Underwater Acoustics,* 24-28 June 1996 vol. II: 649-654.